NASA/CR—2004-212609

Low and High Speed STOVL Configurations in Ground Effect

Thomas J. Vukits
Purdue University, West Lafayette, Indiana

February 2004

The NASA STI Program Office . . . in Profile

Since its founding, NASA has been dedicated to the advancement of aeronautics and space science. The NASA Scientific and Technical Information (STI) Program Office plays a key part in helping NASA maintain this important role.

The NASA STI Program Office is operated by Langley Research Center, the Lead Center for NASA's scientific and technical information. The NASA STI Program Office provides access to the NASA STI Database, the largest collection of aeronautical and space science STI in the world. The Program Office is also NASA's institutional mechanism for disseminating the results of its research and development activities. These results are published by NASA in the NASA STI Report Series, which includes the following report types:

- TECHNICAL PUBLICATION. Reports of completed research or a major significant phase of research that present the results of NASA programs and include extensive data or theoretical analysis. Includes compilations of significant scientific and technical data and information deemed to be of continuing reference value. NASA's counterpart of peer-reviewed formal professional papers but has less stringent limitations on manuscript length and extent of graphic presentations.

- TECHNICAL MEMORANDUM. Scientific and technical findings that are preliminary or of specialized interest, e.g., quick release reports, working papers, and bibliographies that contain minimal annotation. Does not contain extensive analysis.

- CONTRACTOR REPORT. Scientific and technical findings by NASA-sponsored contractors and grantees.

- CONFERENCE PUBLICATION. Collected papers from scientific and technical conferences, symposia, seminars, or other meetings sponsored or cosponsored by NASA.

- SPECIAL PUBLICATION. Scientific, technical, or historical information from NASA programs, projects, and missions, often concerned with subjects having substantial public interest.

- TECHNICAL TRANSLATION. English-language translations of foreign scientific and technical material pertinent to NASA's mission.

Specialized services that complement the STI Program Office's diverse offerings include creating custom thesauri, building customized databases, organizing and publishing research results . . . even providing videos.

For more information about the NASA STI Program Office, see the following:

- Access the NASA STI Program Home Page at ***http://www.sti.nasa.gov***

- E-mail your question via the Internet to help@sti.nasa.gov

- Fax your question to the NASA Access Help Desk at 301–621–0134

- Telephone the NASA Access Help Desk at 301–621–0390

- Write to:
  NASA Access Help Desk
  NASA Center for AeroSpace Information
  7121 Standard Drive
  Hanover, MD 21076

NASA/CR—2004-212609

Low and High Speed STOVL Configurations in Ground Effect

Thomas J. Vukits
Purdue University, West Lafayette, Indiana

Prepared under Grant NAG3–943

National Aeronautics and
Space Administration

Glenn Research Center

February 2004

Acknowledgments

The author wishes to express gratitude to his major professor, John P. Sullivan. His guidance, criticism, and patience during the course of this research are greatly appreciated. The author would also like to thank S.N.B. Murthy and Steven P. Schneider for their support and input as graduate committee professors. Also, the author's appreciation is extended to NASA Glenn Research Center, the sponsors of this research, and to Peter Batterton and James D. Holdeman, who supported and guided the direction of this research. The help and support of this author's fellow graduate students, especially Robert T. Johnston and Robert Hoffenberg, were instrumental in the completion of this research. Special thanks are given to Roderick MacLean, who laid the foundation for this author's work and provided guidance in the initial stages of this research. Finally, the author would like to thank the support staff at the Aerospace Sciences Laboratory. The staff includes: Bob Sanders, Dave Reagan, Bill Bader, Don Bower, Jack Davis, Robert Scott, and Myra Fuqua.

The Propulsion and Power Program at
NASA Glenn Research Center sponsored this work.

Available from

NASA Center for Aerospace Information
7121 Standard Drive
Hanover, MD 21076

National Technical Information Service
5285 Port Royal Road
Springfield, VA 22100

Available electronically at http://gltrs.grc.nasa.gov

TABLE OF CONTENTS

Page

LIST OF TABLES v

LIST OF FIGURES vi

ABSTRACT xvii

CHAPTER 1 INTRODUCTION 1

CHAPTER 2 LITERATURE SURVEY 8

CHAPTER 3 EXPERIMENTAL APPARATUS AND METHOD 13

3.1 Test Models and Jets 13
3.2 Marker Nephelometry 14
3.3 Low Speed Experimental Setup 15
3.4 High Speed Experimental Setup 18
3.5 Test Conditions 21
3.6 Data Processing 21

CHAPTER 4 LOW SPEED - TWO-, THREE-, FOUR-JET STUDY 34

4.1 Ground Plane Measurements: H/D_j=4, U/V_j=0.09 35
4.1.1 Mean Concentration Measurements 36
4.1.2 Single Frame Concentration Measurements 37
4.1.3 RMS Concentration Measurements 38
4.2 Mid-Plane Measurements:
H/D_j=4, U/V_j=0.09 38
4.3 Decreased Forward Speed Measurements:
H/D_j=4, U/V_j=0.03 39
4.4 Measurements at Increased Model Height:
H/D_j=6, U/V_j=0.09 40
4.5 Measurements at Decreased Model Height:
H/D_j=2, U/V_j=0.09, y/D_j=0.6 41

4.6 Vortex Positions Under Parametric Variation 41
4.6.1 H/D_j=2.0 Case 42
4.6.2 H/D_j=4.0 Case 43
4.6.3 H/D_j=6.0 Case 44

CHAPTER 5 LOW SPEED - TWO- AND THREE-JET INLET STUDY 98

5.1 Two-Jet Configuration 98
5.2 Three-Jet Configuration 100

CHAPTER 6 HIGH SPEED - TWO-JET STUDY 111

CHAPTER 7 SUMMARY AND CONCLUSIONS 123

BIBLIOGRAPHY 126

APPENDICES 132

VUKITS VIDEO DESCRIPTION 151

LIST OF TABLES

Table		Page
3.1	Test Parameters	24
4.1	Test Cases for Low Speed - Two-, Three-, and Four-Jet Study	46
5.1	Test Cases for Low Speed - Two- and Three-Jet Inlet Study	102
6.1	Test Cases for High Speed - Two-Jet Study	114

LIST OF FIGURES

Figure		Page
1.1	Hot Gas Ingestion Mechanisms	5
1.2	Flowfield Features in xz Plane From MacLean [28]	6
1.3	Flowfield Features in xy Plane From MacLean [28]	7
3.1	Three-Jet Test Model	25
3.2	Four-Jet Test Model	26
3.3	Adaptor for Three-Jet Test Model	27
3.4	Experimental Setup	28
3.5	Wind Tunnel Velocity Distribution From MacLean [28]	29
3.6	Jet Velocity Profile From MacLean [28]	30
3.7	Laser and Laser Sheet Optics From MacLean [28]	31
3.8	V/STOL Wind Tunnel	32
3.9	V/STOL Wind Tunnel Velocity Profiles	33
4.1	Two-Jet Single Frame Image of Smoke Concentration at Ground Plane $y/D_j=0$, $H/D_j=4$, $U/V_j=0.09$	47
4.2	Two-Jet 127-Frame Average Image of Smoke Concentration at Ground Plane $y/D_j=0$, $H/D_j=4$, $U/V_j=0.09$	48

Figure Page

4.3 Three-Jet Single Frame Image of Smoke Concentration at Ground Plane $y/D_j=0$, $H/D_j=4$, $U/V_j=0.09$ 49

4.4 Three-Jet 127-Frame Average Image of Smoke Concentration at Ground Plane $y/D_j=0$, $H/D_j=4$, $U/V_j=0.09$ 50

4.5 Four-Jet Single Frame Image of Smoke Concentration at Ground Plane $y/D_j=0$, $H/D_j=4$, $U/V_j=0.09$ 51

4.6 Four-Jet 127-Frame Average Image of Smoke Concentration at Ground Plane $y/D_j=0$, $H/D_j=4$, $U/V_j=0.09$ 52

4.7 Two-, Three-, Four-Jet 127-Frame Average Concentration Profiles at Model Centerline: $z/D_j=0$ Laser Sheet at Ground Plane: $y/D_j=0.0$, $H/D_j=4$, $U/V_j=0.09$ 53

4.8 Two-, Three-, Four-Jet 127-Frame Average Concentration Profiles at Jet Centerline: $z/D_j=1.625$ Laser Sheet at Ground Plane: $y/D_j=0.0$, $H/D_j=4$, $U/V_j=0.09$ 54

4.9 Two-, Three-, and Four-Jet 127-Frame Average Concentration Profiles at Forward Jet Centerline: $x/D_j=0$ Laser Sheet at Ground Plane: $y/D_j=0.0$, $H/D_j=4$, $U/V_j=0.09$ 55

4.10 Two-, Three-, Four-Jet Single Frame Concentration Profiles at Model Centerline: $z/D_j=0$ Laser Sheet at Ground Plane: $y/D_j=0.0$, $H/D_j=4$, $U/V_j=0.09$ 56

Figure Page

4.11 Two-, Three-, Four-Jet Single Frame Concentration Profiles at Jet Centerline: z/D_j=1.625 Laser Sheet at Ground Plane: y/D_j=0.0, H/D_j=4, U/V_j=0.09 57

4.12 Two-, Three-, Four-Jet Single Frame Concentration Profiles at Forward Jet Centerline: x/D_j=0 Laser Sheet at Ground Plane: y/D_j=0.0, H/D_j=4, U/V_j=0.09 58

4.13 Two-, Three-, Four-Jet 127-Frame Average RMS Concentration Profiles at Model Centerline: z/D_j=0 Laser Sheet at Ground Plane: y/D_j=0.0, H/D_j=4, U/V_j=0.09 59

4.14 Two-, Three-, Four-Jet 127-Frame Average RMS Concentration Profiles at Jet Centerline: z/D_j=1.625 Laser Sheet at Ground Plane: y/D_j=0.0, H/D_j=4, U/V_j=0.09 60

4.15 Two-, Three-, Four-Jet 127-Frame Average RMS Concentration Profiles at Forward Jet Centerline: x/D_j=0 Laser Sheet at Ground Plane: y/D_j=0.0, H/D_j=4, U/V_j=0.09 61

4.16 Two-Jet 127-Frame Average Image of Smoke Concentration at Mid Plane y/D_j=2, H/D_j=4, U/V_j=0.09 62

4.17 Three-Jet 127-Frame Average Image of Smoke Concentration at Mid Plane y/D_j=2, H/D_j=4, U/V_j=0.09 63

4.18 Four-Jet 127-Frame Average Image of Smoke Concentration at Mid Plane y/D_j=2, H/D_j=4, U/V_j=0.09 64

Figure Page

4.19 Two-, Three-, Four-Jet 127-Frame Average Concentration Profiles at Model Centerline: $z/D_j=0$ Laser Sheet at Mid Plane: $y/D_j=2.0$, $H/D_j=4$, $U/V_j=0.09$ 65

4.20 Two-, Three-, Four-Jet 127-Frame Average Concentration Profiles at Jet Centerline: $z/D_j=1.625$ Laser Sheet at Mid Plane: $y/D_j=2.0$, $H/D_j=4$, $U/V_j=0.09$ 66

4.21 Two-, Three-, Four-Jet 127-Frame Average Concentration Profiles at Forward Jet Centerline: $x/D_j=0$ Laser Sheet at Mid Plane: $y/D_j=2.0$, $H/D_j=4$, $U/V_j=0.09$ 67

4.22 Two-Jet 127-Frame Average Image of Smoke Concentration at Ground Plane $y/D_j=0$, $H/D_j=4$, $U/V_j=0.03$ 68

4.23 Three-Jet 127-Frame Average Image of Smoke Concentration at Ground Plane $y/D_j=0$, $H/D_j=4$, $U/V_j=0.03$ 69

4.24 Four-Jet 127-Frame Average Image of Smoke Concentration at Ground Plane $y/D_j=0$, $H/D_j=4$, $U/V_j=0.03$ 70

4.25 Two-, Three-, Four-Jet 127-Frame Average Concentration Profiles at Model Centerline: $z/D_j=0$ Laser Sheet at Ground Plane: $y/D_j=0.0$, $H/D_j=4$, $U/V_j=0.03$ 71

4.26 Two-, Three-, Four-Jet 127-Frame Average Concentration Profiles at Jet Centerline: $z/D_j=1.625$ Laser Sheet at Ground Plane: $y/D_j=0.0$, $H/D_j=4$, $U/V_j=0.03$ 72

Figure Page

4.27 Two-, Three-, Four-Jet 127-Frame Average Concentration Profiles at Forward Jet Centerline: $x/D_j=0$ Laser Sheet at Ground Plane: $y/D_j=0.0$, $H/D_j=4$, $U/V_j=0.03$ 73

4.28 Two-Jet 127-Frame Average Image of Smoke Concentration at $y/D_j=0.6$ $H/D_j=6$, $U/V_j=0.09$ 74

4.29 Three-Jet 127-Frame Average Image of Smoke Concentration at $y/D_j=0.6$ $H/D_j=6$, $U/V_j=0.09$ 75

4.30 Four-Jet 127-Frame Average Image of Smoke Concentration at $y/D_j=0.6$ $H/D_j=6$, $U/V_j=0.09$ 76

4.31 Two-, Three-, Four-Jet 127-Frame Average Concentration Profiles at Model Centerline: $z/D_j=0$ Laser Sheet at $y/D_j=0.6$, $H/D_j=6$, $U/V_j=0.09$ 77

4.32 Two-, Three-, Four-Jet 127-Frame Average Concentration Profiles at Jet Centerline: $z/D_j=1.625$ Laser Sheet at $y/D_j=0.6$, $H/D_j=6$, $U/V_j=0.09$ 78

4.33 Two-, Three-, Four-Jet 127-Frame Average Concentration Profiles at Forward Jet Centerline: $x/D_j=0$ Laser Sheet at $y/D_j=0.6$, $H/D_j=6$, $U/V_j=0.09$ 79

4.34 Two-Jet 127-Frame Average Image of Smoke Concentration at $y/D_j=0.6$ Plane $H/D_j=2$, $U/V_j=0.09$ 80

4.35 Three-Jet 127-Frame Average Image of Concentration at $y/D_j=0.6$ Plane $H/D_j=2$, $U/V_j=0.09$ 81

Figure Page

4.36 Four-Jet 127-Frame Average Image of Concentration at y/D_j=0.6 Plane H/D_j=2, U/V_j=0.09 82

4.37 Two-, Three-, Four-Jet 127-Frame Average Concentration Profiles at Model Centerline: z/D_j=0 Laser Sheet at Ground Plane: y/D_j=0.6, H/D_j=2, U/V_j=0.09 83

4.38 Two-, Three-, Four-Jet 127-Frame Average Concentration Profiles at Jet Centerline: z/D_j=1.625 Laser Sheet at Ground Plane: y/D_j=0.6, H/D_j=2, U/V_j=0.09 84

4.39 Two-, Three-, Four-Jet 127-Frame Average Concentration Profiles at Forward Jet Centerline: x/D_j=0 Laser Sheet at Ground Plane: y/D_j=0.6, H/D_j=2, U/V_j=0.09 85

4.40 Two-Jet 127-Frame Average Image of Smoke Concentration at y/D_j=0.6 with Inlet Suction H/D_j=4, U/V_j=0.03 86

4.41 Two-Jet 127-Frame Average Image of Smoke Concentration at y/D_j=0.6 without Inlet Suction H/D_j=4, U/V_j=0.03 87

4.42 Three-Jet 127-Frame Average Image of Smoke Concentration at y/D_j=0.6 with Inlet Suction H/D_j=4, U/V_j=0.03 88

4.43 Three-Jet 127-Frame Average Image of Smoke Concentration at y/D_j=0.6 without Inlet Suction H/D_j=4, U/V_j=0.03 89

4.44 Four-Jet 127-Frame Average Image of Smoke Concentration at y/D_j=0.6 with Inlet Suction H/D_j=4, U/V_j=0.03 90

Figure Page

4.45 Four-Jet 127-Frame Average Image of Smoke Concentration at y/D_j=0.6 without Inlet Suction H/D_j=4, U/V_j=0.03 91

4.46 Two-, Three-, Four-Jet Forward Vortex Pair Location Versus Velocity Ratio (U/V_j) With and Without Inlet Suction y/D_j=0.6, H/D_j=2 92

4.47 Two-, Three-, Four-Jet Ground Vortex Location Versus Velocity Ratio (U/V_j) With and Without Inlet Suction y/D_j=0.6, H/D_j=2.0 93

4.48 Two-, Three-, Four-Jet Forward Vortex Pair Location Versus Velocity Ratio (U/V_j) With and Without Inlet Suction y/D_j=0.6, H/D_j=4 94

4.49 Two-, Three-, Four-Jet Ground Vortex Location Versus Velocity Ratio (U/V_j) With and Without Inlet Suction y/D_j=0.6, H/D_j=4 95

4.50 Two-, Three-, Four-Jet Forward Vortex Pair Location Versus Velocity Ratio (U/V_j) With and Without Inlet Suction y/D_j=0.6, H/D_j=6.0 96

4.51 Two-, Three-, Four-Jet Ground Vortex Location Versus Velocity Ratio (U/V_j) With and Without Inlet Suction y/D_j=0.6, H/D_j=6.0 97

5.1 Low Speed Two-Jet Average Smoke Concentration at the Inlet Face Plane [z'y']: H/D_j=4, U/V_j=0.03 103

5.2 Low Speed Two-Jet Average Smoke Concentration at the Inlet Face Plane [z'y']: H/D_j=4, U/V_j=0.09 104

Figure Page

5.3 Low Speed Two-Jet Average Smoke Concentration at the Inlet Face Plane [z'y']: H/D_j=2, U/V_j=0.03 105

5.4 Low Speed Two-Jet Average Smoke Concentration at the Inlet Face Plane [z'y']: H/D_j=2, U/V_j=0.09 106

5.5 Low Speed Two-Jet Average Smoke Concentration at the Inlet Face Plane [z'y']: H/D_j=6, U/V_j=0.03 107

5.6 Low Speed Two-Jet Average Smoke Concentration at the Inlet Face Plane [z'y']: H/D_j=6, U/V_j=0.09 108

5.7 Low Speed Three-Jet Average Smoke Concentration at the Inlet Face Plane [z'y']: H/D_j=4, U/V_j=0.03 109

5.8 Low Speed Three-Jet Average Smoke Concentration at the Inlet Face Plane [z'y']: H/D_j=4, U/V_j=0.09 110

6.1 High Speed Two-Jet Single Frame Image of Smoke Concentration at Ground Plane: M_j=0.5, H/D_j=4.0, U/V_j=0.09 115

6.2 Edge Enhanced High Speed Two-Jet Single Frame Image of Smoke Concentration at Ground Plane: M_j=0.5, H/D_j=4.0, U/V_j=0.09 116

6.3 High Speed Two-Jet 127-Frame Image of Smoke Concentration at Ground Plane: M_j=0.5, H/D_j=4.0, U/V_j=0.09 117

6.4 Two-Jet 127-Frame Average Concentration Profiles Through Model Centerline at Multiple Jet Velocities: H/D_j=4.0, U/V_j=0.03 118

Figure Page

6.5 Two-Jet 127-Frame Average Concentration Profiles Through Jet Centerline at Multiple Jet Velocities: H/D_j=4.0, U/V_j=0.03 119

6.6 Two-Jet 127-Frame Average Concentration Profiles Through Model Centerline at Multiple Jet Velocities: H/D_j=4.0, U/V_j=0.09 120

6.7 Two-Jet 127-Frame Average Concentration Profiles Through Jet Centerline at Multiple Jet Velocities: H/D_j=4.0, U/V_j=0.09 121

6.8 High Speed Two-Jet Forward Vortex Pair and Ground Vortex Position Versus Velocity Ratio (U/V_j) without Inlet Suction: M_j=0.07,0.19,0.50,0.95; H/D_j=4.0 122

Appendix
Figure

A.1 MacLean [28] Four-Jet Single Frame Image of Smoke Concentration at Ground Plane y/D_j=0, H/D_j=4, U/V_j=0.09 133

A.2 Four-Jet Single Frame Image of Smoke Concentration at Ground Plane y/D_j=0, H/D_j=4, U/V_j=0.09 134

A.3 Four-Jet Single Frame Comparison Concentration Profiles at Model Centerline: z/D_j=0 Laser Sheet at Ground Plane: y/D_j=0.0, H/D_j=4, U/V_j=0.09 135

A.4 Four-Jet Single Frame Comparison Concentration Profiles at Jet Centerline: z/D_j=1.625 Laser Sheet at Ground Plane: y/D_j=0.0, H/D_j=4, U/V_j=0.09 136

Appendix
Figure Page

A.5 Four-Jet Single Frame Comparison Concentration Profiles at Forward Jet Centerline: x/D_j=0.0 Laser Sheet at Ground Plane: y/D_j=0.0, H/D_j=4, U/V_j=0.09 137

B.1 Three- and Four-Jet 127-Frame Average Multiple Concentration Profiles at Model Centerline: z/D_j=0 Laser Sheet at Ground Plane: y/D_j=0.0, H/D_j=4, U/V_j=0.09 139

B.2 Three- and Four-Jet 127-Frame Average Multiple Concentration Profiles at Jet Centerline: z/D_j=1.625 Laser Sheet at Ground Plane: y/D_j=0.0, H/D_j=4, U/V_j=0.09 140

B.3 Three- and Four-Jet 127-Frame Average Multiple Concentration Profiles at Forward Jet Centerline: x/D_j=0 Laser Sheet at Ground Plane: y/D_j=0.0, H/D_j=4, U/V_j=0.09 141

C.1 Low Speed Two-Jet Average Smoke Concentration at the Inlet Face Plane [z'y']: H/D_j=4, U/V_j=0.03 143

C.2 Low Speed Two-Jet Average Smoke Concentration at the Inlet Face Plane [z'y']: H/D_j=4, U/V_j=0.09 144

C.3 Low Speed Two-Jet Average Smoke Concentration at the Inlet Face Plane [z'y']: H/D_j=2, U/V_j=0.03 145

C.4 Low Speed Two-Jet Average Smoke Concentration at the Inlet Face Plane [z'y']: H/D_j=2, U/V_j=0.09 146

Appendix
Figure

Page

C.5 Low Speed Two-Jet Average Smoke Concentration at the Inlet Face Plane [z'y']: H/D_j=6, U/V_j=0.03 147

C.6 Low Speed Two-Jet Average Smoke Concentration at the Inlet Face Plane [z'y']: H/D_j=6, U/V_j=0.09 148

C.7 Low Speed Three-Jet Average Smoke Concentration at the Inlet Face Plane [z'y']: H/D_j=4, U/V_j=0.03 149

C.8 Low Speed Three-Jet Average Smoke Concentration at the Inlet Face Plane [z'y']: H/D_j=4, U/V_j=0.09 150

CHAPTER 1

INTRODUCTION

From 1954, with the Lockheed XFV-1, to today, with aircraft like the Harrier, Vertical/Short Take-Off and Landing (V/STOL) and Short Take-Off and Vertical Landing (STOVL) vehicle designs have been pursued. Considerable effort has gone into analyzing and predicting the flowfield around such aircraft. One of the main questions remaining concerns the time varying distortion in the flow and thermal fields at the inlet face particularly in ground effect. It is in ground effect that the phenomenon known as hot gas ingestion can occur. Hot gas ingestion happens when the exhaust is redirected from the jets, back into the inlets. It is a complicated process that is influenced by many factors such as aircraft geometry, jet and cross flow velocities, and height of the aircraft above the ground.

There are two types of ingestion which are known as near and far field ingestion, shown in figure 1.1. Near field ingestion is due to exhaust gases being redirected in the flowfield near the aircraft to the inlet region. Far field ingestion occurs due to redirection of the exhaust gases in the far flowfield.

One approach to addressing the problem of hot gas ingestion is to examine if there are any discernable characteristic features in the flow interaction region beneath the aircraft. The early work on the establishment of the STOVL flowfield in this

manner was done by MacLean [28] and Tafti and Vanka [45]. MacLean conducted an experimental study on a four-jet configuration with cross-flow. An equivalent numerical study was done by Tafti and Vanka. Studies were later presented by Fricker et. al. [14] on a similar numerical model including the effects of splaying the front jets. The two main geometric parameters in those experiments were D_j, the jet diameter, and H, the model height above the ground. The main velocity parameters considered were U, the freestream velocity, and V_j, the jet velocity.

Within the flowfield, three types of vortex structures were identified: (i) the horseshoe ground vortex, (ii) the forward vortex pair, and (iii) the vortices associated with the interaction between the fountain and the jets.

The horseshoe ground vortex is shown in figures 1.2 and 1.3, from MacLean [28]. It forms in the ground plane, and occurs in the region where the wall jet produced by the jets impacting on the ground plane meets the freestream flow. Where they meet, the wall jet rolls up and forms a horseshoe shaped ground vortex. There will also be a second ground vortex in three- and four-jet configurations.

The forward vortex pair is also shown in figures 1.2 and 1.3. It is located in the stagnation region where the flow from between the front jet pair and the freestream flow meet. It is made up of a pair of counter-rotating vortices that are anchored in the ground plane. It is difficult to determine the different factors contributing to the formation of the vortex pair due to its unsteady nature. The third major vortical structure is a pair of counter-rotating vortices between a side pair of jets and the fountain, as seen in figure 1.3.

MacLean [28] showed these vortical structures for a four-jet model experimentally while Tafti and Vanka [45] and Fricker et. al. [14] showed them numerically. Both of those numerical predictions, however, only considered steady flow. The experimental study was able to view instantaneous features of the flowfield.

In the experiments presented here, a non-intrusive technique, marker nephelometry, was chosen to study the flowfield, qualitatively as well as quantitatively. Marker nephelometry is a method of studying concentration fields by injecting (i.e., marking) the feedstream to a flowfield with particles, and detecting particle concentrations with an optical probe based on light scatter techniques. Details on the technique and the method of quantifying the data were given by Becker [3] and Borleteau [4]. The concentration field was also analogous to the temperature field provided the concentration and the temperature were both in the nature of a marker, neither introducing density nor transport differences in the flowfield.

The experiments currently presented were conducted in three parts. In the first part, two-, three- and four-jet configurations at low jet and cross flow speeds with and without momentum matched inlet suction were studied. In the second part, measurements of the concentrations at the inlet entry plane for the two- and three-jet models were made. In the last part, a high speed, two-jet configuration without inlet suction was studied.

The overall objective of the study was to determine the formation and structure of the vortical features in the interaction region between the jets and the cross flow, especially near the inlets.

The specific objectives were to establish the following: (i) the effect of configuration, velocity ratio, model height, and inlet suction on the flowfield; (ii) the distribution of concentrations at the inlet entry plane and the effect of velocity ratio, model height and jet configuration on that distribution; and (iii) the influence of scaling up velocities of both jet and cross flow. It is noted that in (iii) above, the jet velocities were raised to values at which compressibility became an important factor in the jet flow.

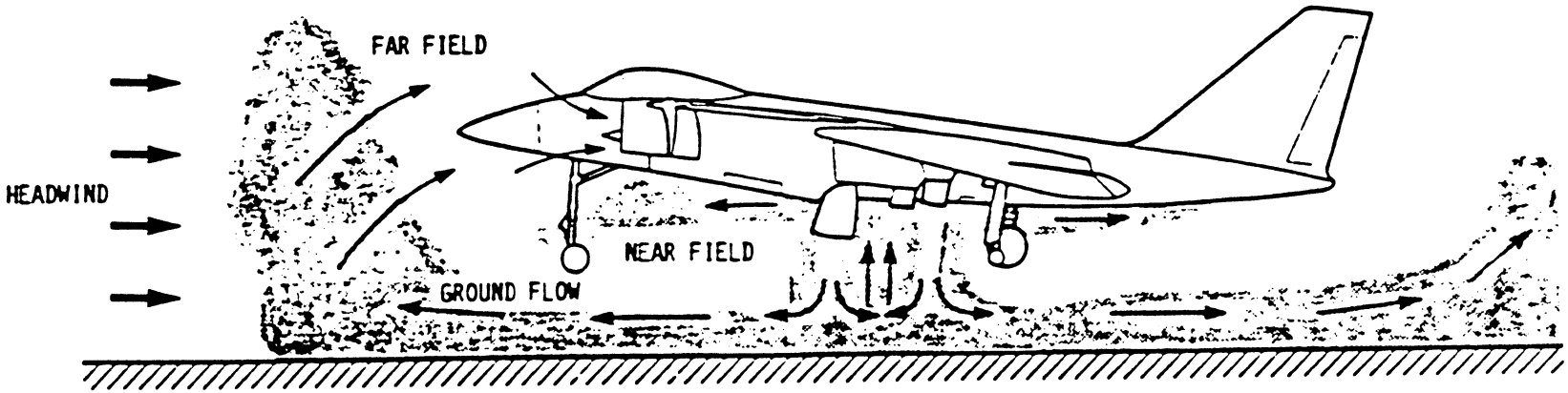

Figure 1.1 Hot Gas Ingestion Mechanisms

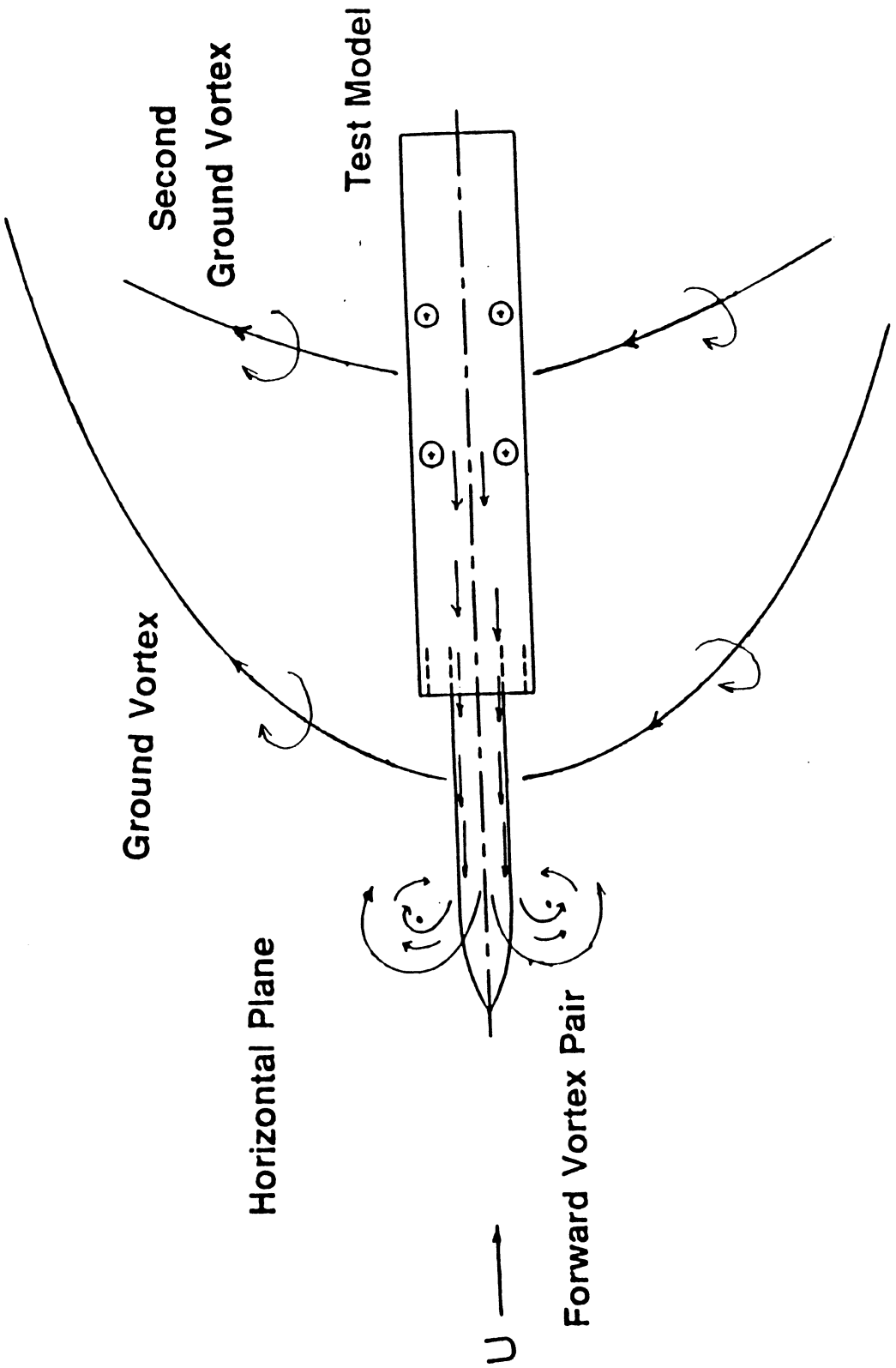

Figure 1.2 Flowfield Features in xz Plane From MacLean [28]

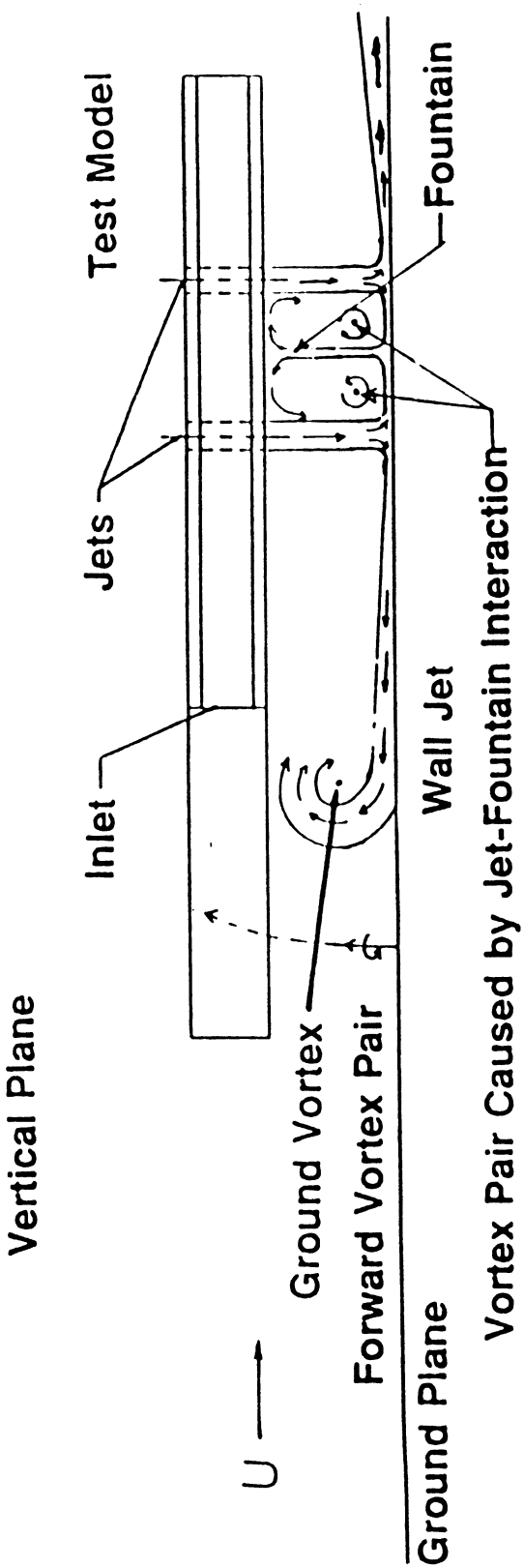

Figure 1.3 Flowfield Features in xy Plane From MacLean [28]

CHAPTER 2

LITERATURE SURVEY

The study of STOVL aircraft configurations has expanded greatly in the last couple of decades. The work for STOVL research was built upon basic studies of single and multiple jets. Free and impinging jets were studied and their basic structures were determined.

Donaldson and Snedeker [11][12] studied the basic structure of a single, free and impinging jet in both the subsonic and underexpanded regimes. The shock structure in the underexpanded cases was clearly described as well as the free jet turbulence structure and impingement heat transfer. Crow and Champagne [10] also examined a single jet. They determined structures within a turbulent jet. Nosseir [33] viewed the turbulent jet as double structured in nature with large scale coherent and small-scale random structures.

Colin and Olivari [9] studied the impingement of a single, circular jet on a flat plate with and without cross flow. Kotansky and Glaze [23] reviewed rectangular jets. Winston [52] compared results from round and square jets and found that square jets reduced lift losses and nose up pitching moments. Shayesteh et. al. [40] measured the turbulence structure of a single three-dimensional impinging jet in a cross stream with

a cross wire and pulsed-wire anemometer. They found that the cross stream kept the turbulent intensities below those found in the jets in still air. They also noted that the effect of compressibility on the turbulence structure of unchoked flows was negligible.

Stewart and Kuhn [44] investigated one-, two- and three-jet STOL configurations and presented a method for evaluating the propulsion induced, aerodynamic effects in ground effect. Kotansky [21] also studied multi-jet impingement flowfields and reviewed a prediction methodology as did Kuhn [24]. They all described the formation of the wall jet, ground vortex, and fountain. When a jet impinges on a ground plane/flat plate, the flow stagnates and turns and radially spreads out forming the wall jet. The ground vortex is created in the presence of cross flow which opposes and rolls back the wall jet. A fountain occurs in configurations with two or more jets. When the aircraft is in ground effect, the wall jets from adjacent jets oppose each other and create an upward directed flow where they meet, known as a fountain. In a two-jet configuration the fountain is a fan shaped sheet of air. With three or more jets, a strong vortical core flow is created where several of these fan shaped fountains meet.

Cimbala et. al. [8] investigated in detail the unsteady ground vortex formed by a single impinging jet in cross flow. They took high speed motion pictures and observed a very low frequency "puffing" action in the ground vortex. The "puffing" could not be correlated with any other oscillations in the flowfield and it was determined to have come from the gross features of the ground vortex itself.

Stewart and Kemmerly [43] examined the ground vortex of a single jet with cross flow in comparison to a moving model without cross flow. The ground boundary

layer was thought to effect the forward extent of the ground vortex in the stationary model case. The moving model case showed a 30% decrease in vortex forward penetration over the stationary jet case and a 50% decrease laterally.

Bray and Knowles [6] studied both single and two-jet configurations. They gave an excellent review of impinging jets in cross flow both experimentally and numerically. They also noted that with a moving model the forward penetration of the ground vortex decreased. The numerical models they evaluated were found to underpredict the jet spreading rate and maximum velocity in fountain upwash region.

Saripalli [35] took laser doppler velocimetry (LDV) measurements of a twin, water jet and found the turbulent intensities in the fountain to be on the order of 50%. Sherrieb [41] performed ground effects tests of two-, three- and four-jet STOL configurations. He determined that the three-jet case had a weaker fountain than the four-jet case and that in the two-jet case, the fountain was even weaker. He also found that the reingestion levels correlated to the strength of fountain flows.

One of the most important parts of studying a STOVL configuration in ground effect is the inlet analysis with respect to the ingestion of hot exhaust gases. Kuhn and Eshleman [25] surveyed the ground effects on V/STOL and STOL aircraft. They identified three basic mechanisms in the ingestion problem: far field ingestion, the fountain flow in the near field, and the ground vortex. Schwantes [37], who also studied the recirculation problem, found that the temperature increase at the intake could take on quite considerable values. The increase in temperature could cause a significant drop in engine power in ground effect and could cause the aircraft to crash. He also found

that wind recirculation (far field) caused only relatively small temperature rises at the intake but this recirculation was much more difficult to combat or eliminate.

Hall and Rogers [17] studied the recirculation effects produced by a pair of heated jets impinging on a ground plane. They noted that maximum levels of inlet temperature rise were seen to occur at low model heights and with close nozzle spacing. Johns [20] performed hot gas ingestion tests on an advanced STOVL configuration in the NASA Lewis 9x15 foot low speed tunnel. He determined that the ground effect range was relatively small. Also, he found that in general, an increase in headwind velocity would result in a higher level of hot gas ingestion, which was caused by the far field separation occurring closer to the inlets. Weber [50] noted that the portion of the inlet with highest temperature reading was the lower sector. Limage's results [26] indicated that near field reingestion would probably not occur without the presence of a fountain. Hammond and McLemore [18] reviewed some design principles to reduce hot gas ingestion.

A non-intrusive, concentration measurement technique known as marker nephelometry has been used to study flowfields. Becker [3], Borleteau [4], and Brandt [5] all provided details on the use of marker nephelometry and the method of quantifying the data. Seal [38] used the method to investigate a single free jet, with and without swirl. Morgan [31] and Dwenger [13] used the technique to study flows in annular combustors. Mueller [32] and Veret [47] applied it to stalled wings and blunt bodies. In terms of studying hot gas ingestion, Johns [20] investigated an advanced STOVL fighter aircraft and MacLean [28][29] studied a general, four-jet STOVL model.

The early work on the establishment of the flowfield for the general STOVL model used in these experiments was described by MacLean [28] and Tafti and Vanka [45]. MacLean conducted an experimental study on a four-jet configuration with cross-flow while Tafti presented an equivalent numerical study. Their models were based on a numerical model used by VanOverbeke and Holdeman [46] who also did numerical studies. The model was a four-jet configuration with two square inlets. Additional studies were presented by Fricker et. al. [14] on the numerical model including the effects of splaying the front jets. The two main geometric parameters in those investigations were D_j, the jet diameter, and H, the model height above the ground. The main velocity parameters were U, the freestream velocity, and V_j, the jet velocity. These were the same parameters that were used in the experiments presented here.

Vukits, Sullivan and Murthy [48] provided the low and high speed results for a multi-jet configuration using the marker nephelometry technique. This thesis provides additional as well as more detailed information of the work presented in that study.

CHAPTER 3

EXPERIMENTAL APPARATUS AND METHOD

In order to study the flowfield around a general Short Take-Off and Vertical Landing (STOVL) aircraft in ground effect, the following experimental apparatus and method were devised. The test model and procedure were based on experimental work done by MacLean [28]. MacLean studied a low speed (75 ft/s), four-jet configuration using a concentration measurement technique known as marker nephelometry. Specific goals in the current work were to determine the effect of configuration and jet velocity on the flowfield with the same technique. In addition, a closer analysis of the inlets was performed in the low speed cases.

3.1 Test Models and Jets

The STOVL model used in the three-jet experiments was based on MacLean's four-jet model [28]. MacLean's model was similar to a numerical model used by VanOverbeke and Holdeman [46], Tafti and Vanka [45], and later by Fricker et. al. [14]. Figures 3.1 and 3.2 show the three- and four-jet models respectively. Each model was constructed with plexiglass with 0.5 inch diameter circular jets and 0.5 x 0.9375 inch rectangular inlets. The short dashed lines in the drawings show the internal channels used for inlet suction. The inlet entrances were 5 inches in front of the front pair of jets

on both models.

Each jet nozzle was made out of aluminum and was 3.625 inches in length, with a 5 to 1 area ratio (1.125 inch to 0.5 inch diameter). The contraction was over the last inch of the nozzle. Straws (2.0 x 0.375 inches), sandwiched between two screens, were inserted into each nozzle just before the contraction in order to reduce unsteady features in the flow. Each jet also had a static pressure port before the contraction. The nozzles were inserted into the plexiglass models.

For the three-jet model, the back two jets on the four-jet model were replaced with one jet at the same x-location on the model centerline (z=0.0). Also, the internal channels for the inlet suction were reconfigured because of the different jet locations. An adaptor, shown in figure 3.3, was designed to simplify the connection of suction hoses by serving as a transition from the two rectangular ports to one circular port.

For all of the two-jet cases presented here, the three-jet model was used with the back jet turned off. The four-jet model could also have been used if the back jet pair was shut off.

3.2 Marker Nephelometry

Marker nephelometry is the method of studying concentration fields by injecting (i.e., marking) the feedstream to a flowfield with particles, and detecting particle concentrations with an optical probe based on light scatter techniques. The optical probe in this experiment involved a laser sheet as the light source and a charged coupled device (ccd) camera as the receiver of the scattered light. The data collected by the

camera was both qualitative (flow visualization) and quantitative (concentrations).

According to Becker [3], the light scattered from the particles is proportional to the number of particles in the region illuminated, if there is independent scattering. The condition for independent scattering is that the center-to-center distance between particles must be greater than 3 radii. This corresponds to a marker volume fraction of about 30%, which was easily met in these experiments. The specific marker particles chosen for the low and high speed experiments are given later.

The concentrations measured with the detector in these experiments were a relative, rather than an absolute, measure. In other words, the exact concentration at a point in the flowfield was not known. It could only be referenced relative to another point in the field. The point of reference used in these experiments was the concentration at the jets, which was the highest concentration in the field.

3.3 Low Speed Experimental Setup

Figure 3.4 shows the experimental setup. The two-, three-, and four-jet models were each mounted upsidedown in front of a small open jet wind tunnel as shown blown up in the lower corner of figure 3.4. The maximum velocity of the tunnel was about 7.5 ft/s. The velocity measurements were made with a Kanomax Anemomaster Model 6611, which was a constant temperature type thermal anemometer. A mean profile of the tunnel, obtained by MacLean [28] is shown in figure 3.5. The mean velocity varied by about ±5% across the test section. The turbulent intensity (u'/U) at the center of the tunnel was measured with a hotwire at a sampling rate of 1000 Hz and with a 500 Hz

low pass filter. The sample size was 4000. The u'/U was found to be 2.0% at a tunnel speed of 6.75 ft/s, which was the corresponding speed for U/V_j=0.09.

The jets of each model were directed upwards toward a 30 inch by 30 inch by 0.25 inch glass plate that served as the ground plane. The arrangement gave the advantage of being able to easily view the planes between the model and the ground. The model could be adjusted to heights between 0 and 14 jet diameters.

A centrifugal blower provided the air supply for the jets by drawing air in through the inlets in order to balance the mass flow rates. The air lines were made from ribbed plastic hosing, plastic tees, and ball valves. The marker particles were injected into a tee in the air line. Then there was about nine feet of hosing where the particles could mix. The ball valves were used to control the air supply for each jet.

In order to calculate the jet velocity, V_j, following equation used was:

$$V_j=\sqrt{2\frac{\Delta p}{1.05\rho}}$$

ΔP was the difference in static pressure between the static pressure port and the jet exit (atmospheric). It was measured with a Validyne pressure transducer. ρ was the air density at the jets. The value 1.05 was the loss coefficient, k. It was calculated as follows:

$$k=\frac{\Delta p}{q}$$

ΔP was again the difference in static pressure between the static pressure port and the jet exit (atmospheric). The dynamic pressure, q, was measured at the jet exit plane with

a pitot-static probe. The loss coefficient was determined to be 1.05. The velocity of each jet (V_j) was 75 ft/s, ±0.3 ft/s. The Reynolds number for the flow was calculated with the following equation:

$$Re = \frac{lV}{\nu}$$

ν is the kinematic viscosity, which is the dynamic viscosity over the density, and for air at room temperature it is $1.5723 \times 10^{-4} ft^2/s$. V and l are the characteristic velocity and length respectively. For these experiments the characteristic length was the jet diameter (D_j=0.5 inch). Therefore, for the low speed experiments the Reynolds number based on jet diameter was about 20,000. A mean velocity profile of one of the jets at exit plane is shown in figure 3.6. The velocity of each jet was adjusted using ball values. The marker particles were generated with a Farval oil mister. Fluid used in the mister was propylene glycol.

In the marker nephelometry technique used, the light source was a five-watt Spectra Physics argon-ion laser. The laser beam was spread into a very wide laser sheet using two convex lens and a cylindrical lens as shown in figure 3.7. In these experiments, the sheet was in the xy plane, parallel to the ground plane.

The detector used in these experiments was a Panasonic Digital 5000, ccd video camera. The camera had a standard RS-170 video output. The camera sent out one field every 1/60th of a second and a full screen image every 1/30 of a second (i.e., one odd field and one even field). Each field represented an average over the 1/60 second period. Consequently, each frame represented an effective average over a 1/30 second

period. A Data Translation DT-2851 frame grabber was used to capture single frame and 127-frame average images for processing. The arrangement of this equipment is shown in the upper portion of figure 3.4.

3.4 High Speed Experimental Setup

The high speed test setup was nearly the same as that used in the low speed cases. In the high speed cases only the two-jet configuration was used. The minimum jet Mach number used was 0.19, which yielded a Reynolds number based on jet diameter of about 5.7×10^4. The maximum jet Mach number used was 0.95, which yielded a Reynolds number of about 2.8×10^5. A new wind tunnel, called the V/STOL tunnel, with an open jet was set up to operate at a maximum speed of about 110 feet/second, which would allow values of tunnel to jet velocities of 0.10 with choked jets at ambient conditions. The tunnel is shown in figure 3.8, but not to scale. Figure 3.9 gives velocity profiles at the tunnel exit plane at a mean velocity of 51.5 ft/s. The data were taken with the test rig in front of the tunnel. A pitot-static probe was used to measure the dynamic pressure of the tunnel and then the Bernoulli equation was used to determine the tunnel velocity. Turbulent intensity (u'/U) measurements of the tunnel were done by Scheuring [36] at the center of the tunnel at a sampling frequency of 600Hz with a low pass filter at 300Hz. The sample set consisted of about 131,000 data points. The average of nine sets showed a u'/U of 0.69%.

In order to obtain the needed high speeds, a Pac-Air compressor was used as an air supply. The air line from the compressor went into a 200 gallon pressure vessel.

Then, after about 25 feet of 1-1/4 inch diameter steel pipe, the air passed through a compressed air regulator. Then air passed through a straight 4 foot section which included a 6 inch section that had straws with two sets of screens on either side. The section was included to help reduce the unsteady features of the flow. Next the line was split with a tee to two shut off valves with rubber hoses leading to each of the jets.

The jet nozzles were the same as those used in the low speed cases. The isentropic gas relation relating the jet pressure ratio to Mach number was used to determine the desired pressures. It is as follows:

$$\frac{P_o}{p} = \left(1 + \left(\frac{\gamma - 1}{2}\right) M_j^2\right)^{\frac{\gamma}{\gamma - 1}}$$

M_j was the desired Mach number. The static pressure at the jet exit, p, was atmospheric since the maximum Mach number was 0.95. The total or reservoir pressure, P_o, was measured from the static port on the jets. When compared to the total pressure measured at the jet exit plane, the error in the port measurement was found to be about 0.6% at 3psi and about 1.7% at 10psi. The total pressure was measured with a Seegers pressure gage. It measured gage pressure down to divisions of 0.05 psi. The ambient pressure was determined from a Wallace and Tiernan absolute pressure gage.

For comparison with the low speed cases, the same velocity ratios (U/V_j) were used. V_j was calculated as follows:

$$V_j = M_j \sqrt{\gamma R T}$$

R is the gas constant for air (1716.47 ft^2/s^2R) and T, is the local static temperature of the jet in Rankine. The jet temperature for a particular M_j was determined with a

Sargent thermometer. The tunnel speed, U, and dynamic pressure were then calculated based on the desired ratio of U/V_j.

The smoke/marker particles were supplied with a smoke wand. The smoke wand heated Fog Juice, Type 1964, traveling through an electrically heated, 4 foot, 1/16 inch diameter stainless steel tube until it was vaporized. The juice was driven through the tube from a reservoir with compressed air. The flow rate was adjusted with a pressure regulator. A variable transformer provided the current to heat the tube. The smoke was injected into the high pressure air line through a 1/8 inch hole that was drilled just downstream of the pressure regulator. The smoke had about four feet of mixing distance before the tee, which included the straw-and-screen section. Then there was a seven foot hose going from the tee to each jet.

A Nd:YAG pulse laser at the 532nm harmonic was used as a light source. It was pulsed at 30 hertz and the duration of each pulse was 10ns. A combination of high energy mirrors and the low energy optics used in the low speed cases was used to produce a laser sheet. The Nd:YAG beam had a flat top, rather than a gaussian, distribution. However, the beam was observed to fluctuate from pulse to pulse at the outer edges of the beam. The beam was centered in the test section and the laser sheet was spread out to about five times the test section width to minimize fluctuations in test section.

In the high speed cases, a Sony XC-77RR full frame camera was used. The camera sent out two fields per frame that were captured at the same time. In a normal (interlaced frame) camera the even field is taken a 1/60 second after the odd field.

Because of the nature of the full frame camera, an Epix Silicon Video Mux frame grabber was used to capture consecutive frames. Wernet [51] gives further details on a full frame camera and its output.

3.5 Test Conditions

The test parameters for the experiments performed are summarized in table 3.1. The conditions chosen for the low speed two- and three-jet experiments were as follows: the velocity of each jet (V_j) was set at 75ft/s (±0.3ft/s); the tests were run at three different model heights: H/D_j=2, 4, and 6; finally, U/V_j was incremented in steps of 0.01 from 0.02 to 0.10. U/V_j was set to a minimum value of 0.02 due to the high degree of uncertainty of vortical structure location at lower values.

In the high speed cases, only a two-jet configuration was used. The main Mach numbers chosen were: 0.19, 0.50, and 0.95. The tests were done at velocity ratios from U/V_j=0.02 to 0.09. Due to the extreme difficulty of obtaining mass balance between the jets and the inlets, there was no inlet suction for these cases.

3.6 Data Processing

Once the low and high speed jet images were digitized from video tape and stored, BASIC programs were used to extract pixel lines from the images. Each point on the pixel lines contained a value between 0-255 indicating the intensity of light, which was proportional to the concentration of marker particles at that point. These values were then normalized with the concentration value at the jets, which was the

maximum for the image. Once normalized, the line cuts from different images were plotted for comparison.

The pixel lines that were chosen for comparison were the ones that best showed the features of the flowfield for all the configurations. Two of the line cuts were parallel to the x-axis. The first one was along the centerline of the model. The second cut was through the centerline of the first jet, (x,z)=(0.0,1.625). The third cut was parallel to the z-axis at the line x=0. Individual frames of data as well as averages over a set of 127 frames were examined. The following equations were used to calculate the mean and rms concentrations respectively:

$$\overline{C}=\frac{\sum_{i=1}^{N} C_i}{N}$$

$$c'=\left[\frac{\sum_{i=1}^{N} C_i^2-\frac{1}{N}\left[\sum_{i=1}^{N} C_i\right]^2}{N-1}\right]^{1/2}$$

where:

$\overline{C}$ = mean concentration

c' = rms concentration

N = number of frames

C_i = i^{th} instantaneous concentration

For the inlet entry plane analysis, seven inlet planes were viewed and background images (i.e., images with no flow) were subtracted at each level to remove background

reflections. Then, one pixel line was cut from each plane at the inlet entrance. Using Tecplot, these seven lines from the xz planes were used to construct a contour plot of concentration in the yz plane at the inlet entry plane.

JET VELOCITY	75-1000 ft/s
VELOCITY RATIO (U/V_J)	0.02-0.10 (selected ratios for different V_J)
JET EXIT LOCATION (H/D_J)	2.0, 4.0, 6.0
NUMBER OF JETS	2, 3, 4
TOTAL NUMBER OF PARAMETER COMBINATIONS	30

Table 3.1 Test Parameters

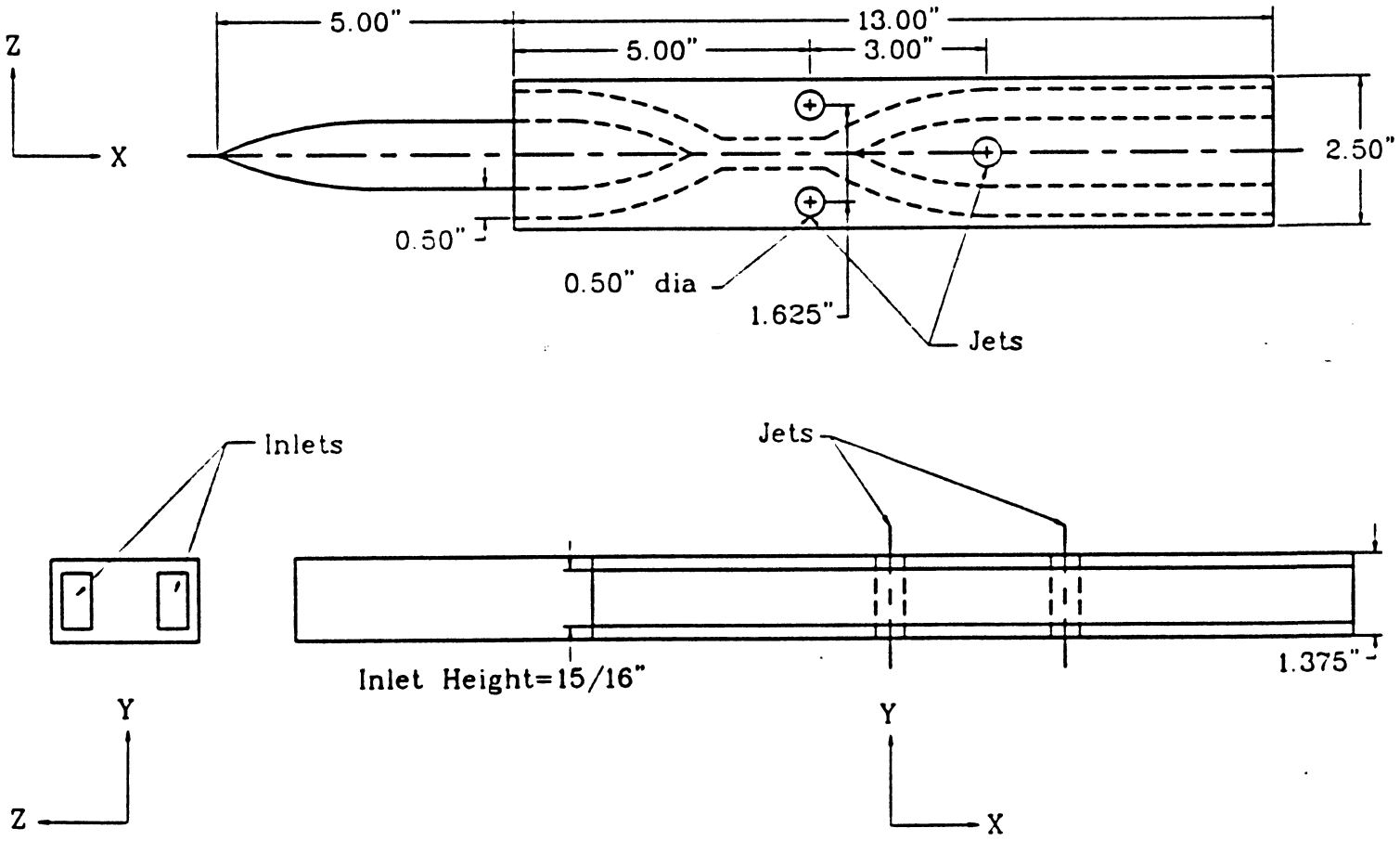

Figure 3.1 Three-Jet Test Model

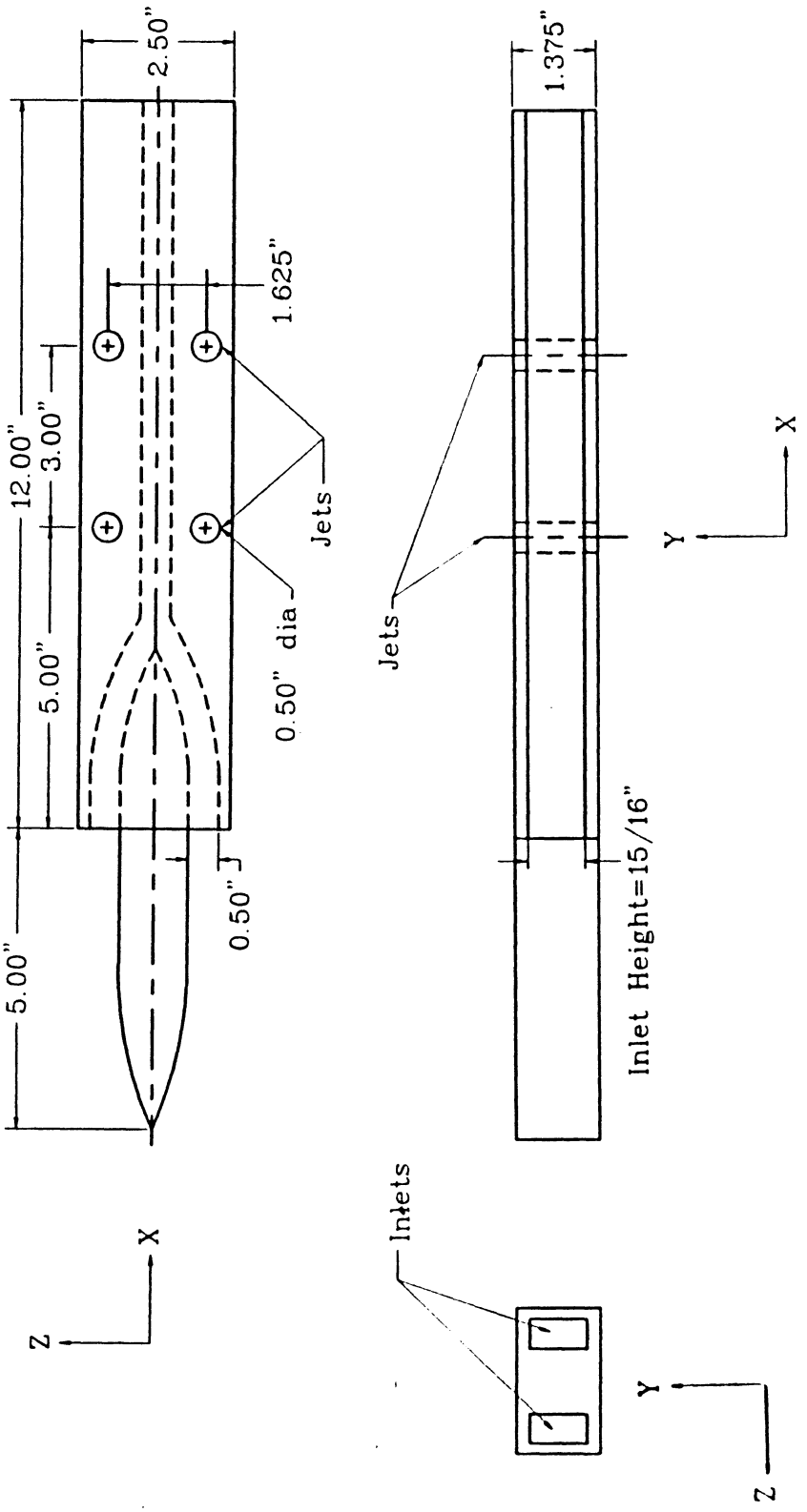

Figure 3.2 Four-Jet Test Model

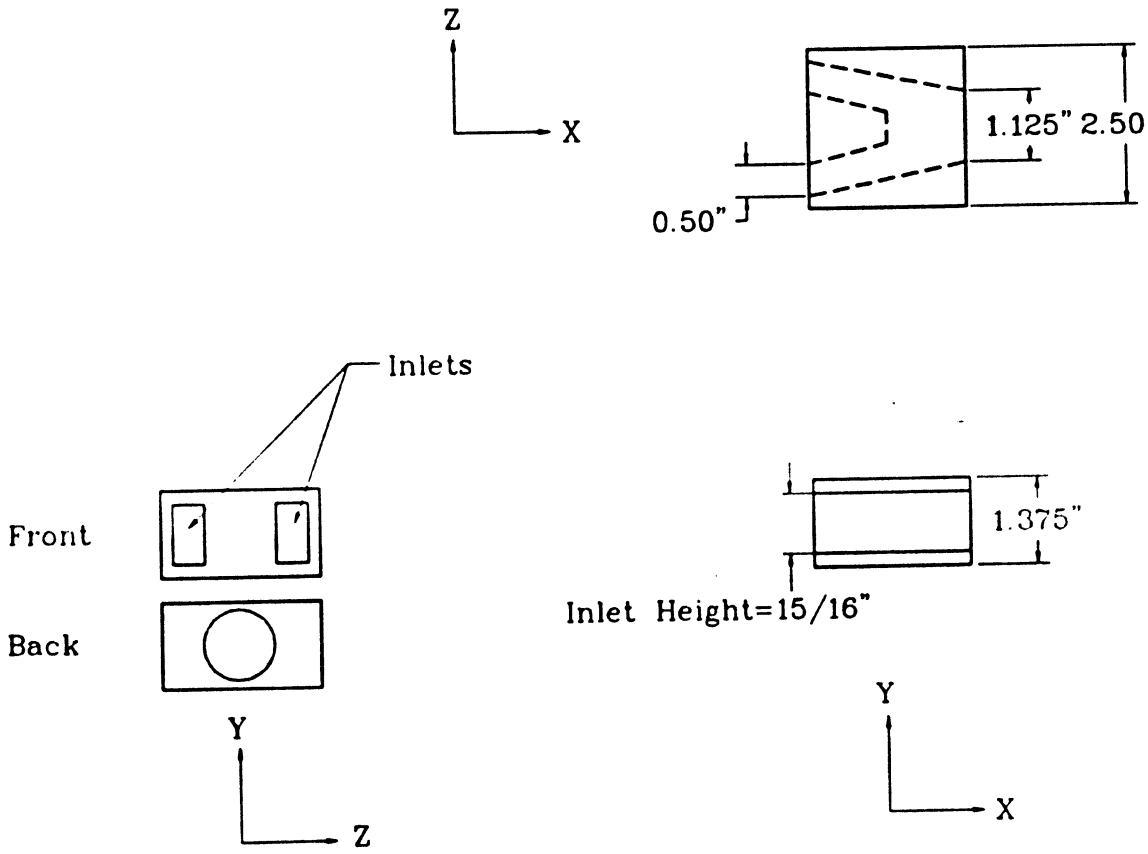

Figure 3.3 Adaptor for Three-Jet Test Model

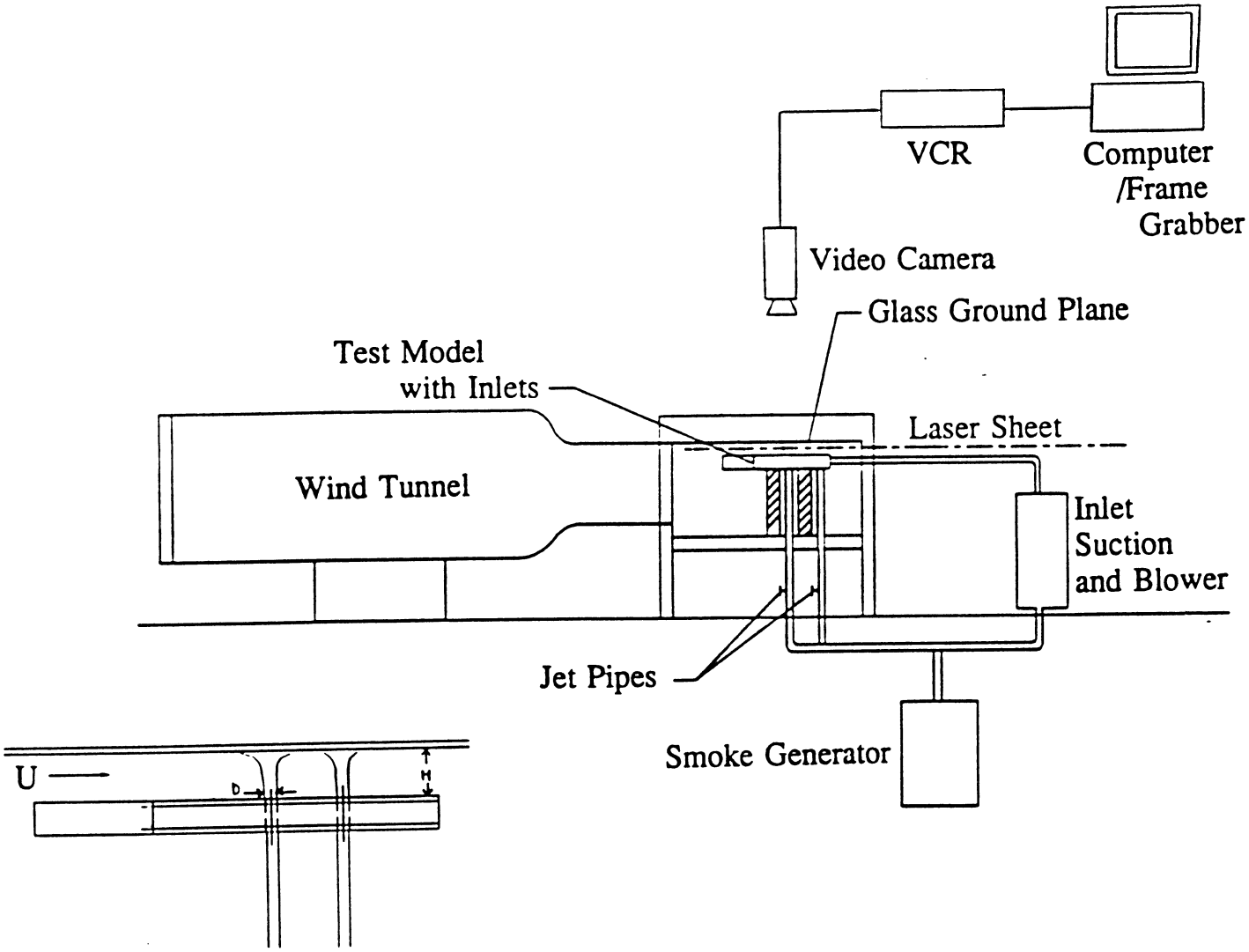

Figure 3.4 Experimental Setup

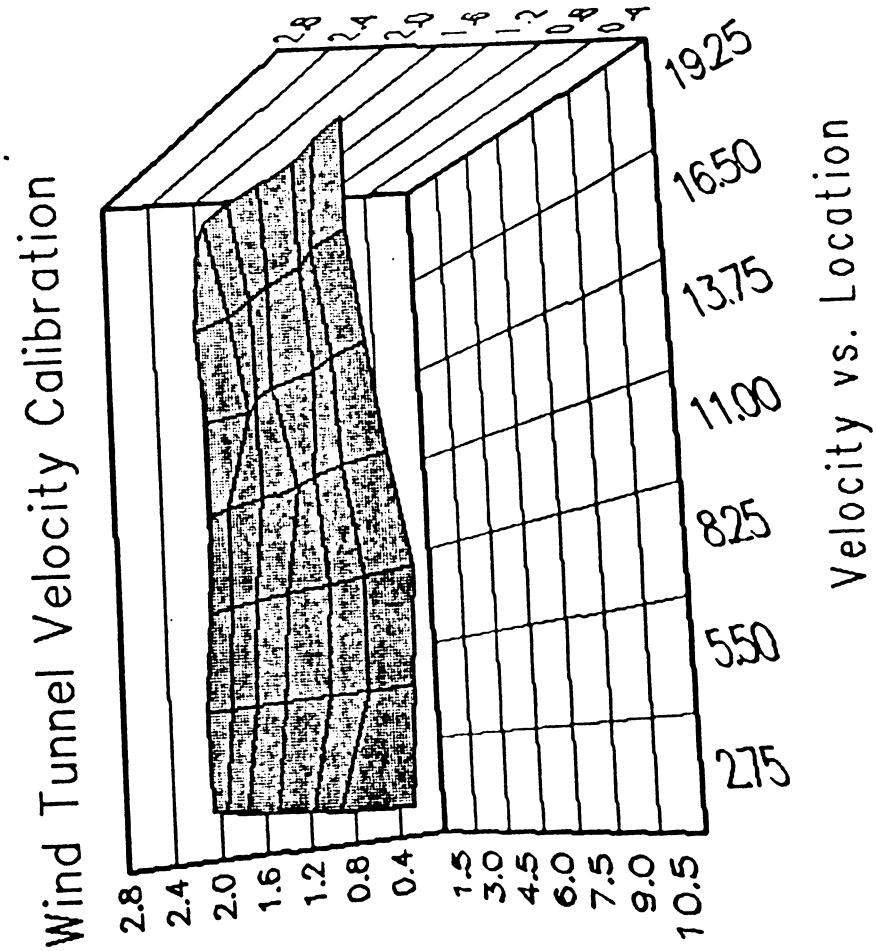

Figure 3.5 Wind Tunnel Velocity Distribution From MacLean [28]

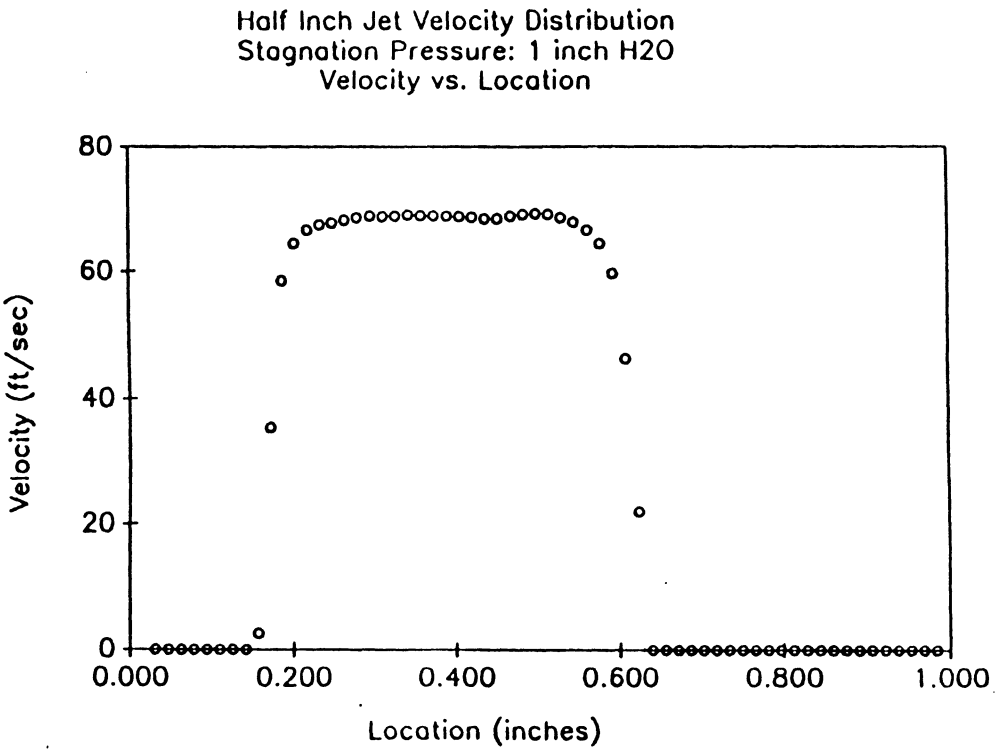

Figure 3.6 Jet Velocity Profile From MacLean [28]

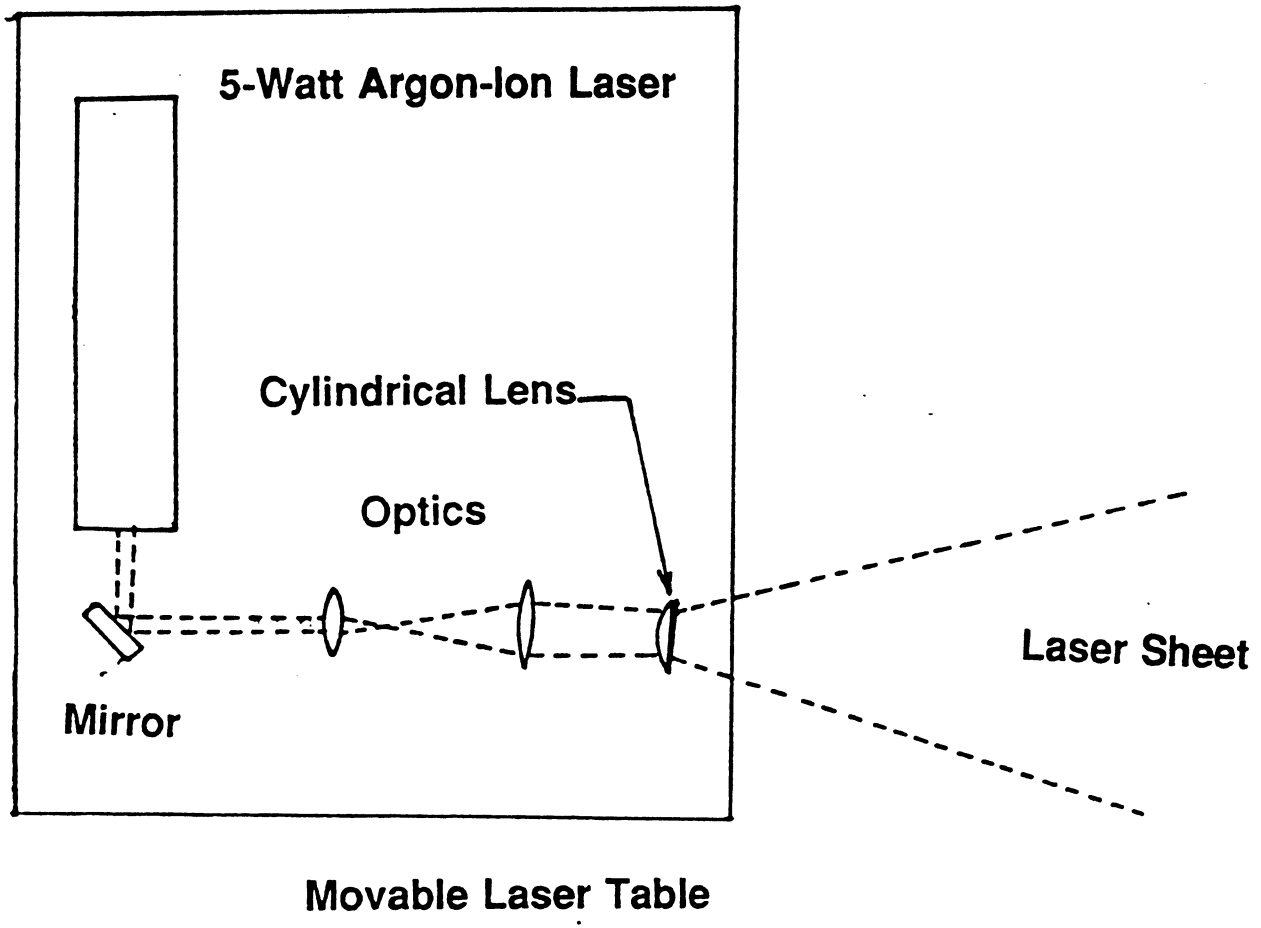

Figure 3.7 Laser and Laser Sheet Optics From MacLean [28]

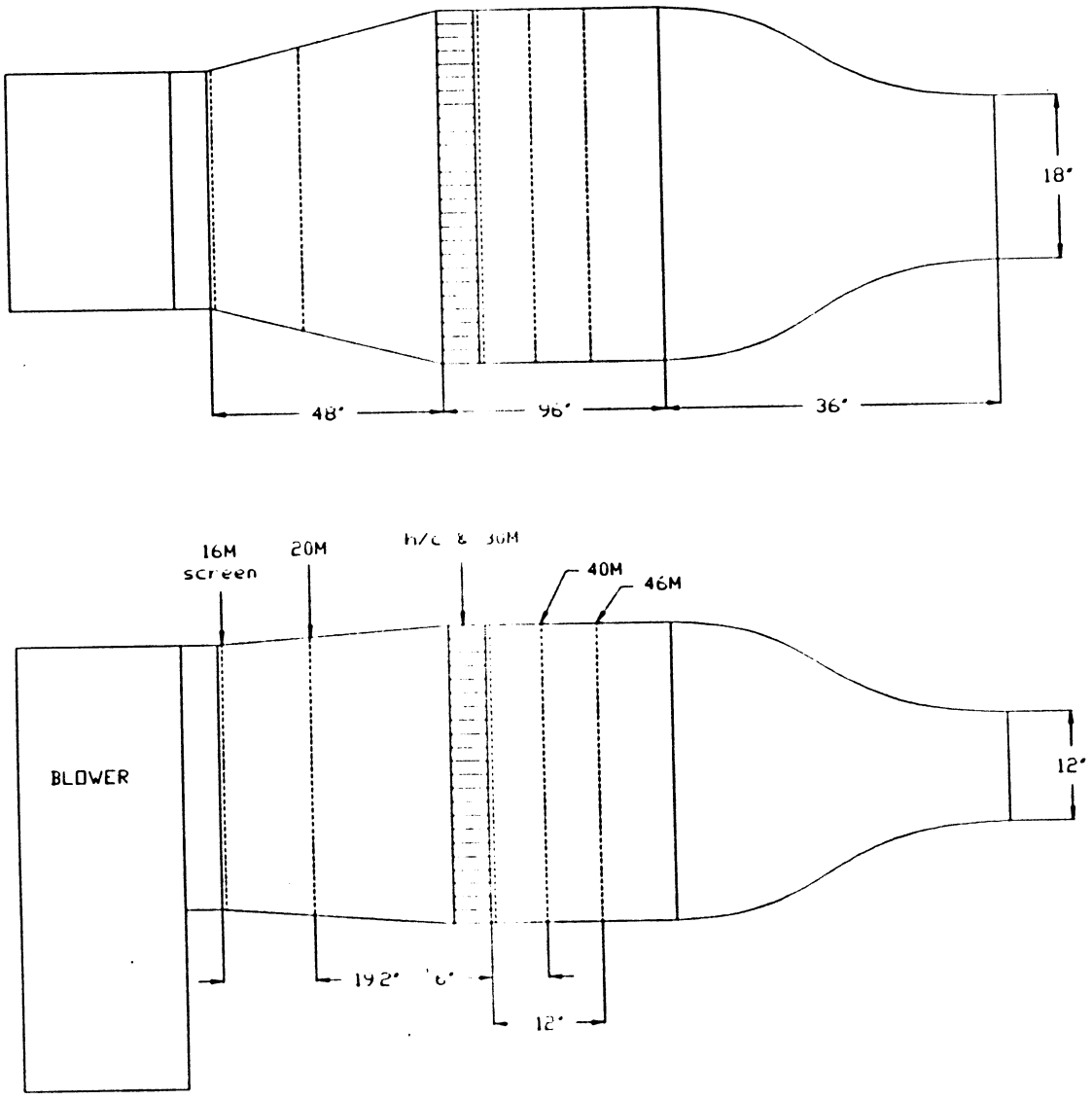

Figure 3.8 V/STOL Wind Tunnel
(Note: Not to Scale)

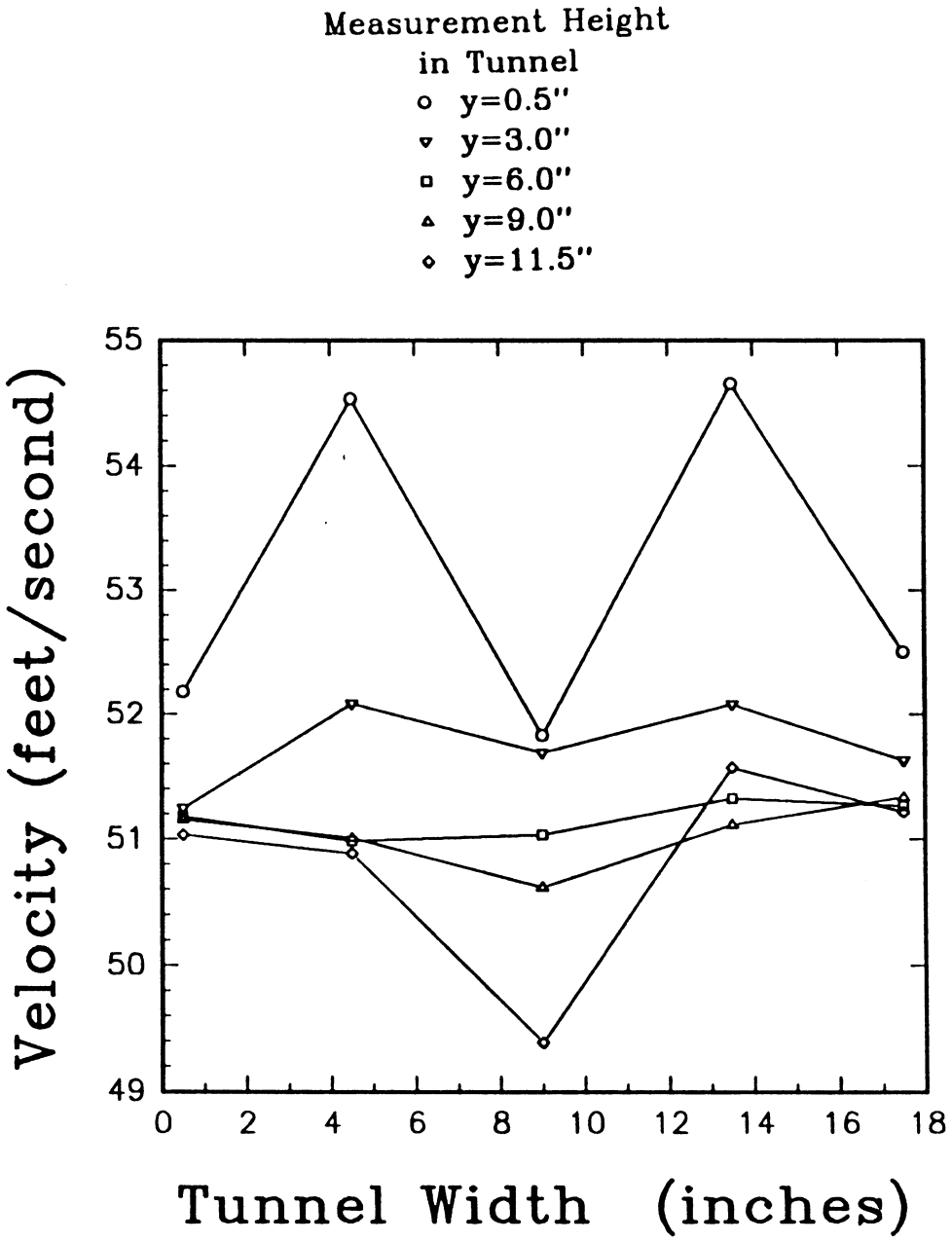

Figure 3.9 V/STOL Wind Tunnel Velocity Profiles

CHAPTER 4

LOW SPEED - TWO-, THREE-, FOUR-JET STUDY

The following is a discussion of the results from the two-, three- and four-jet low speed experiments. The flowfield around each jet configuration had a number of interesting features. These are shown in a series of cases with relevant images of the flowfield extracted from video tape. Single frame, 127-frame average, and root mean square (rms) concentrations are reviewed.

The structures in the flowfield in the ground plane, and then, the mid-plane of each configuration are discussed. Next, the concentrations of the configurations are compared at a decreased forward speed as well as at different model heights. Lastly, the vortex positions for each configuration are reviewed from a parametric variation study.

It should be noted that the videos for each case illustrated clearly both the unsteadiness of the flowfield as well as the shifting asymmetries in the formation and location of vortical structures. In the following, various illustrative cases are referred to by case numbers given in Table 4.1. The four-jet data discussed below was taken from MacLean [28]. A four-jet case was completed to verify the test setup and a comparison with Maclean's data is presented in appendix A. Also, in order to determine the reproducibility of the data, a multiple three-jet comparison was done and is

presented in appendix B.

4.1 Ground Plane Measurements: $H/D_j=4$, $U/V_j=0.09$, $y/D_j=0.0$

Figure 4.1 shows a single frame image of smoke concentration for the two-jet configuration, case 4.1. Figure 4.2 shows a 127-frame average image of the same case. The forward vortex pair is clearly seen in the single frame image but, in the average image, its features are not as discernable. The ground vortex is also seen in each image, especially in the averaged image where a distinct horseshoe shape can be seen. Additionally, the wall jet and the stagnation region between the jets can be seen.

Figure 4.3 and 4.4 show the single and 127-frame average images of the three-jet configuration, case 4.2. The forward vortex pair, ground vortex, and wall jet are seen in these images as in the two-jet case, as well as the stagnation region between the front jet pair. There is also a stagnation region seen between the forward jets and the rear jet. From this region, a secondary ground vortex can be seen.

The single and 127-frame average images for the four-jet case, case 4.3, are shown in figures 4.5 and 4.6. Again the same structures are seen. However, the secondary ground vortex in this case was not as swept downstream as in the three-jet case due to the additional jet at the rear.

The normalized concentrations, at a the ground plane, along the projected model centerline for the three configurations are shown for each comparison given below. Also, the normalized concentrations distributions along the projected horizontal and vertical jet centerlines are given.

4.1.1 Mean Concentration Measurements

In the centerline plot, figure 4.7, there is a peak in concentration, C/Cj, just past x/D_j=0.0 for the two-jet case. It corresponds to the stagnation region between the two-jets. After this peak, the concentrations drop off to zero. For the three-jet centerline profile, the highest peak is at x/D_j=6.0, which is the location of its single back jet. The highest peak for the four-jet centerline plot is at about x/D_j=3.0, which corresponds to the area where the flow from the forward and rear jet pair stagnate.

In the jet centerline concentration plot, figure 4.8, the regions forward of the front jet pair have small differences in normalized concentration levels. Downstream of the front jet pair, the two-jet case again drops to zero. The three-jet case has a peak at about x/D_j=4.0. The concentration peak corresponds to the secondary ground vortex. The four-jet case has a similar peak from its secondary ground vortex but it is further upstream because the additional jet at the rear in this configuration. The three-jet case has one further rise in concentration downstream of the stagnation point which was due to the spread of the back jet. The four-jet case has one last peak at its back jet center.

There are some additional features to note from the jet centerline profiles, figure 4.8, as well as from the centerline profiles, figure 4.7. The first of these is that the two-jet model has lower levels of concentration forward of the inlets (x/D_j<-10). This may be accounted for by the fact that the three- and four-jet models had back jet(s). The back jet(s) gave additional momentum to the flow in the upstream direction. The additional momentum caused the upstream structures to be pushed upstream more than when there were no back jets.

Another interesting feature in the centerline and the jet centerline profiles is that the concentrations for the two-jet configuration increase over the other cases downstream of the inlets up to the jets. The reason may again be attributed to the lesser momentum in the two-jet case. The flow from the jets will tend to be pushed back closer to the jets and thus yield higher concentrations in that region.

For the vertical jet concentration plot, figure 4.9, there is again a close matching of the two-, three-, and four-jet cases. However, the profiles indicate that the lateral spreading of the two-jet case was less than in the three- and four-jet cases.

4.1.2 Single Frame Concentration Measurements

Figures 4.10-4.12 have the three normalized concentration plots from single frame images taken from cases 4.1-4.3. Figure 4.11, the jet centerline case, shows a sharp jump in concentration in all three cases just forward of the inlets. The jump directly corresponds to the location of the forward vortex pair and ground vortex. Since the two vortex structures were so close to each other at the velocity ratio of U/V_j=0.09, they appear as one merged concentration peak. The other structures are the same as those discussed for the 127-frame average cases above. However, there are greater point to point variations in concentrations as compared to the 127-frame case, where the variations were averaged out. These variations give an indication of the degree of unsteadiness of the flowfield. The differences between the two-, three-, and four-jet cases are difficult to compare here due to the unsteady nature of the structures that shows up as variations in positions from frame to frame, especially for the forward

vortex pair.

4.1.3 RMS Concentration Measurements

Figures 4.13-4.15 show the distribution of normalized rms concentration (c'/Cj) along the pixel line cuts taken over 127 frames. The rms value is an indication of the fluctuation of the flow structure positions. It is noted that in the centerline and jet centerline cuts, all of the jet models have the highest level of concentration near the inlets. The location of the concentration peak corresponds to the forward vortex pair location and it indicates that it fluctuated the most for each configuration.

Additionally, the three-jet case shows smaller peaks just forward of the front jet pair and between the front and rear jet(s), as seen in figures 4.13 and 4.14. These indicate that the stagnation regions in front of and between the jets were also unsteady. The four-jet case shows similar, but smaller peaks, indicating that the four-jet case was steadier in these regions. For the vertical jet profile, figure 4.15, there is no definite pattern to indicate the effect of configuration on rms concentration.

4.2 Mid-Plane Measurements: $H/D_j=4$, $U/V_j=0.09$, $y/D_j=2.0$

Figures 4.16-4.18 show 127-frame average images of the two-, three-, and four-jet models for cases 4.4-4.6. At this measurement plane, only a portion of the ground vortex can be seen. For the three- and four-jet cases, the secondary ground vortex is not very discernable. The fluid emanating from between the front jet pair that forms the forward vortex pair can be seen more clearly than in the ground plane. The

concentrations seen between the jets are cross sections of the fountains.

The mean concentration line plots are shown in figures 4.19-4.21. The two-jet case does not match the other cases as well as it did previously. Looking at the centerline and jet centerline profiles, the concentrations for the two-jet configuration are lower upstream of the inlets and higher downstream up to the jets than the other configurations. The same effect was observed in the ground plane case but in the current case, it is more pronounced. As stated above, the higher concentrations of the two-jet case are due to the lower mass flow rate in its forward region. The flow from the jets was pushed closer to the jets and yields higher intensities than found in the other two cases. The effect became more pronounced at the mid-plane. The other flow structures are the same as those discussed above in the ground plane case as indicated by similar concentration distributions in the plots.

4.3 Decreased Forward Speed Measurements: $H/D_j=4$, $U/V_j=0.03$, $y/D_j=0.0$

In cases 4.7-4.9, the forward speed was reduced to 3% of the jet speed. The 127-frame average images are shown in figures 4.22-4.24 for the two-, three-, and four-jet cases respectively. In figure 4.23, there is a line in front of the forward jet pair. The line was caused by excessive reflection from the mounting rig. Overall the structures in each case are not as swept downstream as in cases 4.1-4.3. The ground vortex, stagnation regions, and wall jet are clearly seen in the images. The forward vortex pair is more upstream and its forward edge is much more difficult to determine than in the higher forward speed cases, 4.1-4.3.

In viewing the concentration profiles in figures 4.25-4.27, there are greater differences between the different configurations than at the higher velocity ratio. Since the freestream velocity was decreased, differences in the wall jet velocity (i.e. differences in upstream momentum from the jets) from the different configurations has become more evident. The ground vortex and forward vortex pair are difficult to discern from the plots. However the concentration peaks at the jets and stagnation regions are still evident. The two-jet case still has the lowest overall concentration distribution in the flowfield.

4.4 Measurements at Increased Model Height: H/D_j=6, U/V_j=0.09, y/D_j=0.6

Figures 4.28-4.30 show the smoke concentration distribution for cases 4.10-4.12 respectively. The particular structures, except the wall jet, are the same as in cases 4.1-4.3. The wall jet is only partially seen since the measurements are made slightly out of the ground plane. The other structures appear, however, to be more downstream than in cases 4.1-4.3. The forward vortex pair appears to be closer to the edge of the ground vortex. Overall, the concentration of marker/smoke particles in the flowfield appears to be less than at the lower model height.

Figures 4.31-4.33 give the concentration profiles for these higher model height cases. The normalized concentrations are seen overall to be lower than at the previous lower model height, H/D_j=4.0. The peaks are however more distinct, especially in figure 4.32 where the ground vortex/forward vortex pair concentration peak is almost centered at the inlet location at this measurement plane. The question of whether the

vortices would be downstream of the inlets at the level of the inlet entry plane will be addressed in Chapter 5. Finally, the trends seen in the concentration distributions for the different configurations are the same as those seen in the H/D_j=4 cases.

4.5 Measurements at Decreased Model Height: H/D_j=2, U/V_j=0.09, y/D_j=0.6

The concentration fields for the two-, three-, and four-jet cases at H/D_j=2.0, cases 4.13-4.15, are given in figures 4.34-4.36. Here the concentrations have increased to the point where the wall jet is still clearly seen even though the image plane, y/D_j=0.6, was over a quarter of the way from the ground to the model. Thus, the wall jet was thicker in these cases. The forward vortex pair in each case appears to be directly below the inlets. As stated for the H/D_j=6.0 cases, the question of the concentration at the inlet entry planes will be addressed in the next chapter.

The normalized concentration profiles, figures 4.37-4.39, show an upstream shift in position as compared to cases 4.1-4.3, figures 4.7 and 4.8. The shift was probably due to the jets blocking more of the flow at this height and forcing it upstream. The differences between the different configurations may again be attributed to differences in total momentum.

4.6 Vortex Positions Under Parametric Variation

The position of the forward vortex pair and the ground vortex were studied under various conditions. Each model was placed at three different heights. At each height, the forward speed was varied from 3% to 10% of the jet velocity. These factors were

all varied with and without inlet suction. The uncertainty in position increased from about ± one jet diameter at U/V_j=0.10 to about ± four jet diameters at U/V_j=0.03 for all of the configurations.

Figures 4.40-4.45 show images of the two-, three-, and four-jet configurations with and without inlet suction for case 4.16. The specific velocity ratio for the images was U/V_j=0.03. The effect of inlet suction is difficult to see in the two- and three-jet images. The effect is more clearly seen in the four-jet images, figures 4.44 and 4.45. Without inlet suction, for all the configurations, the structures are further upstream and their boundaries are less distinct, especially for the forward vortex pair.

4.6.1 H/D_j=2.0 Case

The location of the forward vortex pair and ground vortex for case 4.17, the H/D_j=2.0 case, are shown verses velocity ratio in figures 4.46 and 4.47.

The vortex position in the cases without inlet suction were consistently further upstream than in the cases with suction. Increasing the forward speed caused the forward vortex pair and the ground vortex to move downstream toward the inlets. The forward vortex pair moved much more with an increase in forward velocity than did the ground vortex.

The ground vortex eventually moved downstream of the inlet locations toward the jets at higher velocity ratios. At about U/V_j=0.06, the ground vortex in the inlet suction case was downstream of the inlet location. Without inlet suction, the vortex did not move downstream of the inlets until about U/V_j=0.08, and the two-jet case's vortex

was further down stream than the other cases.

The effect of configuration is also evident in the figures. The forward vortex pair for the four-jet configuration was almost always further upstream than for the two-jet configuration. The three-jet case was generally between the other two cases. The distinction between the different configurations was clearer in the cases without inlet suction than cases with suction.

4.6.2 H/D_j=4.0 Case

Figures 4.48 and 4.49 give the forward vortex pair and ground vortex positions at a height of H/D_j=4.0 for case 4.16. It is again clear from these figures that increased cross flow speed caused the vortical structures to move downstream.

For the two-jet configuration, inlet suction did not as appreciably effect the location of the forward vortex pair, figure 4.48, as in case 4.17. The ground vortex, figure 4.49, was only about one jet diameter further upstream without inlet suction for velocity ratios less than 0.07. At this ratio, the structures in both cases were clearly downstream of the inlets. At higher ratios, the ground vortex was about a half jet diameter upstream in the suction case. Thus inlet suction did tend to keep the two-jet ground vortex closer to inlet entry plane.

Referring again to figures 4.48 and 4.49, case 4.16, the effect of velocity ratio and inlet suction for the three-jet configuration can be seen. Until about U/V_j=0.06, there was no appreciable effect of inlet suction on the forward vortex pair. At higher ratios, the vortex pair was consistently about two jet diameters further downstream in

the suction case. The ground vortex for this configuration was about one to two jet diameters further downstream with inlet suction.

Comparing the different concentration profile plots given above along with figures 4.48 and 4.49, case 4.16, it is evident that the four-jet configuration had the highest overall normalized concentration distributions and its structures were further upstream than for the other configurations. The two-jet configurations had the most swept back features expect when blocking effects occurred near the jets.

Overall, the differences between the configurations were greater at lower velocity ratios where the differences in total momentum became more apparent. At higher velocity ratios, the structures began to experience the blocking effect of the jets. Thus the differences in momentum were less apparent as the structures were pushed back toward the jets. Also, at this model height, inlet suction did not have as great of an effect as at the H/D_j=2.0 case.

4.6.3 H/D_j=6.0 Case

At the increased model height of H/D_j=6.0, case 18, the effects of configuration and inlet suction were small. Figures 4.50 and 4.51 give the forward vortex pair and ground vortex positions for this case respectively. It is only at lower velocity ratios (U/V_j<0.06) that the effect of configuration and suction is seen in the figures. The effect was the same as that at the lower model heights, but not as appreciable. The same was also true of the ground vortex where its locations were almost the same for all of the configurations, with and without inlet suction. The effects of velocity ratio,

however, remained the same for both vortex structures.

Overall, case 17, at H/D_j=2.0, was clearly in ground effect and the effects of inlet suction and configuration were apparent on the vortical structures. Case 16, H/D_j=4.0, was further out of ground effect and the parametric variations did not have as much of an effect. At H/D_j=6.0, the model appeared to be almost out of ground effect and the parametric variations had a minimal effect on the vortical structures.

Case Number	Jet Velocity (ft/s)	Velocity Ratio U/V_j	Model Height H/D_j	Laser Sheet Height y/D_j	Number of Jets	Inlet Suction
4.1	75.0	0.09	4.0	0.0	2	Yes
4.2	75.0	0.09	4.0	0.0	3	Yes
4.3	75.0	0.09	4.0	0.0	4	Yes
4.4	75.0	0.09	4.0	2.0	2	Yes
4.5	75.0	0.09	4.0	2.0	3	Yes
4.6	75.0	0.09	4.0	2.0	4	Yes
4.7	75.0	0.03	4.0	0.0	2	Yes
4.8	75.0	0.03	4.0	0.0	3	Yes
4.9	75.0	0.03	4.0	0.0	4	Yes
4.10	75.0	0.09	6.0	0.6	2	Yes
4.11	75.0	0.09	6.0	0.6	3	Yes
4.12	75.0	0.09	6.0	0.6	4	Yes
4.13	75.0	0.09	2.0	0.6	2	Yes
4.14	75.0	0.09	2.0	0.6	3	Yes
4.15	75.0	0.09	2.0	0.6	4	Yes
4.16	75.0	0.03-0.10	4.0	0.6	2, 3, 4	Yes/No
4.17	75.0	0.03-0.10	2.0	0.6	2, 3, 4	Yes/No
4.18	75.0	0.03-0.10	6.0	0.6	2, 3, 4	Yes/No

Table 4.1 Test Cases for Low Speed - Two-, Three-, and Four-Jet Study

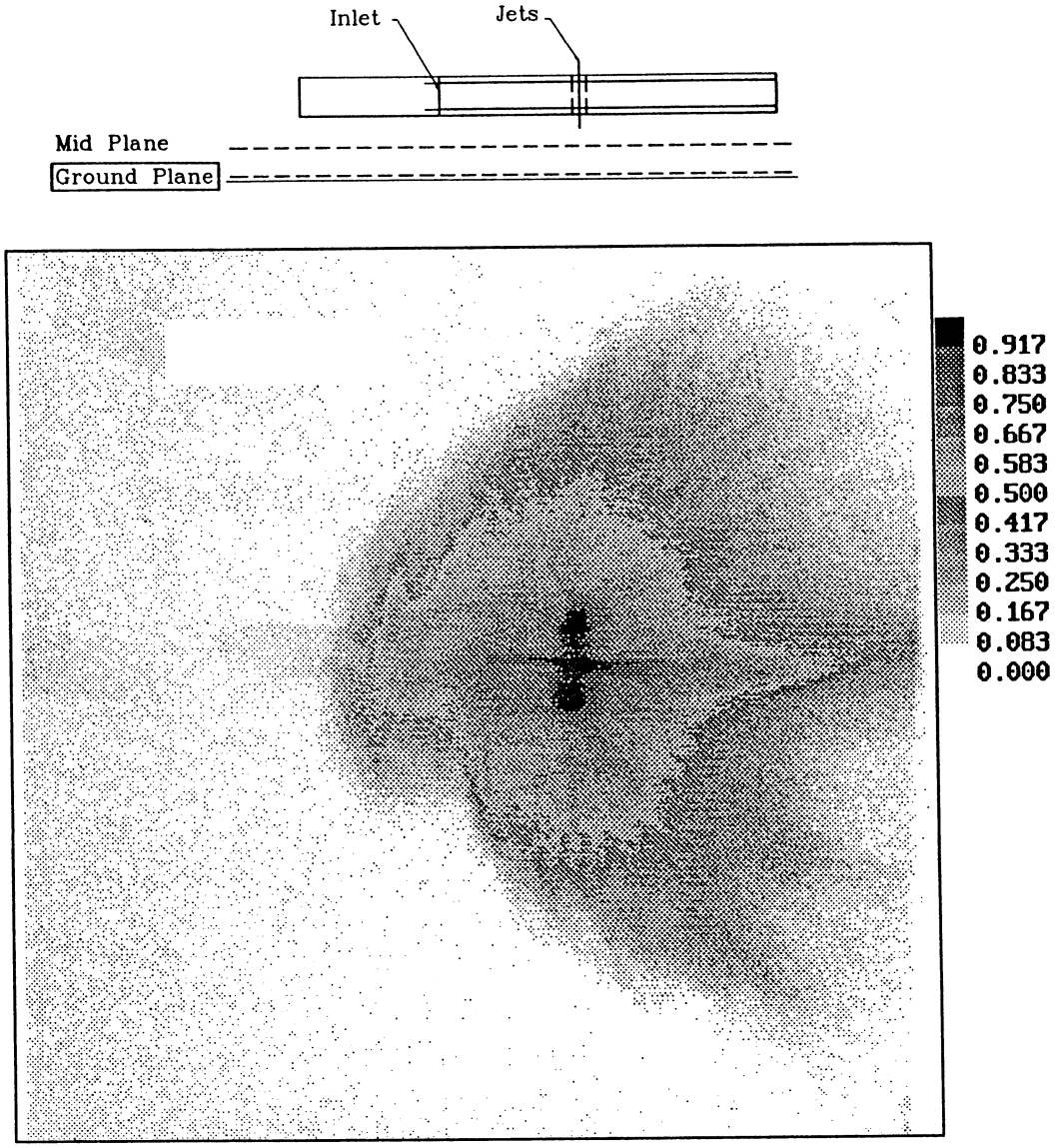

Figure 4.1 Two-Jet Single Frame Image of Smoke Concentration at Ground Plane
$y/D_j=0$, $H/D_j=4$, $U/V_j=0.09$

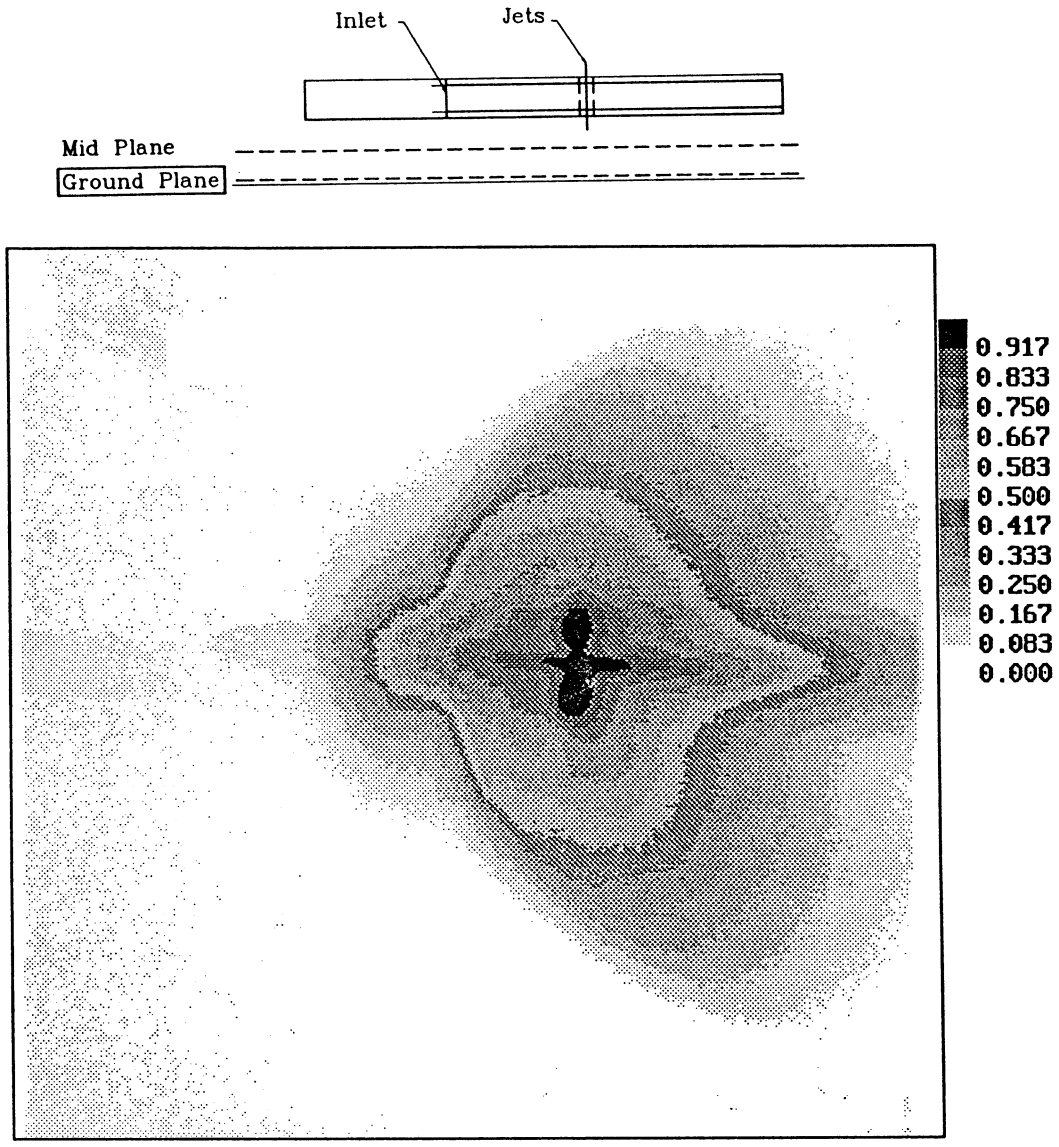

Figure 4.2 Two-Jet 127-Frame Average Image of Smoke Concentration at Ground Plane
$y/D_j=0$, $H/D_j=4$, $U/V_j=0.09$

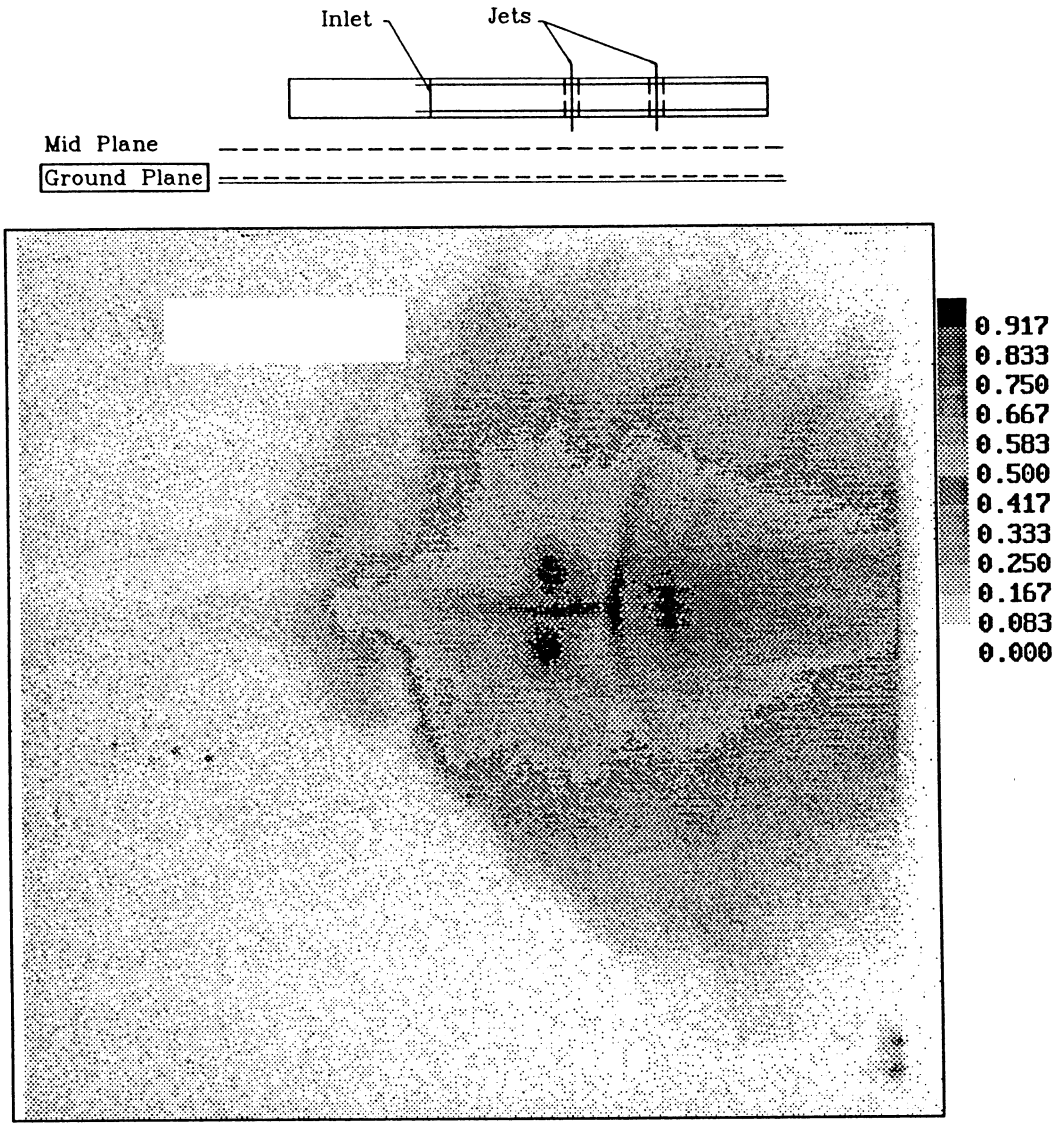

Figure 4.3 Three-Jet Single Frame Image of Smoke Concentration at Ground Plane
$y/D_j=0$, $H/D_j=4$, $U/V_j=0.09$

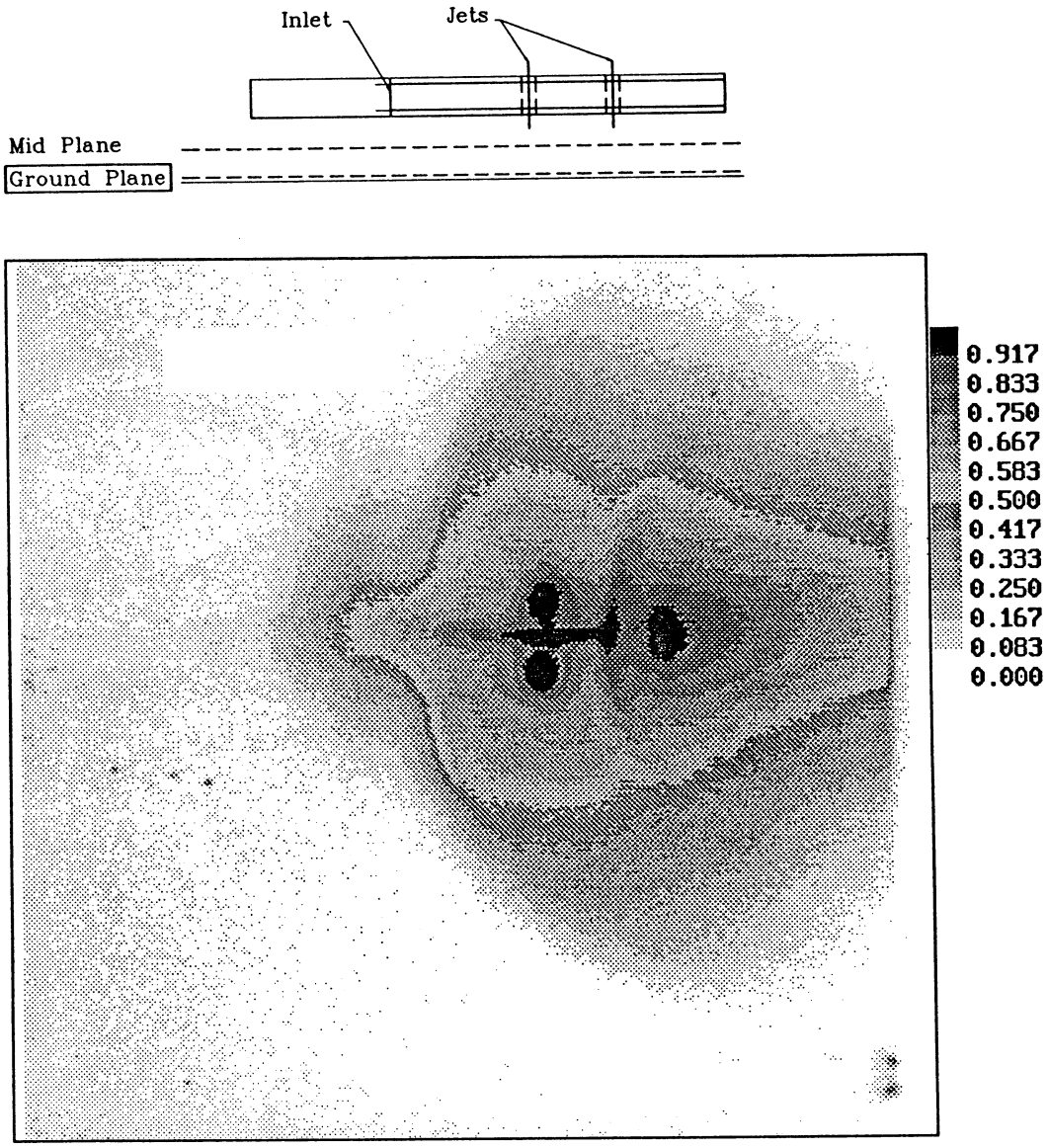

Figure 4.4 Three-Jet 127-Frame Average Image of Smoke Concentration at Ground Plane
$y/D_j=0$, $H/D_j=4$, $U/V_j=0.09$

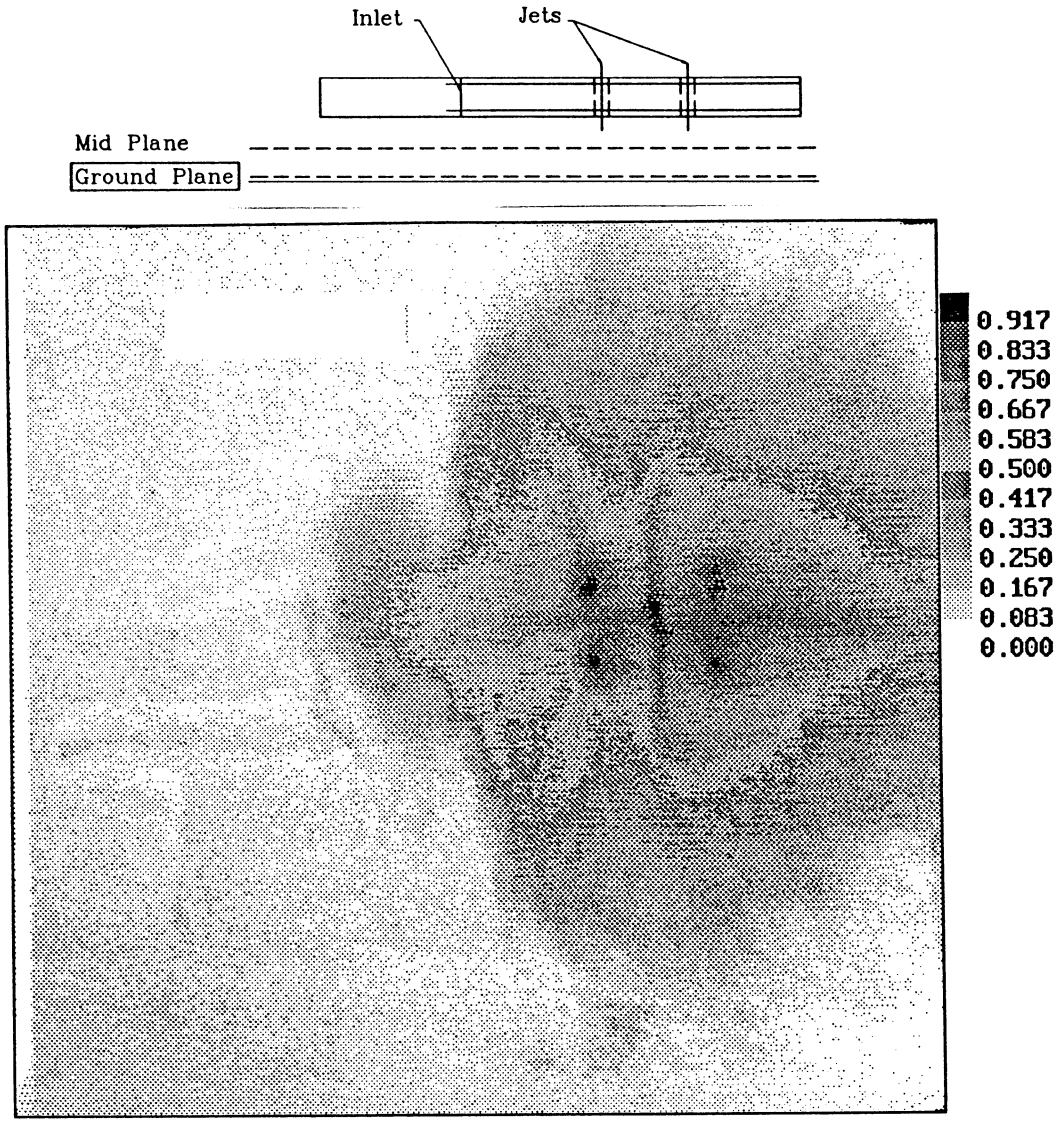

Figure 4.5 Four-Jet Single Frame Image of Smoke Concentration at Ground Plane
$y/D_j=0$, $H/D_j=4$, $U/V_j=0.09$

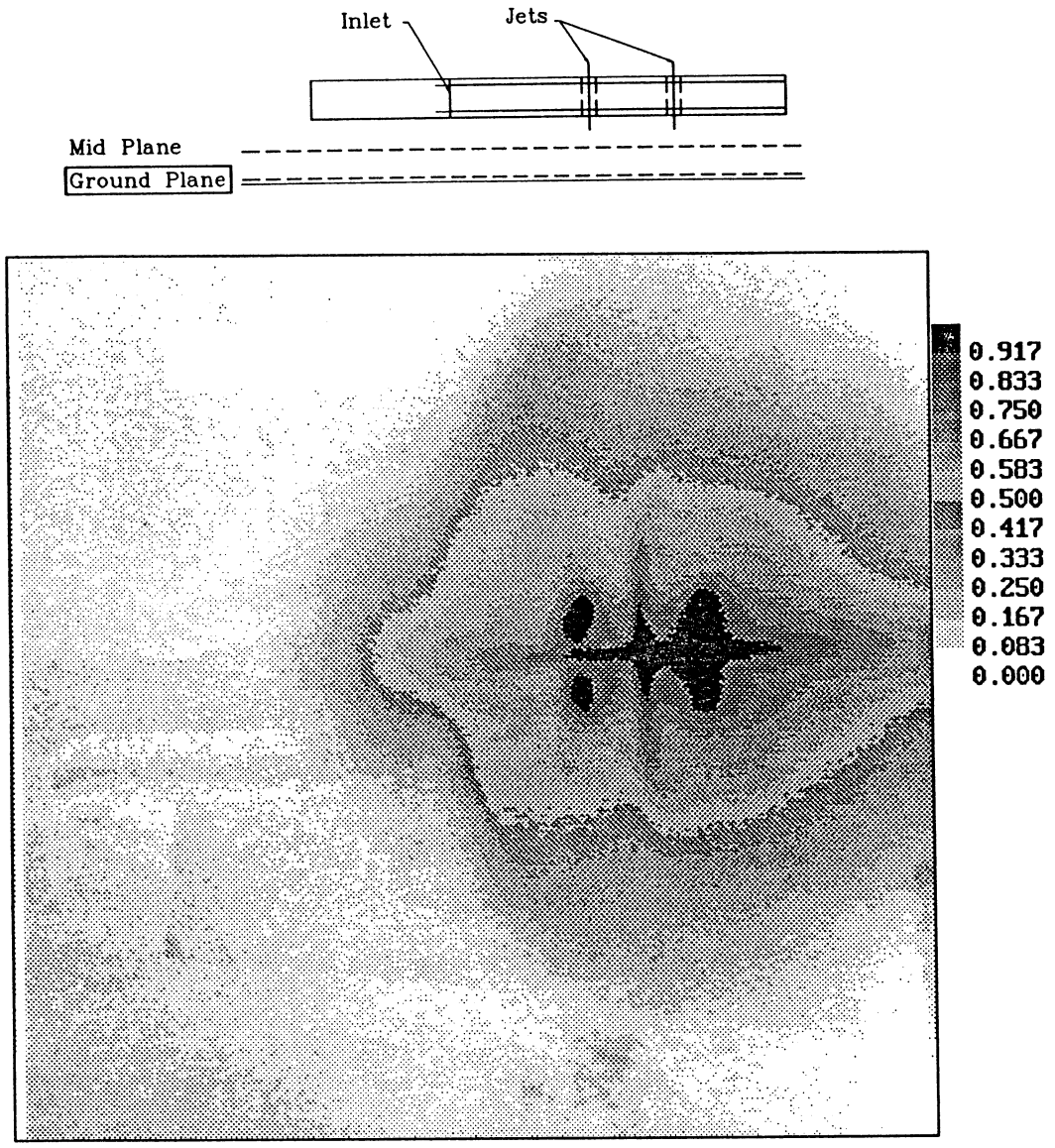

Figure 4.6 Four-Jet 127-Frame Average Image of Smoke Concentration at Ground Plane
$y/D_j=0$, $H/D_j=4$, $U/V_j=0.09$

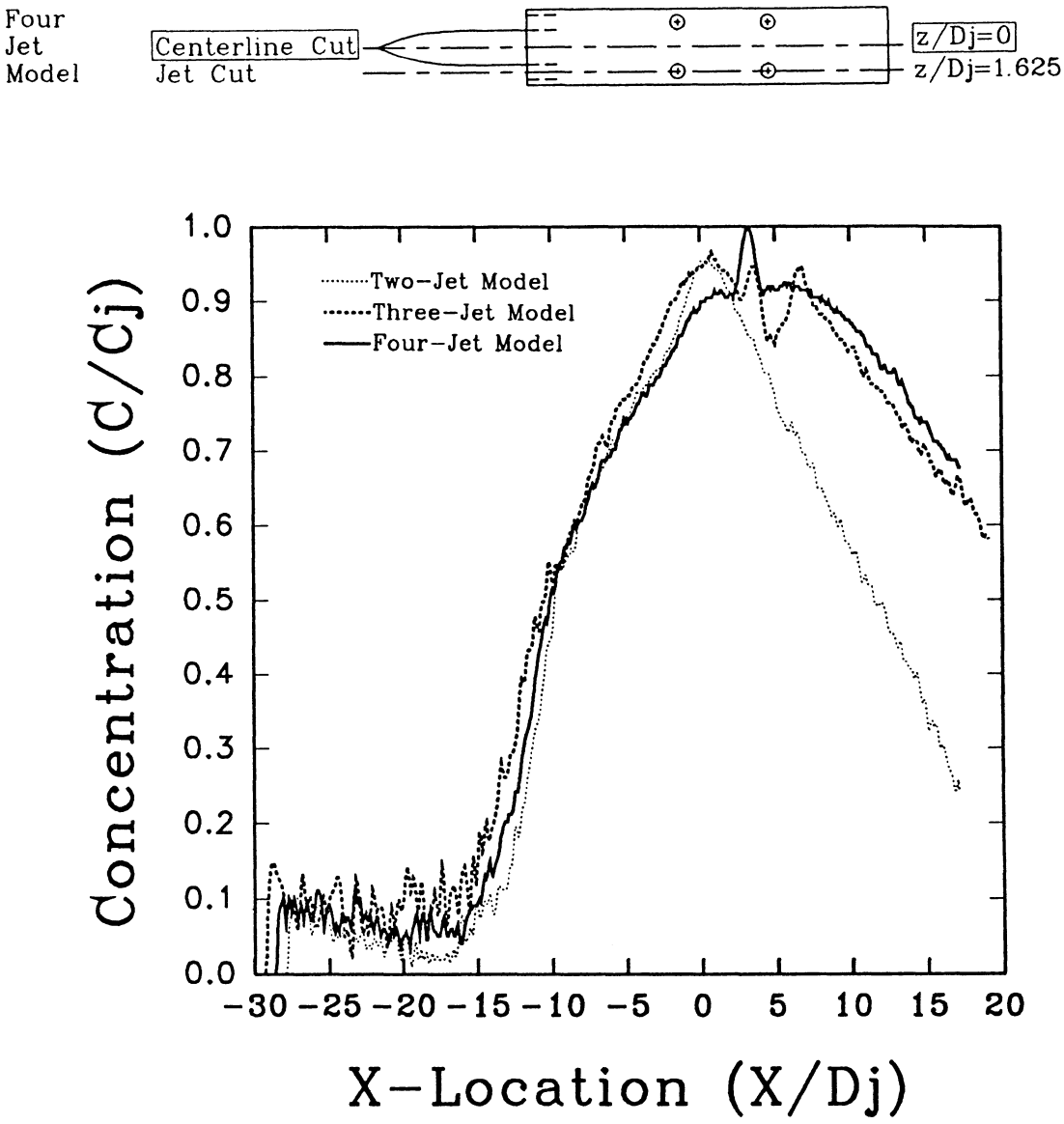

Figure 4.7 Two-, Three-, Four-Jet 127-Frame Average Concentration Profiles at Model Centerline: $z/D_j=0$ Laser Sheet at Ground Plane: $y/D_j=0.0$, $H/D_j=4$, $U/V_j=0.09$

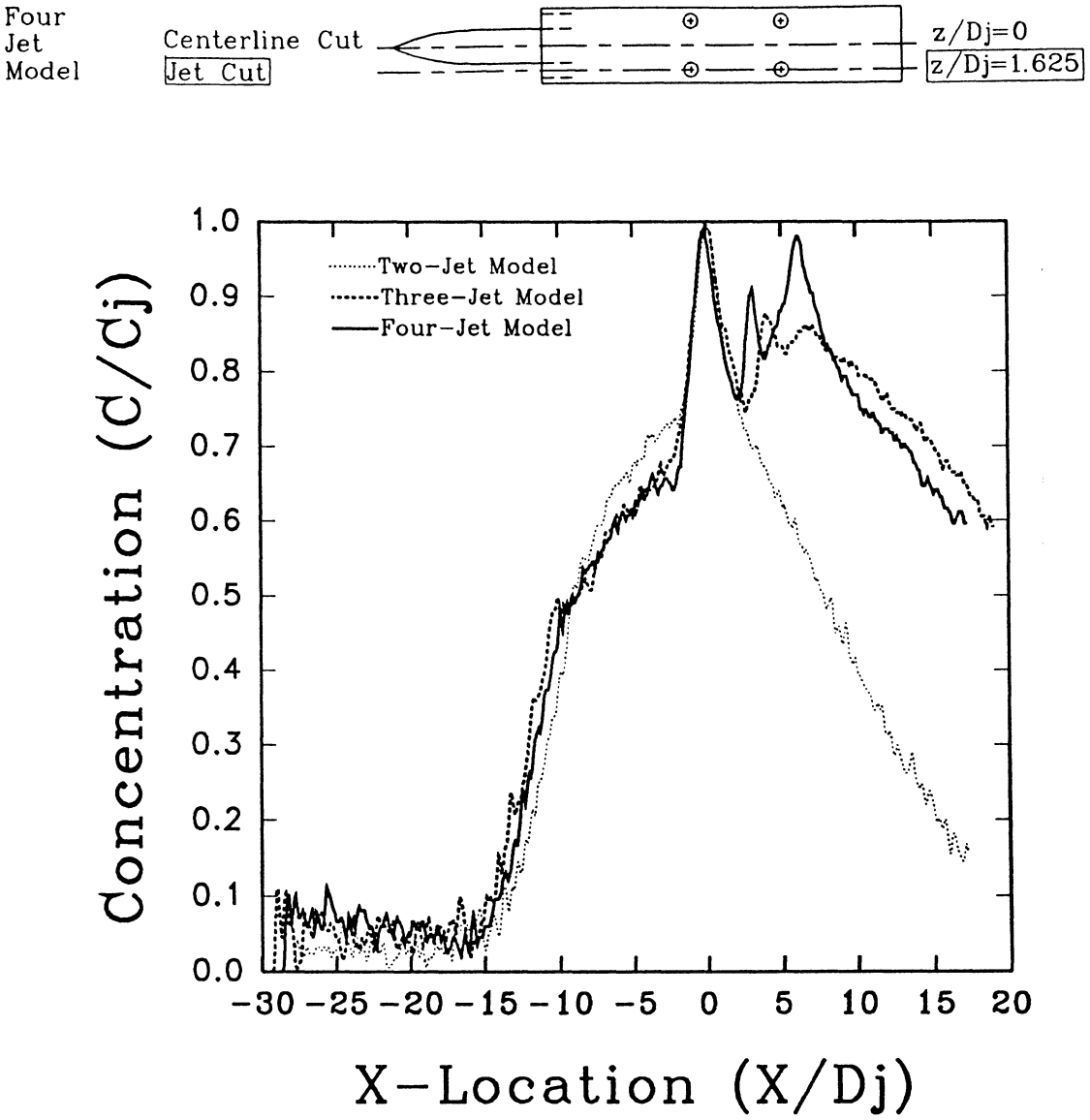

Figure 4.8 Two-, Three-, Four-Jet 127-Frame Average Concentration Profiles at Jet Centerline: z/D_j=1.625 Laser Sheet at Ground Plane: y/D_j=0.0, H/D_j=4, U/V_j=0.09

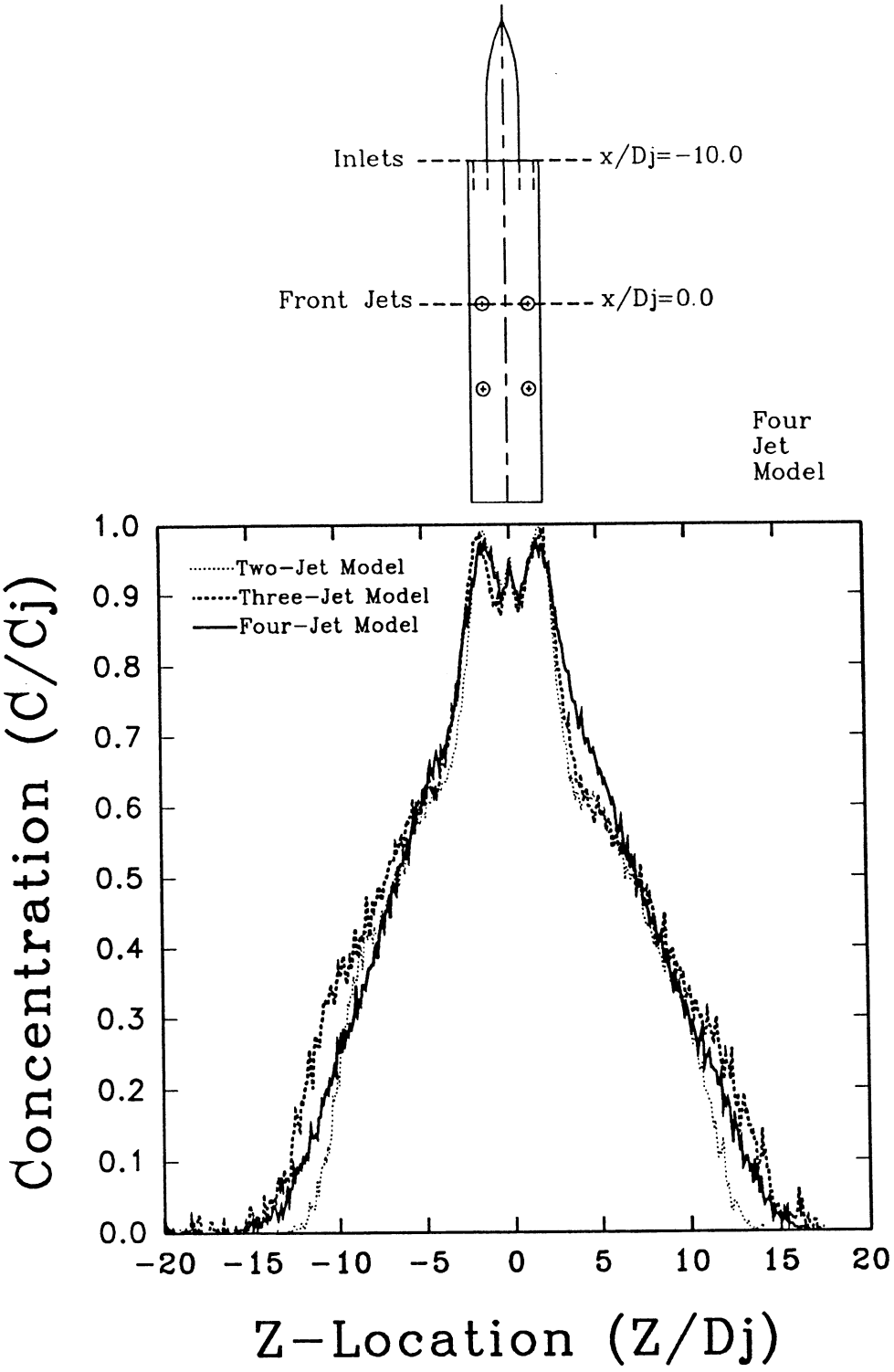

Figure 4.9 Two-, Three-, and Four-Jet 127-Frame Average Concentration Profiles at Forward Jet Centerline: $x/D_j=0$ Laser Sheet at Ground Plane: $y/D_j=0.0$, $H/D_j=4$, $U/V_j=0.09$

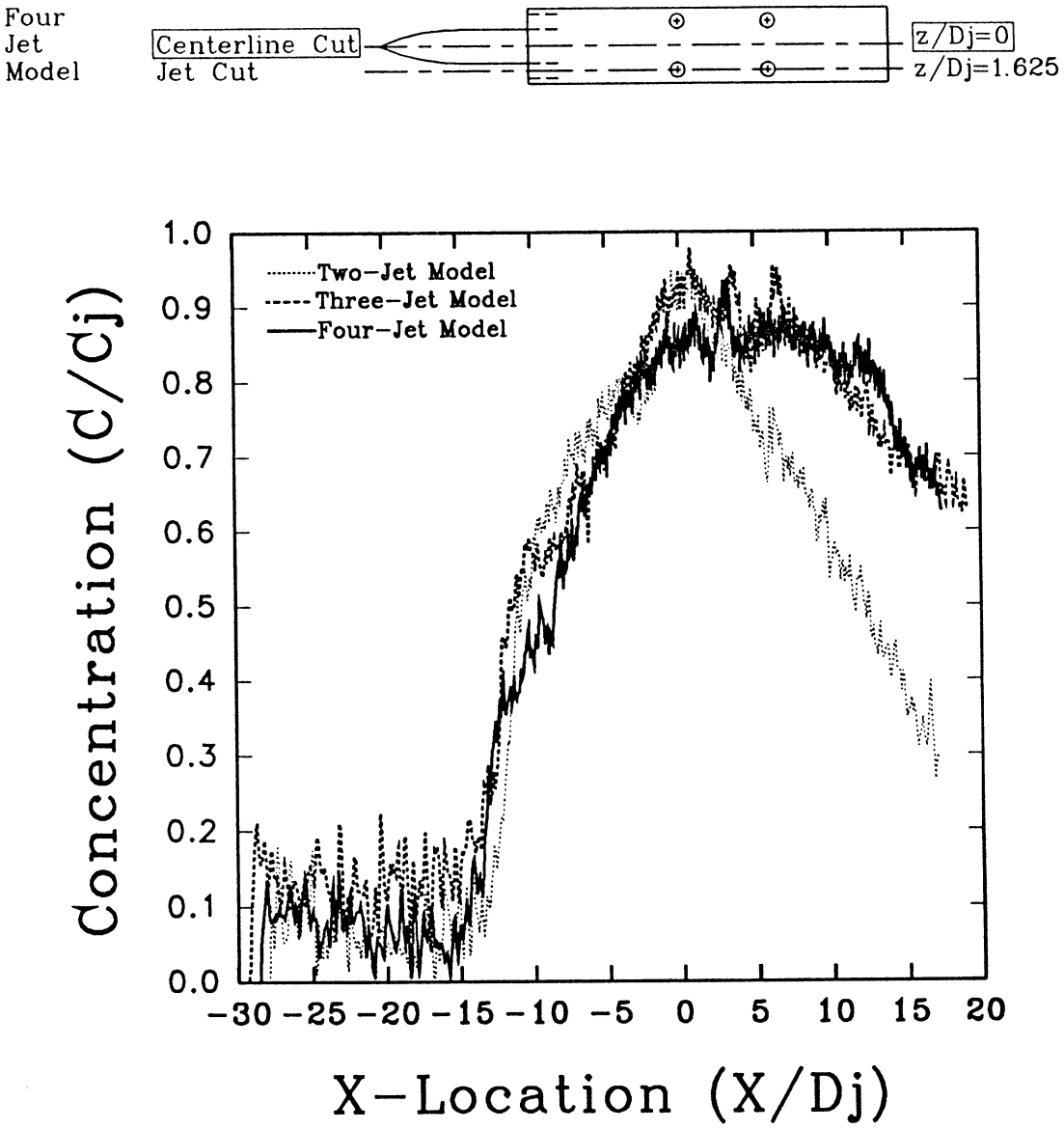

Figure 4.10 Two-, Three-, Four-Jet Single Frame Concentration Profiles at Model Centerline: $z/D_j=0$ Laser Sheet at Ground Plane: $y/D_j=0.0$, $H/D_j=4$, $U/V_j=0.09$

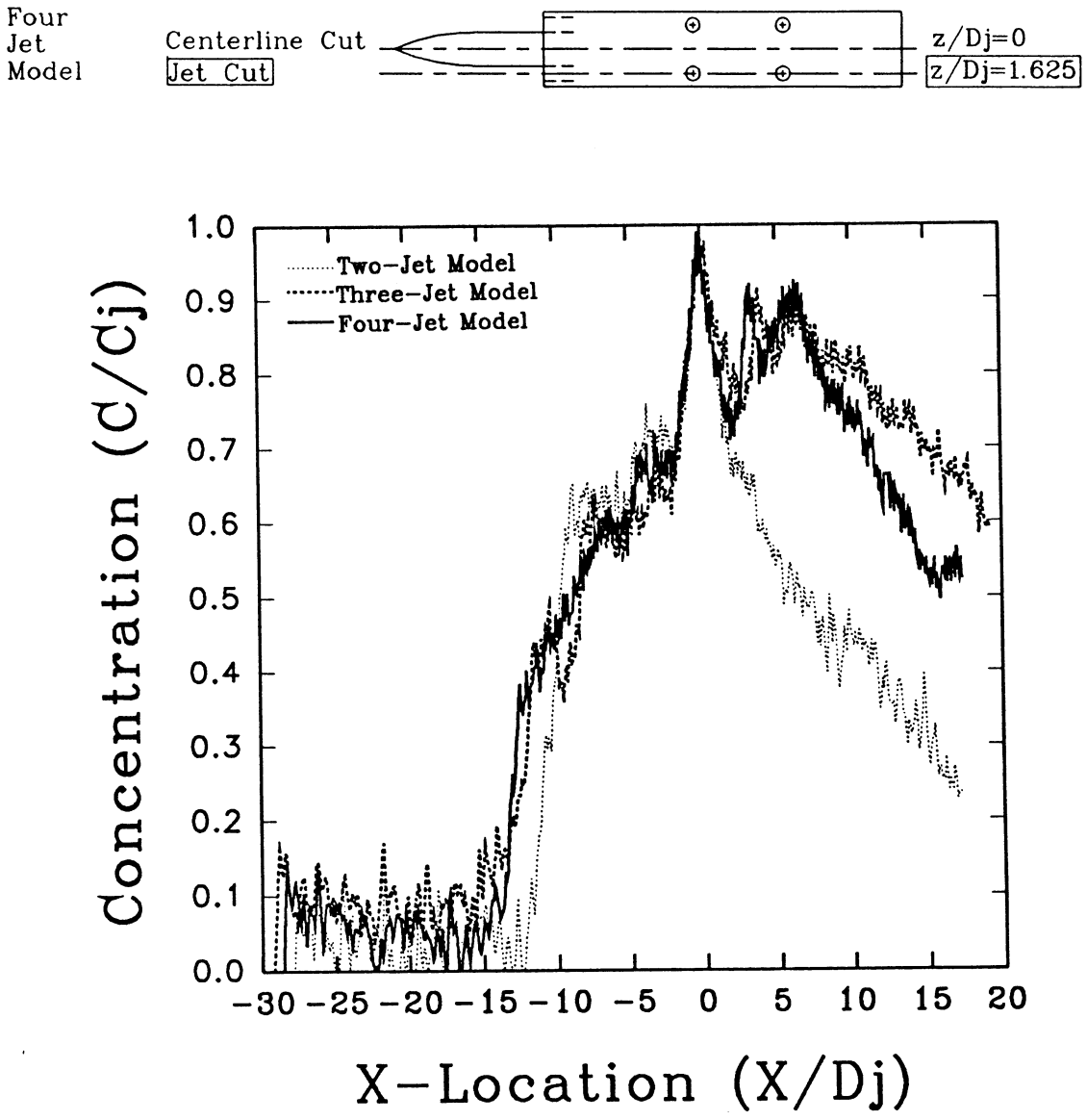

Figure 4.11 Two-, Three-, Four-Jet Single Frame Concentration Profiles at Jet Centerline: z/D_j=1.625 Laser Sheet at Ground Plane: y/D_j=0.0, H/D_j=4, U/V_j=0.09

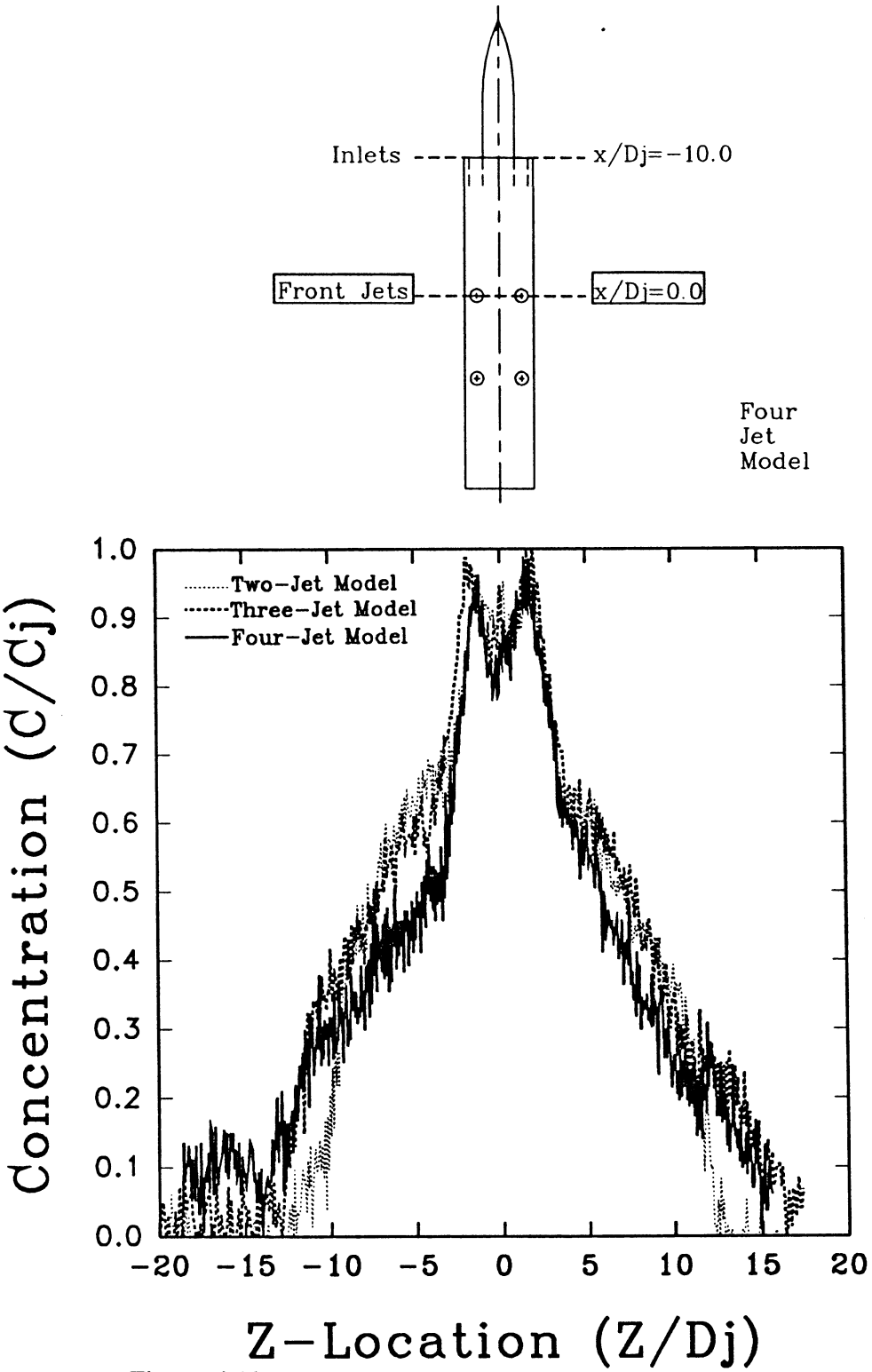

Figure 4.12 Two-, Three-, Four-Jet Single Frame Concentration Profiles at Forward Jet Centerline: $x/D_j=0$ Laser Sheet at Ground Plane: $y/D_j=0.0$, $H/D_j=4$, $U/V_j=0.09$

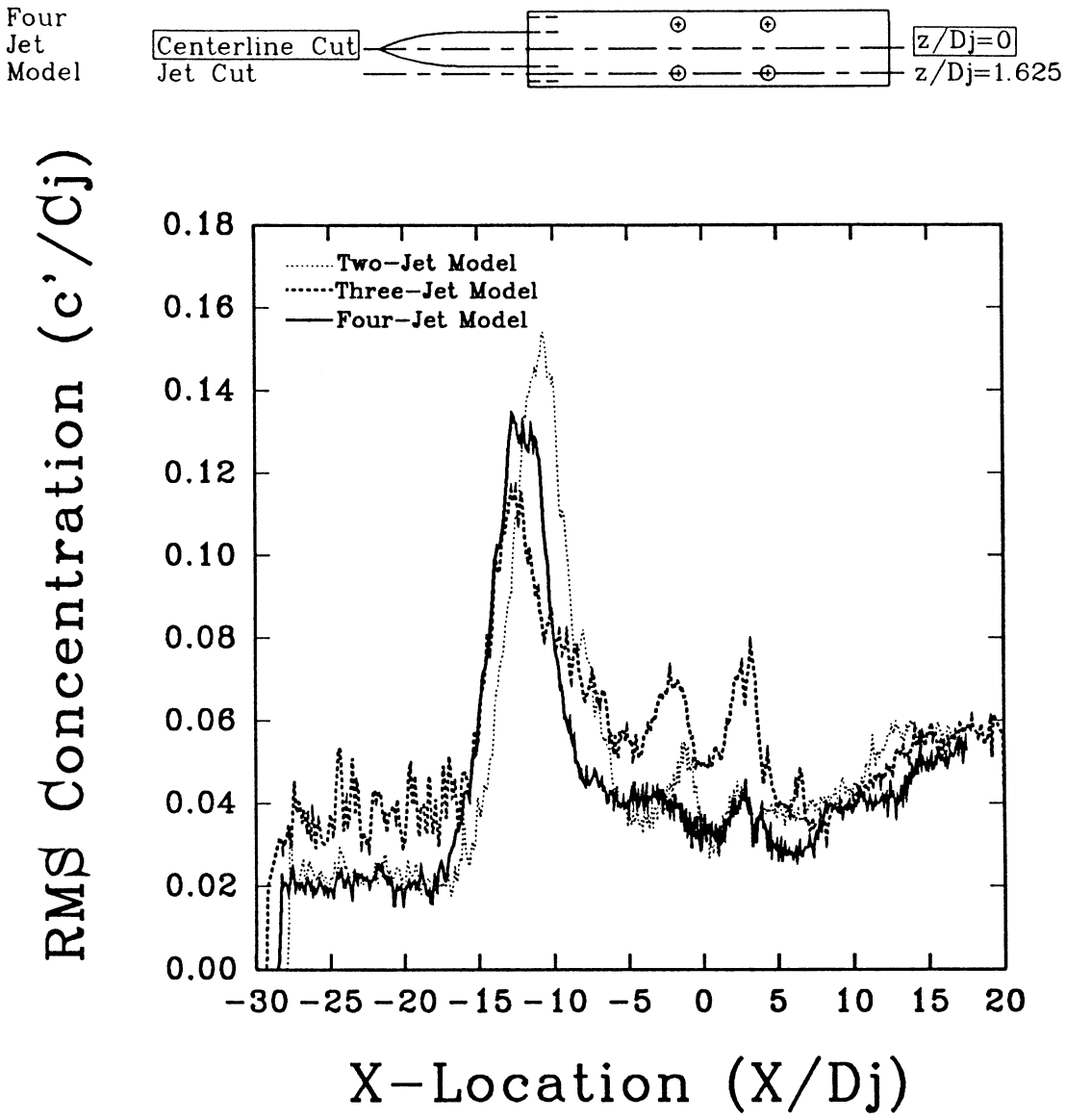

Figure 4.13 Two-, Three-, Four-Jet 127-Frame Average RMS Concentration Profiles at Model Centerline: $z/D_j=0$ Laser Sheet at Ground Plane: $y/D_j=0.0$, $H/D_j=4$, $U/V_j=0.09$

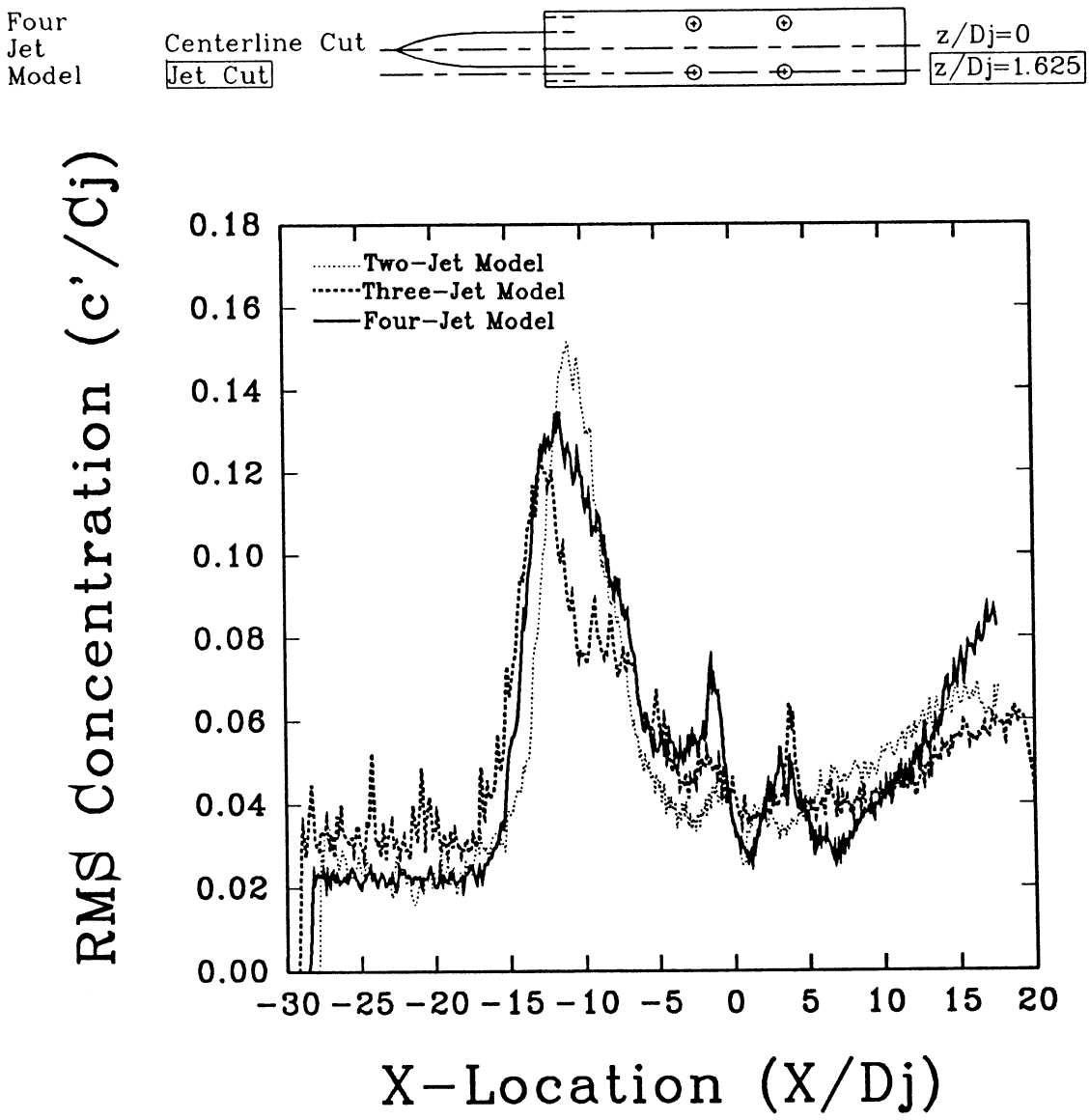

Figure 4.14 Two-, Three-, Four-Jet 127-Frame Average RMS Concentration Profiles at Jet Centerline: z/D_j=1.625 Laser Sheet at Ground Plane: y/D_j=0.0, H/D_j=4, U/V_j=0.09

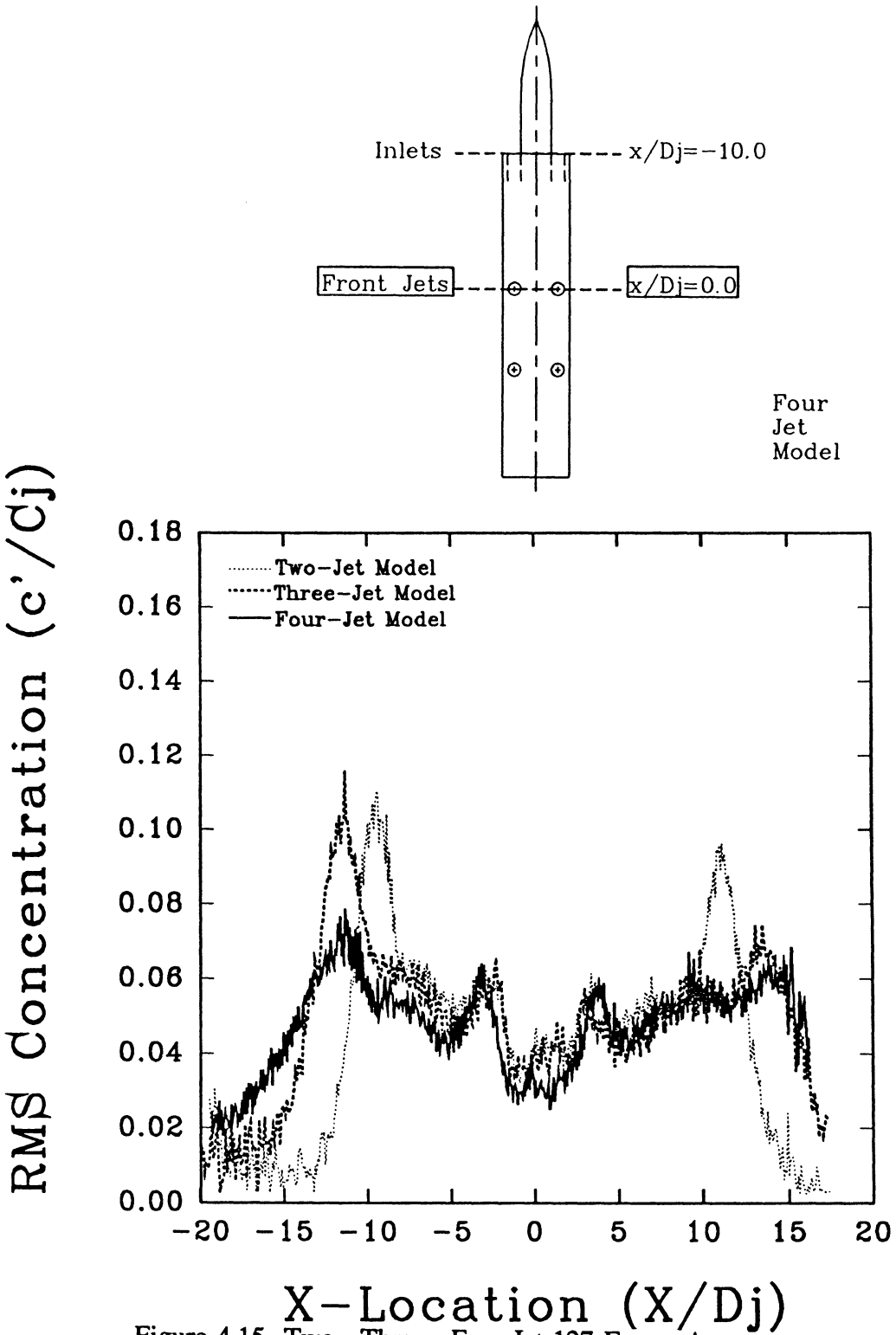

Figure 4.15 Two-, Three-, Four-Jet 127-Frame Average RMS Concentration Profiles at Forward Jet Centerline: $x/D_j=0$ Laser Sheet at Ground Plane: $y/D_j=0.0$, $H/D_j=4$, $U/V_j=0.09$

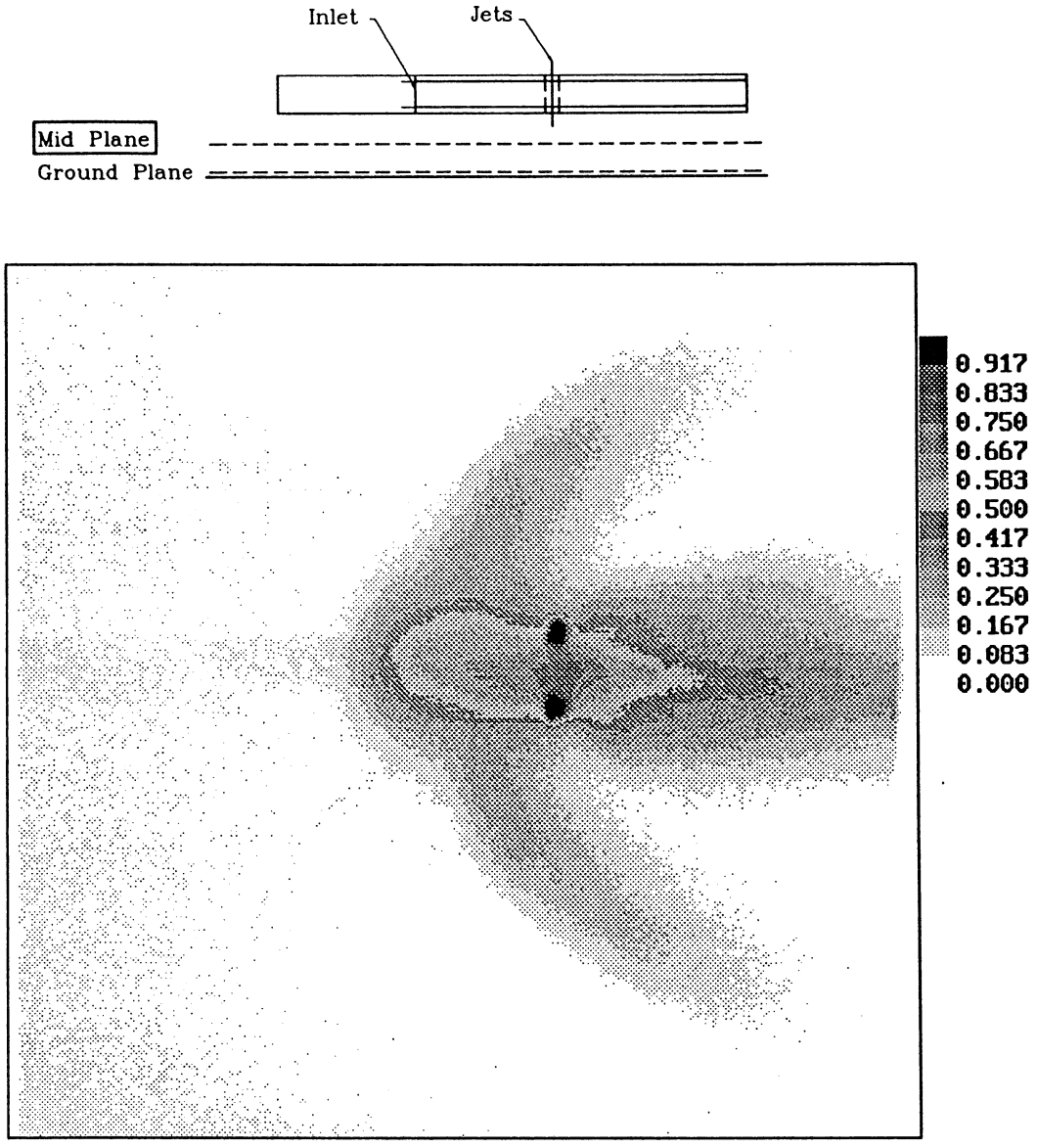

Figure 4.16 Two-Jet 127-Frame Average Image of Smoke Concentration at Mid Plane
y/D_j=2, H/D_j=4, U/V_j=0.09

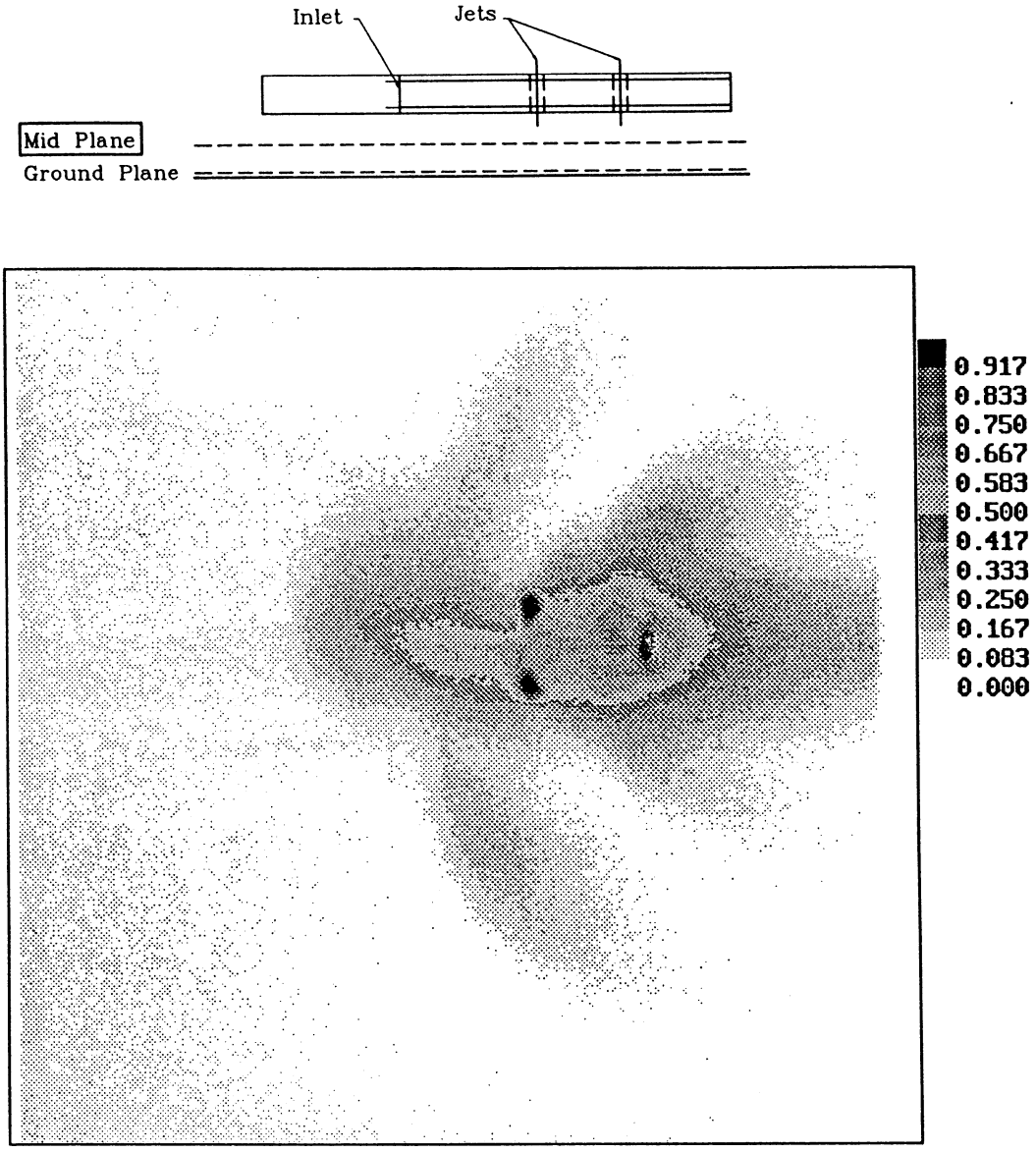

Figure 4.17 Three-Jet 127-Frame Average Image of Smoke Concentration at Mid Plane
$y/D_j=2$, $H/D_j=4$, $U/V_j=0.09$

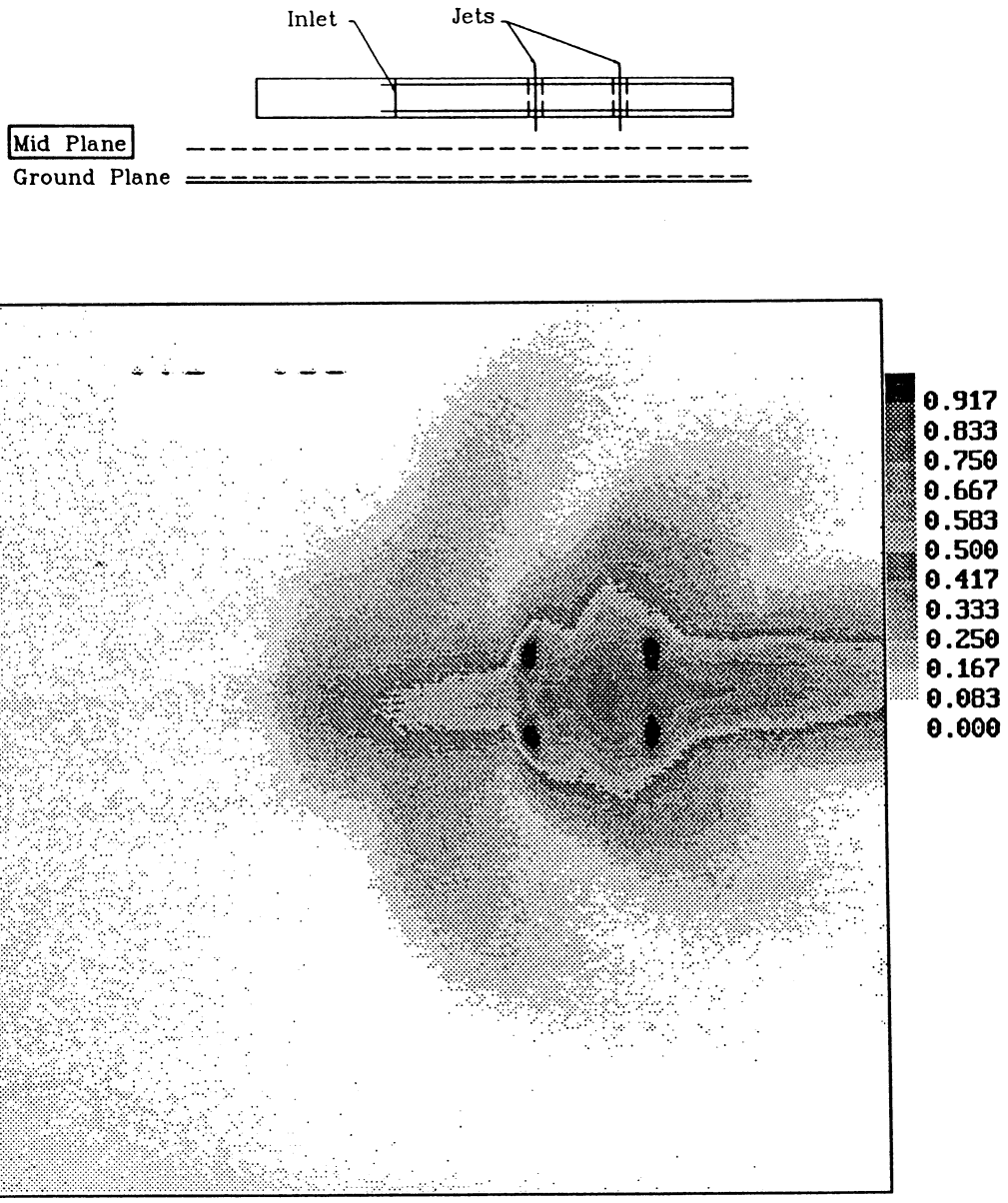

Figure 4.18 Four-Jet 127-Frame Average Image of Smoke Concentration at Mid Plane
$y/D_j=2$, $H/D_j=4$, $U/V_j=0.09$

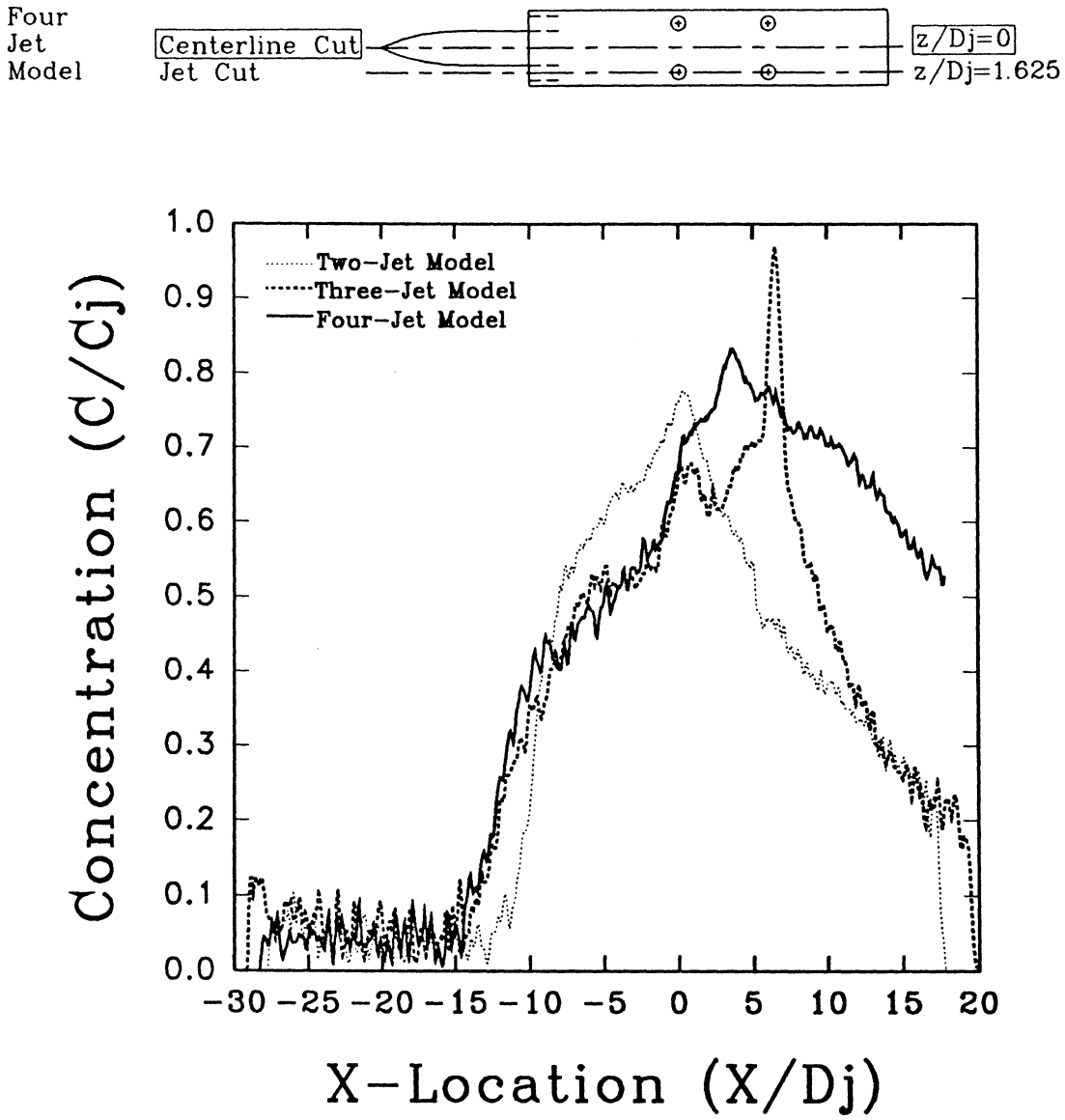

Figure 4.19 Two-, Three-, Four-Jet 127-Frame Average Concentration Profiles at Model Centerline: $z/D_j=0$ Laser Sheet at Mid Plane: $y/D_j=2.0$, $H/D_j=4$, $U/V_j=0.09$

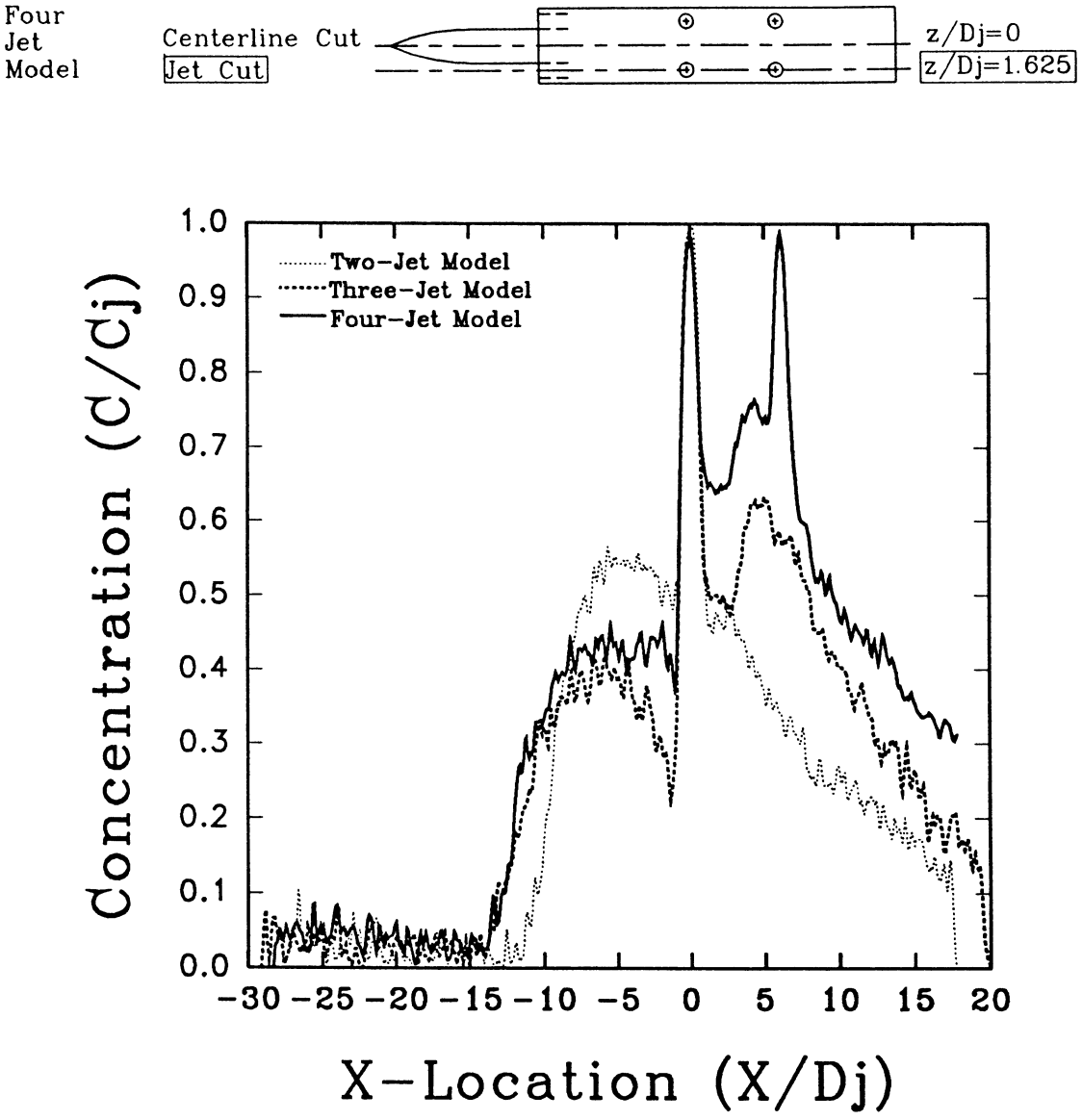

Figure 4.20 Two-, Three-, Four-Jet 127-Frame Average Concentration Profiles at Jet Centerline: $z/D_j=1.625$ Laser Sheet at Mid Plane: $y/D_j=2.0$, $H/D_j=4$, $U/V_j=0.09$

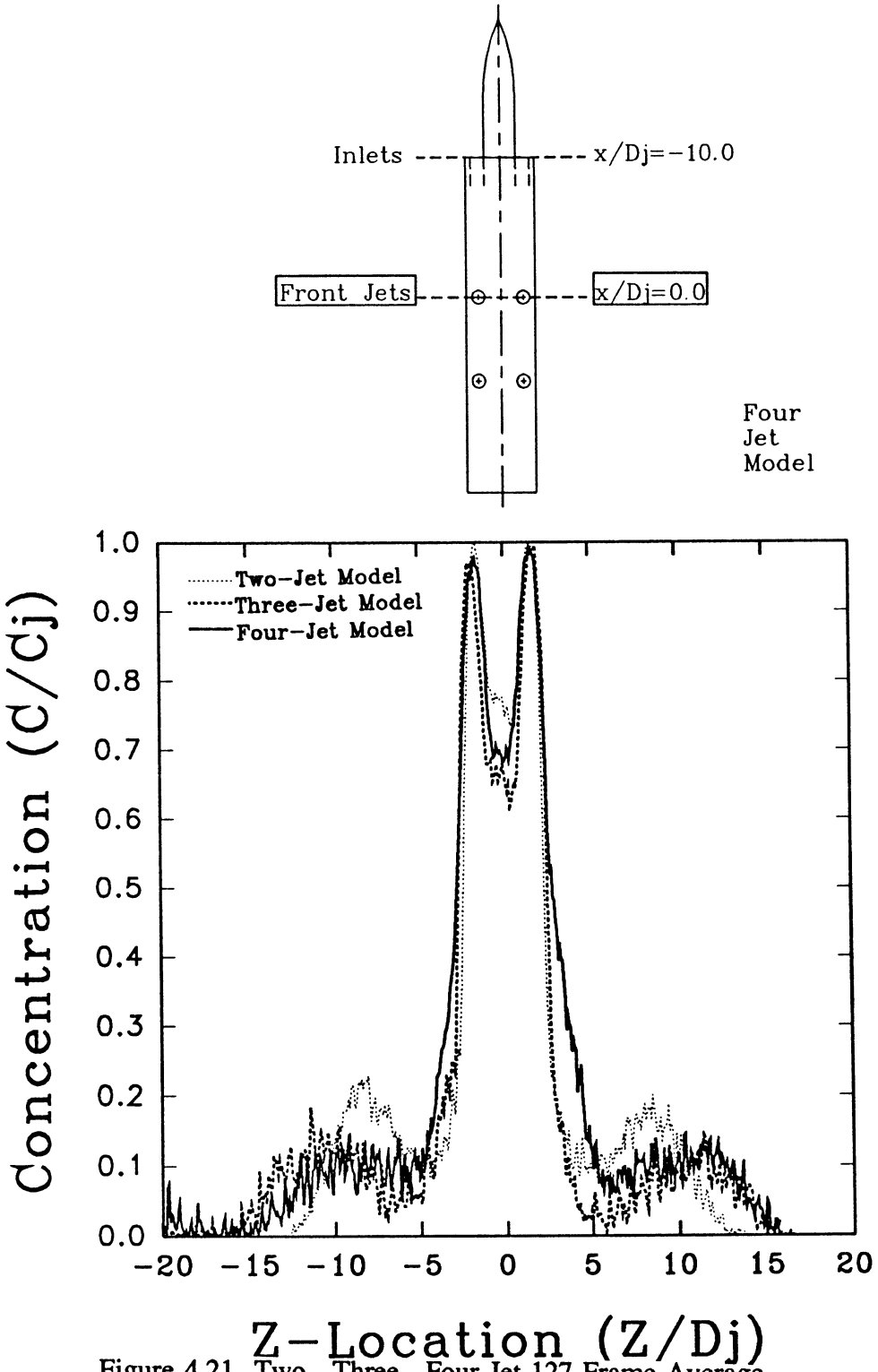

Figure 4.21 Two-, Three-, Four-Jet 127-Frame Average Concentration Profiles at Forward Jet Centerline: $x/D_j=0$ Laser Sheet at Mid Plane: $y/D_j=2.0$, $H/D_j=4$, $U/V_j=0.09$

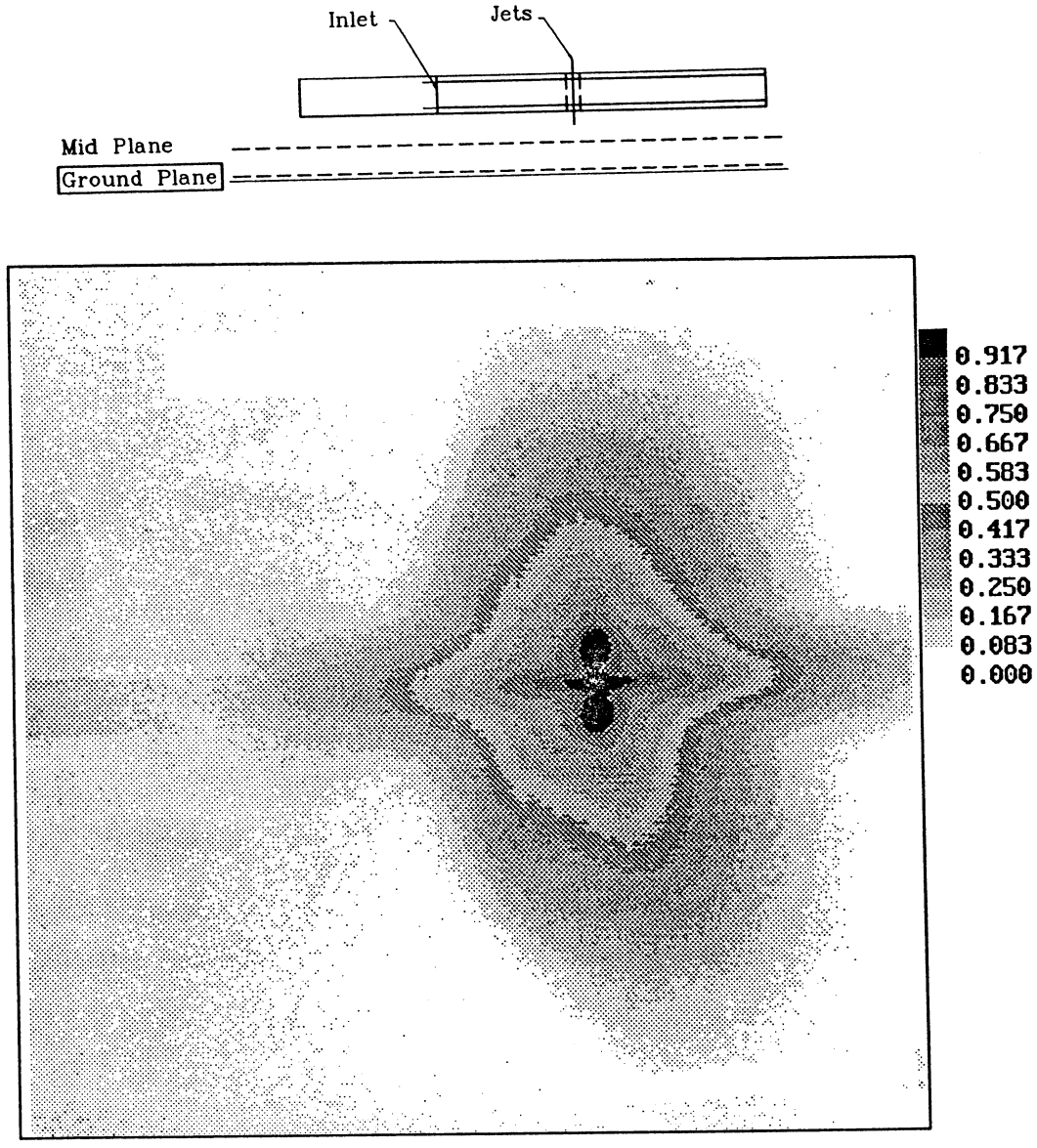

Figure 4.22 Two-Jet 127-Frame Average Image of Smoke Concentration at Ground Plane
$y/D_j=0$, $H/D_j=4$, $U/V_j=0.03$

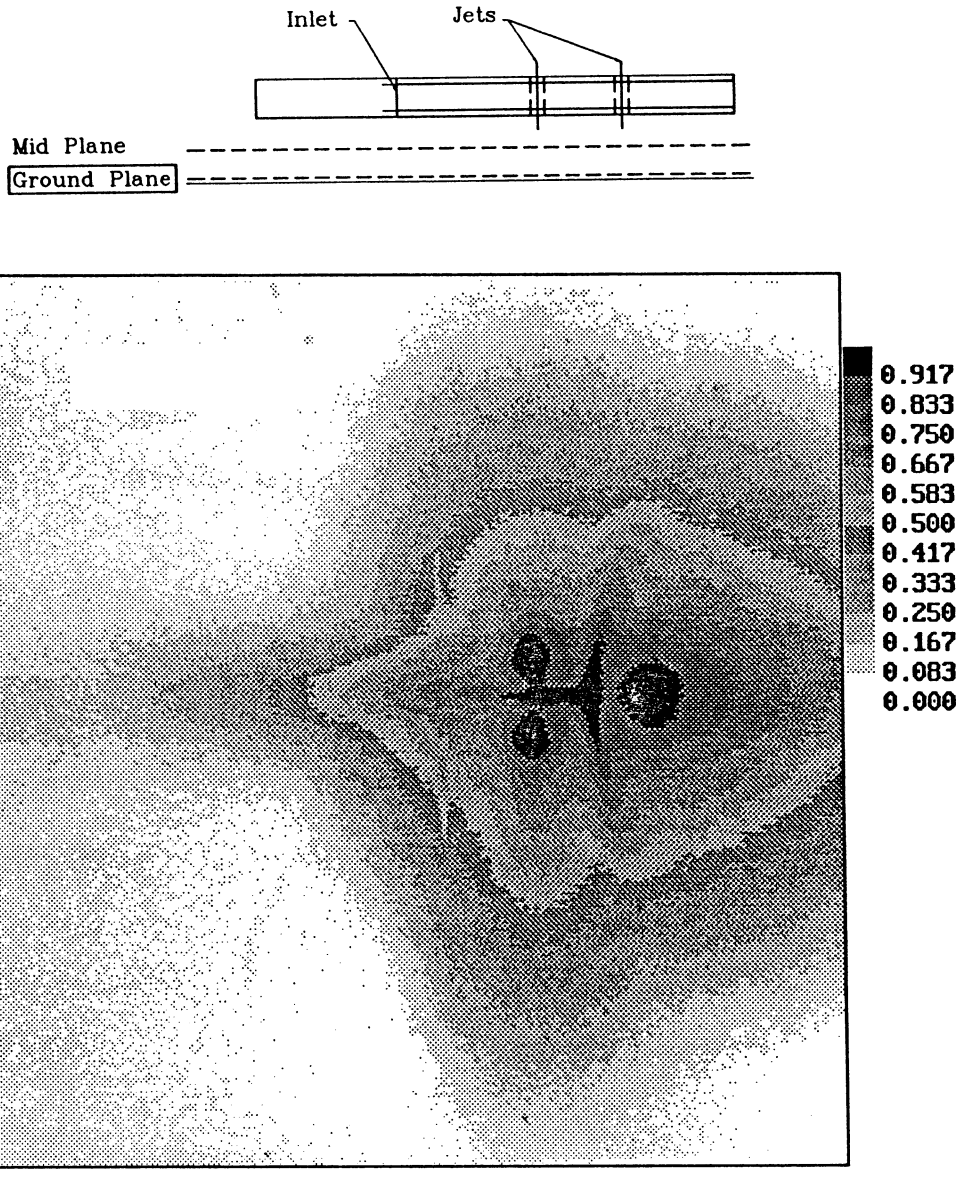

Figure 4.23 Three-Jet 127-Frame Average Image of Smoke Concentration at Ground Plane $y/D_j=0$, $H/D_j=4$, $U/V_j=0.03$

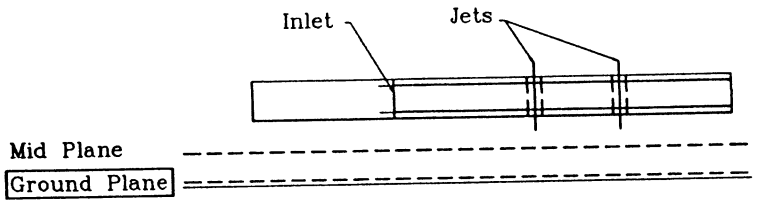

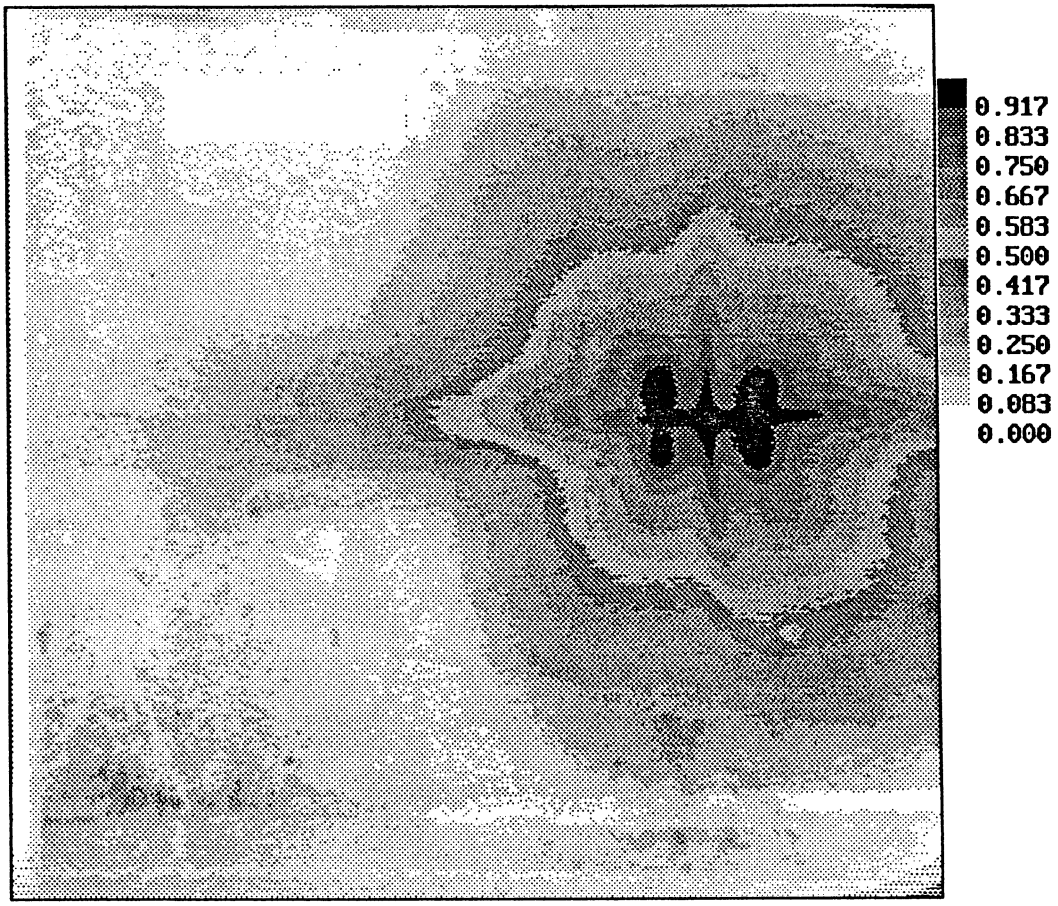

Figure 4.24 Four-Jet 127-Frame Average Image of Smoke Concentration at Ground Plane $y/D_j=0$, $H/D_j=4$, $U/V_j=0.03$

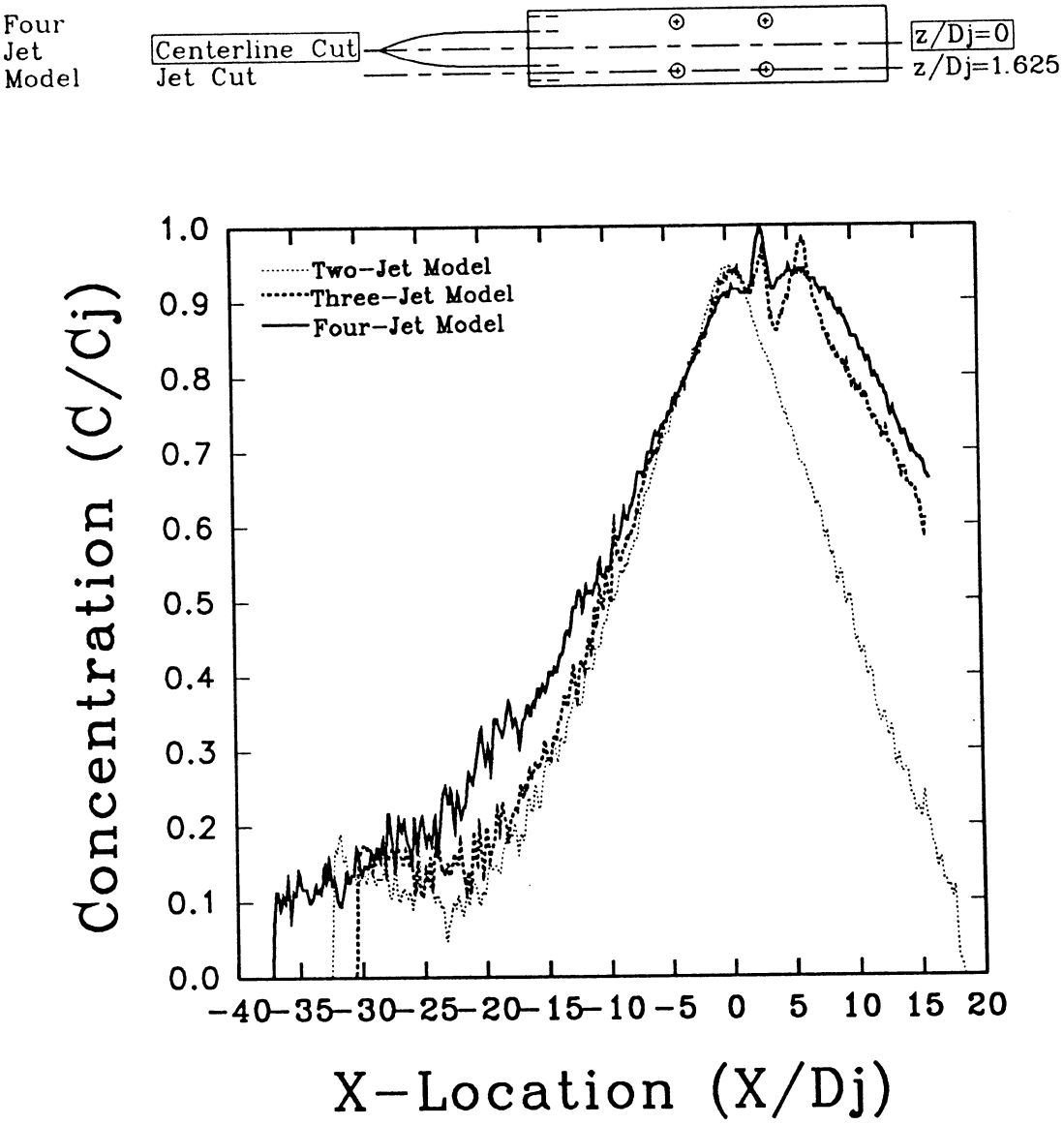

Figure 4.25 Two-, Three-, Four-Jet 127-Frame Average Concentration Profiles at Model Centerline: $z/D_j=0$ Laser Sheet at Ground Plane: $y/D_j=0.0$, $H/D_j=4$, $U/V_j=0.03$

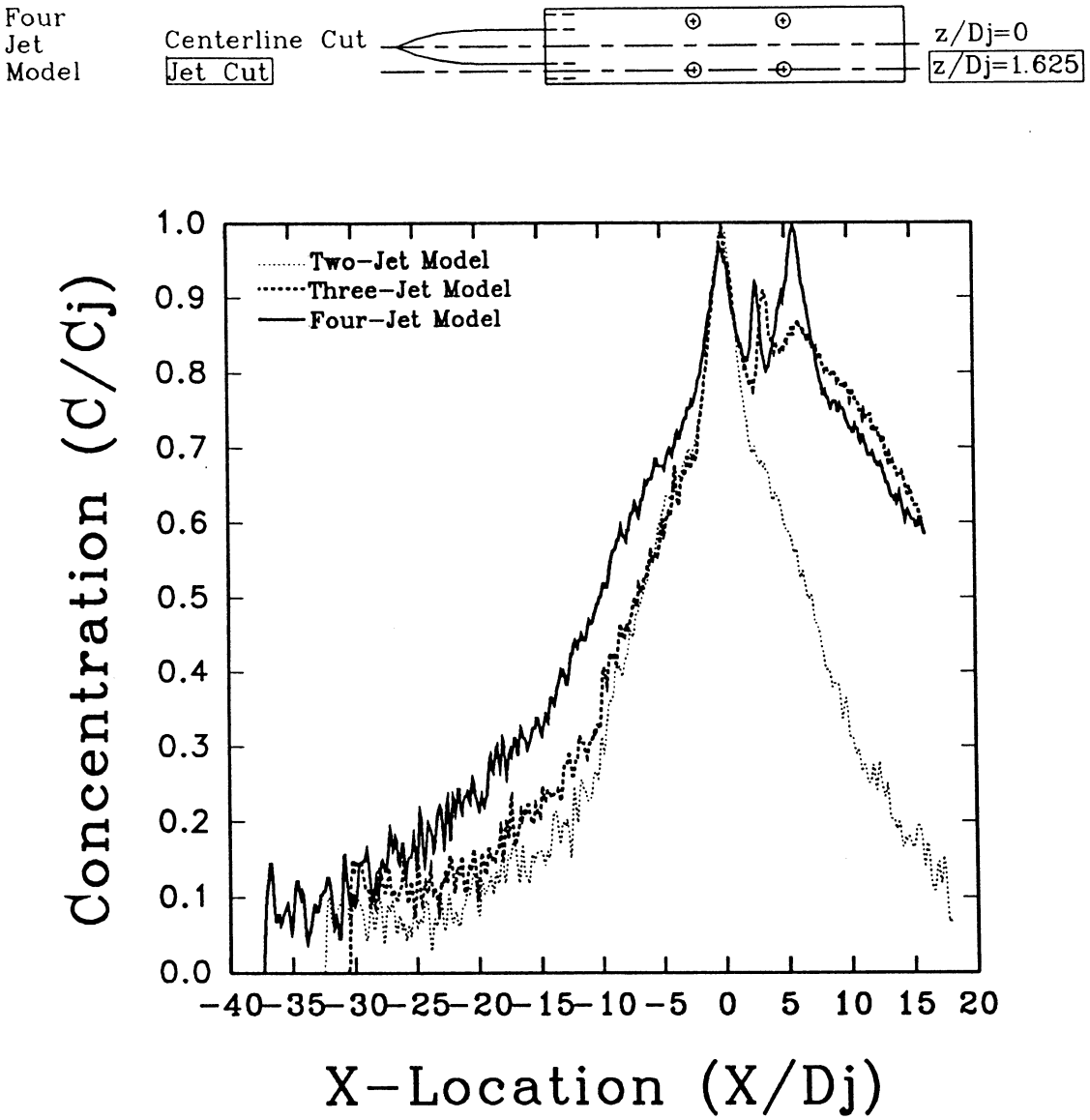

Figure 4.26 Two-, Three-, Four-Jet 127-Frame Average Concentration Profiles at Jet Centerline: z/D_j=1.625 Laser Sheet at Ground Plane: y/D_j=0.0, H/D_j=4, U/V_j=0.03

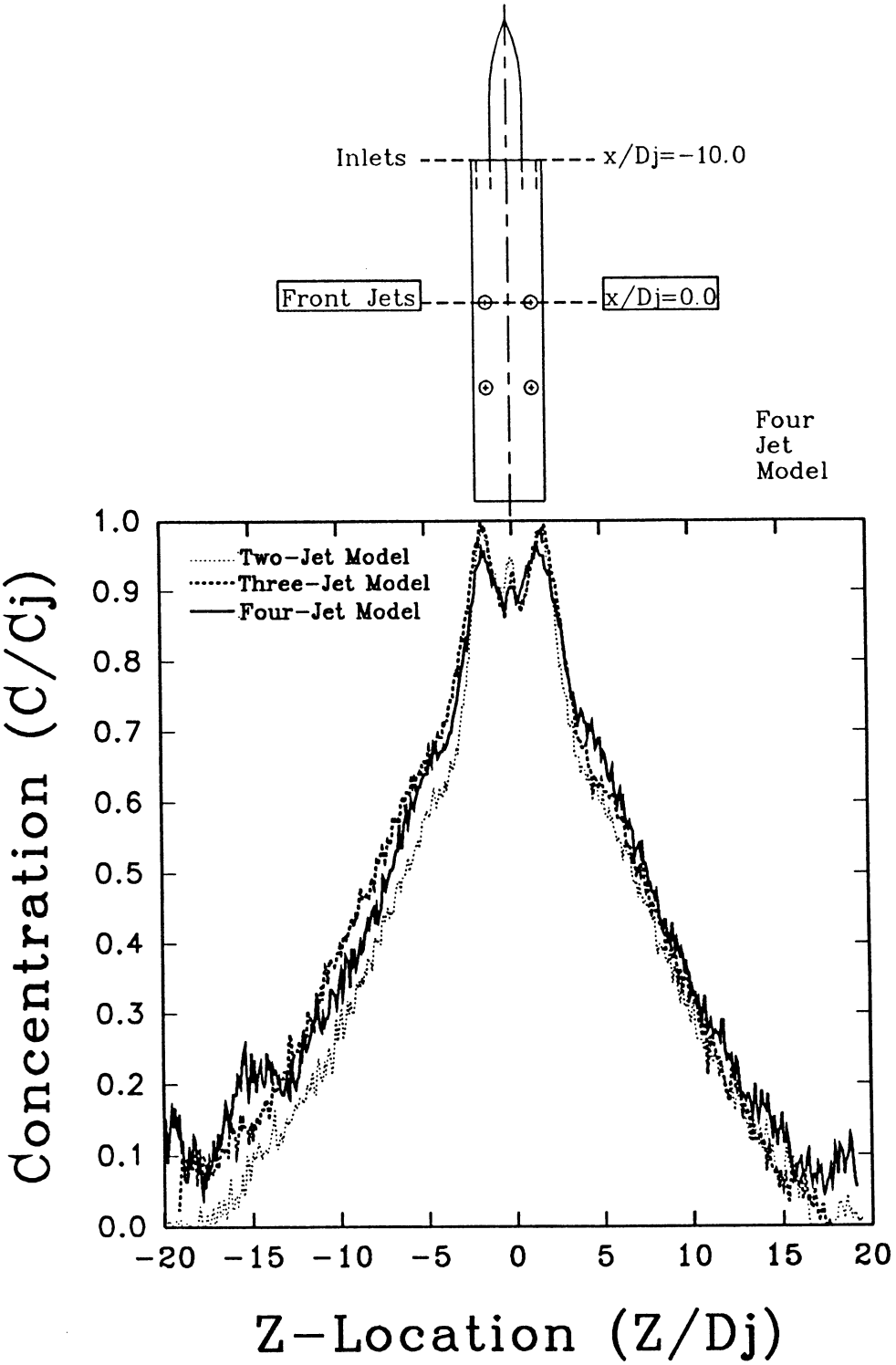

Figure 4.27 Two-, Three-, Four-Jet 127-Frame Average Concentration Profiles at Forward Jet Centerline: $x/D_j=0$ Laser Sheet at Ground Plane: $y/D_j=0.0$, $H/D_j=4$, $U/V_j=0.03$

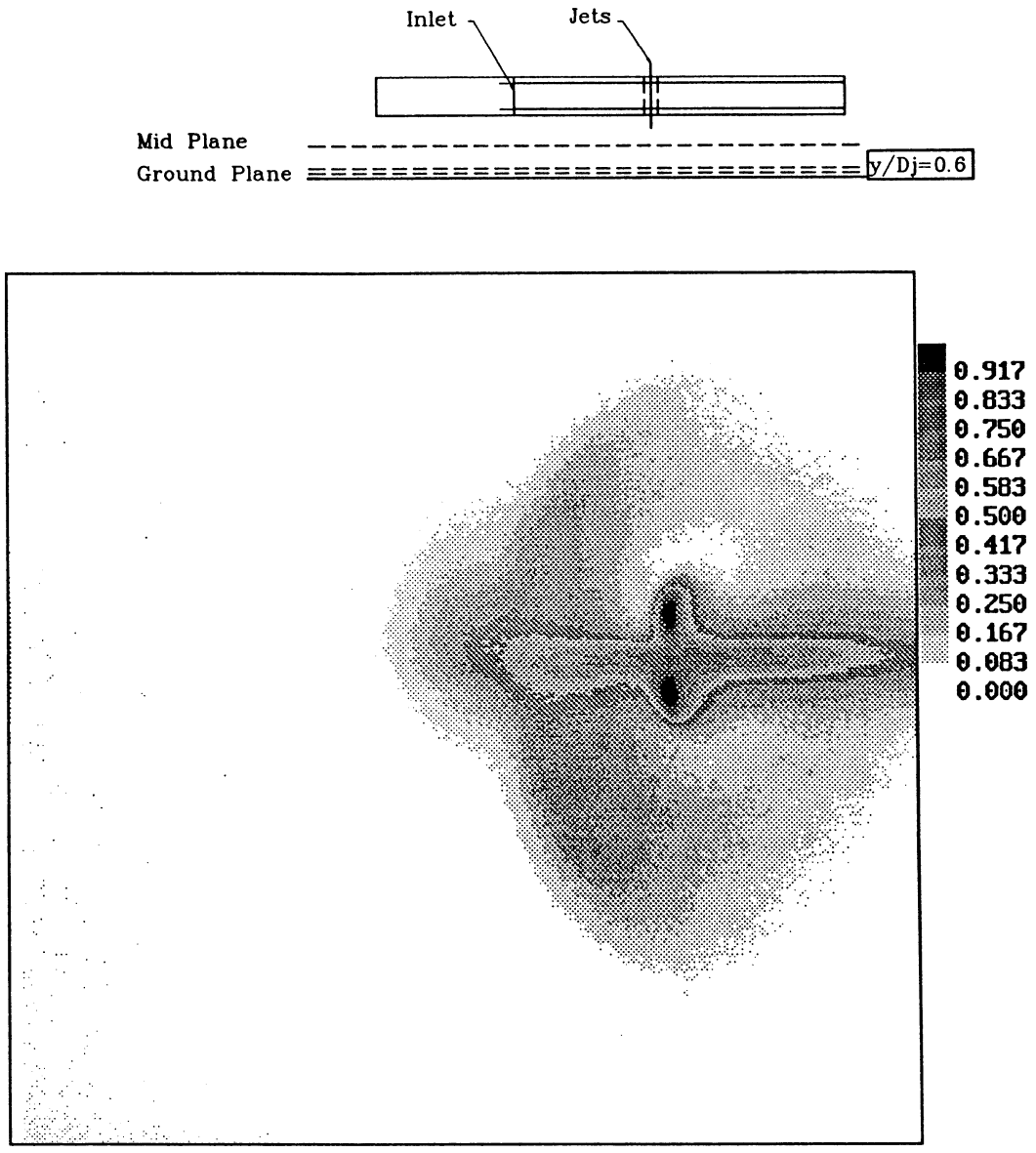

Figure 4.28 Two-Jet 127-Frame Average Image of Smoke Concentration at $y/D_j=0.6$
$H/D_j=6$, $U/V_j=0.09$

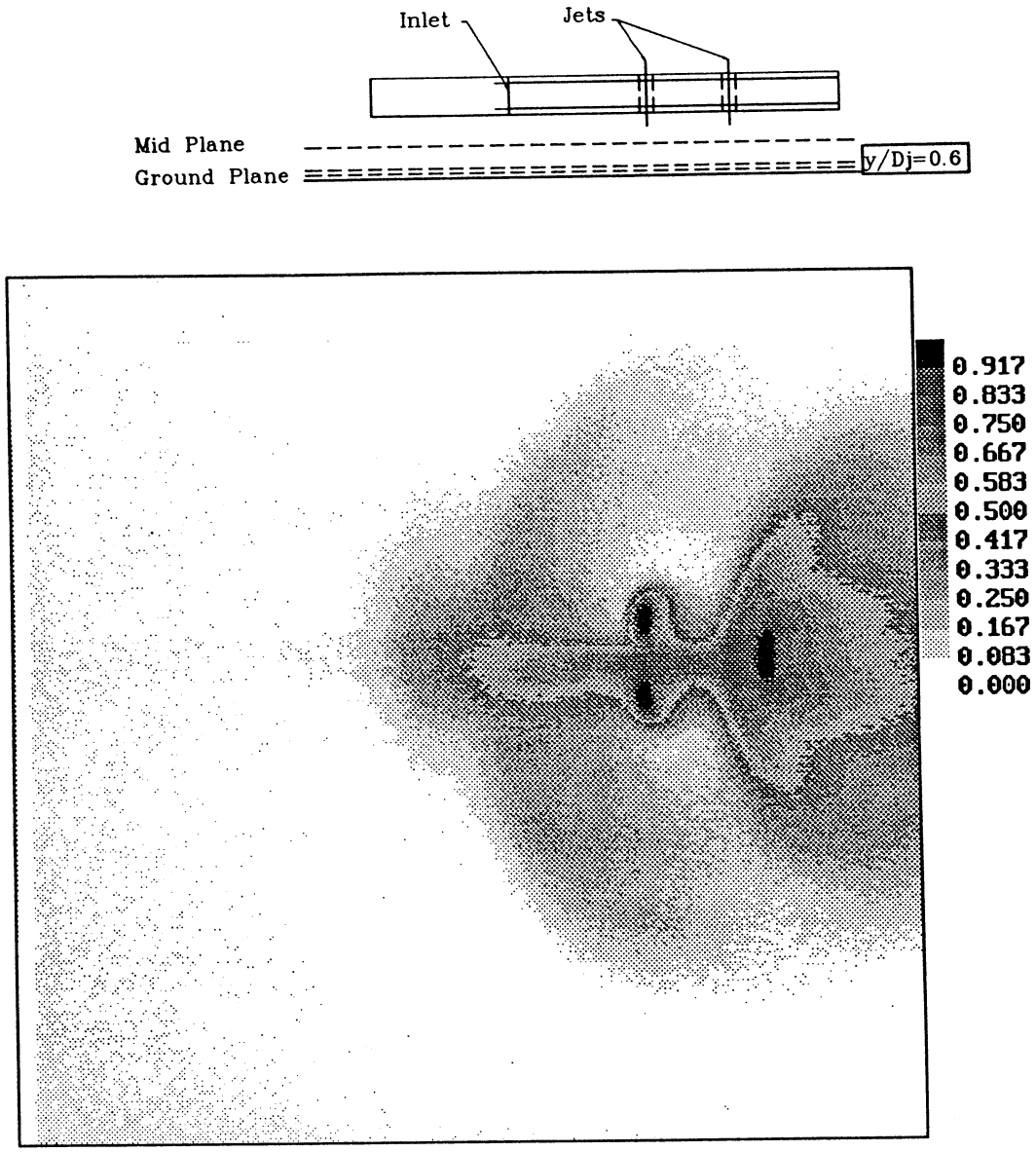

Figure 4.29 Three-Jet 127-Frame Average Image of Smoke Concentration at y/D_j=0.6
H/D_j=6, U/V_j=0.09

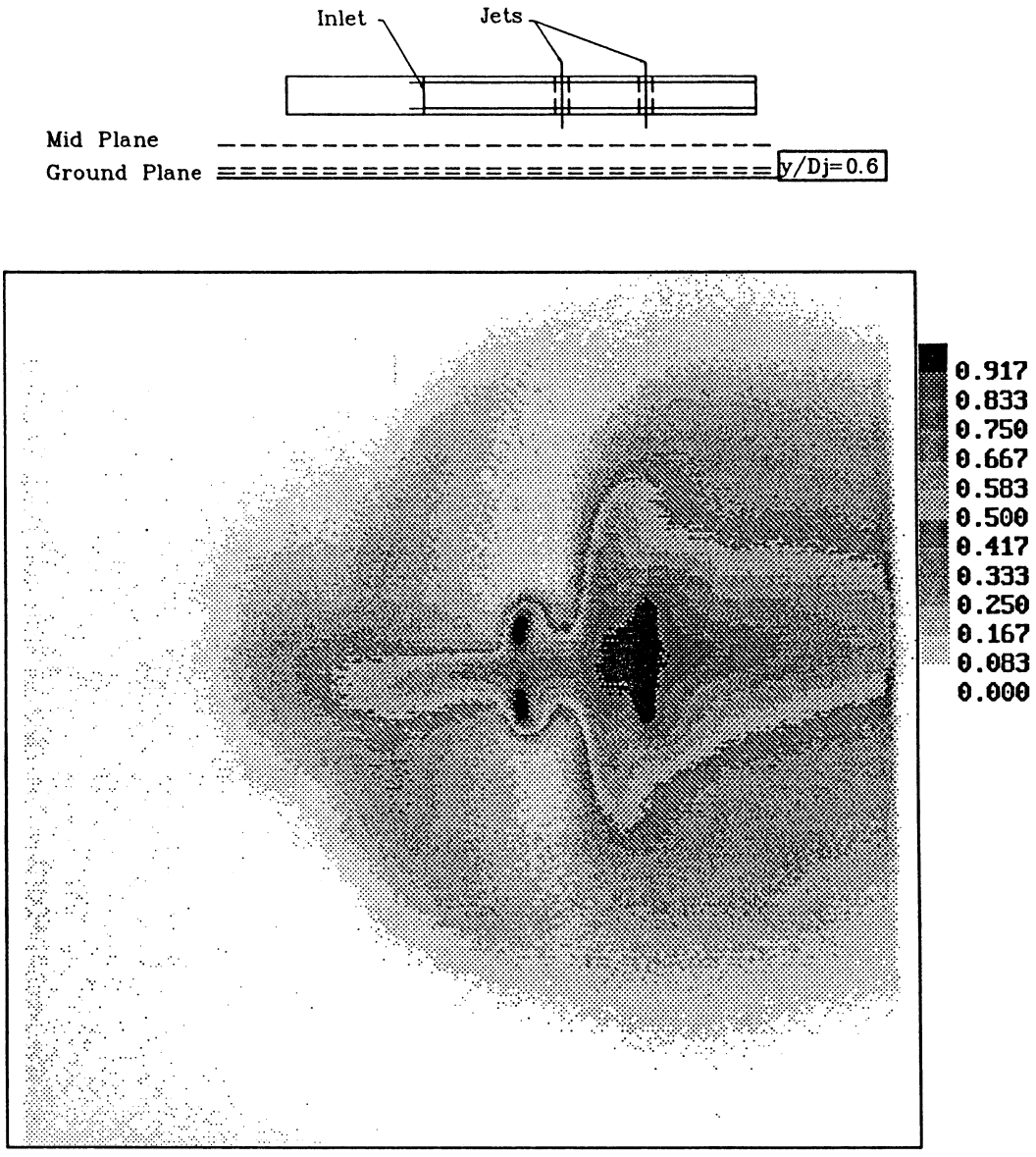

Figure 4.30 Four-Jet 127-Frame Average Image of Smoke Concentration at y/D_j=0.6
H/D_j=6, U/V_j=0.09

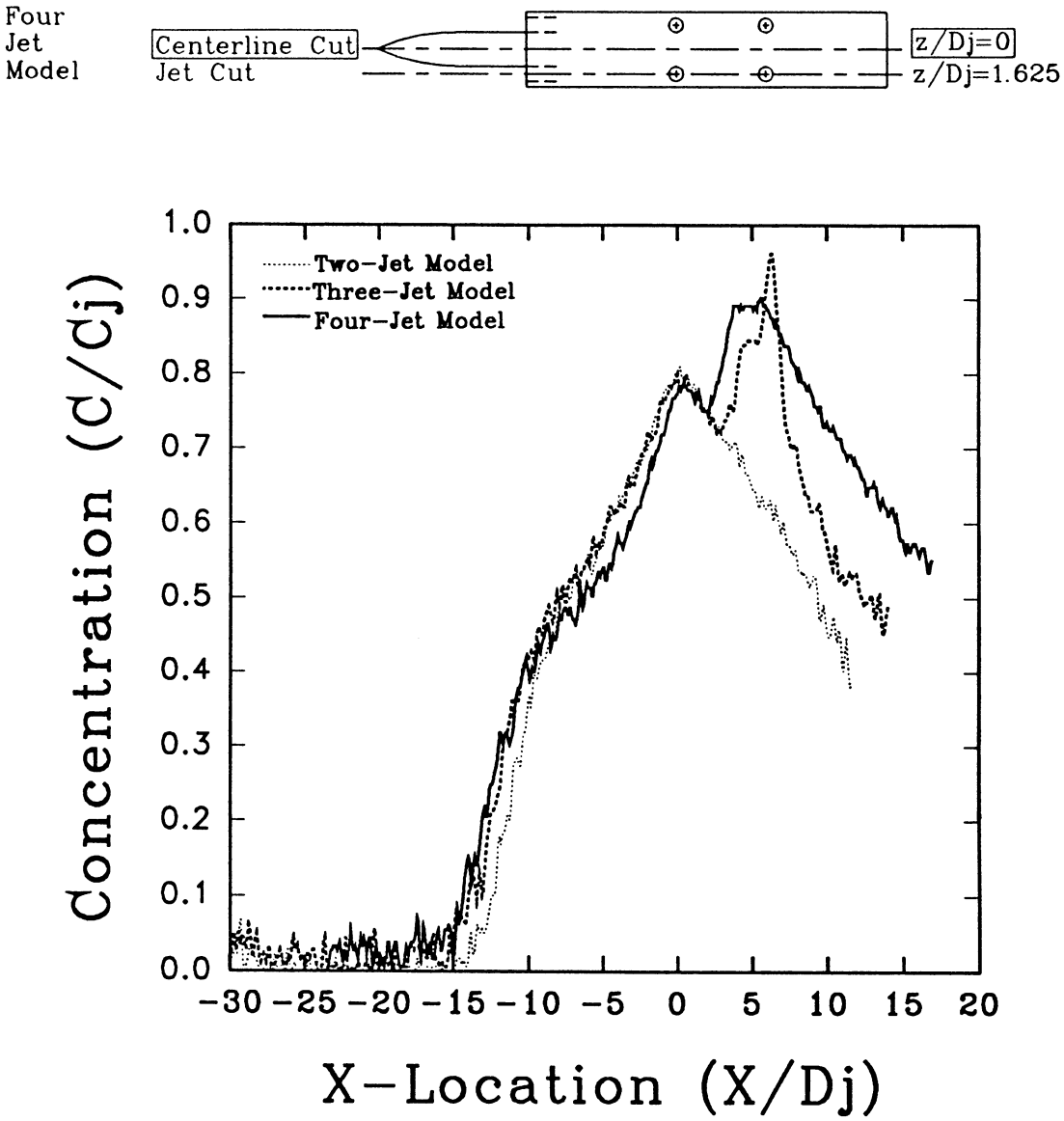

Figure 4.31 Two-, Three-, Four-Jet 127-Frame Average Concentration Profiles at Model Centerline: $z/D_j=0$ Laser Sheet at $y/D_j=0.6$, $H/D_j=6$, $U/V_j=0.09$

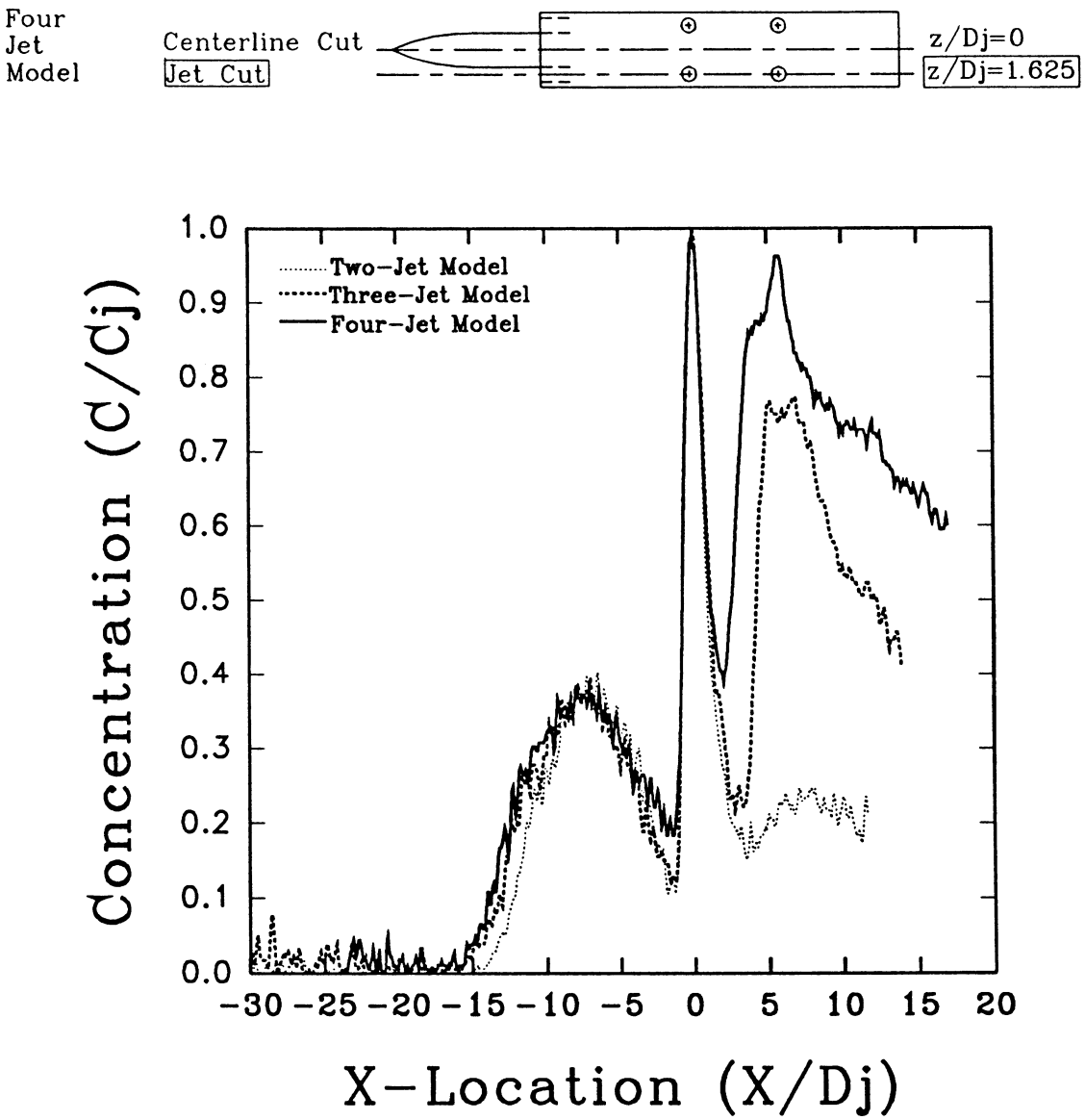

Figure 4.32 Two-, Three-, Four-Jet 127-Frame Average Concentration Profiles at Jet Centerline: z/D_j=1.625 Laser Sheet at y/D_j=0.6, H/D_j=6, U/V_j=0.09

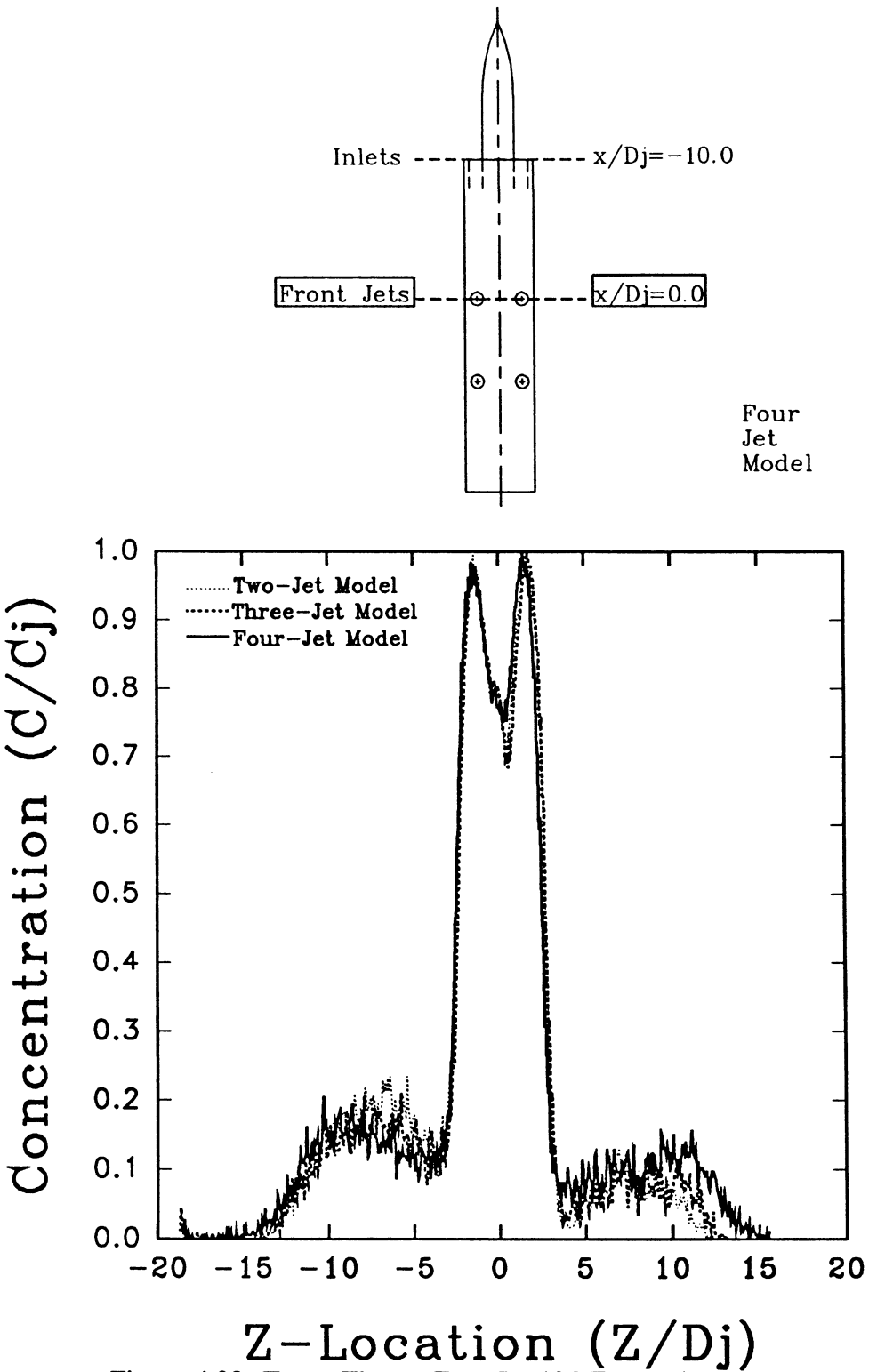

Figure 4.33 Two-, Three-, Four-Jet 127-Frame Average Concentration Profiles at Forward Jet Centerline: $x/D_j=0$ Laser Sheet at $y/D_j=0.6$, $H/D_j=6$, $U/V_j=0.09$

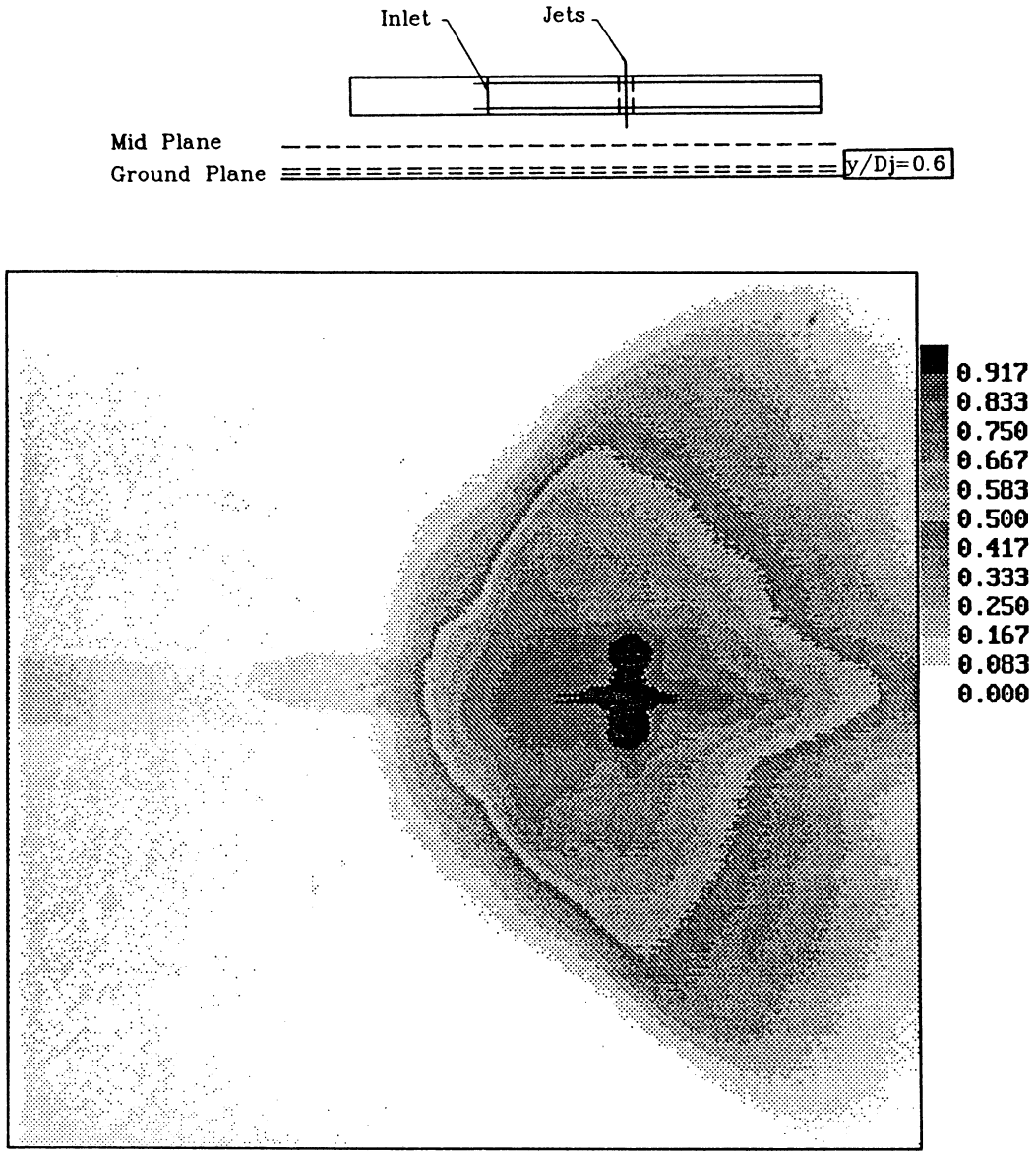

Figure 4.34 Two-Jet 127-Frame Average Image of Smoke Concentration at y/D_j=0.6 Plane
H/D_j=2, U/V_j=0.09

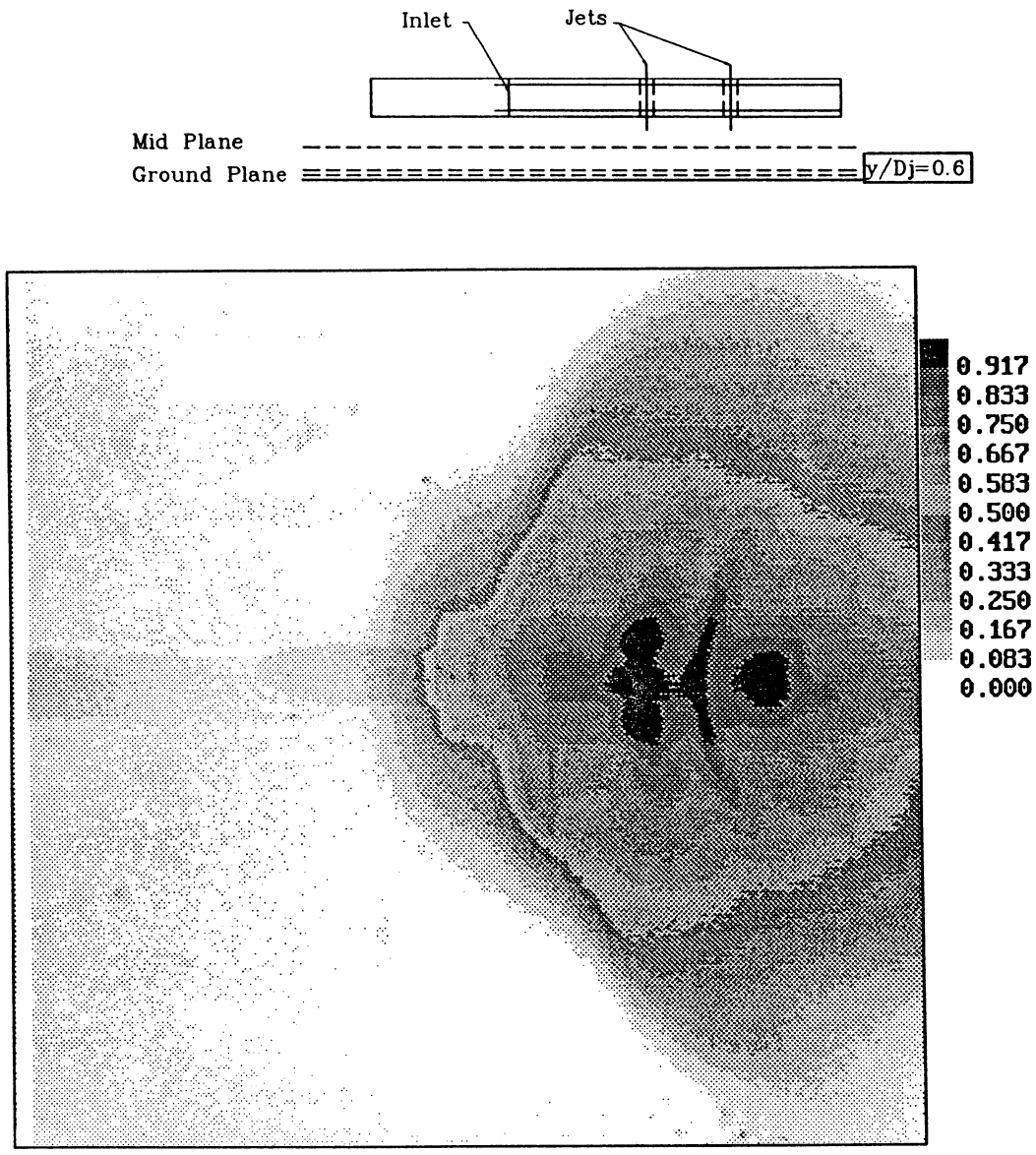

Figure 4.35 Three-Jet 127-Frame Average Image of Concentration at y/D_j=0.6 Plane
H/D_j=2, U/V_j=0.09

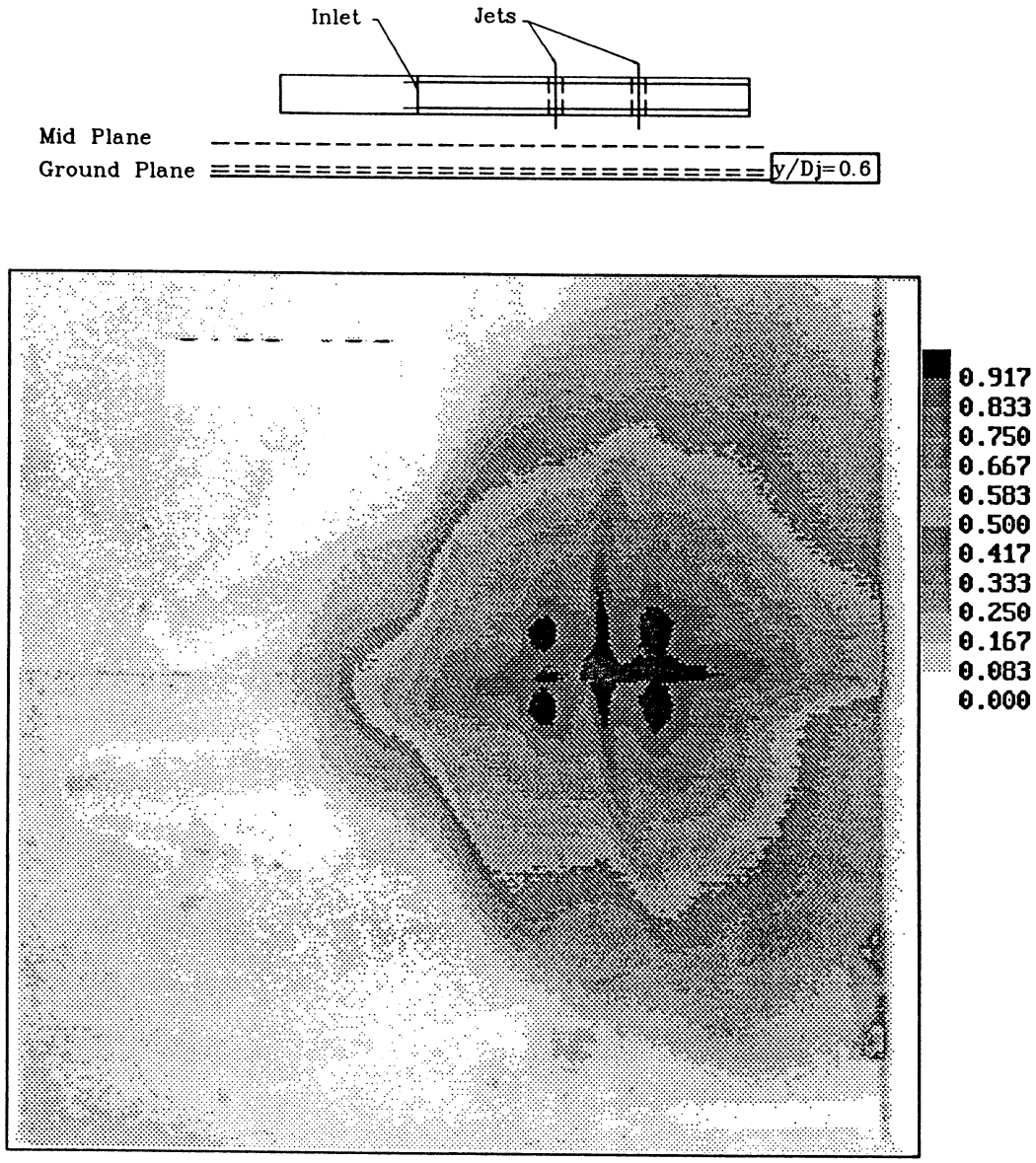

Figure 4.36 Four-Jet 127-Frame Average Image of Concentration at y/D_j=0.6 Plane
H/D_j=2, U/V_j=0.09

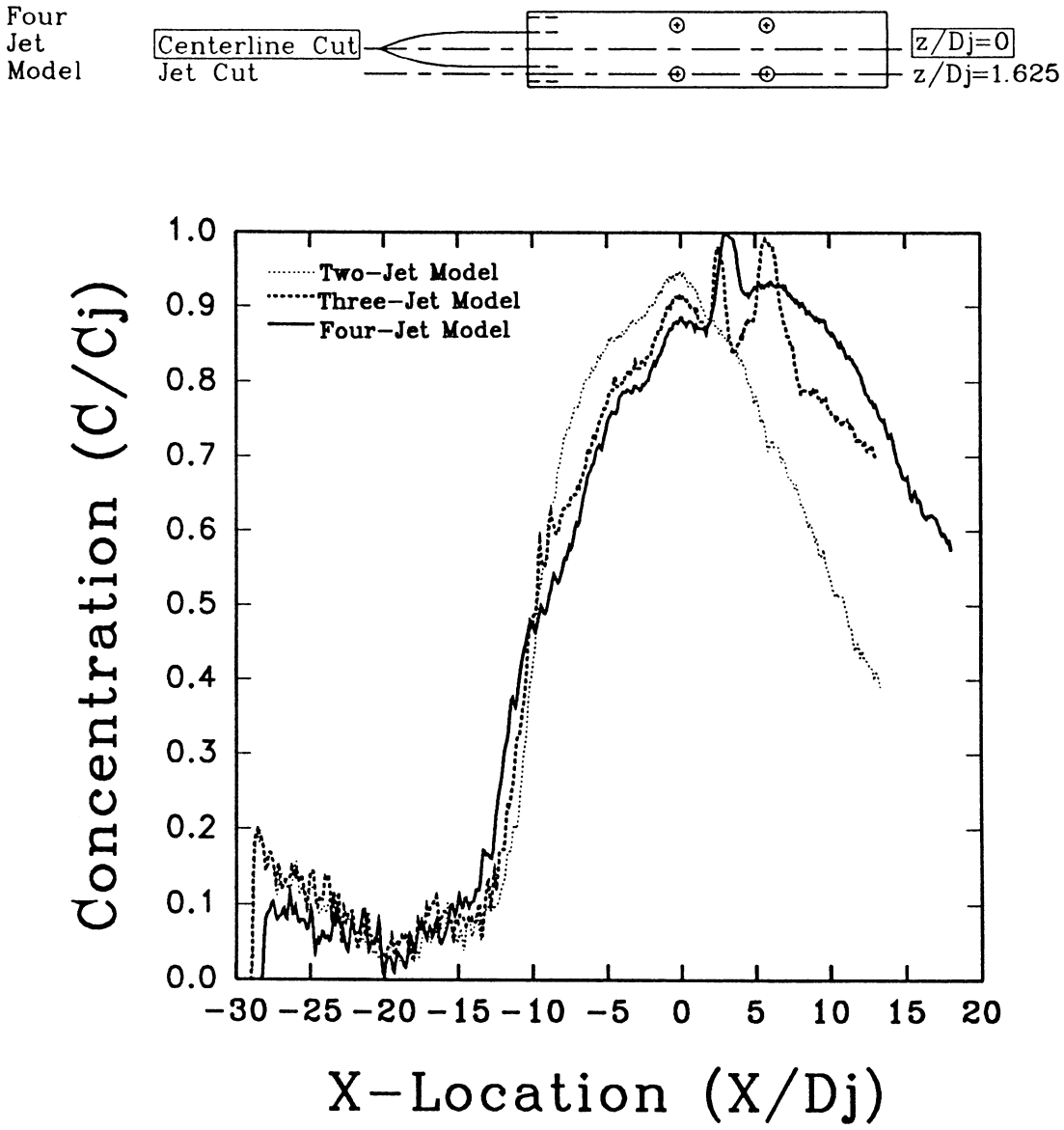

Figure 4.37 Two-, Three-, Four-Jet 127-Frame Average Concentration Profiles at Model Centerline: $z/D_j=0$ Laser Sheet at Ground Plane: $y/D_j=0.6$, $H/D_j=2$, $U/V_j=0.09$

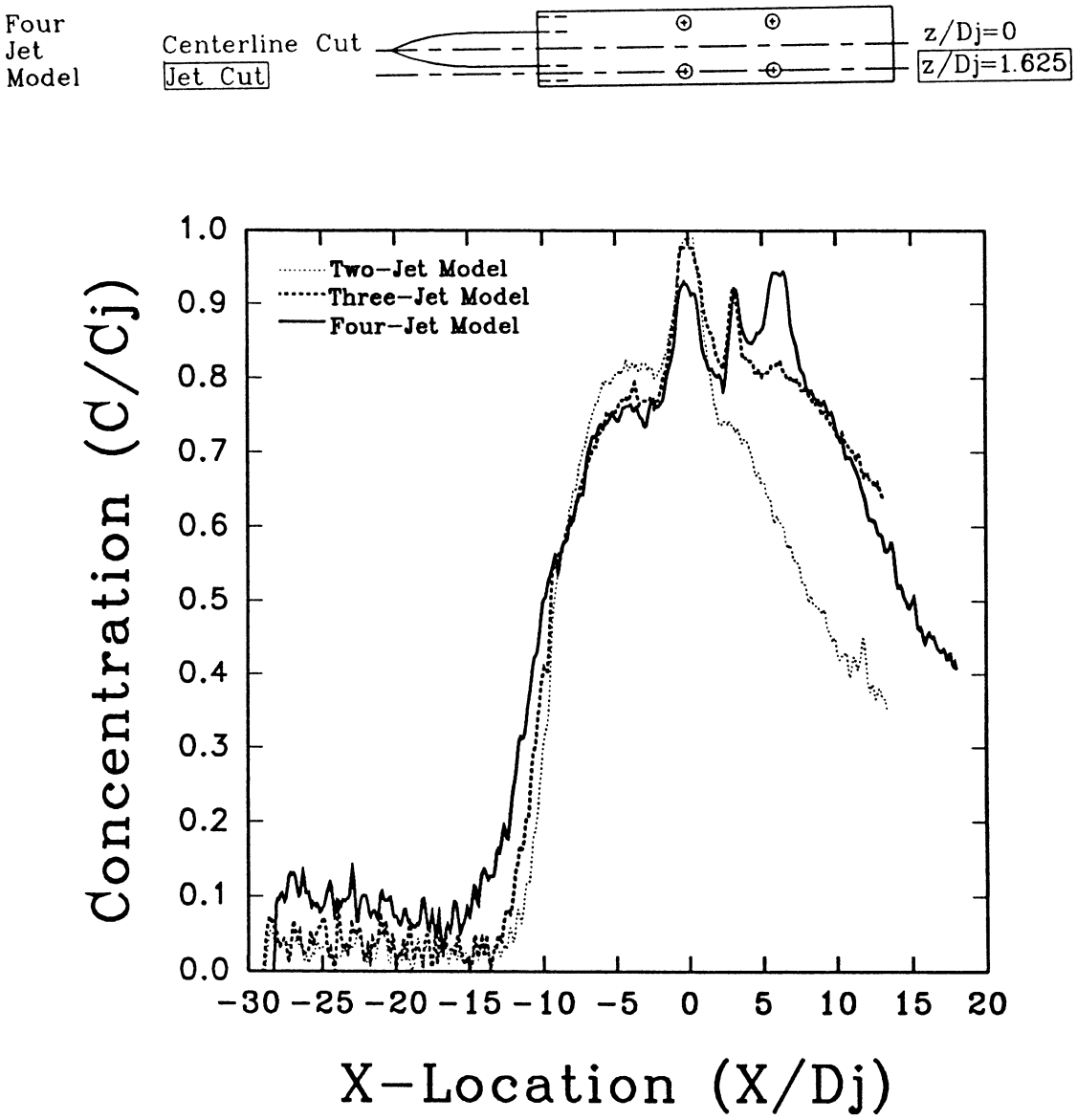

Figure 4.38 Two-, Three-, Four-Jet 127-Frame Average Concentration Profiles at Jet Centerline: z/D_j=1.625 Laser Sheet at Ground Plane: y/D_j=0.6, H/D_j=2, U/V_j=0.09

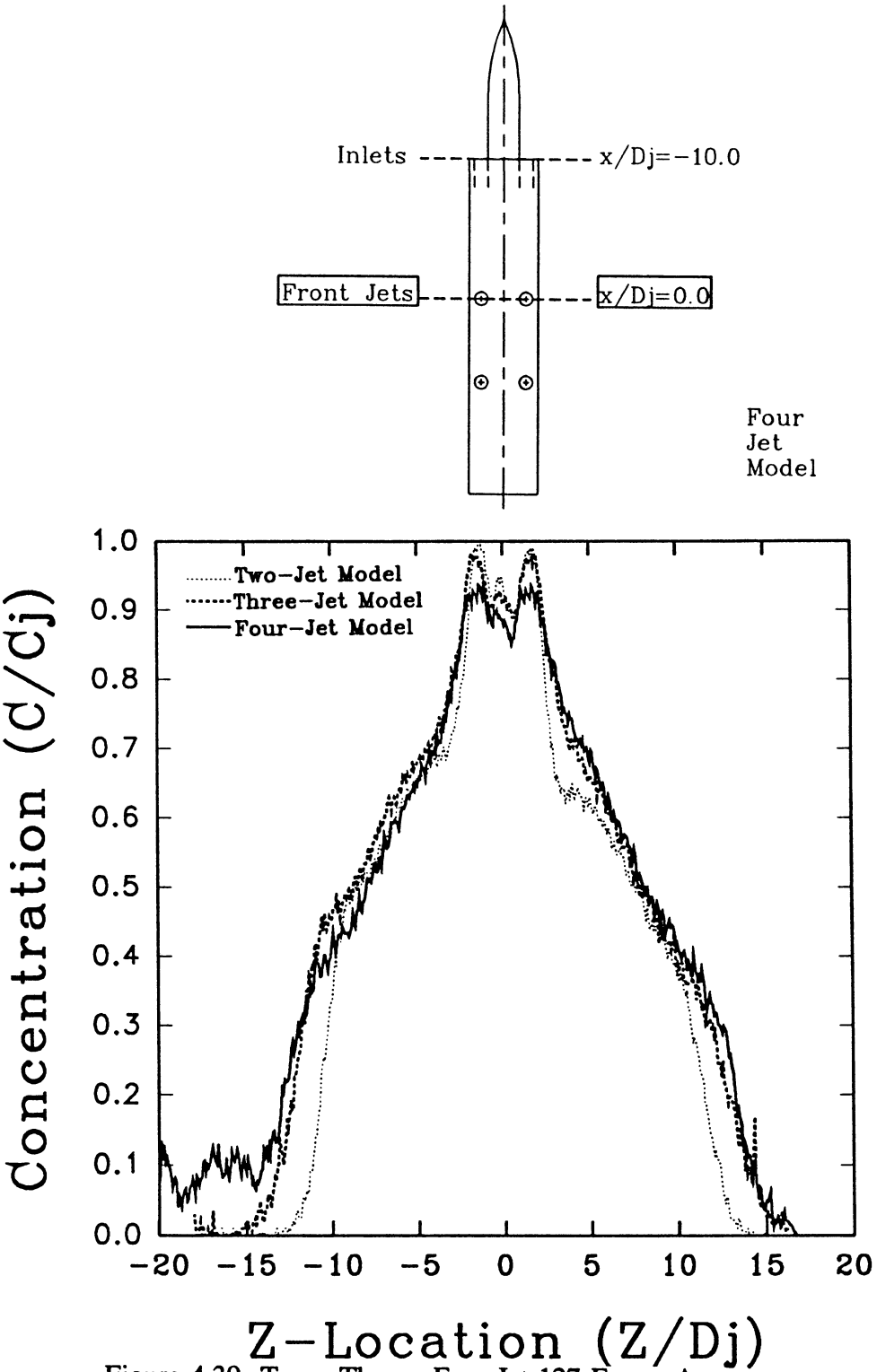

Figure 4.39 Two-, Three-, Four-Jet 127-Frame Average Concentration Profiles at Forward Jet Centerline: $x/D_j=0$ Laser Sheet at Ground Plane: $y/D_j=0.6$, $H/D_j=2$, $U/V_j=0.09$

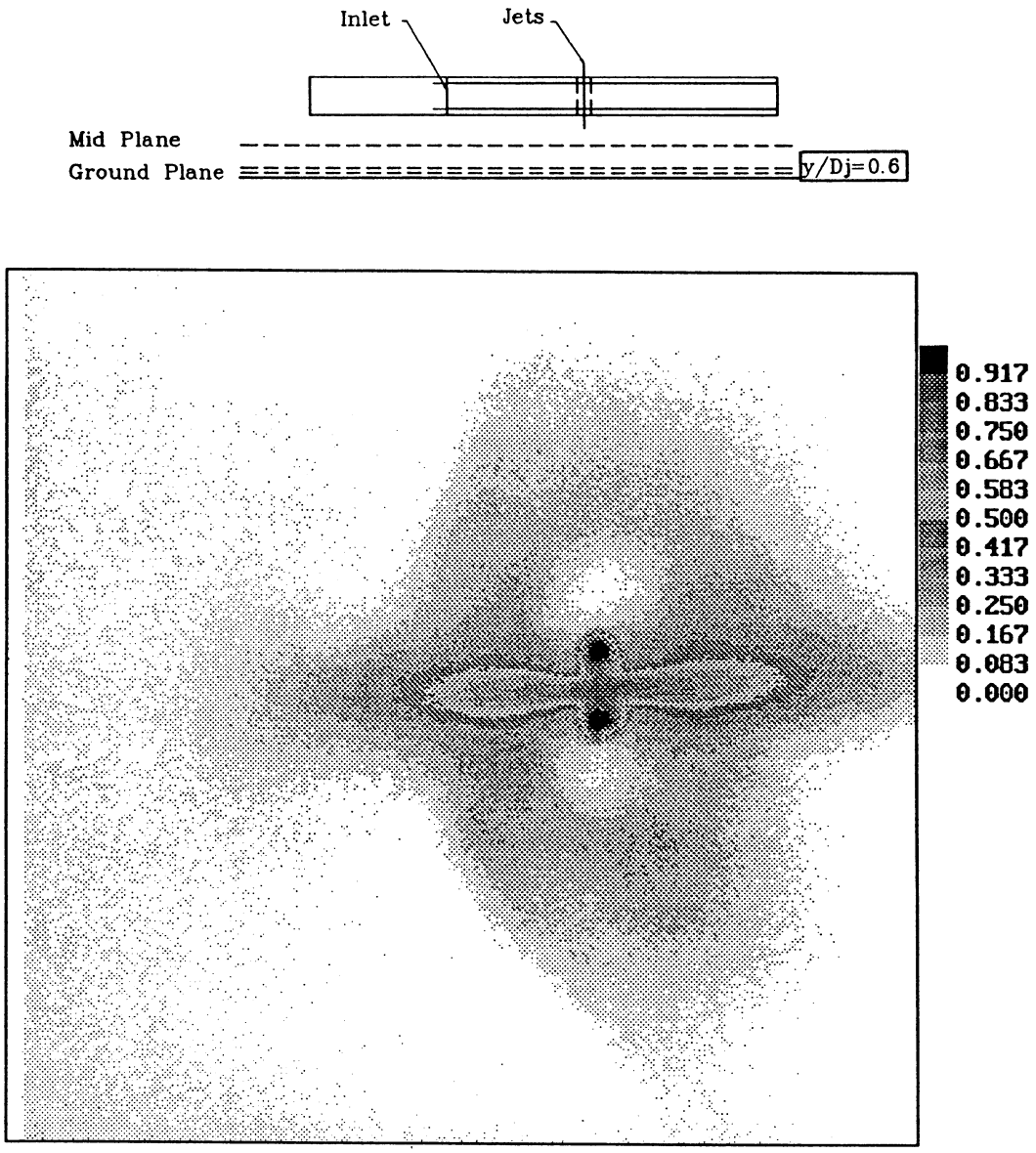

Figure 4.40 Two-Jet 127-Frame Average Image of Smoke Concentration at y/D_j=0.6 with Inlet Suction H/D_j=4, U/V_j=0.03

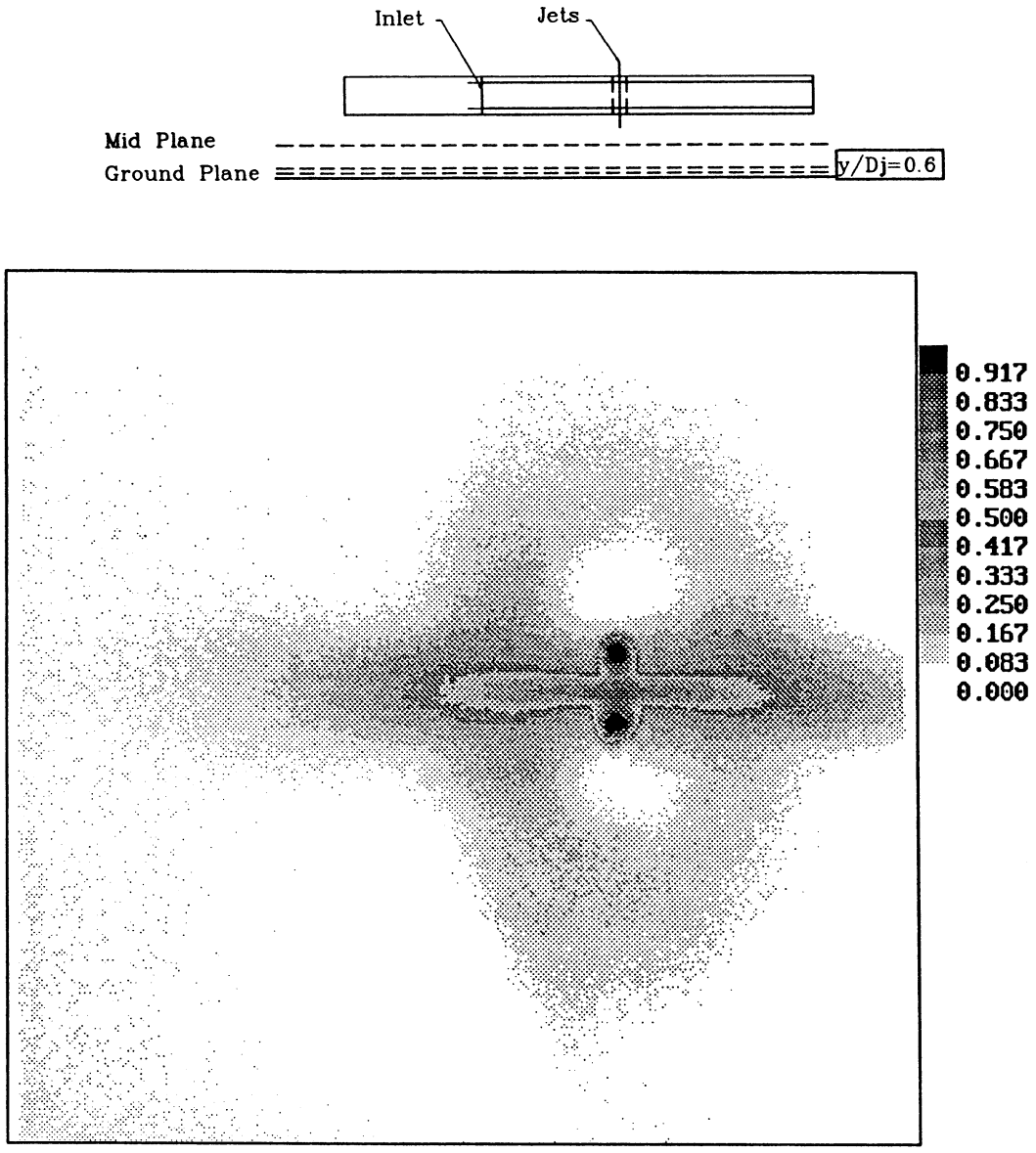

Figure 4.41 Two-Jet 127-Frame Average Image of Smoke Concentration at y/D_j=0.6 without Inlet Suction H/D_j=4, U/V_j=0.03

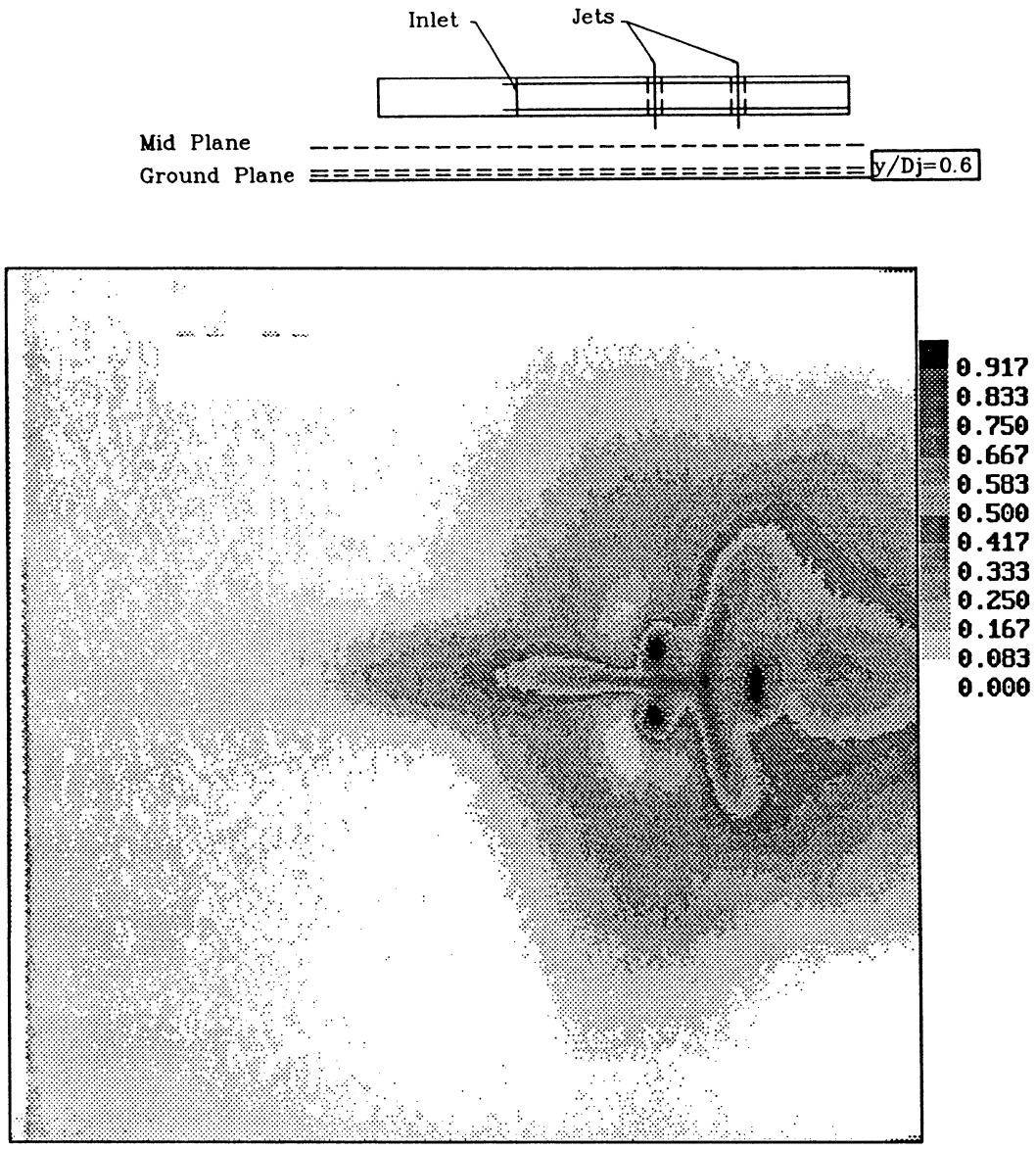

Figure 4.42 Three-Jet 127-Frame Average Image of Smoke Concentration at y/D_j=0.6 with Inlet Suction H/D_j=4, U/V_j=0.03

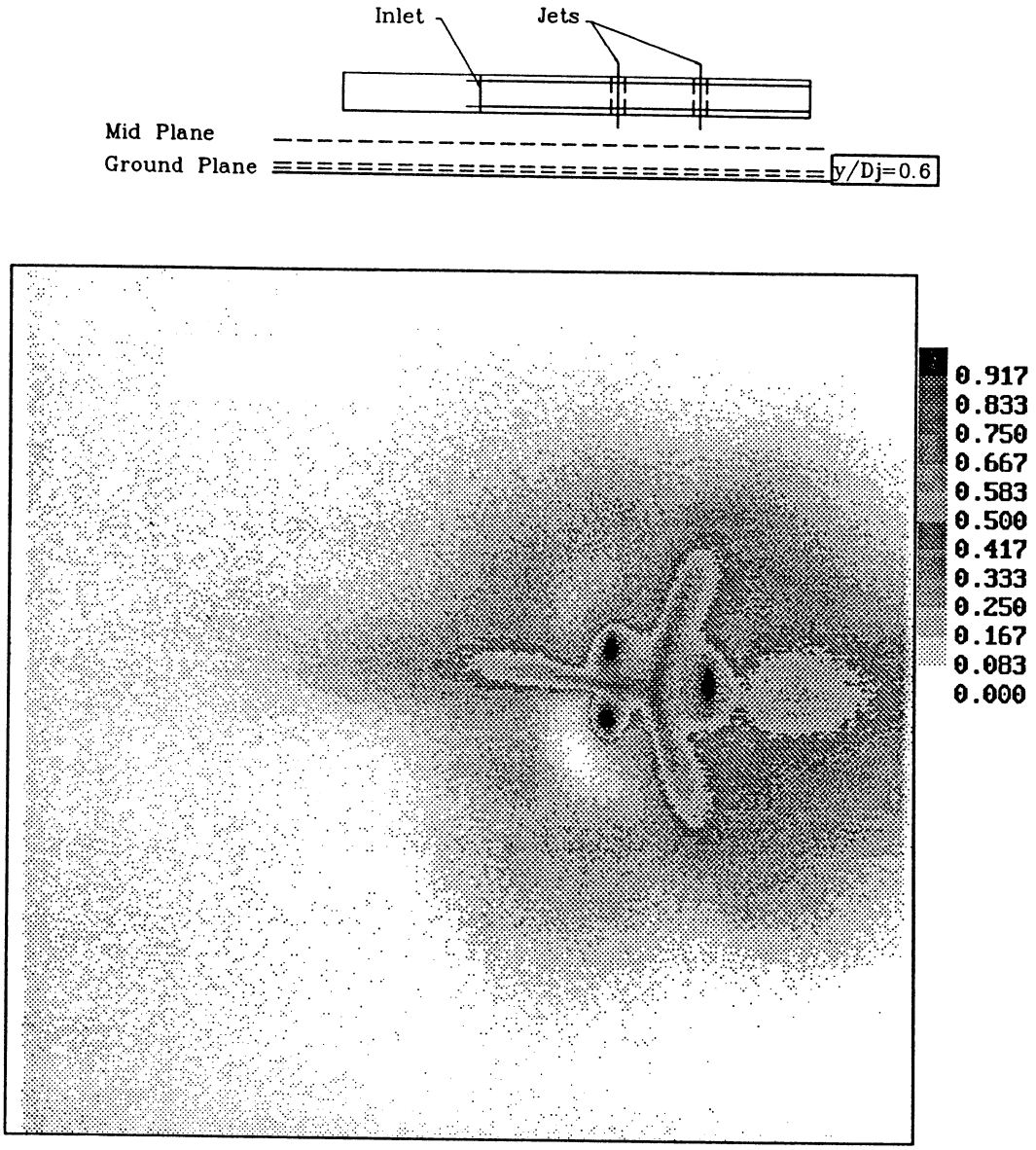

Figure 4.43 Three-Jet 127-Frame Average Image of Smoke Concentration at y/D_j=0.6 without Inlet Suction H/D_j=4, U/V_j=0.03

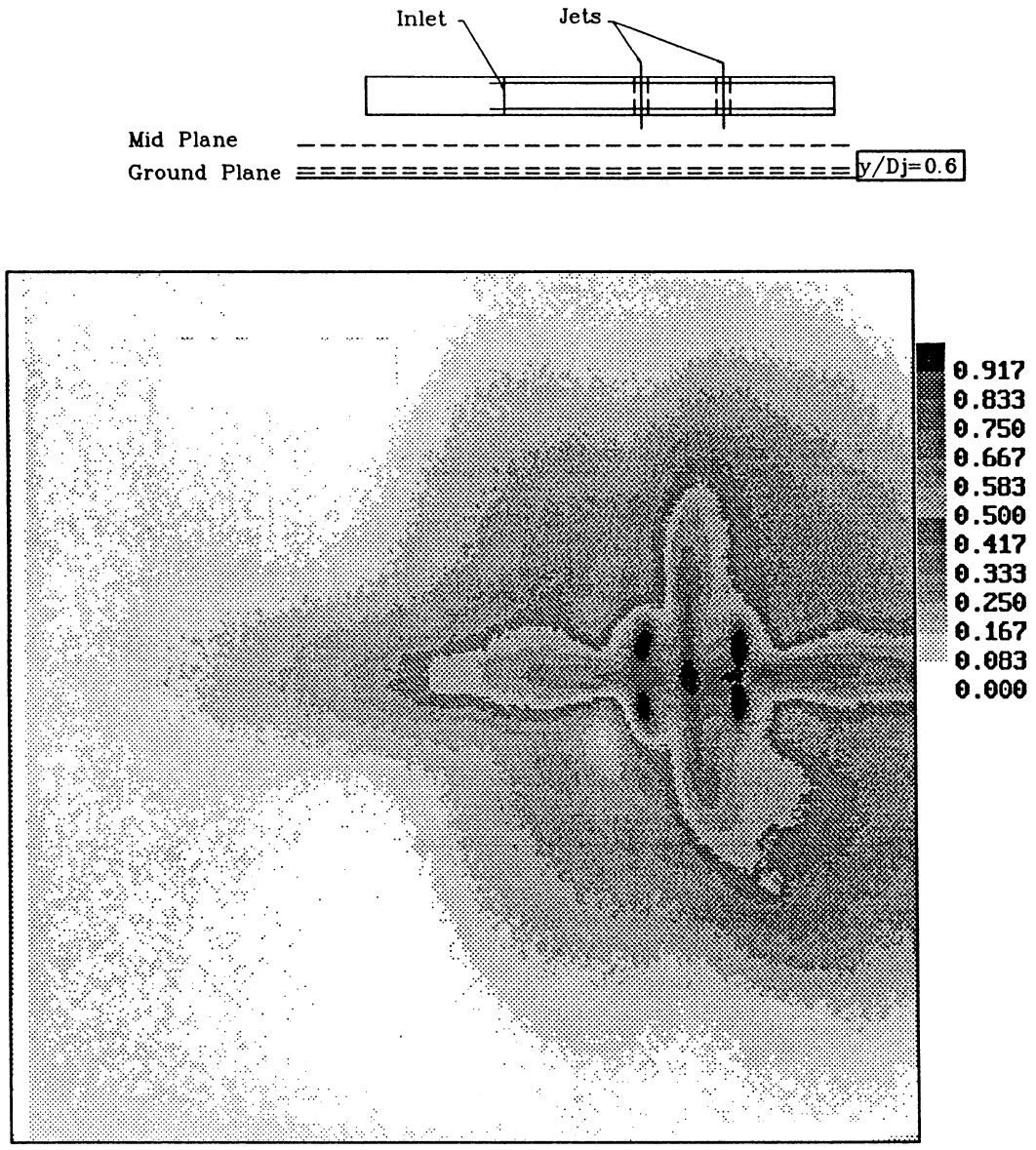

Figure 4.44 Four-Jet 127-Frame Average Image of Smoke Concentration at y/D_j=0.6 with Inlet Suction H/D_j=4, U/V_j=0.03

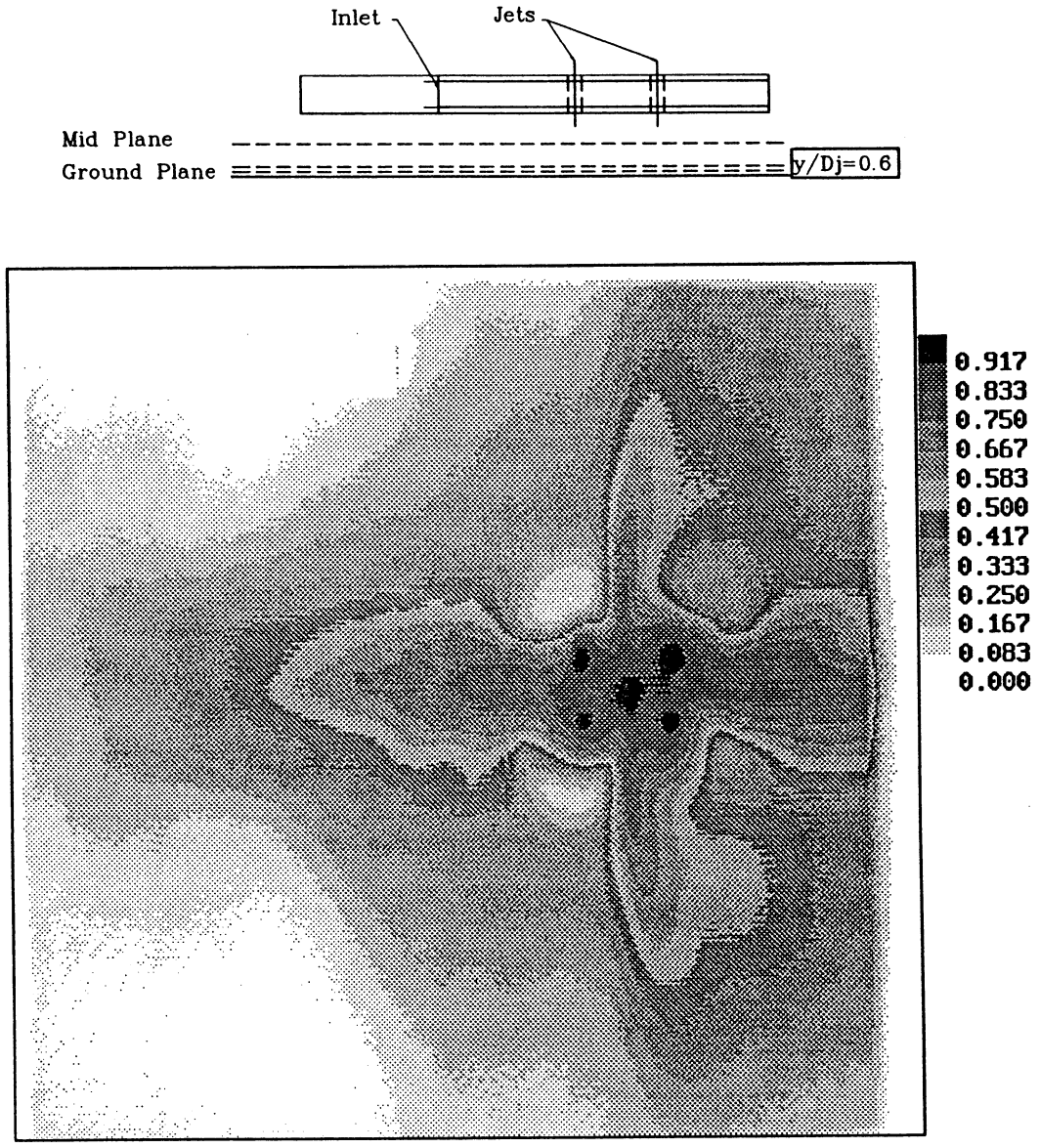

Figure 4.45 Four-Jet 127-Frame Average Image of Smoke Concentration at y/D_j=0.6 without Inlet Suction H/D_j=4, U/V_j=0.03

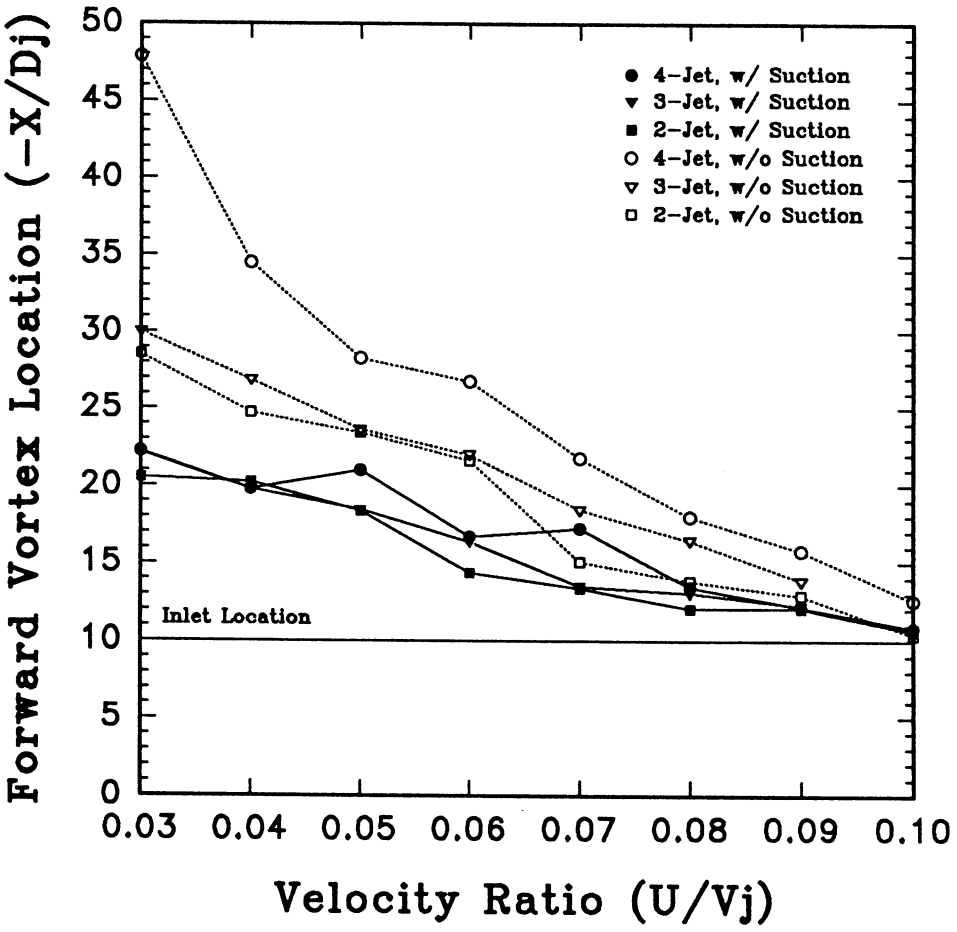

Figure 4.46 Two-, Three-, Four-Jet
Forward Vortex Pair Location Versus Velocity Ratio (U/V_j)
With and Without Inlet Suction
y/D_j=0.6, H/D_j=2.0

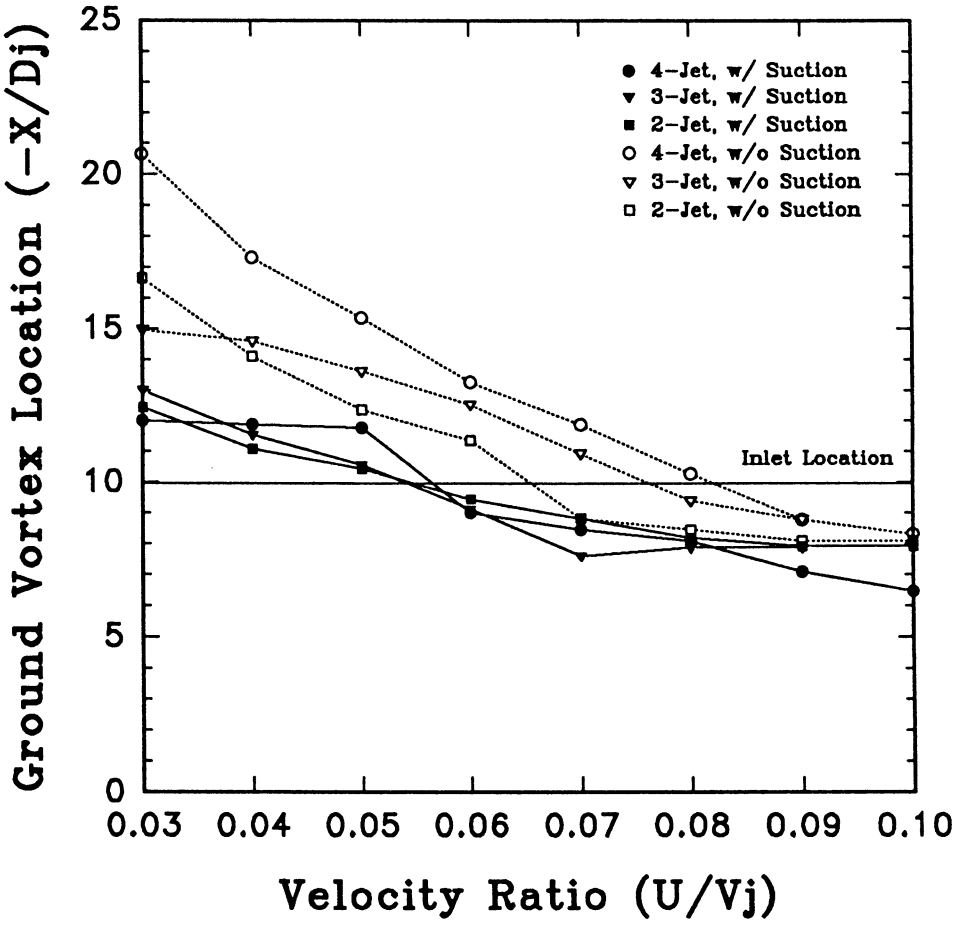

Figure 4.47 Two-, Three-, Four-Jet
Ground Vortex Location Versus Velocity Ratio (U/V_j)
With and Without Inlet Suction
y/D_j=0.6, H/D_j=2.0

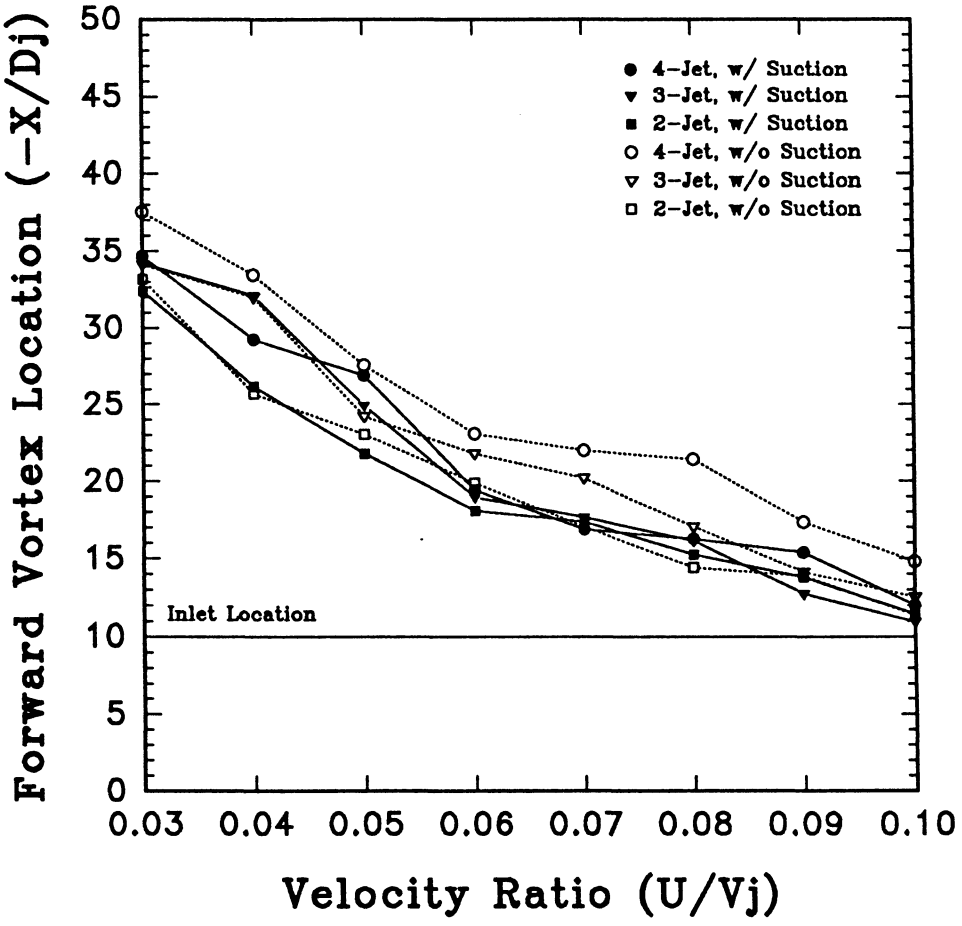

Figure 4.48 Two-, Three-, Four-Jet
Forward Vortex Pair Location Versus Velocity Ratio (U/V_j)
With and Without Inlet Suction
y/D_j=0.6, H/D_j=4.0

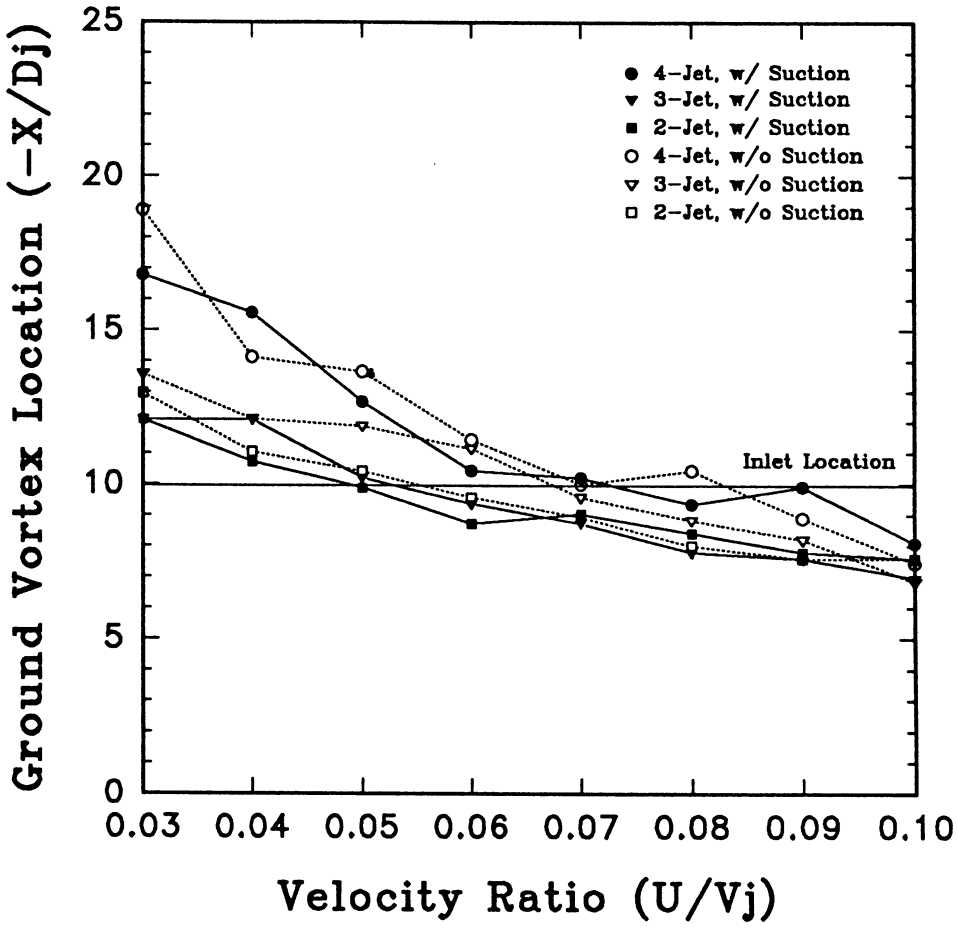

Figure 4.49 Two-, Three-, Four-Jet
Ground Vortex Location Versus Velocity Ratio (U/V_j)
With and Without Inlet Suction
y/D_j=0.6, H/D_j=4.0

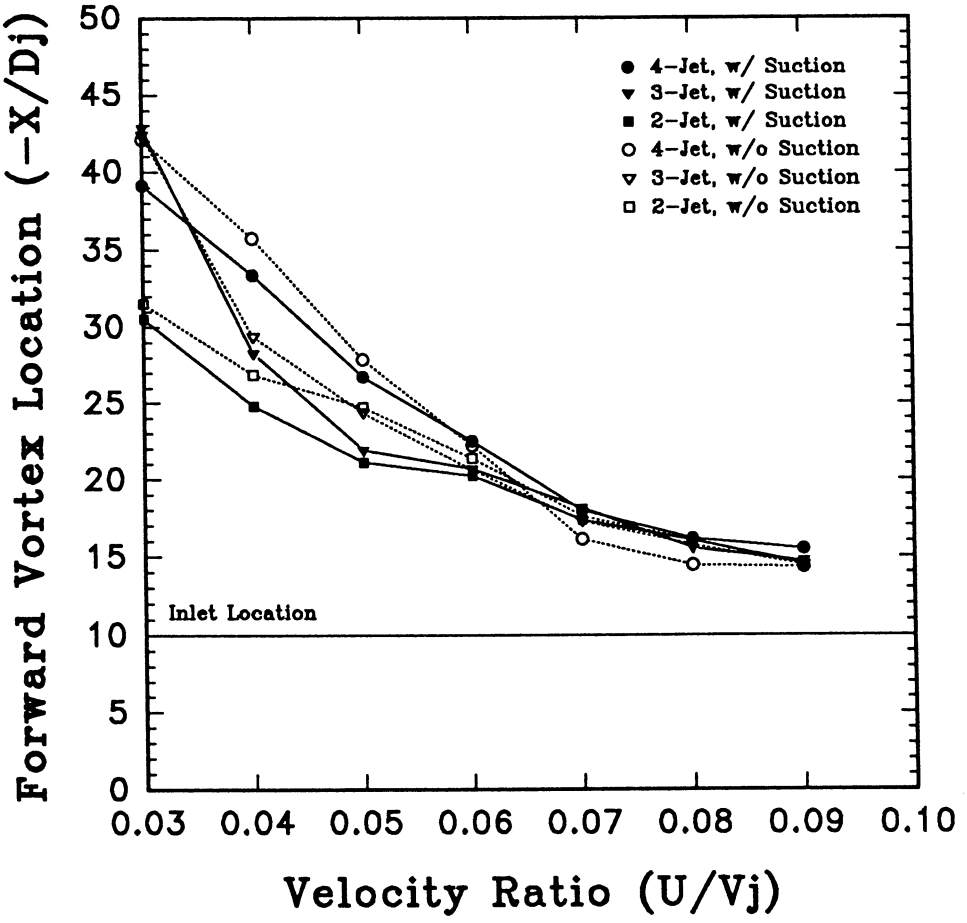

Figure 4.50 Two-, Three-, Four-Jet
Forward Vortex Pair Location Versus Velocity Ratio (U/V_j)
With and Without Inlet Suction
y/D_j=0.6, H/D_j=6.0

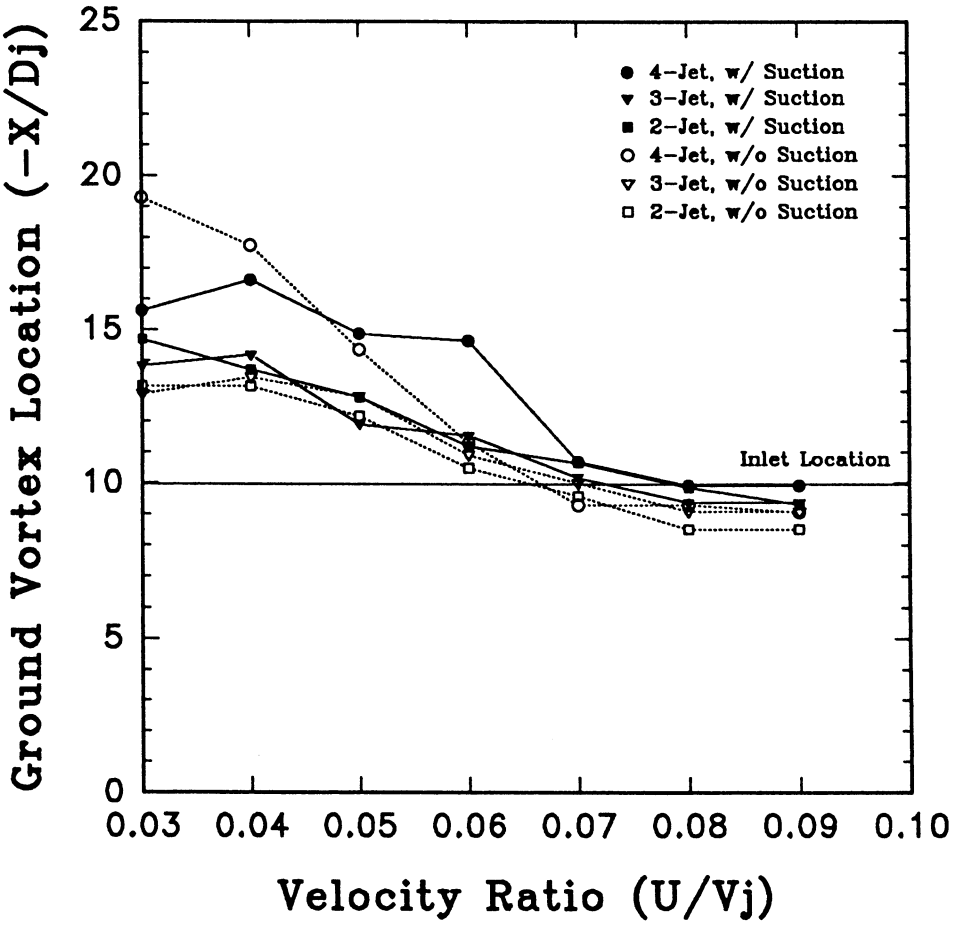

Figure 4.51 Two-, Three-, Four-Jet
Ground Vortex Location Versus Velocity Ratio (U/V_j)
With and Without Inlet Suction
y/D_j=0.6, H/D_j=6.0

CHAPTER 5

LOW SPEED - TWO- AND THREE-JET INLET STUDY

Below, constructed three-dimensional images of averaged concentration at the inlet entry plane for the two- and three-jet low speed models under different conditions are discussed. The effect of model height was seen to greatly effect ingestion concentration levels while configuration had a small effect. Table 5.1 gives a summary of the cases discussed and their conditions which will be referred to by case number below. Appendix C gives equivalent two-dimensional concentration contour plots for the three-dimensional projections given below to aid in the overall study.

5.1 Two-Jet Configuration

Figures 5.1 and 5.2 show constructed images at the two-jet inlet entrance plane at a model height of H/D_j=4.0 for cases 5.1 and 5.2 respectively. From the video tape, it was seen that ingestion was not a continuous process, but rather an intermittent one, especially in the upper portion of the inlets.

The averaged results in general showed that there were higher concentrations in the lower inside corner of the inlets. The fountain flow that impinges on the model undersurface, flows forward to the inlet vicinity. Furthermore, since the jet configurations were symmetric, the majority of undersurface upstream flow would be

along the centerline and would enter the inlets in the lower corners. Limage [26] noted in a correlation study that the fountain was the main, if not the only, source of near field ingestion.

It should be noted that at U/V_j=0.09, the far field structures (ground vortex and forward vortex pair) were located nearly directly below the model inlets. A question of terminology comes into play as to whether they may still be considered as far field structures. Furthermore, since they were so close to the inlets, they would have caused higher concentrations in the lower portion of the inlets. Therefore, the near and "far" field ingestion contributions would be difficult, if not impossible, to distinguish between.

In comparison to case 5.2, the higher velocity ratio case, case 5.1 had higher concentration near the nose cone and higher in the inlet. It was noted in the video that the smoke was being drawn into the inlet from upstream along the nose cone thus yielding the higher concentration near the sides and indicating that far field ingestion was occurring.

Also, it is noted that case 5.1 had higher concentrations than case 5.2. Work done Tafti and Vanka [45] on an equivalent numerical model for the four-jet model, agreed with this trend. The major difference from the numerical work was the underprediction of the concentration in the 0.09 cases. An explanation for this may be that the numerical cases underpredicted the degree of upstream penetration of the vortex structures.

Cases 5.3 and 5.4, shown in figures 5.3 and 5.4, were at a decreased model height of H/D_j=2.0. In these cases, the U/V_j=0.09 case had higher concentrations than

U/V_j=0.03 case. The forward vortex pair was seen in the video to be directly below the inlet and it increased the ingestion levels to a maximum of just over 62% of the jet concentration, as seen in figure 5.4. The reason for the higher concentrations was that the model was closer the ground. At U/V_j=0.03, the vortical structures were further upstream and thus yielded lower inlet concentrations than in the U/V_j=0.09 case.

The averaged concentrations at the inlet entrance plane at an increased model height of H/D_j=6.0 are shown in figures 5.5 and 5.6 from cases 5.5 and 5.6. The maximum concentrations for the lower velocity ratio case, figure 5.5 and case 5.5, was about 15% of the jet concentration which was comparable to 14% for the H/D_j=4.0 case. The concentrations however were not as distributed in the inlet plane as they were at lower model heights, indicating that the model was almost out of ground effect, at least with respect to reingestion. For the U/V_j=0.09 case, figure 5.6 and case 5.6, it was clear that the vortical structures were almost entirely downstream of the inlet. This was indicated by a maximum concentration of only 3% of the jet concentration at the inlets. Only weak fountain flow from the near field and possibly some flow from the vortical structures in the "far" field contributed to the concentrations at the inlets at the U/V_j=0.09 case.

5.2 Three-Jet Configuration

Figures 5.7 and 5.8 show constructed images at the inlet entrance plane for the two-jet cases, 5.7 and 5.8 respectively. Limage [26] showed in the comparison of two-, three- and four-jet configurations, that the two-jet configuration produced the minimum

upward fountain flow. It was also noted in Chapter 4, that the two-jet structures were more swept back than in the three-jet case due to the lower total momentum. Therefore, at U/V_j=0.09, the two-jet flow on the underside of the model and the ground structures were swept further out of the inlet entrainment region than in the three jet case. These are given as the reasons for the lower concentrations in case 5.2 verses case 5.8. The three jet case had nearly twice the maximum concentration of the two jet case.

At U/V_j=0.03, the two- and three-jet cases had the same maximum concentration, cases 5.1 and 5.7 respectively. In comparison to the U/V_j=0.09 cases, these cases had higher concentration near the nose cone and higher in the inlet and again indicate far field ingestion.

Case Number	Jet Velocity (ft/s)	Velocity Ratio U/V_j	Model Height H/D_j	Laser Sheet Height y/D_j	Number of Jets	Inlet Suction
5.1	75.0	0.03	4.0	Inlet Planes	2	Yes
5.2	75.0	0.09	4.0	Inlet Planes	2	Yes
5.3	75.0	0.03	2.0	Inlet Planes	2	Yes
5.4	75.0	0.09	2.0	Inlet Planes	2	Yes
5.5	75.0	0.03	6.0	Inlet Planes	2	Yes
5.6	75.0	0.09	6.0	Inlet Planes	2	Yes
5.7	75.0	0.03	4.0	Inlet Planes	3	Yes
5.8	75.0	0.09	4.0	Inlet Planes	3	Yes

Table 5.1 Test Cases for Low Speed - Two- and Three-Jet Inlet Study

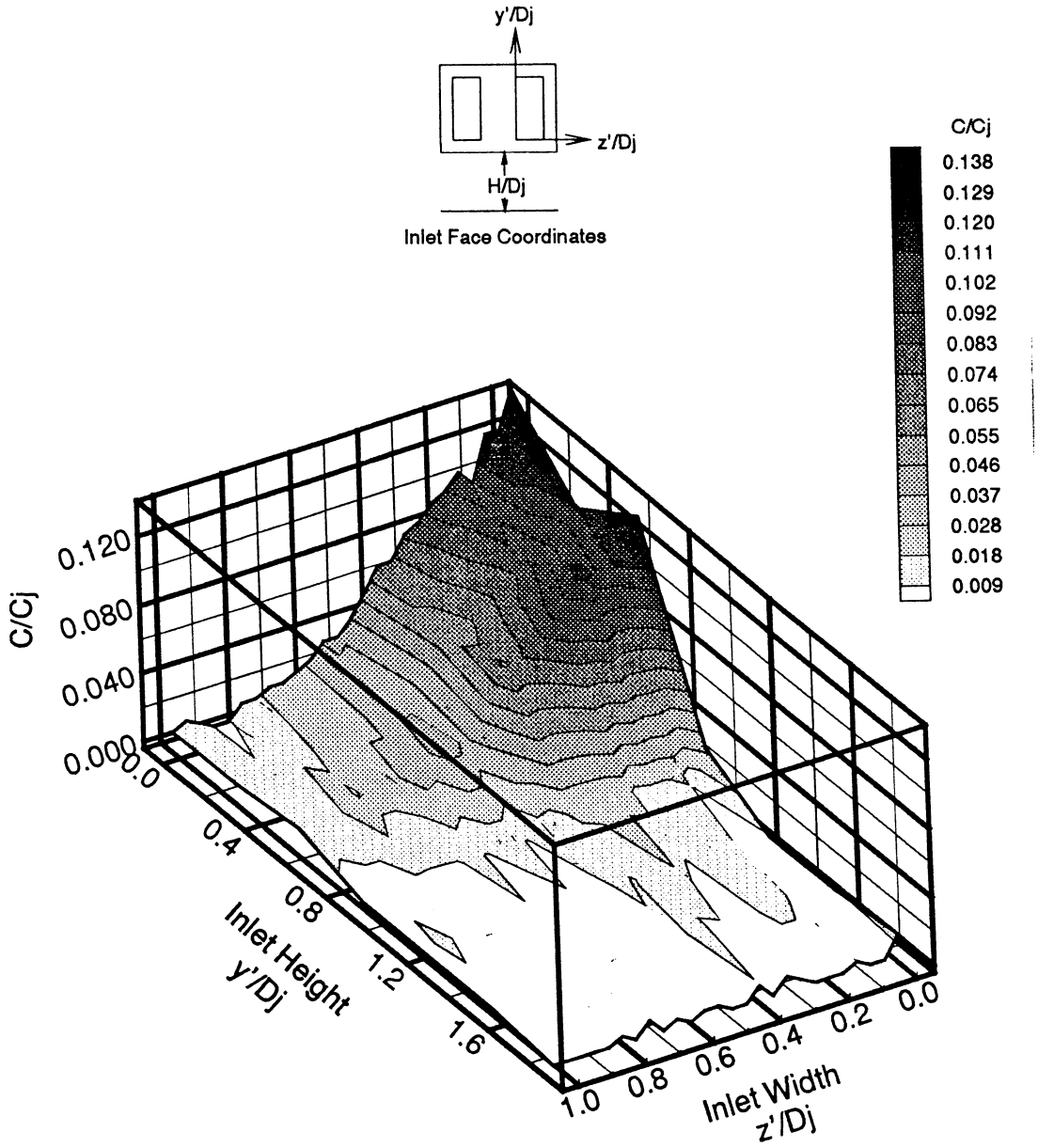

Figure 5.1 Low Speed Two-Jet Average Smoke Concentration at the Inlet Face
Plane [z'y']: H/D_j=4, U/V_j=0.03

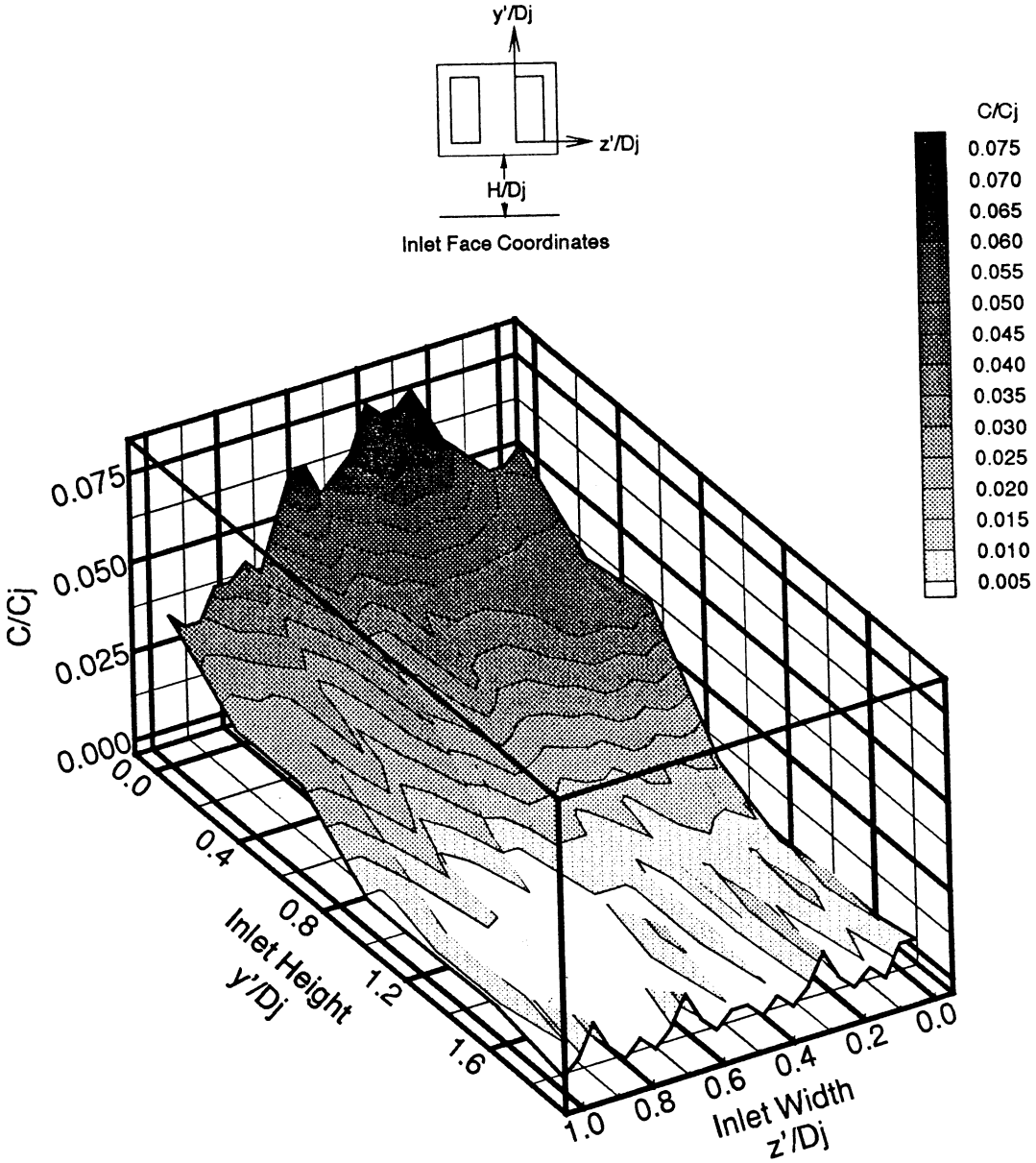

Figure 5.2 Low Speed Two-Jet Average Smoke Concentration at the Inlet Face Plane [z'y']: H/D_j=4, U/V_j=0.09

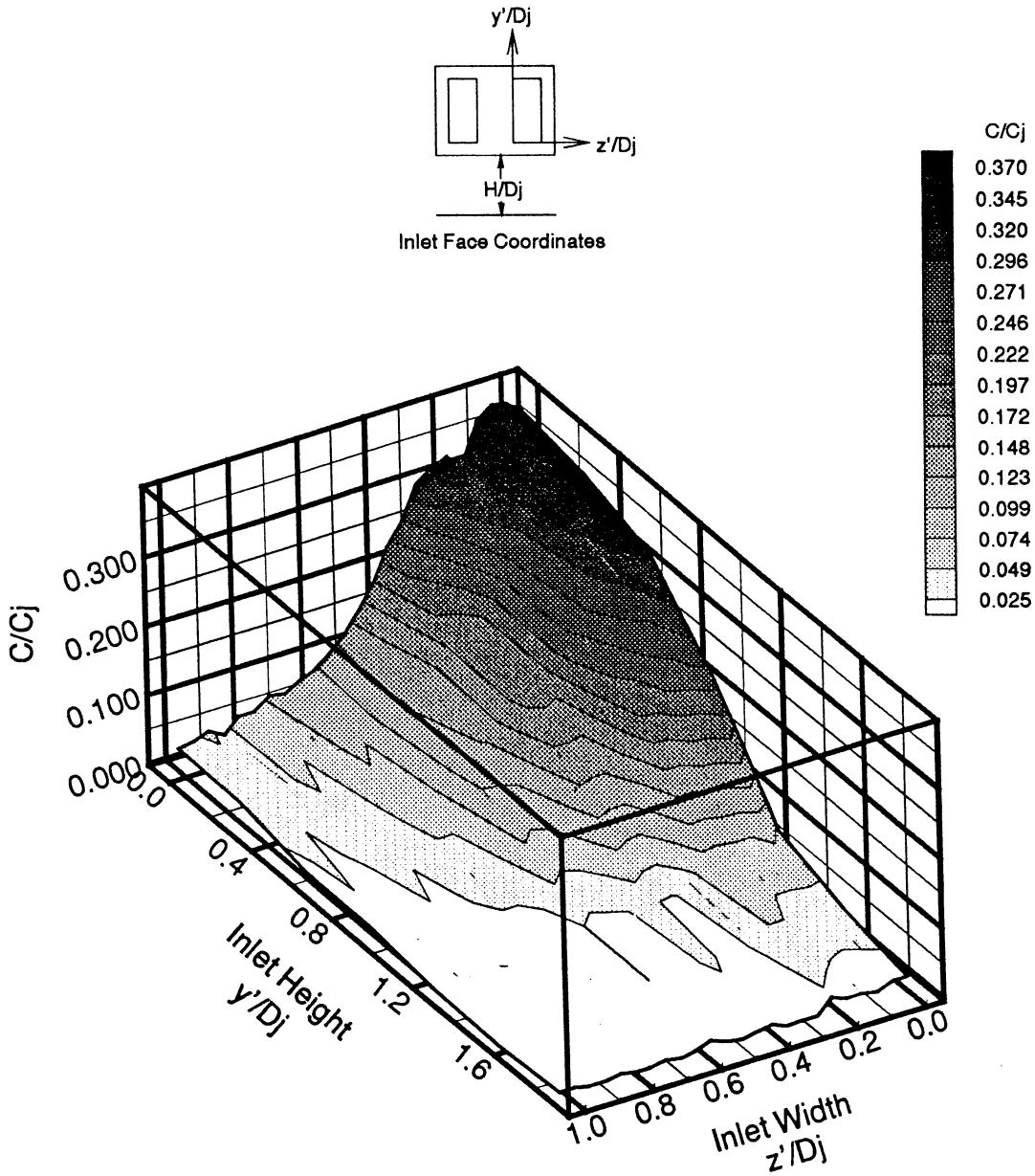

Figure 5.3 Low Speed Two-Jet Average Smoke Concentration at the Inlet Face
Plane [z'y']: H/D_j=2, U/V_j=0.03

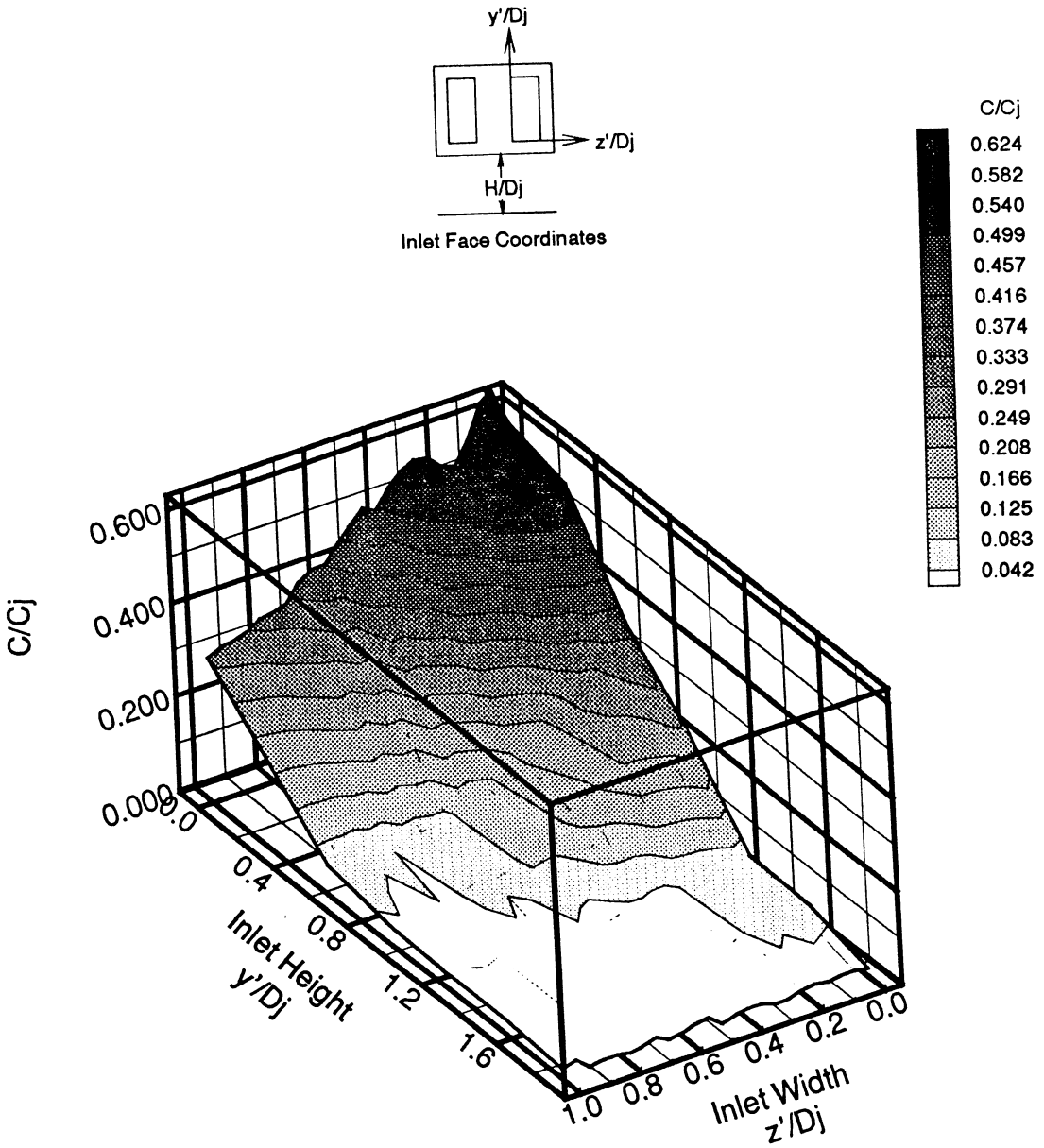

Figure 5.4 Low Speed Two-Jet Average Smoke Concentration at the Inlet Face
Plane [z'y']: $H/D_j=2$, $U/V_j=0.09$

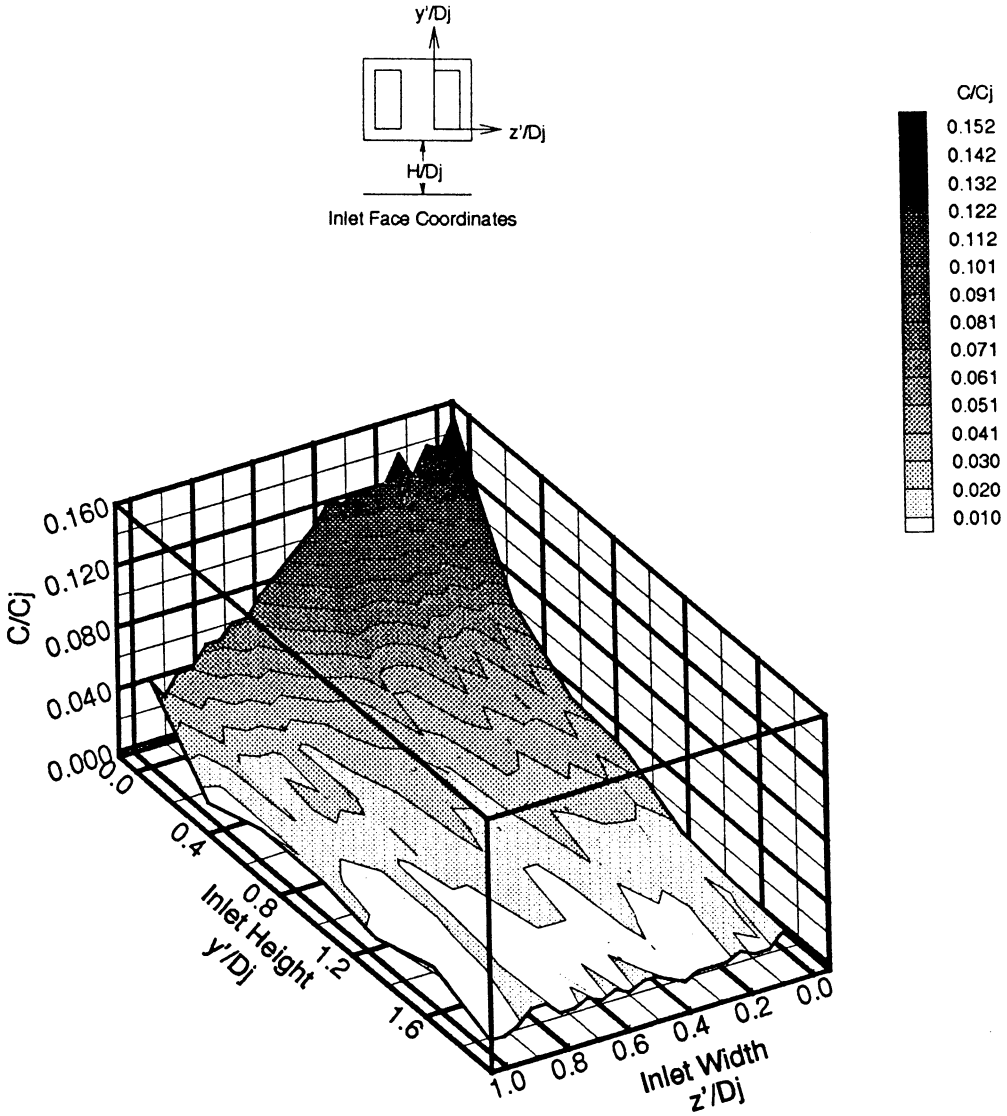

Figure 5.5 Low Speed Two-Jet Average Smoke Concentration at the Inlet Face Plane [z'y']: $H/D_j=6$, $U/V_j=0.03$

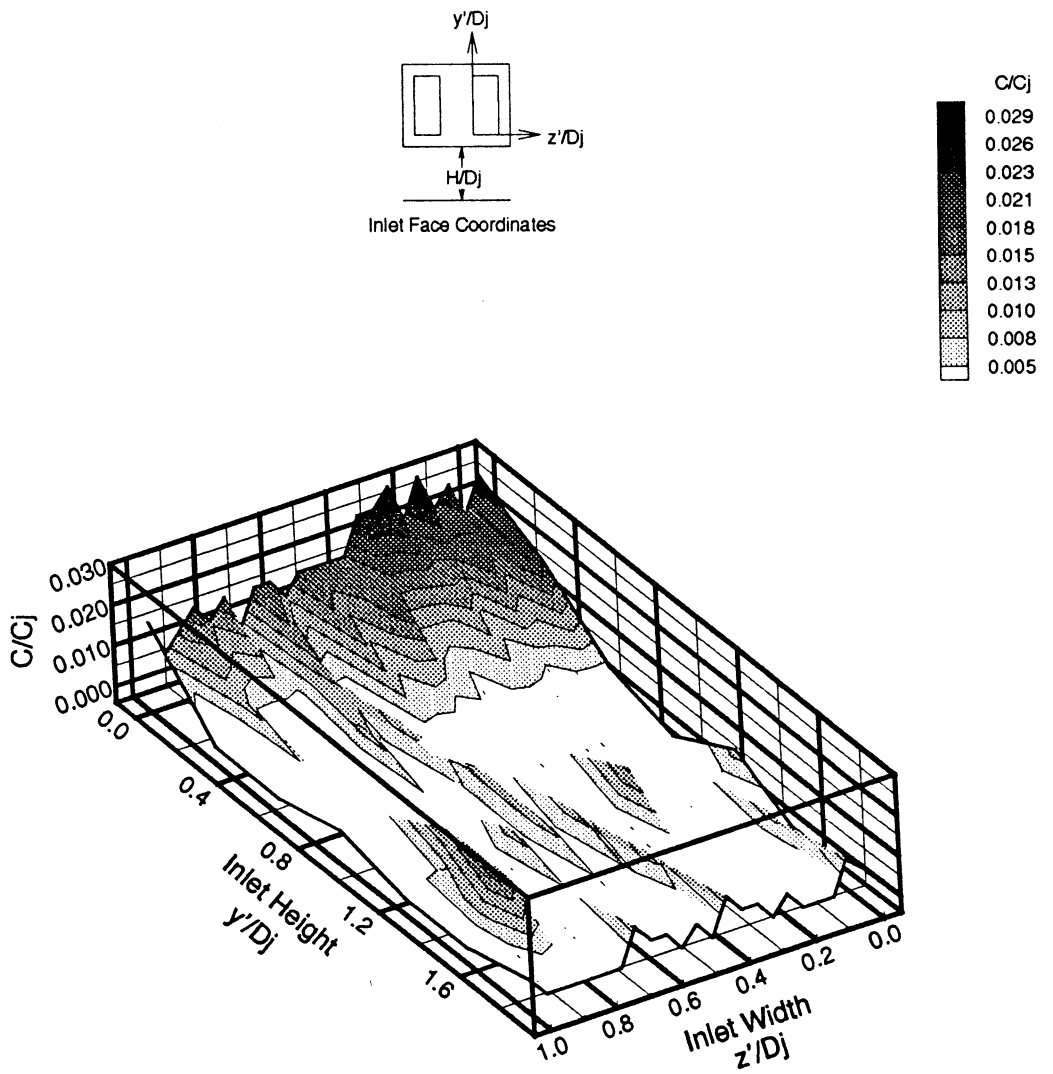

Figure 5.6 Low Speed Two-Jet Average Smoke Concentration at the Inlet Face
Plane [z'y']: H/D_j=6, U/V_j=0.09

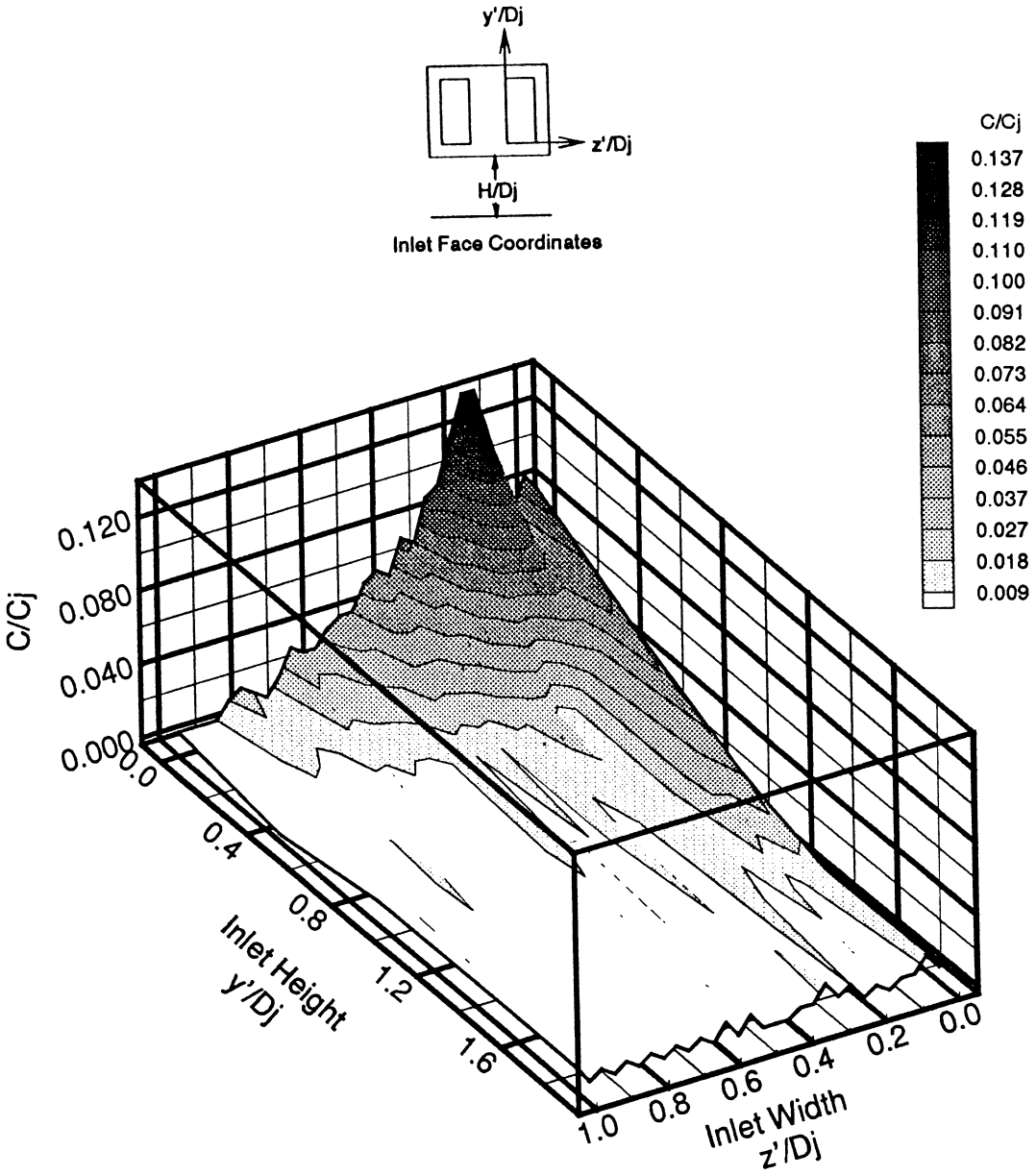

Figure 5.7 Low Speed Three-Jet Average Smoke Concentration at the Inlet Face Plane [z'y']: H/D_j=4, U/V_j=0.03

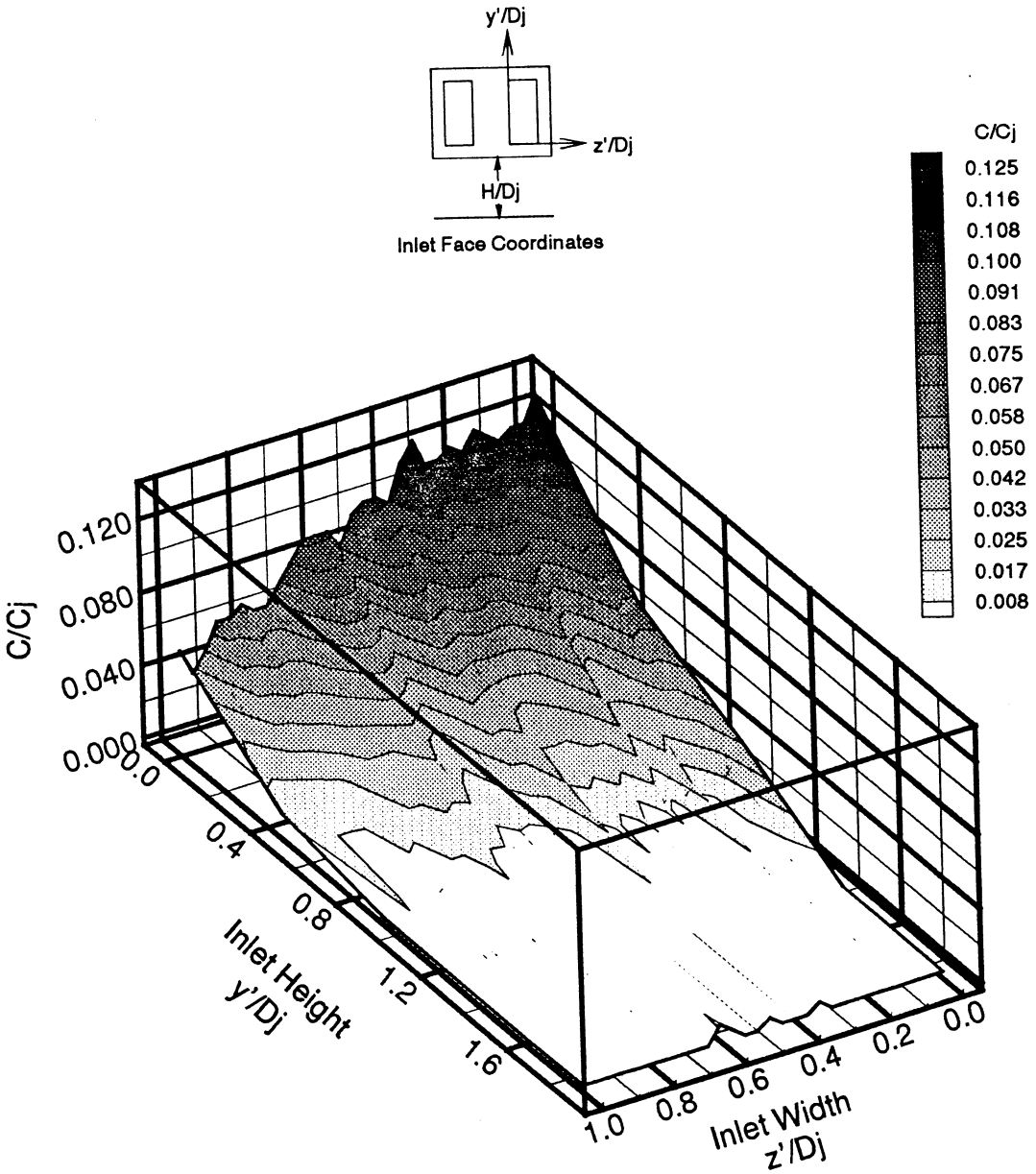

Figure 5.8 Low Speed Three-Jet Average Smoke Concentration at the Inlet Face Plane [z'y']: H/D_j=4, U/V_j=0.09

CHAPTER 6

HIGH SPEED - TWO-JET STUDY

A high speed two-jet configuration without inlet suction has been studied. The overall objective of the study was to determine the formation and structure of the vortical features in the interaction between the jet and the cross flow. The specific objective of the study was to establish the influence of scaling up the velocities of both the jet and the cross flow. It is noted that the jet velocities were raised to values at which compressibility became an important factor in the jet flow. The cases discussed in this chapter are summarized in Table 6.1 and will be referred to later by case numbers.

A Nd:YAG pulse laser was used in these experiments. The duration of each pulse was 10ns. In the low speed experiments, the argon laser had a continuous output and the camera took an average of the flowfield over a 1/30 second period for each frame. The Nd:Yag, however, had only one pulse per frame and the camera averaged only over the period of the pulse. Figure 6.1 shows the single frame image for case 6.1. The wall jet in the image does not appear to be continuous, but rather to be made up of multiple, broken concentric rings issuing forth from the point of impingement. The rings can be better seen in figure 6.2, which shows an edge enhanced single frame image for the same case. The large scale structures in a turbulent jet are ring vortices.

Crow and Champagne [10] noted that for a free turbulent jet of a Reynolds number of 10^4 and higher, a "train" of large scale axisymmetric, vortical puffs (i.e., ring vortices) issued forth from the jet. In these high speed experiments, the Reynolds number ranged from $5.7x10^4$ to $2.8x10^5$. Cimbala et. al. [8] further noted that these vortices were turned upstream when a ground plane was present and that they appeared to combine with the ground vortex. The rings viewed in figures 6.1 and 6.2 may be a cross section of those vortices. They appeared to be issuing outward from the point of impingement and moving radially out and breaking up. The upstream portions seemed to collect in the ground vortex.

Figure 6.3 shows a 127-frame average image for case 6.1. The individual structures seen in the single frame image have been averaged out and yielded a lower overall concentration field. This may be attributed to the unsteadiness in the flowfield which was evident in the video where the frame-to-frame changes in flow structure positions and symmetry were large.

The model and jet centerline concentration profiles were chosen for comparison. Figures 6.4 and 6.5 show a comparison of normalized concentration line cuts from 127-frame average images for case 6.2 and figures 6.6 and 6.7 show the comparison for case 6.3. From the comparisons of these cases it appears that the inlet ingestion levels in the high speed cases would be higher in the U/V_j=0.03 case than in the U/V_j=0.09 case because of the higher concentration levels near the inlets. A comparison is also given in these plots to the previous low speed cases. From these figures it appears that the high speed cases are more similar to each other than to the low speed cases. It is noted

that the given low speed concentration measurements were taken slightly out of the ground plane (y/D_j=0.6) which decreases the overall normalized concentrations. The concentrations would be higher in the ground plane and thus the differences between the high and low speed cases would be even greater.

Figures 6.4-6.7 also show that with an increase in Mach number, the overall normalized concentrations generally decreased upstream of the jets. Figure 6.8 shows the effect of velocity ratio on the forward vortex pair and ground vortex position for case 6.4. Increasing the velocity ratio caused the forward vortex pair to move downstream but not downstream of the inlets while the ground vortex did move downstream of the inlets at a ratio of about U/V_j=0.06. These velocity ratio effects were the same as those seen in the low speed cases.

Increasing the jet velocity at the same velocity ratio, also shown in figure 6.8 from cases 6.2 and 6.3, had the general effect of moving the flow structures downstream more. The effects observed currently seem to indicate Reynolds number, rather than Mach number, effects. For the same velocity ratio, an increase in jet speed requires an increase in freestream velocity. Kuhn and Eshleman [25] noted that for a STOVL aircraft in ground effect, the high velocities in the wall jet, which were very close to the ground, penetrated further against the relatively lower velocities in the ground boundary layer than would be possible against the freestream velocity. They noted that a moving model would have no boundary layer and the ground vortex would have much smaller penetration. The further swept back features observed with increased jet velocity at the same velocity ratio may be due to the reduction in the ground plane boundary layer.

Case Number	Mach Number	Velocity Ratio U/V_j	Model Height H/D_j	Laser Sheet Height y/D_j	Number of Jets	Inlet Suction
6.1	0.50	0.09	4.0	0.0	2	No
6.2	0.19, 0.50, 0.95	0.03	4.0	0.0	2	No
6.3	0.19, 0.50, 0.95	0.09	4.0	0.0	2	No
6.4	0.50	0.02, 0.03, 0.06, 0.09	4.0	0.0	2	No

Table 6.1 Test Cases for High Speed - Two-Jet Study

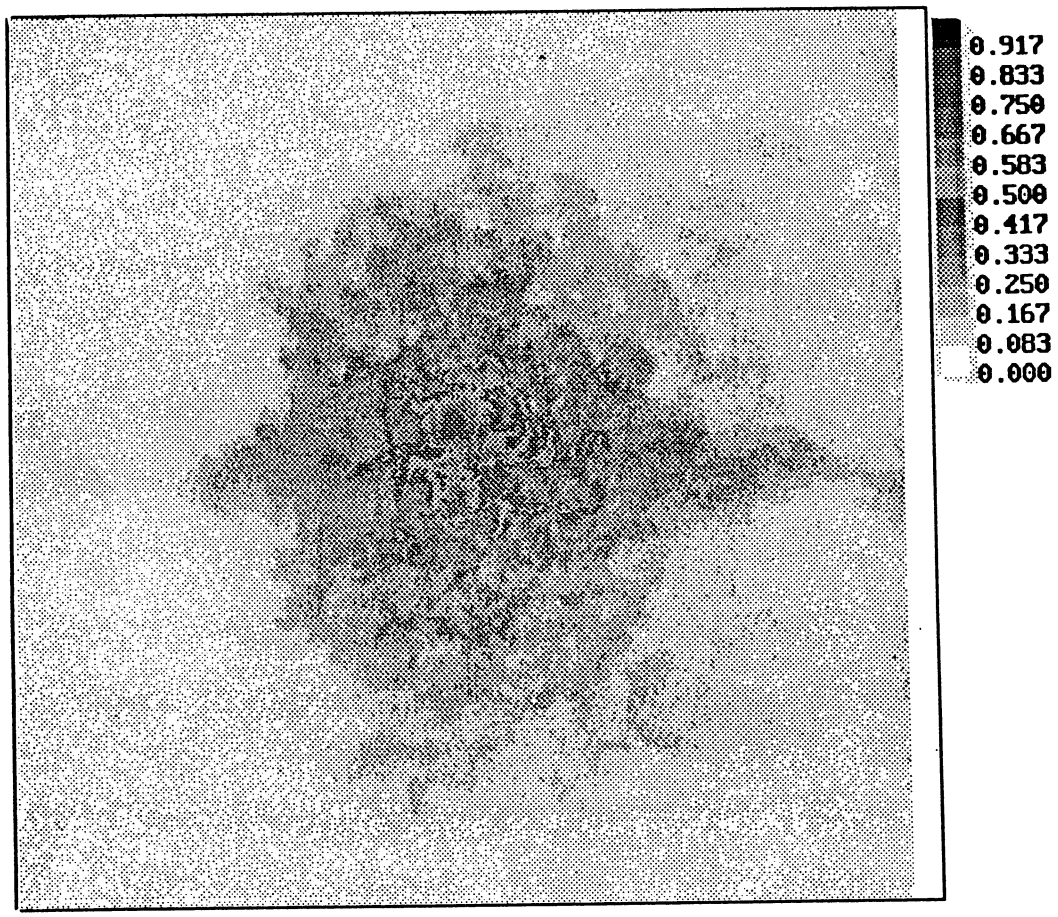

Figure 6.1 High Speed Two-Jet Single Frame Image of Smoke Concentration at Ground Plane: M_j=0.5, H/D_j=4.0, U/V_j=0.09

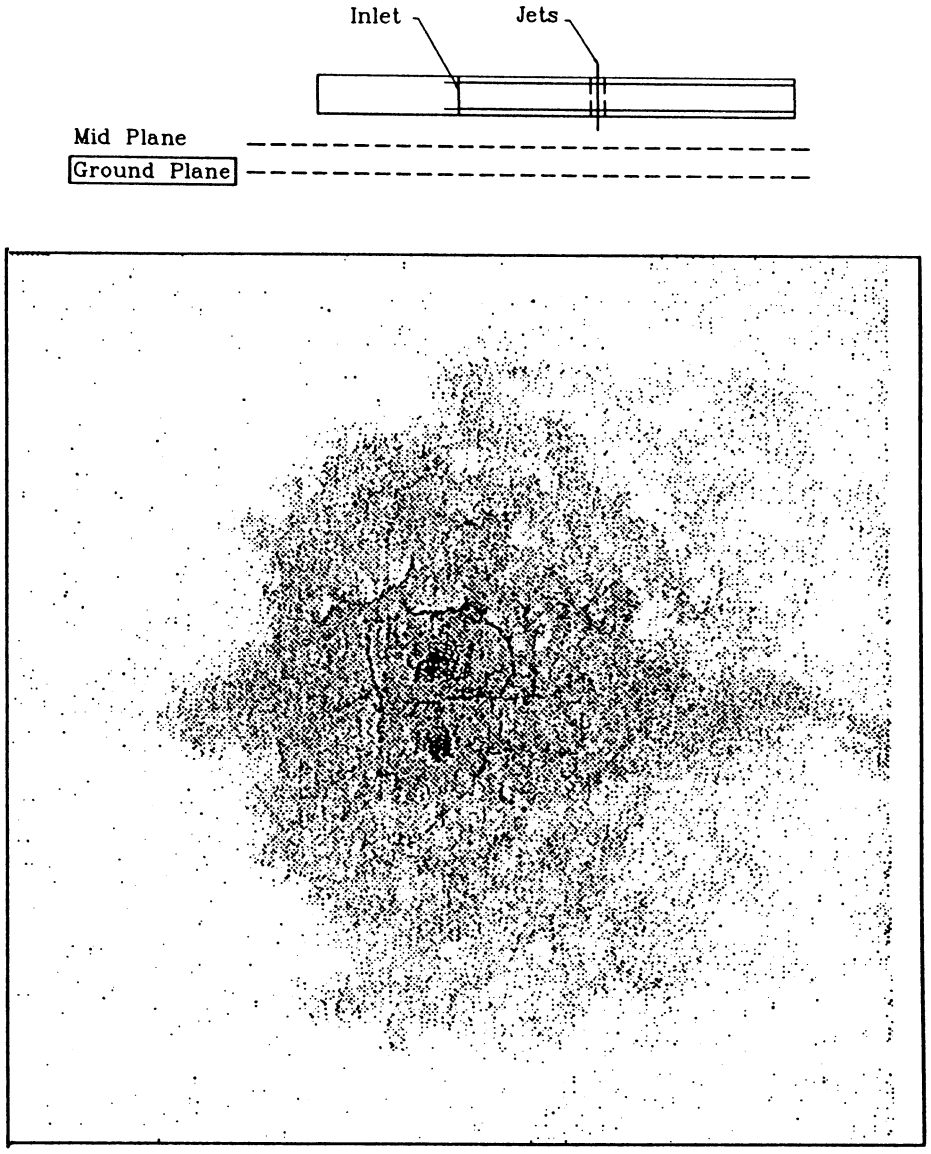

Figure 6.2 Edge Enhanced High Speed Two-Jet Single Frame Image of Smoke Concentration at Ground Plane: M_j=0.5, H/D_j=4.0, U/V_j=0.09

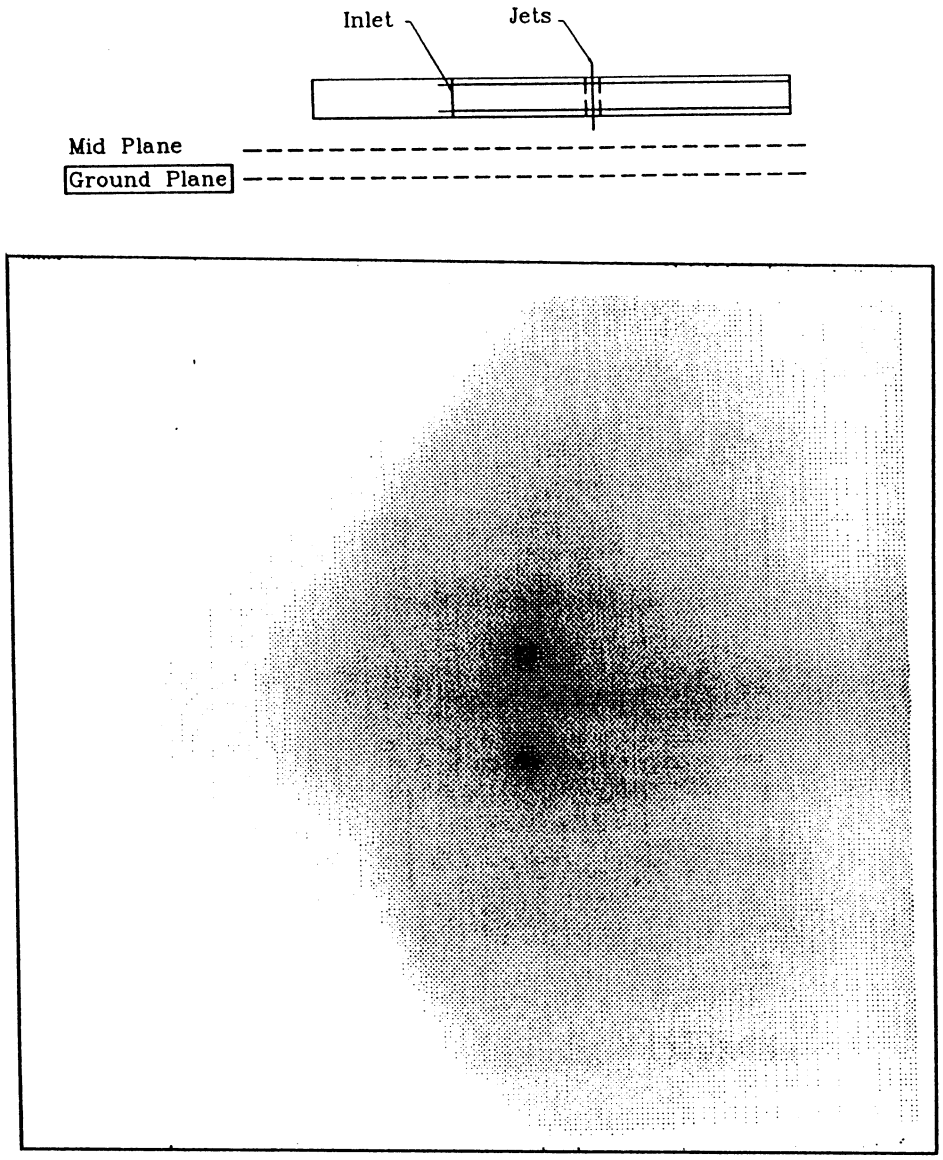

Figure 6.3 High Speed Two-Jet 127-Frame Image of Smoke Concentration at Ground Plane: M_j=0.5, H/D_j=4.0, U/V_j=0.09

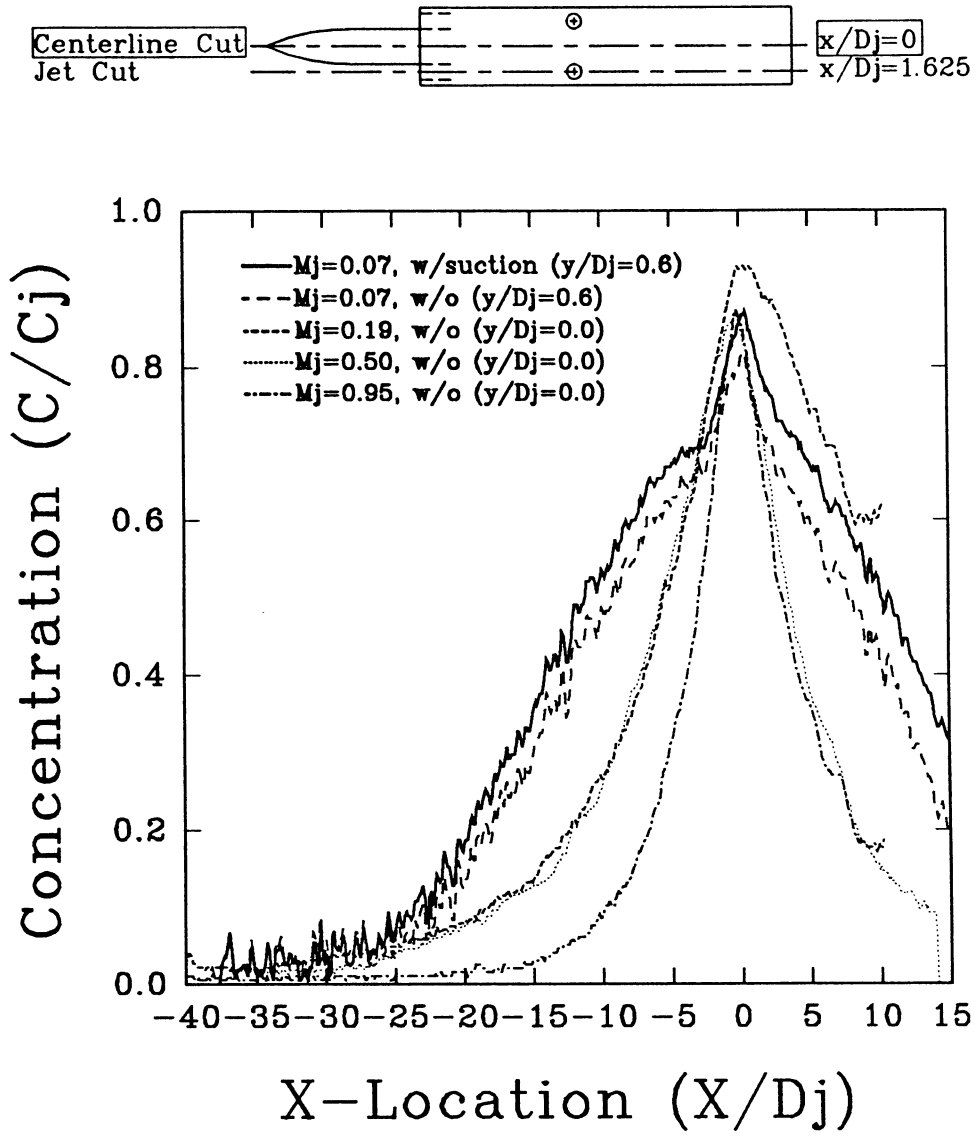

Figure 6.4 Two-Jet 127-Frame Average Concentration Profiles Through Model Centerline at Multiple Jet Velocities: H/D_j=4.0, U/V_j=0.03

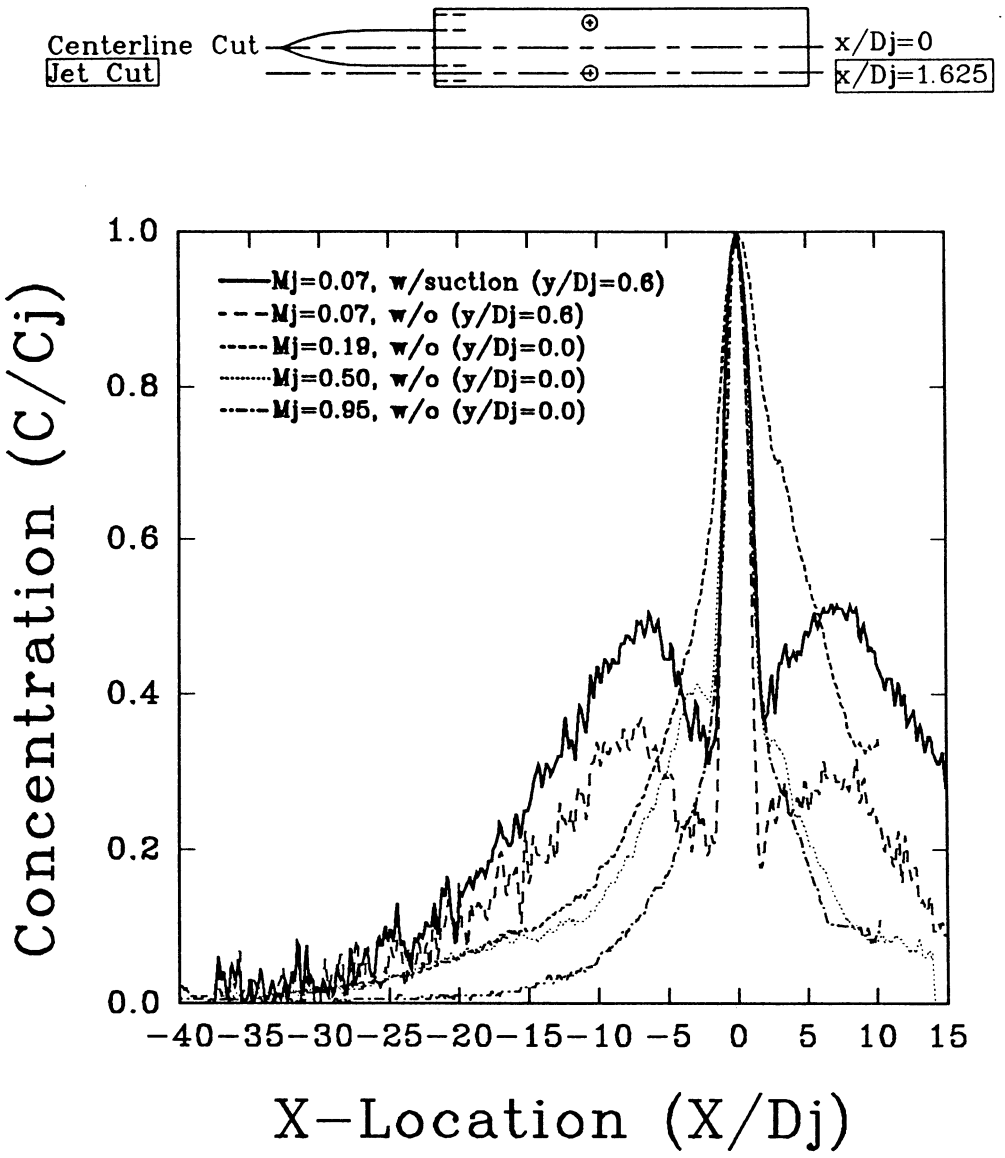

Figure 6.5 Two-Jet 127-Frame Average Concentration Profiles Through Jet Centerline at Multiple Jet Velocities: H/D_j=4.0, U/V_j=0.03

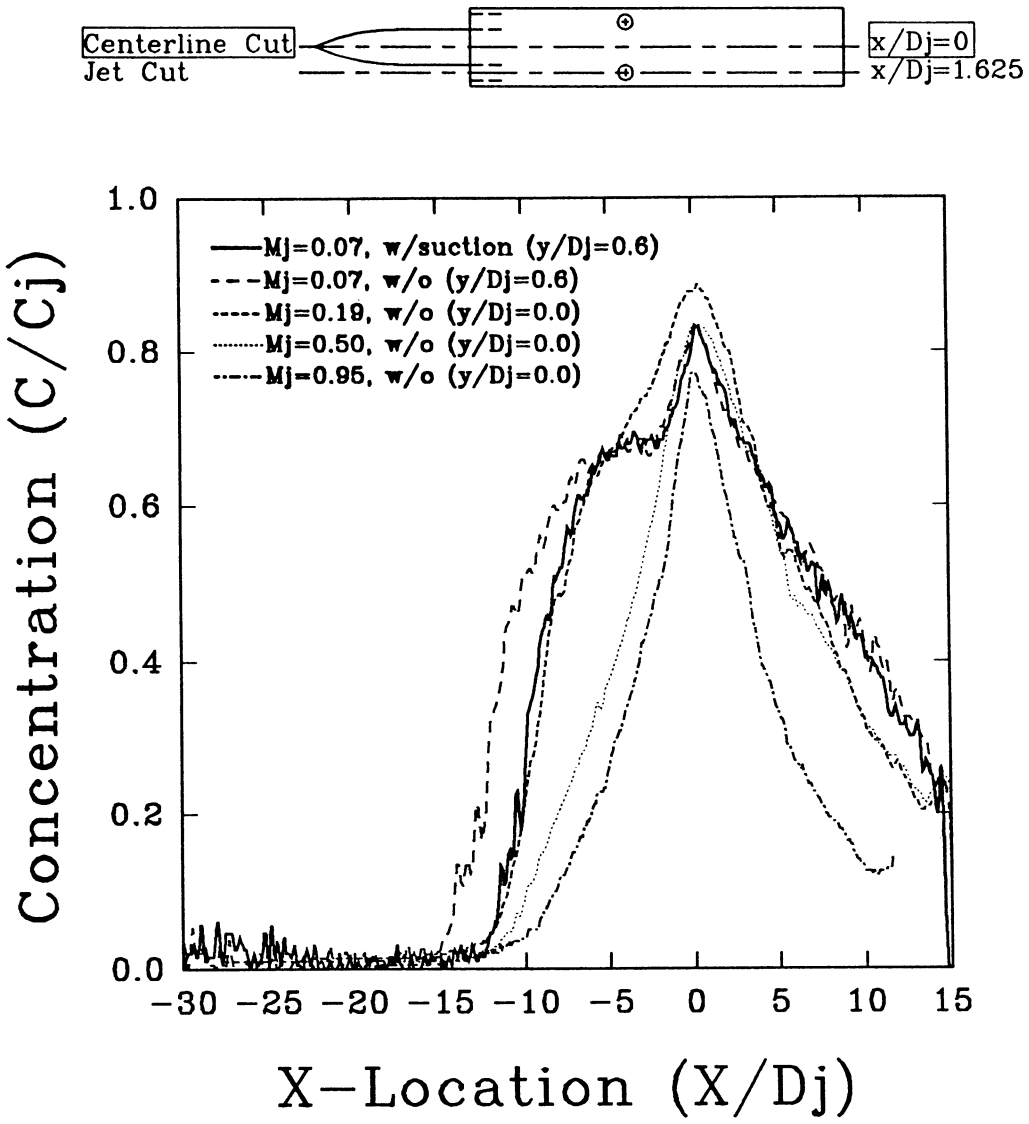

Figure 6.6 Two-Jet 127-Frame Average Concentration Profiles Through Model Centerline at Multiple Jet Velocities: H/D_j=4.0, U/V_j=0.09

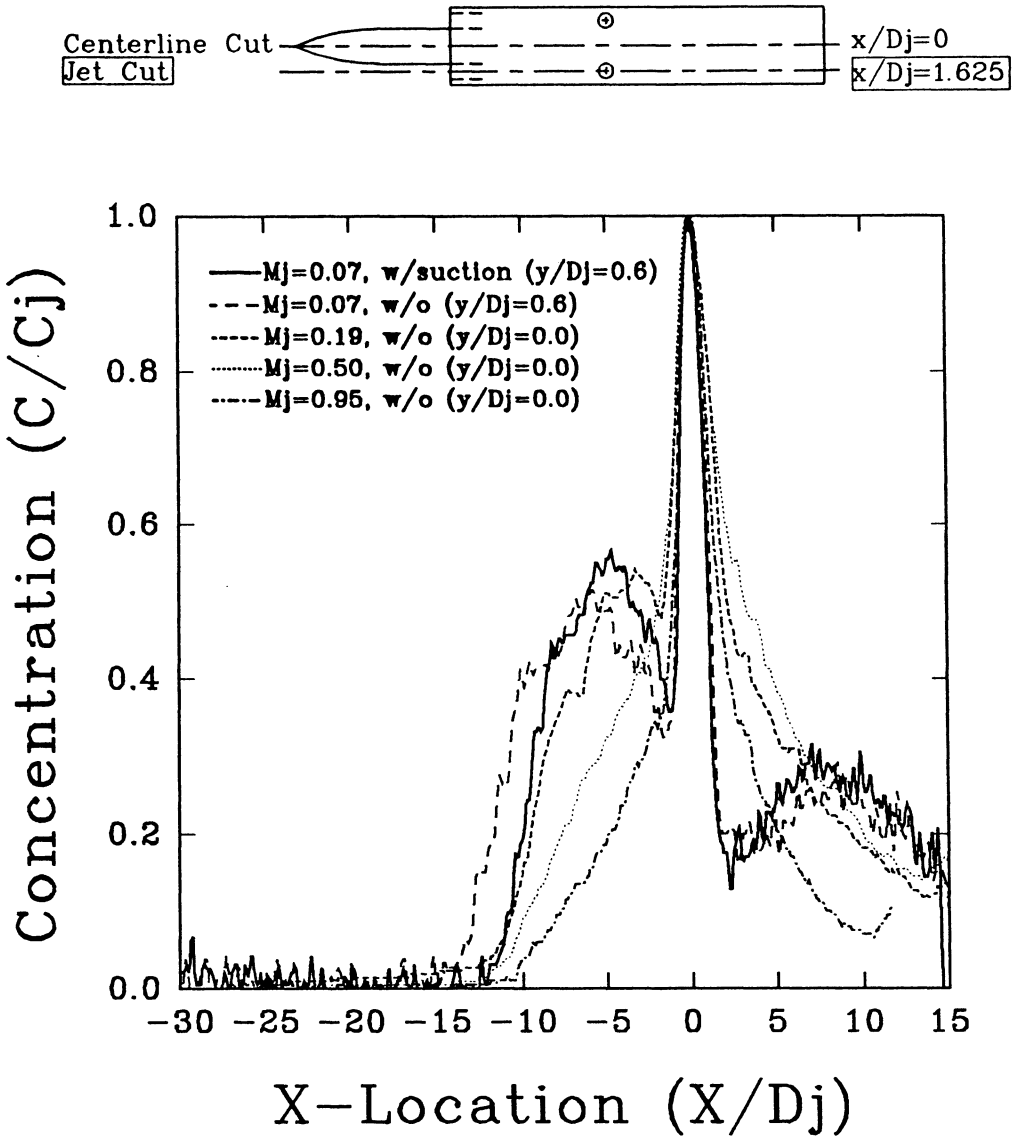

Figure 6.7 Two-Jet 127-Frame Average Concentration Profiles Through Jet Centerline at Multiple Jet Velocities: H/D_j=4.0, U/V_j=0.09

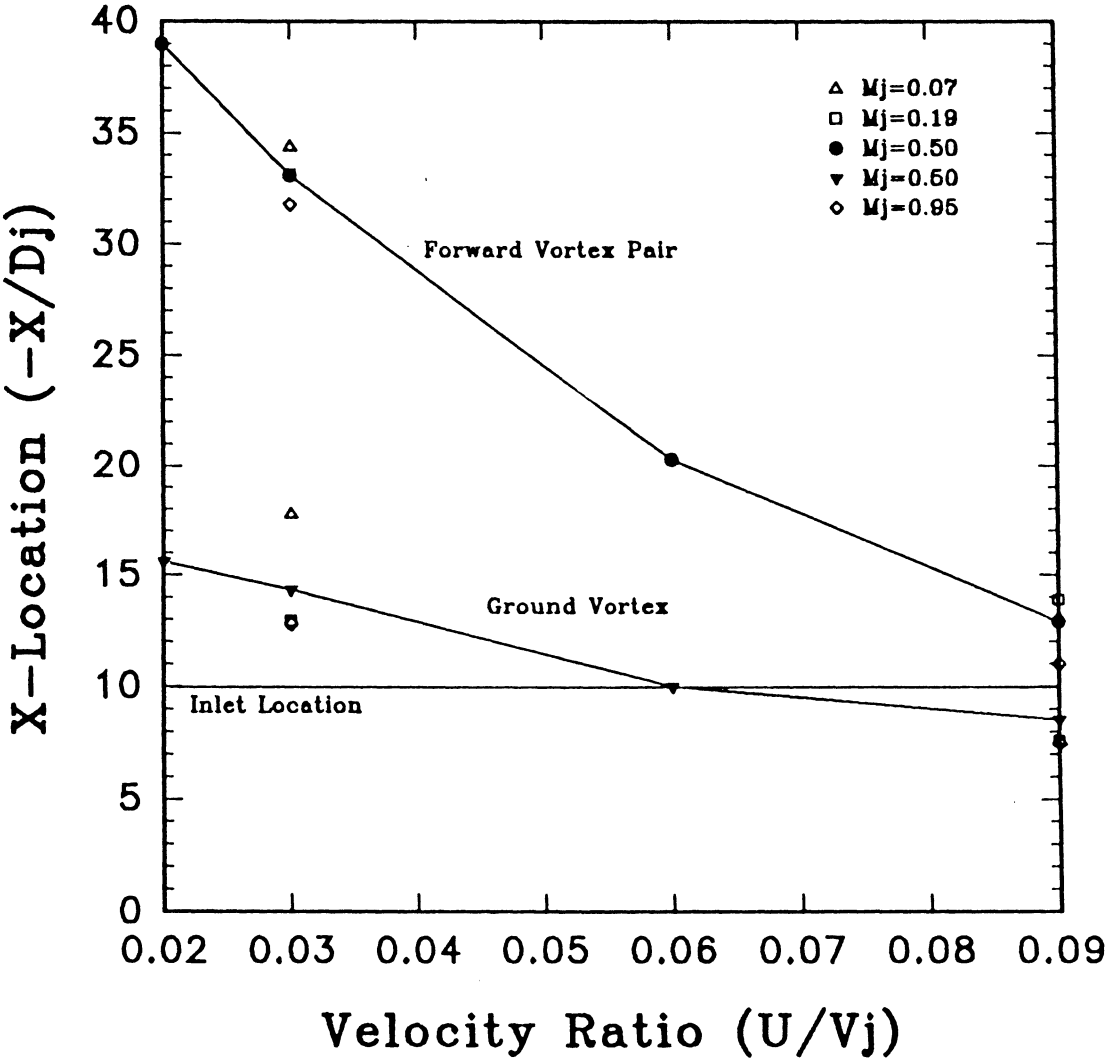

Figure 6.8 High Speed Two-Jet Forward Vortex Pair and Ground Vortex Position Versus Velocity Ratio (U/V_j) without Inlet Suction: M_j=0.07,0.19,0.50,0.95; H/D_j=4.0

CHAPTER 7

SUMMARY AND CONCLUSIONS

Ground impinging, two-, three-, and four-poster jets operating in the presence of cross flow, were studied. The emphasis of the study was the reingestion of exhaust gases into the inlets. The results were based on a quantitative, marker concentration distribution, supported by direct observations from video.

The first part of the study involved a comparison of low speed two-, three-, and four-poster jet configuration, with respect to the flowfield in the region of interaction between the forward and the jet flows. These cases had mass balanced inlet suction. In the second part, measurements were made at the inlet entry plane of the low speed two- and three-poster jet cases. Finally, a high speed, two-jet configuration without inlet suction was studied.

Overall, the same flow structures were present upstream of the front jet pair for the two-, three-, and four-jet configurations. There were, however, differences downstream of the front jet pair. The two-jet configuration had no aft jets and therefore, no downstream stagnation region. The three-jet model had a rear stagnation region and secondary ground vortex like the four-jet case, but the structures were swept further downstream.

At lower U/V_j's the matching of the normalized concentration fields between the

two- three- and four-jet cases was not as close as at higher ratios. The normalized concentrations increased overall from the two- to three- to four-jet case. The reason for the differences was that the total momentum of each case was different. In the two-jet case, the momentum flux from the jets was 50% lower than the four-jet case and 33.3% lower than three-jet case. At the higher velocity ratios, the freestream velocity was greater and it caused the structures to move closer together as they approached the front jet pair. Thus, the effect of configuration became less apparent at higher velocity ratios.

For a particular velocity ratio and model height, the normalized concentration distributions near the inlets were nearly the same for all of the low speed jet configurations. However, the two-jet case had somewhat lower normalized concentrations overall. There was an exception in the region between the inlets and the jets. The two jet case had lower momentum and the spread from the jets was pushed back closer toward the jets than in the other configurations.

Considering the inlet planes, the ingestion of smoke was not a continuous process, but rather, an intermittent one. Therefore, in the average of 127 frames, the intensities appeared lower because of the periods when little or no smoke was being ingested. Also, it was noted that the inlet concentrations were highest in the lower portion of the inlets. The results for the two- and three-jet cases were generally the same, with the differences attributed to total momentum differences.

At a velocity ratio of U/V_j=0.03, the inlets drew in marker particles from upstream along the nose cone. It was clear that far field ingestion occurred at this ratio. At U/V_j=0.09, the ground vortex and forward vortex pair were very near the inlets. The

distinction between near and "far" field became difficult to distinguish. The ingestion of the flow from the underside of the model body and from the ground plane both tended to enter the lower portions of the inlets. It was clear though, that at higher model heights, H/D_j= 4.0 and 6.0, the flow tended to get pushed back out of the inlet entrainment region and thus had lower concentrations at the inlet plane at higher velocity ratios. At a model height of H/D_j=2, the vortical structures were in the inlet plane region which yielded the highest overall inlet plane concentrations.

In the two-jet, high speed cases, it appeared that vortices from the jets were seen in the ground plane which seemed to collect in the ground vortex. As jet velocity increased at a particular velocity ratio, the flow structures were on the average, swept further downstream and thus yielded lower overall normalized concentrations upstream of the jets. Furthermore, the M_j=0.50 and M_j=0.95 cases were more similar than either of them were with the low speed, nearly incompressible flow cases. Thus indicating that simple scaling parameters may not exist in relating the jet and the forward speeds to instantaneous distortion parameters at the inlet except when the initial conditions under consideration differ little for the cases being compared.

In future studies, the ground plane boundary layer should be investigated in both the low and high speed cases. It is of particular interest to isolate the causes of the differences between the two cases. Also, the effect of splaying the nozzles should be studied. Finally, a method for obtaining mass balanced inlet suction should be investigated for the high speed cases.

BIBLIOGRAPHY

1. Aoyagi,, Kiyoshi, and Snyder, Phillip K., "Experimental Investigation of a Jet Inclined to a Subsonic Crossflow," December, 1981, AIAA Paper No. 81-2610.

2. Balint, J. L., Ayrault, M., and Scon, J. P., "Quantitative Investigation of the Velocity and Concentration Fields of Turbulent Flows Combining Visualization and Image Processing," Flow Visualization III, Proceedings of the Third International Symposium on Flow Visualization, September, 1983, University of Michigan, Ann Arbor, Michigan, Edited by W. J. Yang, Hemisphere Publishing Corp., Washington, D.C.

3. Becker, H. A., "Mixing, Concentration Fluctuations and Marker Nephelometry," Studies in Convection, Volume 2: Theory, Measurement, and Application, Edited by B. E. Launder, Academic Press, New York, NY, 1977.

4. Borleteau, J.P., "Concentration Measurement with Digital Image Processing," ICIASF '83 Record, pp. 37-42, St. Louis, France, September 1983.

5. Brandt, A., "Hydrodynamic Flowfield Imaging," Flow Visualization III, Proceedings of the Third International Symposium on Flow Visualization, September, 1983, University of Michigan, Ann Arbor, Michigan, Edited by W. J. Yang, Hemisphere Publishing Corp., Washington, D.C.

6. Bray, D., and Knowles, K., "A Review of Impinging Jets in Crossflows-Experimentation and Computation," 30th Aerospace Sciences Meeting and Exhibit, Reno, Nevada, January, 1992, AIAA Paper No. 92-0633.

7. Childs, E., and Patel, B., "Turbulence Model Performance in V/STOL Flow Field Simulation," AIAA/SAE/ASME/ASEE 26th Joint Propulsion Conference, Orlando, Florida, July, 1990, AIAA Paper No. 90-2248.

8. Cimbala, J.M., Gaublomme, D.P., Stinebring, D.R., and Billet, M.L., "Experiments on the Unsteady Ground Vortex," Aerospace Technology Conference and Exposition, Anaheim, California, September 1989, SAE Paper No. 892281.

9. Colin, F.E., and Olivari, D., "The Impingement of a Circular Jet Normal to a Flat Surface With and Without Crossflow," European Research Office, United States Army Report No., AD-688953, January 1969.

10. Crow, S.C., and Champagne, F.H., "Orderly Structure in Jet Turbulence," Journal of Fluid Mechanics, Vol. 48, Part 3, pp. 547-591, 1971.

11. Donaldson, Coleman Dup., and Snedeker, Richard S., "A Study of Free Jet Impingement. Part 1. Mean Properties of Free and Impinging Jets," Journal of Fluid Mechanics, Vol. 45, Part 2, pp. 281-319, 1971.

12. Donaldson, Coleman Dup., Snedeker, Richard S., and Margolis, David P., "A Study of Free Jet Impingement. Part 2. Free Jet Turbulence Structure and Impingement Heat Transfer," Journal of Fluid Mechanics, Vol. 45, Part 3, pp. 477-512, 1971.

13. Dwenger, Richard, "Laser Doppler Velocimeter Measurements and Laser Sheet Imaging in an Annular Combustor Model," M.S. Thesis, Purdue University, August, 1990.

14. Fricker, D.M., Holdeman, J.D., and Vanka, S.P., "Calculations of Hot Gas Ingestion for a STOVL Aircraft Model," 30th Aerospace Sciences Meeting and Exhibit, Reno, Nevada, January, 1992, AIAA Paper No. 92-0385.

15. Gittner, U., Hoffert, F., and Lotz, M., "Interaction Between Airframe-Powerplant Integration and Hot Gas Ingestion for Jet Lift V/STOL Transport Aircraft," Agard Conference Proceeding 27: Integration of Propulsion Systems in Airframes, September 1967.

16. Goldstein, Richard J., Fluid Mechanics Measurements, Hemisphere Publishing Corp., Washington D.C., 1983.

17. Hall, Gordon R., and Rogers, Kenneth H., "Recirculation Effects Produced by a Pair of Heated Jets Impinging on a Ground Plane," NASA CR-1307, Northrop Corporation, September, 1969.

18. Hammond, Alexander D., and McLemore, H. Clyde, "Hot-Gas Ingestion and Jet Interference Effects for Jet V/STOL Aircraft," Agard Conference Proceeding 27: Integration of Propulsion Systems in Airframes, September 1967.

19. Hoad, Danny R., "Techniques and Problems Associated With Wind-Tunnel Testing of Multi-Fan VTOL Aircraft Models," Presented at the Navy Workshop on Prediction Methods for Jet V/STOL Propulsion Aerodynamics, Washington, D.C., July, 1975.

20. Johns, Albert L., "Hot Gas Ingestion Testing of an Advanced STOVL Concept in the NASA Lewis 9- by 15-Foot Low Speed Wind Tunnel With Flow Visualization," AIAA/ASME/SAE/ASEE 24th Joint Propulsion Conference, Boston, Massachusetts, July 1988, AIAA Paper No. 88-3025.

21. Kotansky, Donald R., "Multiple Jet Impingement Flowfields," Recent Advances in Aerodynamics, Edited by Anjaneyulu Krothapalli and Charles A. Smith, Springer-Verlag, New York, NY 1986.

22. Kotansky, D. R., and Bower, W. W., "A Basic Study of the VTOL Ground Effect Problem for Planar Flow," AIAA/NASA Ames V/STOL Conference, Palo Alto, California, June, 1977, AIAA Paper No. 77-614.

23. Kotansky, D. R., and Glaze, L. W., "Impingement of Rectangular Jets on a Ground Plane," AIAA Journal, Vol. 20, No. 5, May 1982, pp. 585-586.

24. Kuhn, Richard E., "The Induced Aerodynamics of Jet and Fan Powered V/STOL Aircraft," Recent Advances in Aerodynamics, Edited by Anjaneyulu Krothapalli and Charles A. Smith, Springer-Verlag, New York, NY, 1986.

25. Kuhn, Richard E., and Eshleman, James, "Ground Effects on V/STOL and STOL Aircraft--A Survey," AIAA/AHS/ASEE Aircraft Design Systems and Operations Meeting, Colorado Springs, Colorado, October 1985, AIAA Paper No. 85-4033.

26. Limage, C.R., "Evaluation of Inlet Reingestion for Large Bypass Ratio V/STOL Aircraft," AIAA Paper No. 78-1079, AIAA/SAE 14th Joint Propulsion Conference, July 1978.

27. Lord, P. A., "Development and Usage of a Small-Scale V/STOL Ground Effects Simulator," AIAA/AHS/ASEE Aircraft Design Systems and Operations Meeting, Colorado Springs, Colorado, October, 1985, AIAA Paper No. 85-4037.

28. MacLean, Roderick J., "The Flowfield Around a STOVL Aircraft Model in Ground Effect," M.S. Thesis, Purdue University, December 1990.

29. MacLean, R., Sullivan, J.P., and Murthy, S.N.B., "Hot Gas Environment Around STOVL Aircraft in Ground Proximity, Part I: Experimental Study," AIAA/SAE/ASME/ASEE 26th Joint Propulsion Conference, Orlando, Florida, July 1990, AIAA Paper No. 90-2269.

30. Mineck, Raymond E., "Comparison of Theoretical and Experimental Interference Effects on a Jet VTOL Airplane Model," Presented at the Navy Workshop on Prediction Methods for Jet V/STOL Propulsion Aerodynamics, Washington, D.C., July 1975.

31. Morgan, Douglas C., "Concentration Measurements in a Cold Flow Model Annular Combustor Using Laser Induced Fluorescence," M. S. Thesis, Purdue University, August 1988.

32. Mueller, Thomas J., "Recent Developments in Smoke Flow Visualization," Flow Visualization III, Proceedings of the Third International Symposium on Flow Visualization, September, 1983, University of Michigan, Ann Arbor, Michigan, Edited by W. J. Yang, Hemisphere Publishing Corp., Washington, D.C.

33. Nosseir, Nagy S., "Chapter 13: Impinging Jets," Encyclopedia of Fluid Mechanics, pp.349-366, Gulf Publishing, 1986.

34. Nosseir, N. S., and U. Peled, "The Pressure Field Generated by Jet-Jet Impingement," AIAA 10th Aeroacoustics Conference, Seattle, WA, July 1986, AIAA Paper No. 86-1951.

35. Saripalli, K. R., "Laser Doppler Velocimeter Measurements in a 3-D Impinging Twin-Jet Fountain Flow," AIAA/AHS/ASEE Aircraft Design Systems and Operations Meeting, Colorado Springs, Colorado, October, 1985, AIAA Paper No. 85-4036.

36. Scheuring, Jason, "Turbulence Intensity of the V/STOL and Boeing Wind Tunnels," Private Communication to John P. Sullivan, Purdue University, May, 1992.

37. Schwantes, E., "The Recirculation Flow Pattern of a VTOL Lift Engine," NASA TT F-14,912, June 1973.

38. Seal, Michael Damian II, "An Experimental Study of Swirling Flows as Applied to Annular Combustors," M. S. Thesis, Purdue University, May 1988.

39. Settles, Gary S., "Modern Developments in Flow Visualization," AIAA Journal, Vol. 24, No. 8, August, 1986, pp. 1313-1323.

40. Shayesteh, M. V., Shapaka, I. M. M. A., and P. Bradshaw, "Turbulence Structure of a Three Dimensional Impinging Jet in a Cross Stream," AIAA 23rd Aerospace Sciences Meeting, Reno, Nevada, January, 1985, AIAA Paper No. 85-0044.

41. Sherrieb, H. E., "Ground Effects Testing of Two-, Three-, and Four-Jet Configurations," Journal of Aircraft, Vol. 16, No. 6, June 1979, pp. 393-397.

42. Siclari, M. J., Migdal, D., Luzzi, T. W., Barche, J., and Palcza, J. L., "Development of Theoretical Models for Jet-Induced Effects on V/STOL Aircraft," Journal of Aircraft, Vol. 13, No. 12, December 1976, pp. 938-244.

43. Stewart, V., and Kemmerly, G., "Characteristics of the Ground Vortex Formed by a Jet Moving Over a Fixed Ground Plane," 27th Aerospace Sciences Meeting, Reno, Nevada, January 1989, AIAA Paper No. 89-0650.

44. Stewart, V. R., and Kuhn, R. E., "A Method for Estimating the Propulsion Induced Aerodynamic Characteristics of STOL Aircraft in Ground Effect,"Report No. NADC 80226-60, August 1983.

45. Tafti, D., and Vanka, S. P., "Hot Gas Environment Around STOVL Aircraft in Ground Proximity, Part II: Numerical Study," AIAA/SAE/ASME/ASEE 26th Joint Propulsion Conference, Orlando, Florida, July 1990, AIAA Paper No. 90-2270.

46. VanOverbeke, Thomas J., and Holdeman, James D., "A Numerical Study of the Hot Gas Environment Around a STOVL Aircraft in Ground Proximity," AIAA/ASME/SAE/ASEE 24th Joint Propulsion Conference, Boston, Massachusetts, July, 1988, AIAA Paper No. 88-2882.

47. Veret, C., "Flow Visualization by Light Sheet," Flow Visualization III, Proceedings of the Third International Symposium on Flow Visualization, September, 1983, University of Michigan, Ann Arbor, Michigan, Edited by W. J. Yang, Hemisphere Publishing Corp., Washington, D.C.

48. Vukits, T.J., Sullivan, J.P., and Murthy, S.N.B., "Two-, Three-, and Four-Poster Jets in Cross Flow," 31st Aerospace Sciences Meeting and Exhibit, Reno, Nevada, January 1993, AIAA Paper No. 93-0023.

49. Waesche, J. E., and Migdal, D., "High-Performance Jet V/STOL Development," Journal of Aircraft, Vol 14, No. 2, February 1977, pp. 97-103.

50. Weber, Henry A. "VTOL Recirculation and Impingement Model Testing," Presented at the AIAA/SAE Ninth Propulsion Conference, Las Vegas, Nevada, November, 1973, AIAA Paper No. 73-1183.

51. Wernet, Mark P., "Particle Displacement Tracking Applied to Air Flows," Fourth International Conference on Laser Anemometry, Cleveland, Ohio, August 1991. (NASA TM 104481)

52. Winston, Matthew M., "Propulsion-Induced Aerodynamic Interference Effects on Jet Lift VTOL Aircraft," Presented at the Navy Workshop on Prediction Methods for Jet V/STOL Propulsion Aerodynamics, Washington, D.C., July 1975.

53. Wohllebe, F. A., and Siclari, M. J., "Fountain and Upwash Flowfields of Multi-jet Arrangements," Journal of Aircraft, Vol. 15, No. 8, August 1978, pp. 468-473.

54. Yanta, William J., "Use of the LDV in Subsonic and Supersonic Flow," The Use of the Laser Doppler Velocimeter for Flow Measurements, Project Squid Report, Purdue University, March 1972.

55. Yanta, W.J., Gates, D.F., "The Use of a Laser Doppler Velocimeter in Supersonic Flow," AIAA 6th Aerodynamic Testing Conference, Albuquerque, New Mexico, March 1971, AIAA Paper No. 71-287.

APPENDICES

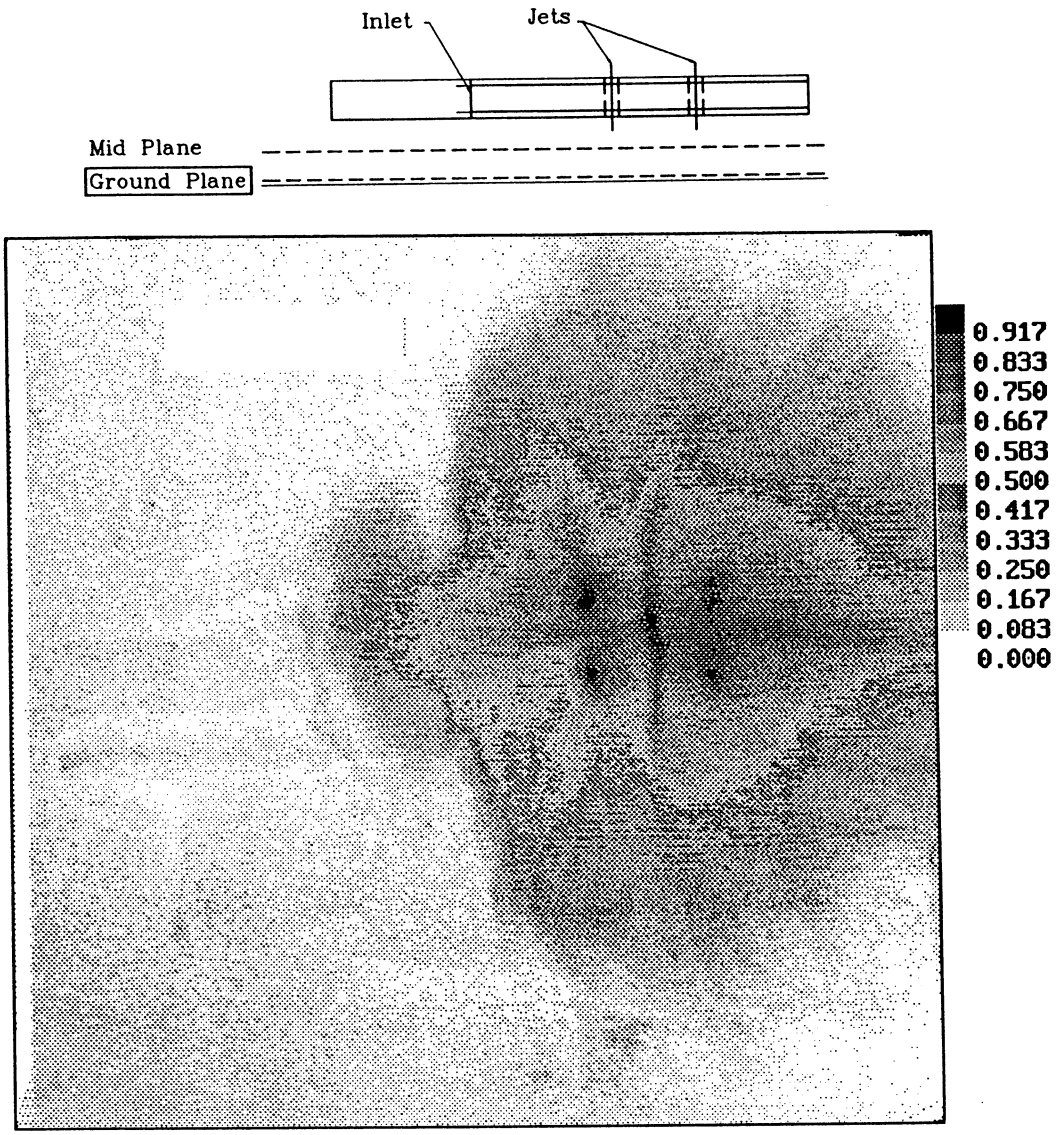

Figure A.1 MacLean [28] Four-Jet Single Frame Image of Smoke Concentration at Ground Plane
$y/D_j=0$, $H/D_j=4$, $U/V_j=0.09$

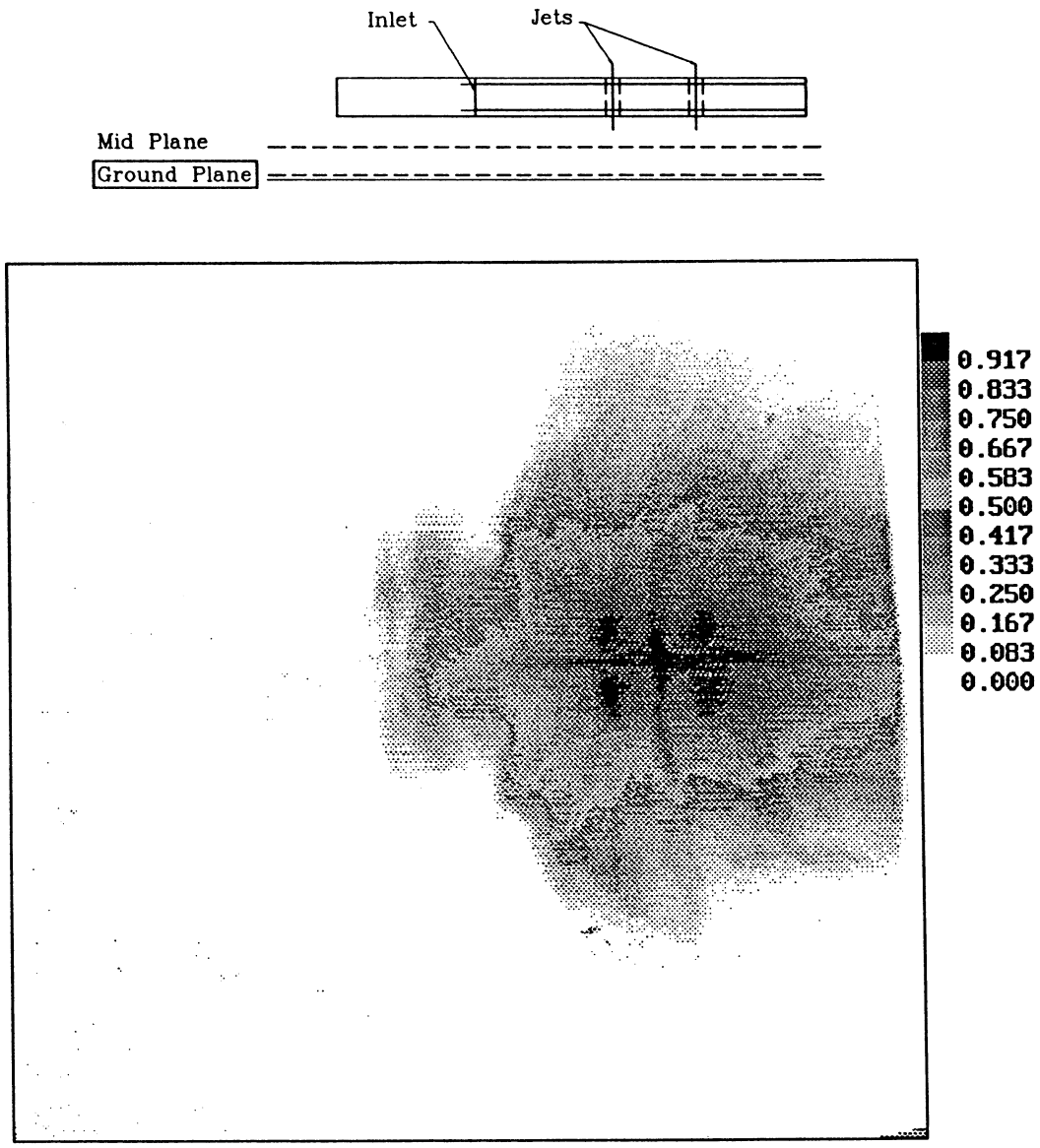

Figure A.2 Four-Jet Single Frame Image of Smoke Concentration at Ground Plane
$y/D_j=0$, $H/D_j=4$, $U/V_j=0.09$

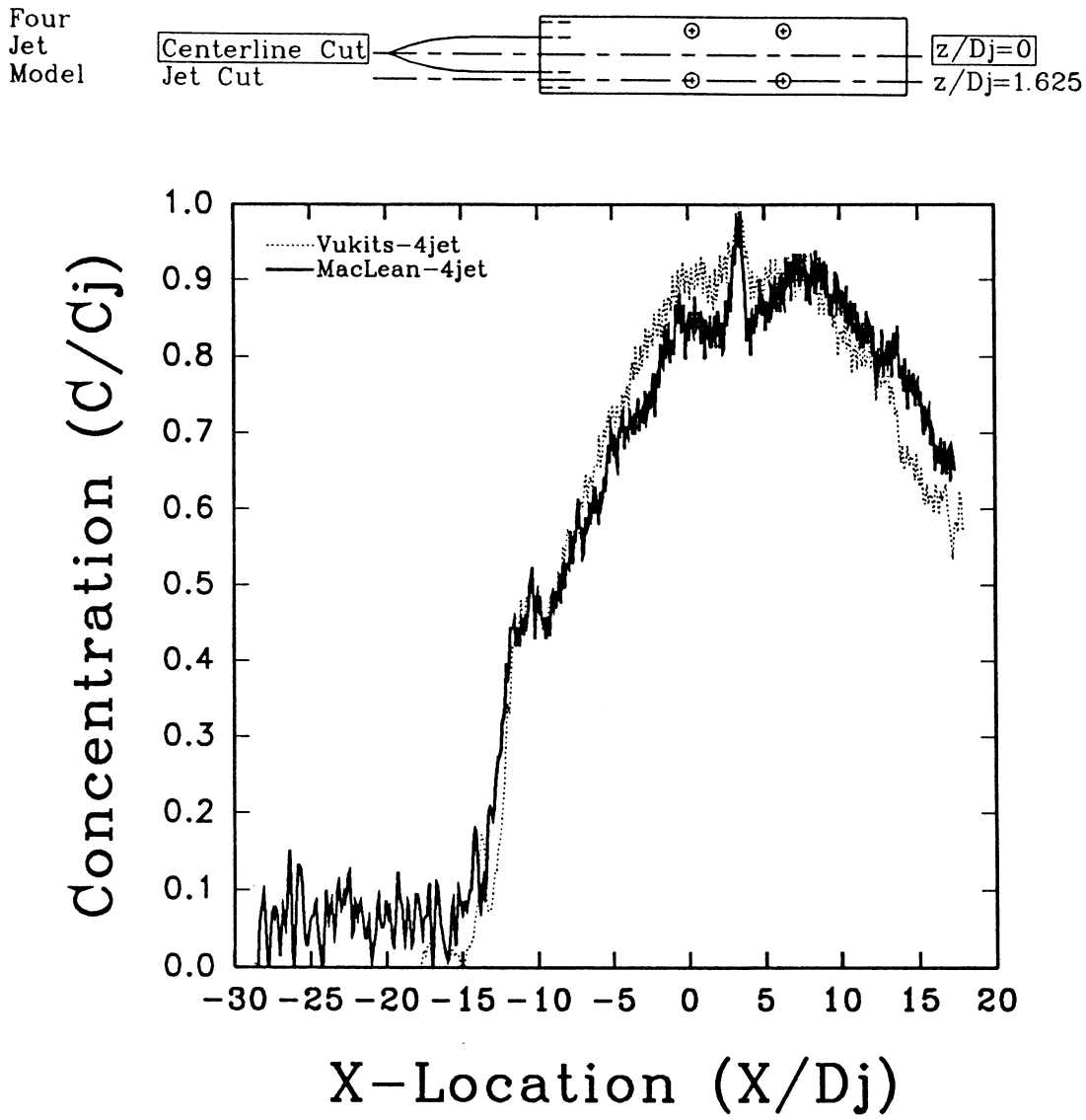

Figure A.3 Four-Jet Single Frame Comparison
Concentration Profiles at Model Centerline: $z/D_j=0$
Laser Sheet at Ground Plane: $y/D_j=0.0$, $H/D_j=4$, $U/V_j=0.09$

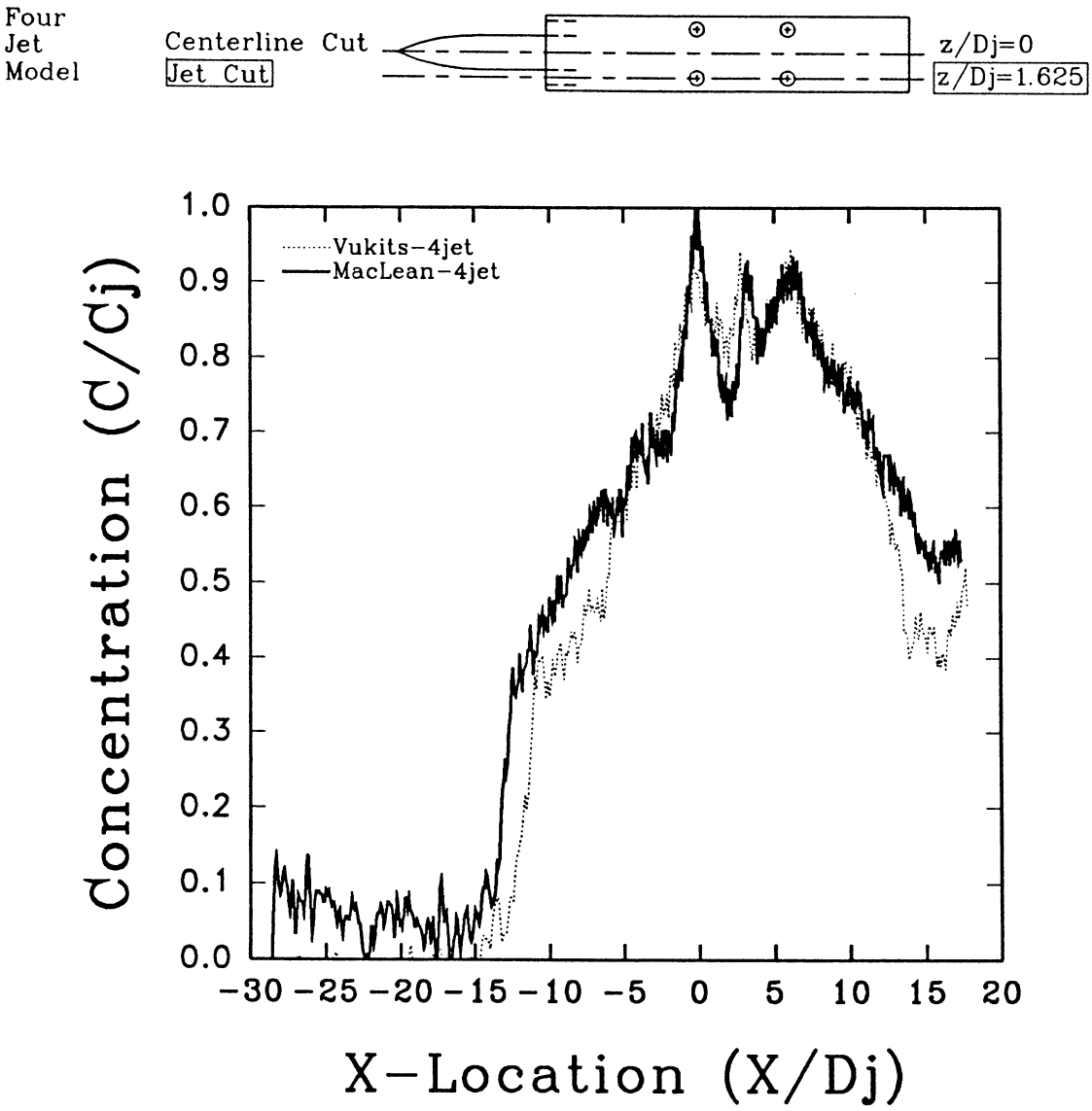

Figure A.4 Four-Jet Single Frame Comparison
Concentration Profiles at Jet Centerline: z/D_j=1.625
Laser Sheet at Ground Plane: y/D_j=0.0, H/D_j=4, U/V_j=0.09

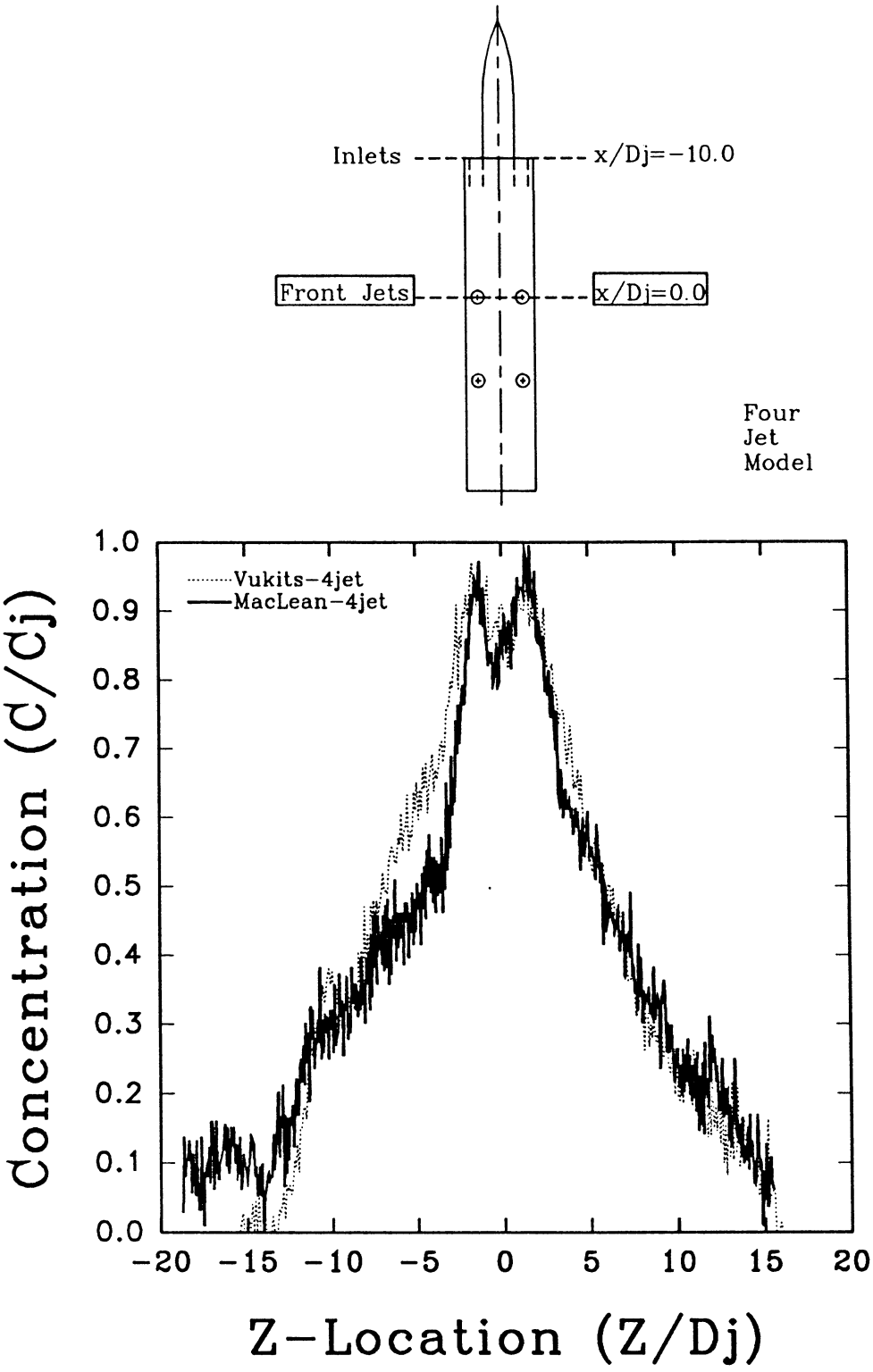

Figure A.5 Four-Jet Single Frame Comparison
Concentration Profiles at Forward Jet Centerline: $x/D_j=0.0$
Laser Sheet at Ground Plane: $y/D_j=0.0$, $H/D_j=4$, $U/V_j=0.09$

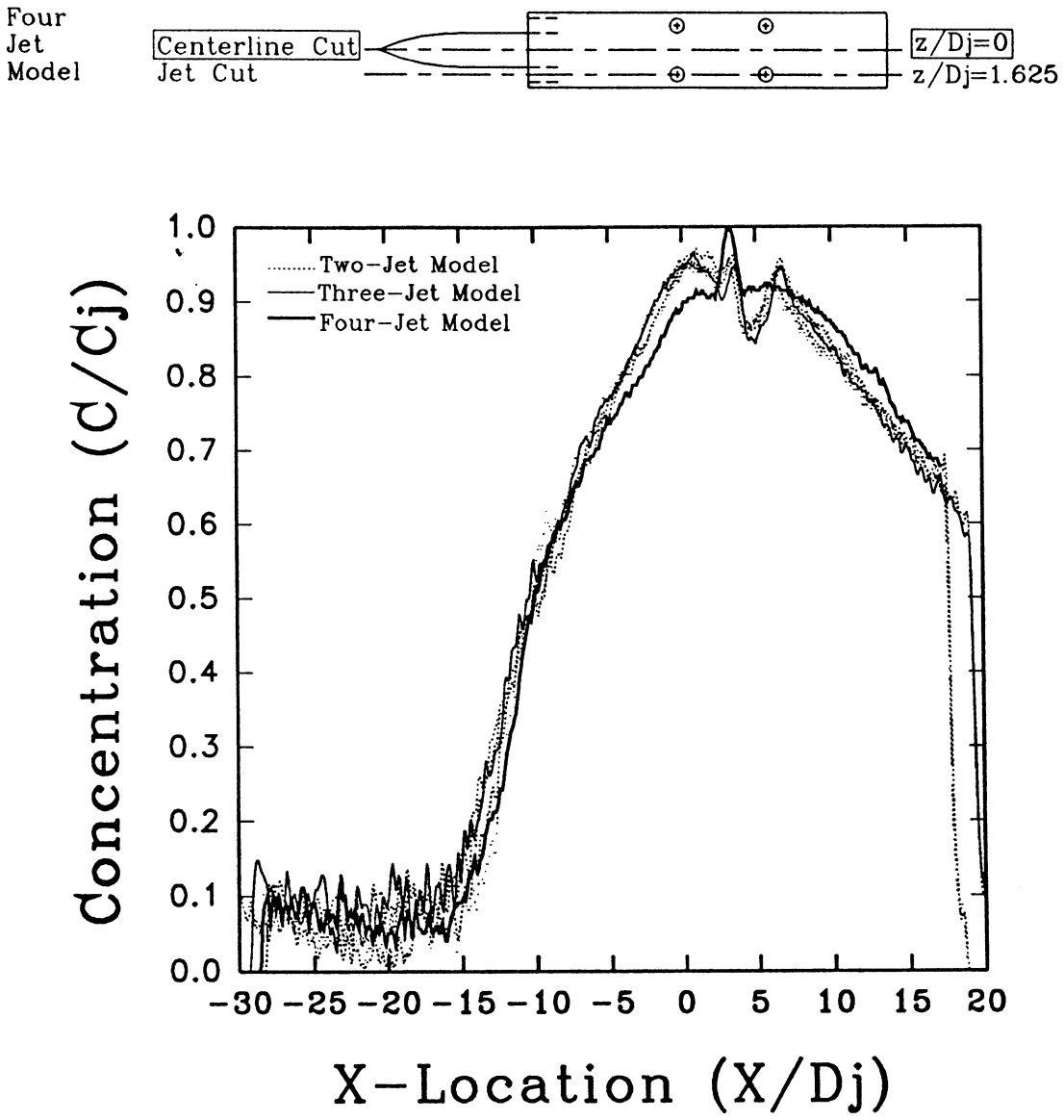

Figure B.1 Three- and Four-Jet 127-Frame Average Multiple Concentration Profiles at Model Centerline: $z/D_j=0$ Laser Sheet at Ground Plane: $y/D_j=0.0$, $H/D_j=4$, $U/V_j=0.09$

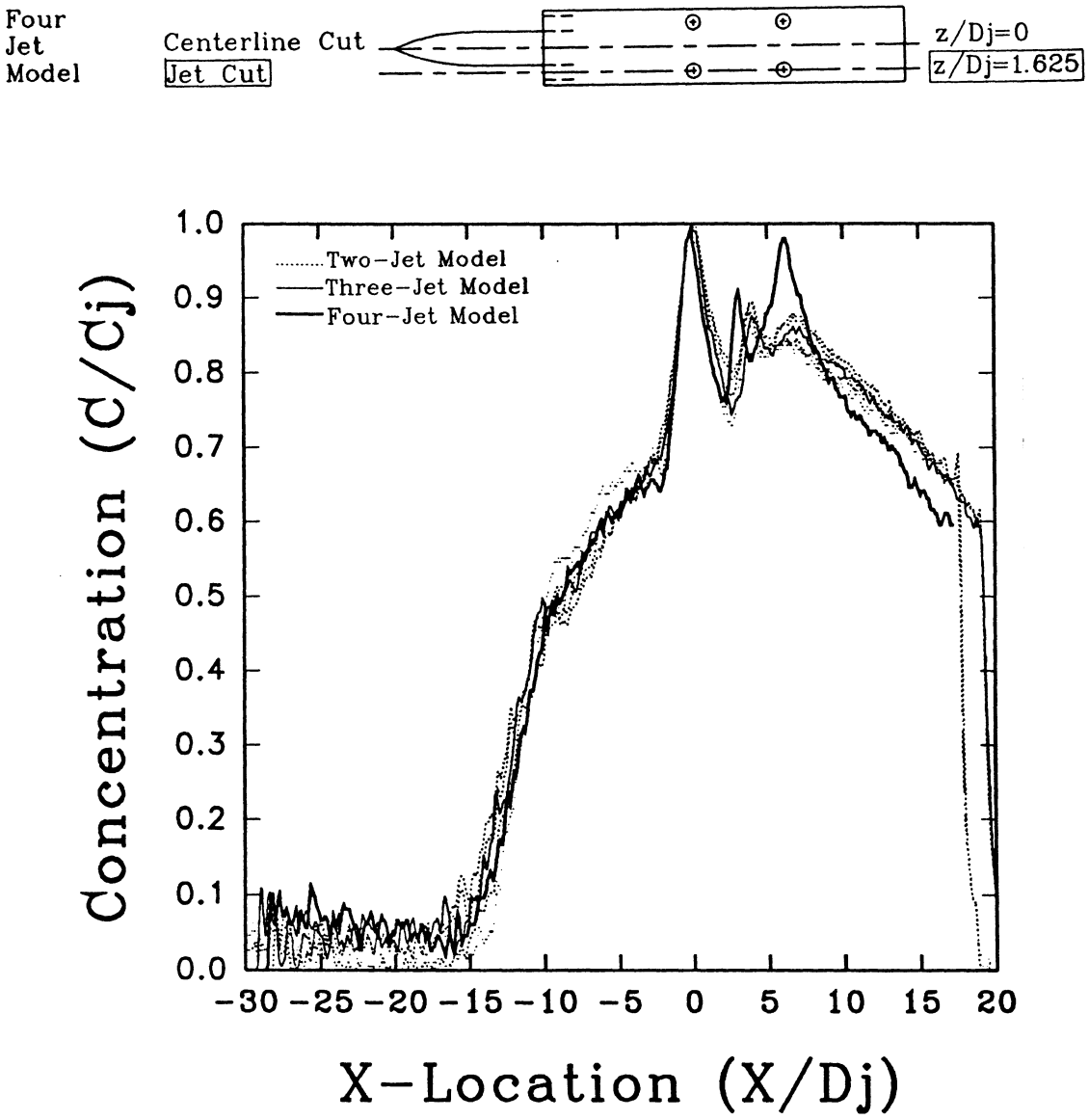

Figure B.2 Three- and Four-Jet 127-Frame Average Multiple Concentration Profiles at Jet Centerline: z/D_j=1.625 Laser Sheet at Ground Plane: y/D_j=0.0, H/D_j=4, U/V_j=0.09

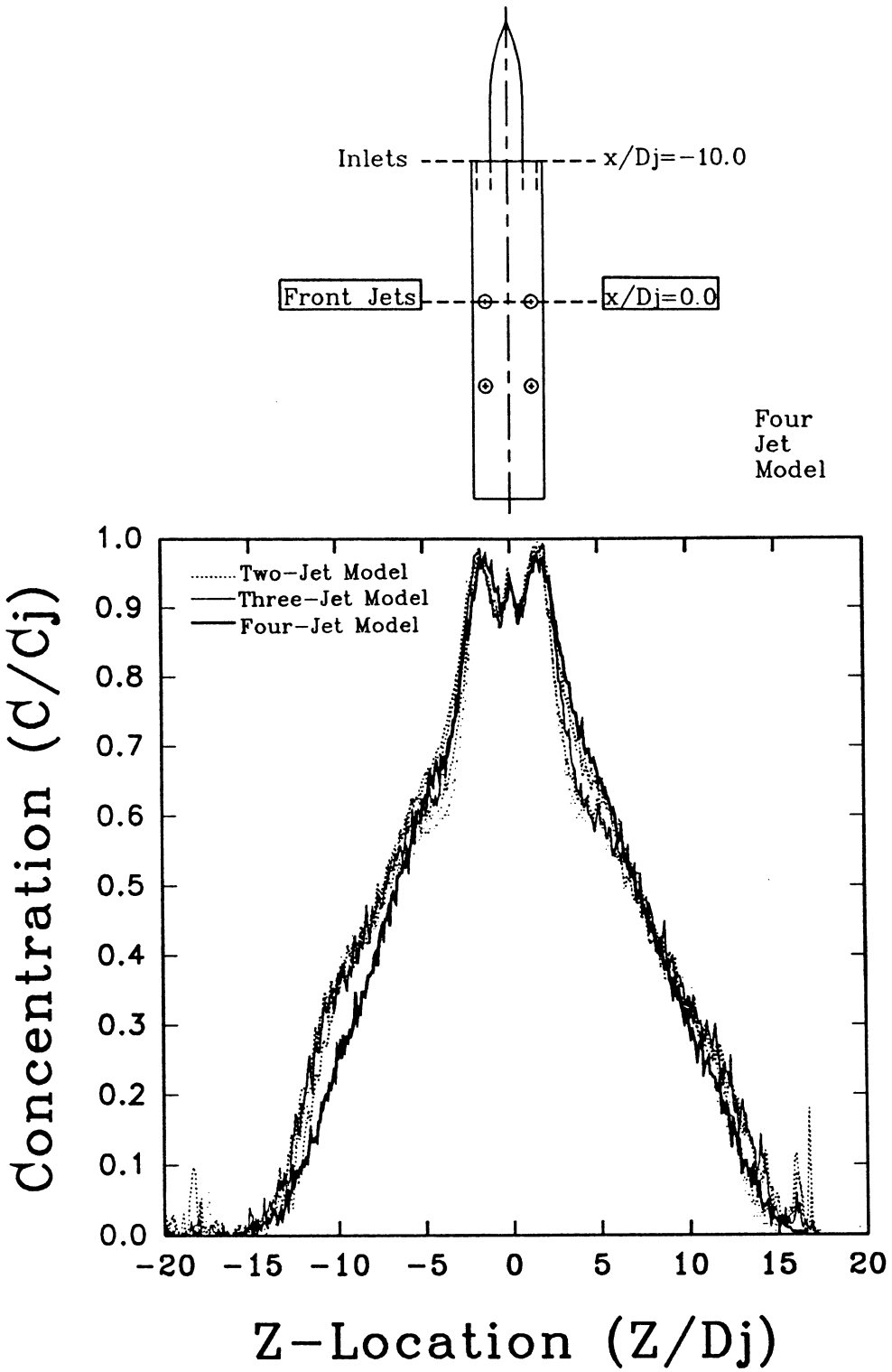

Figure B.3 Three- and Four-Jet 127-Frame Average Multiple Concentration Profiles at Forward Jet Centerline: $x/D_j=0$ Laser Sheet at Ground Plane: $y/D_j=0.0$, $H/D_j=4$, $U/V_j=0.09$

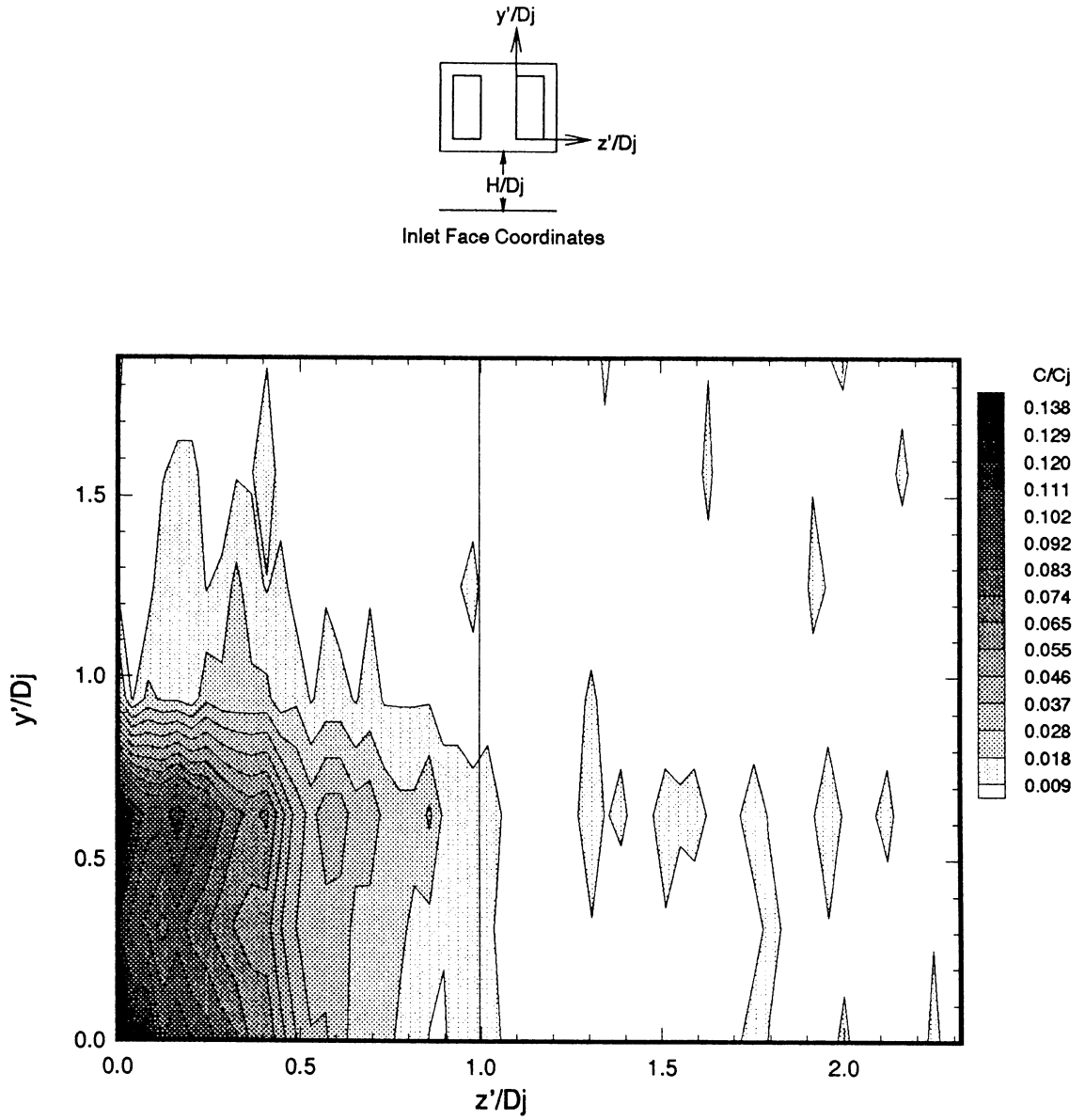

Figure C.1 Low Speed Two-Jet Average Smoke Concentration at the Inlet Face
Plane [z'y']: H/D_j=4, U/V_j=0.03

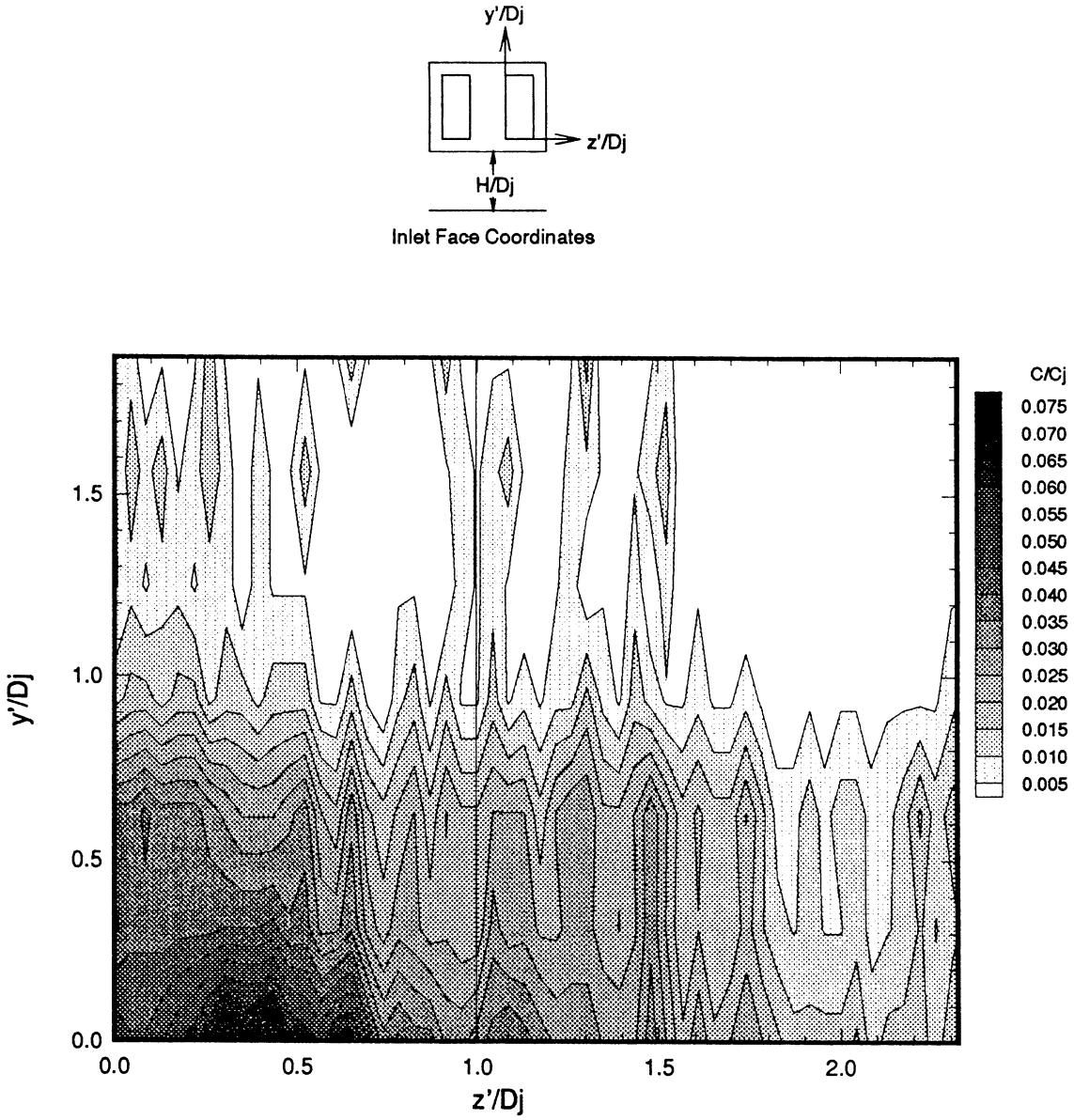

Figure C.2 Low Speed Two-Jet Average Smoke Concentration at the Inlet Face
Plane [z'y']: H/D_j=4, U/V_j=0.09

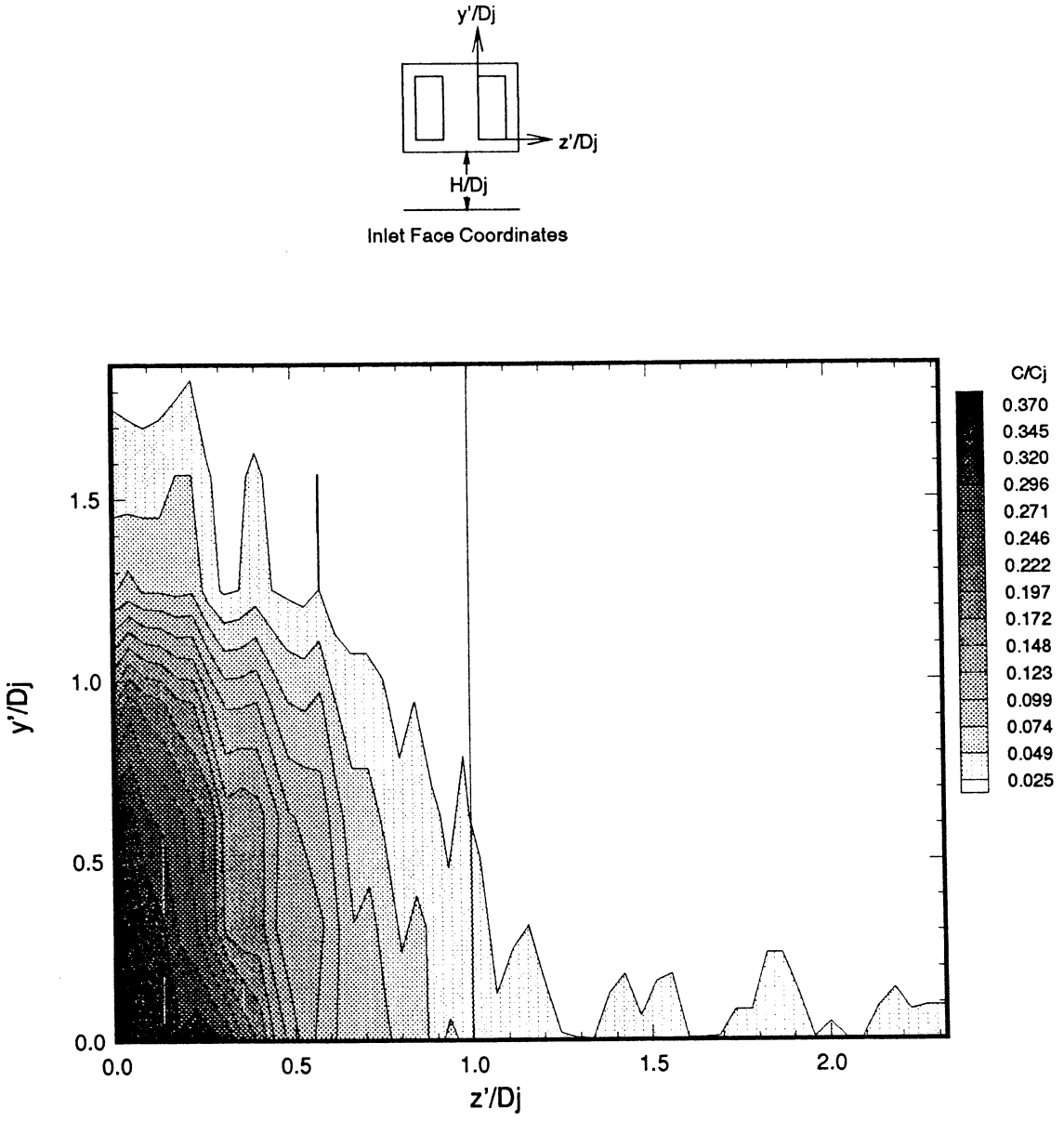

Figure C.3 Low Speed Two-Jet Average Smoke Concentration at the Inlet Face
Plane [z'y']: H/D_j=2, U/V_j=0.03

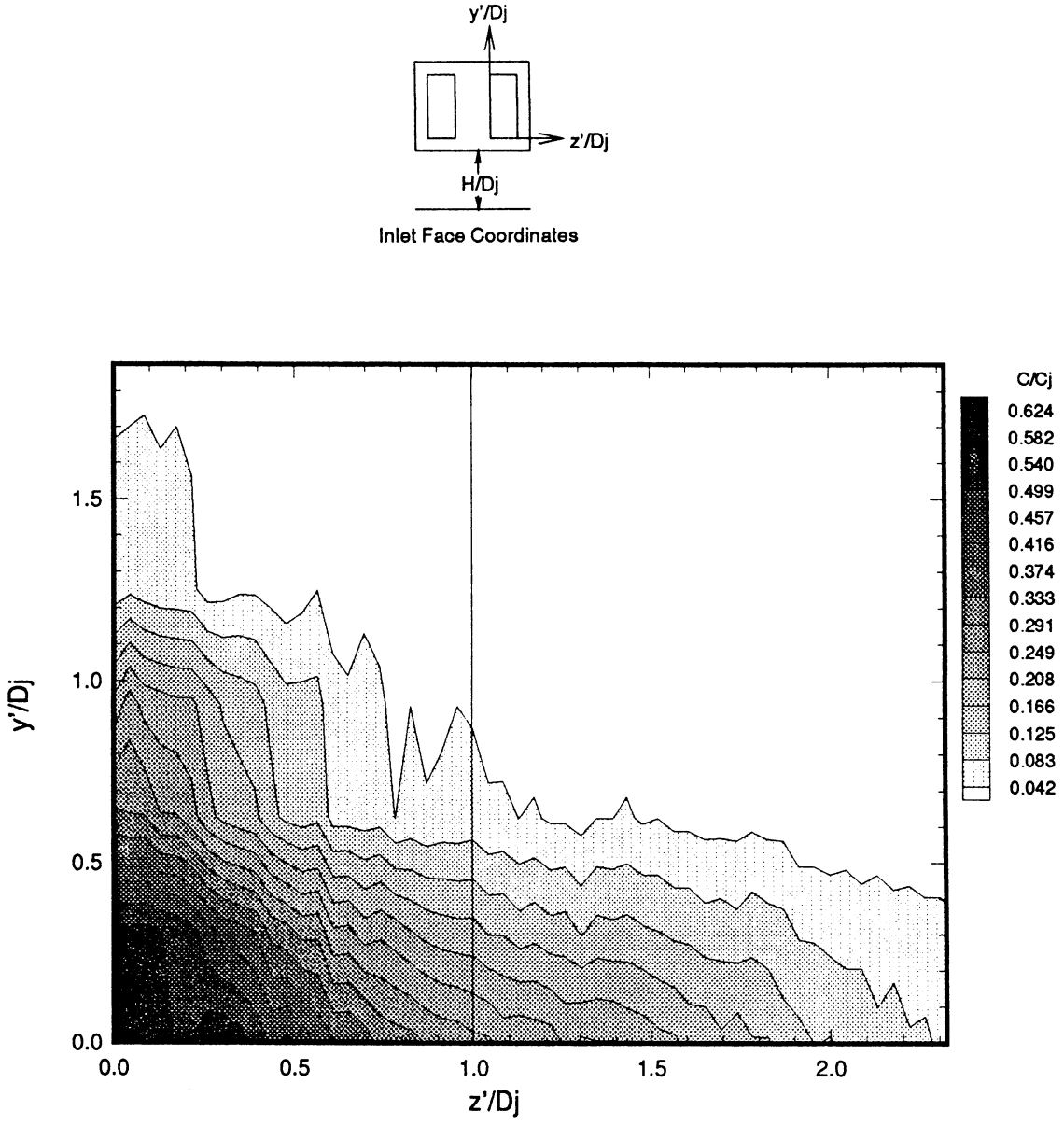

Figure C.4 Low Speed Two-Jet Average Smoke Concentration at the Inlet Face
Plane [z'y']: H/D_j=2, U/V_j=0.09

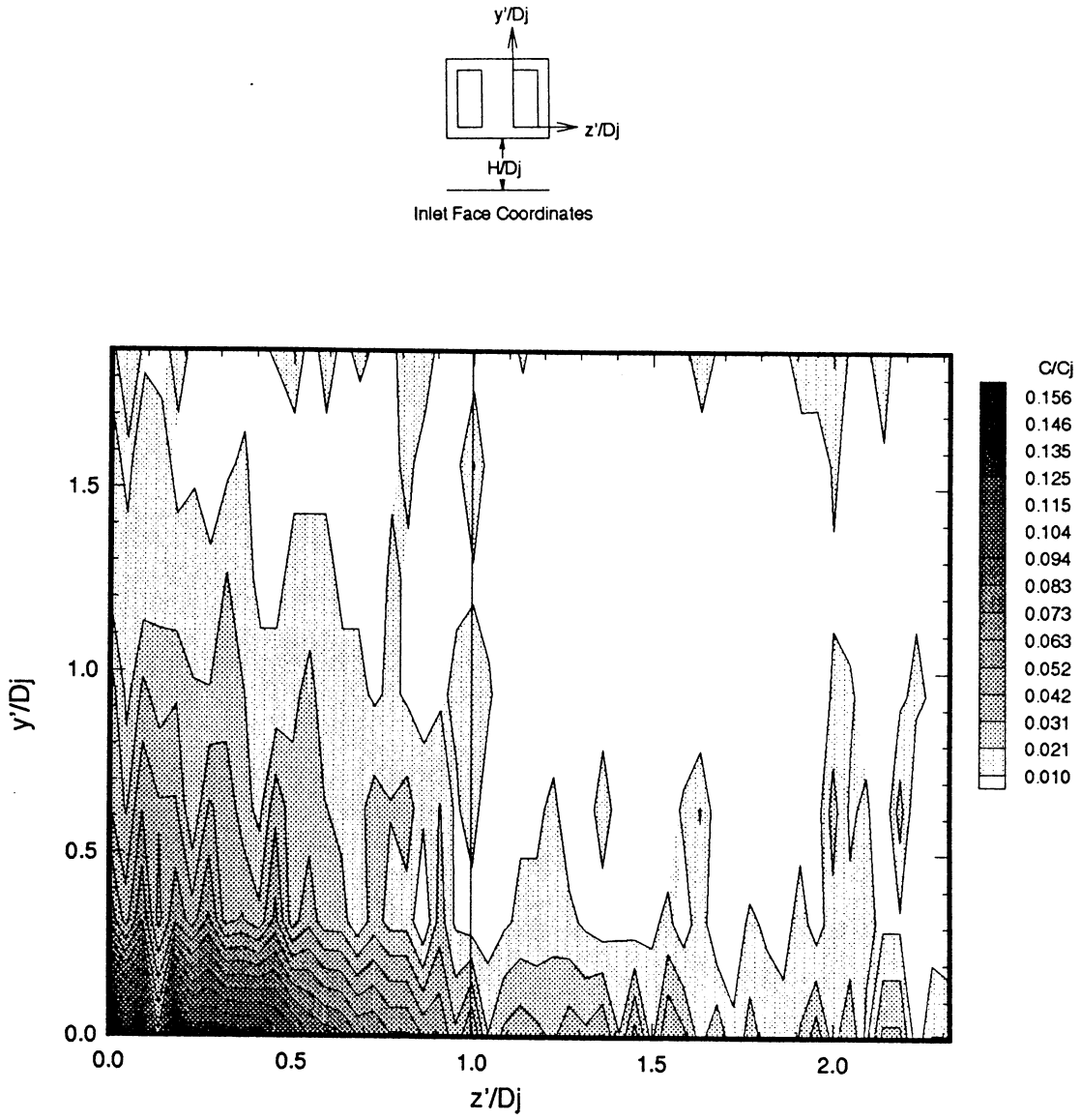

Figure C.5 Low Speed Two-Jet Average Smoke Concentration at the Inlet Face
Plane [z'y']: H/D_j=6, U/V_j=0.03

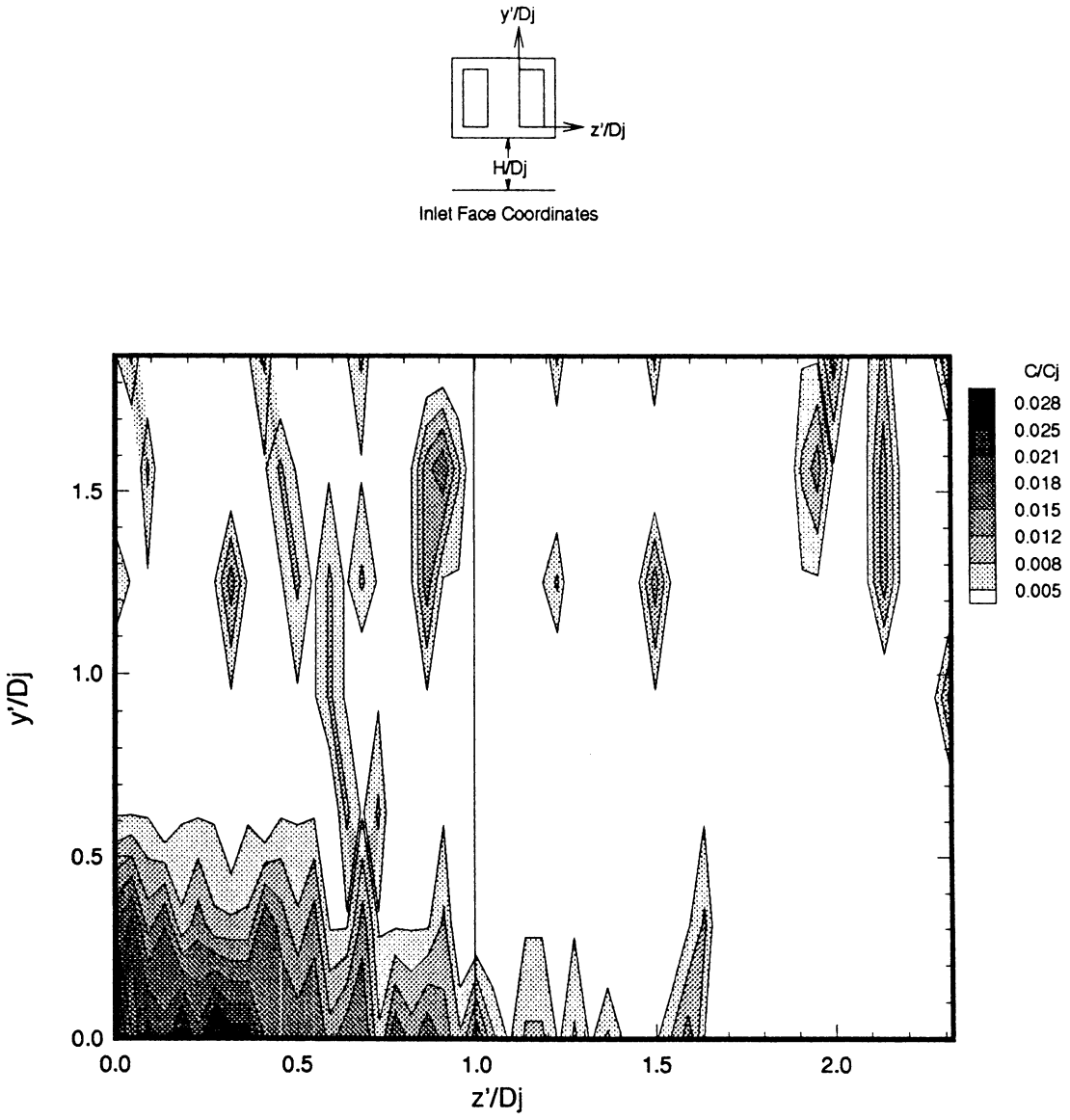

Figure C.6 Low Speed Two-Jet Average Smoke Concentration at the Inlet Face
Plane [z'y']: H/D_j=6, U/V_j=0.09

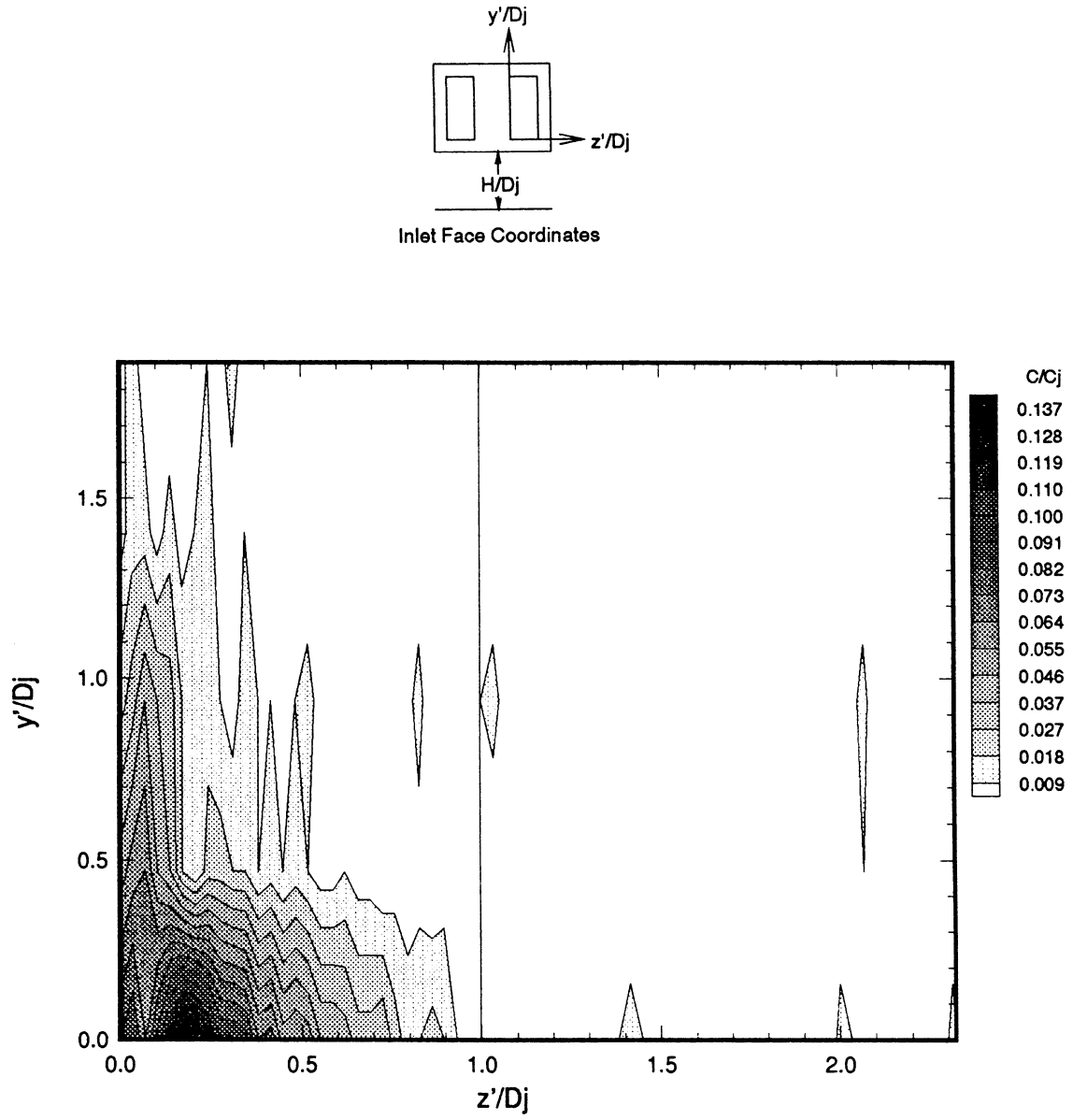

Figure C.7 Low Speed Three-Jet Average Smoke Concentration at the Inlet Face Plane [z'y']: H/D_j=4, U/V_j=0.03

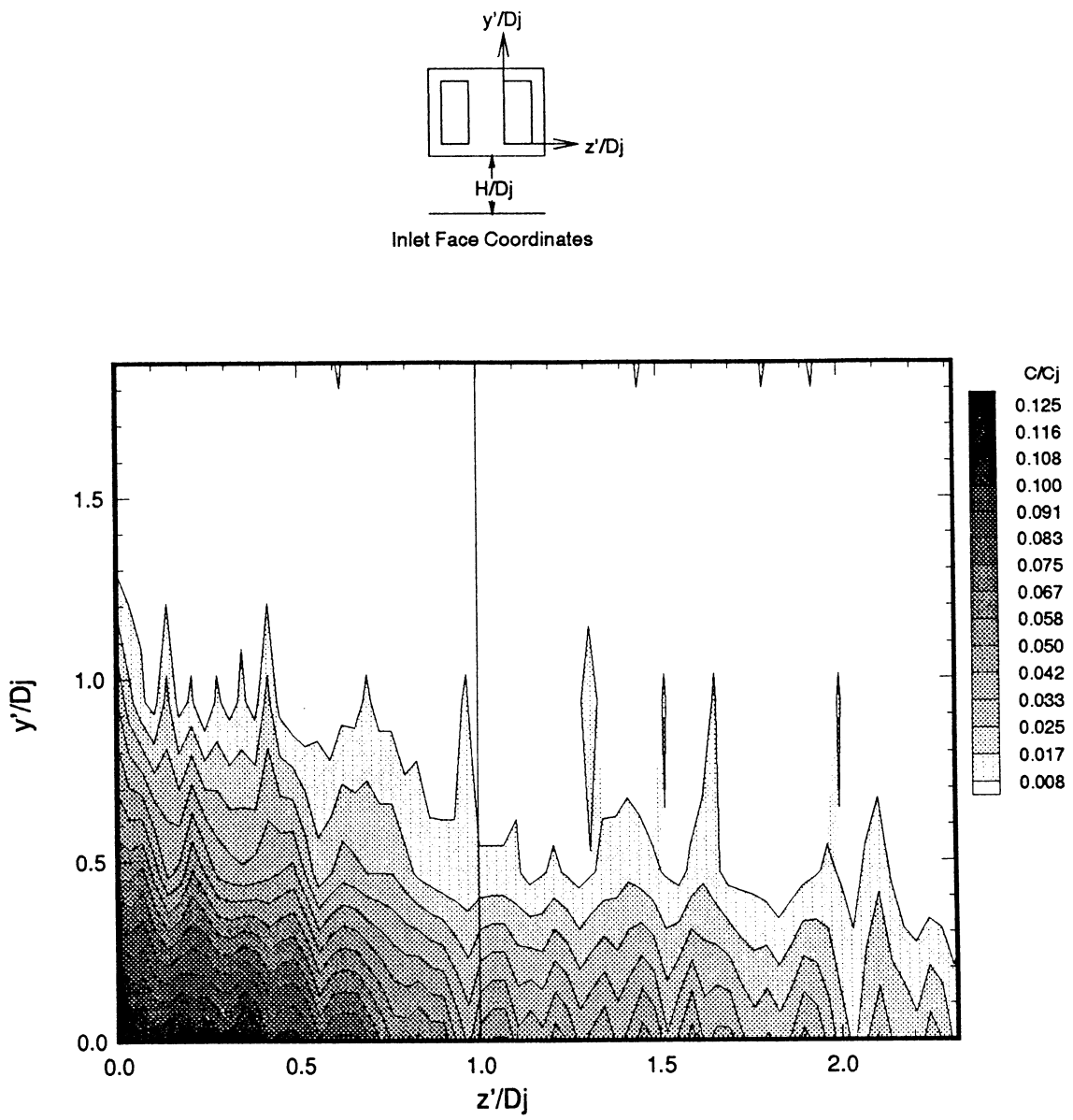

Figure C.8 Low Speed Three-Jet Average Smoke Concentration at the Inlet Face Plane [z'y']: H/D_j=4, U/V_j=0.09

VUKITS VIDEO DESCRIPTION

1). Low Speed Configuration Measurements in Ground Plane - $H/D_j = 4.0$

a). Two-Jet- $U/V_j = 0.03$ and 0.09
b). Three-Jet- $U/V_j = 0.03$ and 0.09
c). Four-Jet- $U/V_j = 0.03$ and 0.09

2). Low Speed Two-Jet Inlet Plane Measurements

a). $H/D_j=4$, $U/V_j = 0.03$
b). $H/D_j=4$, $U/V_j = 0.09$
c). $H/D_j=2$, $U/V_j = 0.03$
d). $H/D_j=2$, $U/V_j = 0.09$

For each case, the laser sheet was in the xz plane at the following planes:
-model plane
-lower inlet plane (closest to the ground)
-mid inlet plane
-top inlet plane

3). High Speed Two-Jet Measurements in Ground Plane - $H/D_j = 4.0$

a). $M_j = 0.50$, $U/V_j=0.03$
b). $M_j = 0.50$, $U/V_j=0.09$
c). $M_j = 0.95$, $U/V_j=0.03$
d). $M_j = 0.95$, $U/V_j=0.09$

REPORT DOCUMENTATION PAGE

Form Approved
OMB No. 0704-0188

1. AGENCY USE ONLY (*Leave blank*)	2. REPORT DATE	3. REPORT TYPE AND DATES COVERED
	February 2004	Final Contractor Report

4. TITLE AND SUBTITLE

Low and High Speed STOVL Configurations in Ground Effect

5. FUNDING NUMBERS

WBS–22–708–90–21
NAG3–943

6. AUTHOR(S)

Thomas J. Vukits

7. PERFORMING ORGANIZATION NAME(S) AND ADDRESS(ES)

Purdue University
Main Campus
West Lafayette, Indiana 47907

8. PERFORMING ORGANIZATION REPORT NUMBER

E–14167

9. SPONSORING/MONITORING AGENCY NAME(S) AND ADDRESS(ES)

National Aeronautics and Space Administration
Washington, DC 20546–0001

10. SPONSORING/MONITORING AGENCY REPORT NUMBER

NASA CR—2004-212609

11. SUPPLEMENTARY NOTES

Project Manager, James D. Holdeman, Turbomachinery and Propulsion Systems Division, NASA Glenn Research Center, organization code 5830, 216–433–5846.

12a. DISTRIBUTION/AVAILABILITY STATEMENT

Unclassified - Unlimited
Subject Category: 07 Distribution: Nonstandard

Available electronically at http://gltrs.grc.nasa.gov

This publication is available from the NASA Center for AeroSpace Information, 301–621–0390.

12b. DISTRIBUTION CODE

13. ABSTRACT ***(Maximum 200 words)***

The problem of hot gas ingestion in V/STOL and STOVL aircraft has motivated a set of experimental studies. Two-, three-, and four-jet configurations in cross flow were studied in ground effect. The results presented here were based on a quantitative, concentration measurement technique know as marker nephelometry. The effects of configuration, velocity ratio (freestream over jet velocity), model height, and inlet suction were investigated. The experiments were conducted in three parts. In the first part, comparisons of low speed two-, three-, and four-jet configurations were made. Measurements were made in the planes beneath the models in ground effect. As the number of jets increased, the vortical structures in the flowfield were found to move further upstream due to the increased total momentum. In the second part of the experiments, measurements were made at the inlet entry plane of the low speed two- and three-jet configurations in ground effect. The results indicated that ingestion occurred intermittently, especially in the upper portions of the inlets. The highest levels of concentrations were measured at a model height of two jet diameters. As the model height increased, the concentration levels decreased. Finally, a high speed, two-jet configuration without inlet suction was studied. The flowfield structures were generally found to move further downstream as the jet velocity increased at a constant velocity ratio.

14. SUBJECT TERMS

STOVL aircraft; Hot gas ingestion; Jet in crossflow

15. NUMBER OF PAGES

170

16. PRICE CODE

17. SECURITY CLASSIFICATION OF REPORT	18. SECURITY CLASSIFICATION OF THIS PAGE	19. SECURITY CLASSIFICATION OF ABSTRACT	20. LIMITATION OF ABSTRACT
Unclassified	Unclassified	Unclassified	